

Fluorescent fusions of key enzymes of plant fatty acid modification: functionality and localization

Dissertation

Zur Erlangung des

Doktorgrades der Naturwissenschaften (Dr. rer. nat.)

der Naturwissenschaftlichen Fakultät I – Biowissenschaften –

der Martin-Luther-Universität

Halle-Wittenberg,

vorgelegt von

Frau Larissa Launhardt

Geb. am 22.11.1993 in Buchholz i. d. Nordheide

Gutachterinnen und Gutachter:

Prof. Dr. Ingo Heilmann

Prof. Dr. Bettina Hause

Prof. Dr. Johnathan Napier

Tag der Verteidigung: 29. August 2022

Table of Contents

Abbreviations	V
Figures	VIII
Tables	X
Summary	XI
Zusammenfassung	XIII
1. Introduction	1
1.1 Structure and function of glycerolipids in plants	2
1.2 Lipid biosynthesis and modification	5
1.2.1 Fatty acid synthesis in the plastid	6
1.2.2 Lipid assembly in the chloroplast: the prokaryotic pathway	7
1.2.3 Lipid assembly and fatty acid modification at the ER: the eukaryotic pathway ...	8
1.2.4 Fatty acid desaturation by membrane-bound FADs	9
1.3 Seed oil biogenesis and oil body formation	10
1.3.1 Synthesis of seed oils	11
1.3.2 Lipid droplets engulf accumulating TAG that would destabilize the bilayer	12
1.3.3 The role of PC in seed oil biogenesis	13
1.4 Characterization of FAD2 and FAD3 from <i>A. thaliana</i>	13
1.5 TAG assembly by DGATs and PDAT	15
1.6 Technical modification of oil biogenesis and its challenges	18
2. Aims and Objectives	21
3. Results	22
3.1 Fluorescence-tagged enzyme variants of FAD2 and FAD3 are functional in yeast	22
3.2 Fluorescence-tagged enzyme variants of FAD2 and FAD3 complement Arabidopsis mutants	24
3.2.1 Phenotypic defects of <i>fad2-1</i> and <i>fad3-2</i> are restored by the respective expression of EYFP-FAD2 or EYFP-FAD3	25
3.2.2 Fatty acid compositions of <i>fad2-1</i> and <i>fad3-2</i> are restored by the respective expression of EYFP-FAD2 or EYFP-FAD3	29
3.3 Functional EYFP-FAD2 and EYFP-FAD3 fusions decorate donut-shaped structures in complemented plant lines	33
3.4 Fluorescent fusions of FAD2 associate with Golgi-particles in close proximity to the ER in Arabidopsis mesophyll protoplasts	36
3.5 FAD3 associated with the ER of Arabidopsis mesophyll protoplasts	47
3.6 Partial colocalization of FAD2 and FAD3 in Arabidopsis mesophyll protoplasts	49

3.7	Coexpression of the transcription factor WRINKLED1 enables detection of mCherry-FAD3 expressed from its intrinsic promoter in Arabidopsis mesophyll protoplasts.....	51
3.8	FAD2 and FAD3 interact with acyltransferases in yeast two-hybrid studies	54
3.9	Fluorescence-tagged enzyme variants of PDAT and DGAT1 are functional in yeast	57
3.10	PDAT and DGAT1 localize to the ER in Arabidopsis mesophyll protoplasts	59
3.11	FAD2 interacts with FAD3 and PDAT in BiFC experiments at ER-like structures	62
4.	Discussion	67
4.1	Fluorescence-tagged enzyme variants of FAD2 and FAD3 are functional and complement the respective Arabidopsis mutants.....	68
4.2	A possible role of FAD2 at the Golgi.....	70
4.3	FAD2 and FAD3 interact with each other at the ER membrane	73
4.4	Novel interactions between fatty acid desaturases and acyl-transferases	76
4.5	In a nutshell and future perspectives	78
5.	Materials and Methods.....	80
5.1	Devices and Equipment.....	80
5.2	Chemicals	80
5.3	Standards, enzymes, molecular size markers	80
5.4	Consumables and kits	80
5.5	Microorganisms.....	80
5.6	Plants	81
5.7	Culture media and growth conditions.....	81
5.7.1	Growth conditions for <i>E. coli</i>	82
5.7.2	Growth conditions for <i>A. tumefaciens</i>	82
5.7.3	Growth conditions for yeast	82
5.7.4	Growth conditions for Arabidopsis	83
5.8	Salt treatment and root length measurements of Arabidopsis.....	83
5.9	Vectors.....	83
5.10	Molecular biology methods.....	86
5.10.1	Isolation of RNA from seeds and siliques	86
5.10.2	Isolation of RNA from leaves and seedlings	87
5.10.3	Concentration measurements of nucleic acid	87
5.10.4	cDNA-Synthesis	87
5.10.5	Isolation of genomic DNA.....	87

5.10.6	Amplification of DNA fragments via PCR	88
5.10.7	Separation of DNA and RNA fragments in agarose gels.....	88
5.10.8	Extraction of DNA fragments from agarose gels	88
5.10.9	Restriction of DNA fragments	89
5.10.10	Ligation of DNA fragments	89
5.10.11	Clonase™-mediated Gateway™ reaction	89
5.11	Amplification of plasmid-DNA in <i>E. coli</i>	90
5.11.1	Preparation of chemo competent <i>E. coli</i>	90
5.11.2	Transformation of chemo competent <i>E. coli</i>	90
5.11.3	Isolation of plasmid DNA from <i>E. coli</i>	91
5.12	Sequencing	91
5.13	Cloning strategies.....	91
5.13.1	Recombinant plasmids for heterologous protein expression in yeast.....	91
5.13.2	Recombinant plasmids for yeast two-hybrid analyses	92
5.13.3	Recombinant plasmids for bimolecular fluorescence complementation (BiFC) .	93
5.13.4	Recombinant plasmids for heterologous protein expression in plant cells.....	94
5.14	Preparation and transformation of chemo competent <i>A. tumefaciens</i>	95
5.15	Preparation and transformation of competent <i>S. cerevisiae</i>	95
5.16	Preparation and transformation of Arabidopsis mesophyll protoplasts.....	96
5.17	Generation of stably transformed Arabidopsis plants.....	98
5.18	SDS-PAGE.....	98
5.19	Western blotting and immunodetection of specific proteins	99
5.20	Heterologous expression of different cDNA clones in yeast.....	100
5.20.1	Heterologous expression of FAD2 and FAD3 in the yeast strain INVSc1	100
5.20.2	Heterologous expression of PDAT and DGAT1 in the yeast strain H1246	101
5.21	Lipid extraction and fatty acid analyses	101
5.21.1	Isolation of total lipids from yeast.....	101
5.21.2	Isolation of total lipids from plant material	102
5.21.3	Separation of lipid classes with solid phase adsorption chromatography	102
5.21.4	Thin layer chromatography (TLC).....	103
5.21.5	Extraction and transmethylation of fatty acids form single seeds	103
5.21.6	Base-catalyzed transmethylation of fatty acids with sodium methoxide	104
5.21.7	Acid-catalyzed transmethylation of fatty acids	104
5.21.8	Gas chromatography of FAMES	104

5.22	Protein-protein interaction studies	105
5.22.1	Split-ubiquitin-based yeast two-hybrid system	105
5.22.2	Yeast two-hybrid tests	105
5.22.3	Interaction analysis by bimolecular fluorescence complementation	106
5.23	Microscopy and image analysis	106
5.23.1	Fluorescence microscopy using the LSM880	106
5.23.2	Fluorescence microscopy using a spinning disc microscope	107
5.23.3	Image analysis using Fiji	107
5.24	Statistical analyses	108
6.	References	109
7.	Appendix	XV
7.1	Additional information to the obtained results	XV
7.2	Additional information to materials and methods	XXII
7.2.1	Specification of devices	XXII
7.2.2	Specification of chemicals	XXIII
7.2.3	Lipid and fatty acid standards	XXIV
7.2.4	Molecular size markers and enzymes	XXIV
7.2.5	Consumables and kits	XXV
7.2.6	AGI numbers of genes used in this work	XXVI
7.2.7	Oligonucleotides	XXVI
	Acknowledgment – Danksagung	XXXI
	Curriculum vitae	XXXIII
	Erklärung	XXXIV

Abbreviations

16:0	palmitic acid
16:1 ^{Δ9}	palmitoleic acid
16:3	hexadecatrienoic acid
18:0	stearic acid
18:1 ^{Δ9}	oleic acid
18:2 ^{Δ9,12}	linoleic acid
18:3 ^{Δ9,12,15}	α-linolenic acid
20:1 ^{Δ11}	gondoic acid, 11-eicosenoic acid
ACC	acetyl-CoA carboxylase
ACP	acyl carrier protein
Alg5	dolichyl-phosphate beta-glucosyltransferase
APS	ammonium persulfate
Arabidopsis	<i>Arabidopsis thaliana</i>
ATP	adenosine triphosphate
<i>A. tumefaciens</i>	<i>Agrobacterium tumefaciens</i>
AWAK2	wall-associated kinase 2 from <i>Arabidopsis thaliana</i>
<i>Bn</i>	<i>Brassica napus</i>
BSA	bovine serum albumin, Albumin Fraction V
β-X-gal	5-bromo-4-chloro-3-indolyl-β-D-galactopyranoside
cDNA	complementary DNA
CDP	cytidine diphosphate
CFP	cyan fluorescent protein
ChlA	chlorophyll A
CoA	coenzyme A
CTCF	corrected total cell fluorescence
CTP	cytidine triphosphate
Cub	C-terminal half of ubiquitin (amino acids 35 to 76)
D	aspartate
DAG	diacylglycerol
DGAT	diacylglycerol:acyl-CoA acyltransferase
DGDG	digalactosyldiacylglycerol
DMF	di-methyl formamide
DMSO	dimethyl sulfoxide
DNA	deoxyribonucleic acid
DTT	dithiothreitol
E	glutamate
<i>E. coli</i>	<i>Escherichia coli</i>
EDTA	ethylenediaminetetraacetic acid
ER	endoplasmic reticulum
EYFP	enhanced yellow fluorescent protein
FA	fatty acid
FAD	fatty acid desaturase
FAME	fatty acid methyl ester

FAS	fatty acid synthase
FID	flame ionization detector
G3P	glycerol-3-phosphate
GC	gas chromatography
GFP	green fluorescent protein
<i>GmMan1</i>	1,2- α -mannosidase 1 from <i>Glycine max.</i>
GOI	gene of interest
GPAT	glycerol-3-phosphate acyltransferase
G3P	glycerol-3-phosphate
H	histidine
HEPES	4-(2-hydroxyethyl)-1-piperazineethanesulfonic acid
HRP	horse radish peroxidase
HSPB	high salt precipitation buffer
I	isoleucine
IAA	isoamyl alcohol
IPTG	isopropyl β -D-1-thiogalactopyranoside
IQR	interquartile range
K	lysine
L	leucine
LACS	long-chain acyl-CoA synthetase
LD	lipid droplet
LDAP	lipid droplet associated protein
LDIP	LDAP-interacting protein
LiAc	lithium acetate
LPA	lyso-phosphatidic acid
LPAAT	lyso-phosphatidic acid acyltransferase
LPC	lyso-phosphatidylcholine
LPCAT	lyso-phosphatidylcholine:acyl-CoA acyltransferase
LSM	laser scanning microscopy
MBS	main beam splitter
MCC	Manders' colocalization coefficient
mCherry	monomeric red fluorescent protein
mcs	multiple cloning site
MES	2-(N-morpholino) ethanesulfonic acid
MGDG	monogalactosyldiacylglycerol
N	asparagine
NADH	nicotinamide adenine dinucleotide
NADPH	nicotinamide adenine dinucleotide phosphate
Nub	N-terminal half of ubiquitin (amino acid 1-34)
NubG	N-terminal half of ubiquitin (amino acid 1-34) with point mutation: isoleucin 13 to glycine
OCS	octopin synthase
ORF	open reading frame
OD ₆₀₀	optical density at 600 nm
OD-unit	volume corresponding to the volume of a solution with OD ₆₀₀ of 1

OLE3	oleosin3
PA	phosphatidic acid
PAP	phosphatidic acid phosphatase
PC	phosphatidylcholine
PCC	Pearson's correlation coefficient
PCR	polymerase chain reaction
PDAT	phosphatidylcholine:diacylglycerol acyltransferase
PDCT	phosphatidylcholine:diacylglycerol cholintransferase
PE	phosphatidylethanolamine
PEG	polyethylene glycol
PG	phosphatidylglycerol
PGP	phosphatidylglycerol phosphate
PI	phosphatidylinositol
PS	phosphatidylserine
Q	glutamine
R	arginine
<i>Rc</i>	<i>Ricinus communis</i> L. (castor bean)
<i>Rc</i> PDAT	PDAT from <i>Ricinus communis</i> L.
RFP	red fluorescent protein
RNA	ribonucleic acid
RNAi	ribonucleic acid interference
S	serine
SAD	$\Delta 9$ stearoyl-ACP desaturase
<i>S. cerevisiae</i>	<i>Saccharomyces cerevisiae</i>
ScOLE1	$\Delta 9$ -desaturase from <i>Saccharomyces cerevisiae</i>
SD	spinning disc microscopy
SDS	sodium dodecyl sulfate
SDS-PAGE	sodium dodecyl sulfate polyacrylamide gel electrophoresis
TAE	tris, acetic acid and EDTA buffer
TAG	triacylglycerol
TBS	tris buffered saline
TE	tris buffer with EDTA
TEMED	N,N,N',N'-tetramethyl-ethylenediamine
TLC	thin layer chromatography
TMSH	trimethylsulfonium hydroxide
UDP	uridine diphosphate
Ura	uracil
VAP27-1	vesicle associated protein 27-1
<i>Vf</i>	<i>Vernicia fordii</i> (tung tree)
<i>Vf</i> DGAT1/2	DGAT1/2 from <i>Vernicia fordii</i>
<i>Vf</i> FAD3	FAD3 from <i>Vernicia fordii</i>
W	tryptophane
WRI1	WRINKLED1

Figures

Figure 1.1. Structures of different lipid classes.	3
Figure 1.2. Overview of fatty acid synthesis and lipid assembly in plants.	5
Figure 1.3. Topology model of integral membrane desaturases.	10
Figure 1.4. Proposed membrane topology of DGAT1 and DGAT2 from tung tree.	15
Figure 3.1. Functionality of fluorescence-tagged fatty acid desaturases FAD2 and FAD3 from <i>Arabidopsis</i> heterologously expressed in yeast.	23
Figure 3.2. Phenotypic comparison of Col-0 wild type, <i>fad2-1</i> and <i>fad2-1</i> lines expressing EYFP-FAD2.	25
Figure 3.3. Complementation of <i>fad2-1</i> salt sensitivity by expression of EYFP-FAD2. ...	26
Figure 3.4. Expression of EYFP-FAD3 complements the phenotypic growth defect of the <i>Arabidopsis fad3-2</i> mutant.	28
Figure 3.5. Expression of EYFP-FAD2 reconstitutes a wild type-like fatty acid composition in the <i>Arabidopsis fad2-1</i> mutant.	30
Figure 3.6. Expression of EYFP-FAD3 reconstitutes a wild type-like fatty acid composition in the <i>Arabidopsis</i>	32
Figure 3.7. Subcellular distribution of EYFP-FAD2 in roots and in leaves of transgenic <i>Arabidopsis</i> plants.	34
Figure 3.8. Subcellular distribution of EYFP-FAD3 in roots and in leaves of transgenic <i>Arabidopsis</i> plants.	35
Figure 3.9. Subcellular distribution of EYFP-FAD2 in <i>Arabidopsis</i> mesophyll protoplasts.	37
Figure 3.10. Subcellular distribution of EYFP-FAD2 relative to the ER and the Golgi in <i>Arabidopsis</i> mesophyll protoplasts.	41
Figure 3.11. Detailed analysis of the subcellular distribution of EYFP-FAD2 relative to the ER and to Golgi stacks.	43
Figure 3.12. Subcellular distribution of EYFP-FAD2 relative to peroxisomes and oil bodies in <i>Arabidopsis</i> mesophyll protoplasts.	45
Figure 3.13. Subcellular distribution of mCherry-FAD3 in <i>Arabidopsis</i> mesophyll protoplasts.	48
Figure 3.14. Relative subcellular distribution of EYFP-FAD2 and mCherry-FAD3 in <i>Arabidopsis</i> mesophyll protoplasts.	50
Figure 3.15. Subcellular distribution of mCherry-FAD3 driven by an intrinsic promoter fragment upon coexpression with WRI1-EYFP.	52
Figure 3.16. Interaction of enzymes involved in fatty acid desaturation and TAG assembly according to split-ubiquitin based yeast two-hybrid analyses.	56

Figure 3.17. Functionality of the fluorescence-tagged acyltransferases PDAT and DGAT1 in the yeast strain H1246.	58
Figure 3.18. Subcellular distribution of fluorescence-tagged PDAT in Arabidopsis mesophyll protoplasts.	60
Figure 3.19. Subcellular distribution of DGAT1 in Arabidopsis mesophyll protoplasts. ...	62
Figure 3.20. BiFC-analyses for in vivo interactions between FAD2, FAD3 and PDAT. ...	64
Figure 3.21. Quantitative evaluation of BiFC analyses.	65
Figure 7.1. Subcellular distribution of mCherry-FAD2 in Arabidopsis mesophyll protoplasts.	XV
Figure 7.2. Immunodetection of tagged FAD2 expressed in Arabidopsis mesophyll protoplasts.	XVI
Figure 7.3. Subcellular distribution of two different ER markers.	XVII
Figure 7.4. MCCs for selected colocalization experiments in Arabidopsis mesophyll protoplasts.	XVIII
Figure 7.5. Subcellular distribution of EYFP-FAD3 relative to the ER in Arabidopsis mesophyll protoplasts.	XIX
Figure 7.6. Immunodetection of fluorescence-tagged FAD3 expressed in Arabidopsis mesophyll protoplasts.	XX
Figure 7.7. Immunodetection of fluorescence-tagged PDAT expressed in Arabidopsis mesophyll protoplasts.	XX
Figure 7.8. Immunodetection of DGAT1-EYFP expressed in Arabidopsis mesophyll protoplasts.	XXI

Tables

Table 5.1. Antibiotics and supplements.....	81
Table 5.2. Recombinant plasmids for protein expression in INVScI cloned or used in this work.....	92
Table 5.3. Recombinant plasmids for yeast two-hybrid analyses cloned or used in this work.....	93
Table 5.4. Recombinant plasmids for BiFC analyses cloned and used in this work.....	93
Table 5.5. Recombinant plasmids for transient transformation of Arabidopsis protoplasts cloned or used in this work.....	94
Table 5.6. Recombinant plasmids for stable and transient transformation of Arabidopsis generated and used in this work.....	95
Table 5.7. Organelle markers used for colocalization experiments in Arabidopsis protoplasts.....	97
Table 5.8. Composition of self-cast SDS-PAGE-gels.....	99
Table 5.9. Primary and secondary polyclonal antibodies.....	100
Table 5.10. Developing solvents and developing time for thin layer chromatography.....	103
Table 5.11. Microscopy settings at the LSM880.....	106
Table 7.1. Devices used in this work.....	XXII
Table 7.2. Chemicals used in this work.....	XXIII
Table 7.3. Lipid- and fatty acid standards.....	XXIV
Table 7.4. Molecular size markers and enzymes.....	XXIV
Table 7.5. Consumables and kits.....	XXV
Table 7.6. AGI numbers of genes used in this work.....	XXVI
Table 7.7. Oligonucleotides used for cloning.....	XXVI
Table 7.8. Oligonucleotides used for sequencing.....	XXIX

Summary

Unsaturated fatty acids influence the physiological function of membranes and are also incorporated into triacylglycerol (TAG), a major component of seed storage oil. The fatty acid desaturases FAD2 and FAD3 sequentially convert oleic acid (18:1^{Δ9}) to linoleic acid (18:2^{Δ9,12}) and linolenic acid (18:3^{Δ9,12,15}), respectively. FAD2 and FAD3 are thought to reside in the endoplasmic reticulum (ER) where they modify phospholipid-associated fatty acids. The acyltransferases DGAT1, DGAT2 and PDAT are also assumed to reside in the ER and produce TAG by transferring fatty acids to diacylglycerol (DAG). DGAT1 and DGAT2 use CoA-bound fatty acids as acyl donor, while PDAT utilizes the membrane phospholipids as acyl donor. Previous research indicates that besides the metabolic context and the interaction and cooperation of the enzymes involved in fatty acid desaturation and TAG assembly, the subcellular distribution seemingly plays a role in the production of TAG. Fusion variants of FAD2 and FAD3 with N-terminal fluorescence tags were generated and successfully converted oleic or linoleic acids, respectively, upon expression in yeast (*Saccharomyces cerevisiae*). Furthermore, ectopic expression of EYFP-FAD2 or EYFP-FAD3 rescued macroscopic and biochemical phenotypes of *fad2-1* or *fad3-2* Arabidopsis mutants, respectively, indicating functionality of the fluorescent fusions. In the generated plant lines, EYFP-FAD2 or EYFP-FAD3 decorated ER-associated flattened donut-shaped structures. Coexpression in Arabidopsis mesophyll protoplasts with different organelle markers correlated these structures with Golgi-particles. Quantitative evaluation of the colocalization supported the Golgi-association of EYFP-FAD2 and comparisons with other organelle markers indicated that the observed colocalization of EYFP-FAD2 and Golgi particles was not coincidental. In contrast to the punctuate distribution of EYFP-FAD3 in complemented plants, fluorescence-tagged FAD3 variants associated with the ER network in Arabidopsis mesophyll protoplasts. The expression of FAD3 under the control of its endogenous promoter was enhanced by coexpression with the transcription factor for lipid biosynthesis WRINKLED1 (WRI1), indicating a prominent role for FAD3 in oleogenic tissues. Interaction analyses using the split-ubiquitin-based yeast two-hybrid system revealed novel interactions of the fatty acid desaturases FAD2 and FAD3 with the acyltransferases PDAT, DGAT1 and DGAT2. Expression of fluorescence-tagged variants of PDAT and DGAT1 resulted in the production of TAG in the *S. cerevisiae* acyltransferase quadruple mutant H1246 deficient in TAG production, respectively, indicating functionality of the fluorescent fusions. Localization analyses in Arabidopsis mesophyll protoplasts revealed an ER-association of fluorescence-tagged PDAT and DGAT1. Bimolecular fluorescence complementation

analyses verified the observed interactions of FAD2 with FAD3 and PDAT. Reconstituted EYFP-fluorescence was seen in a network-like structure resembling the ER, suggesting the ER membrane to be the site of interaction. Overall, the data suggest different roles for FAD2 and FAD3 depending on the cell type and/or metabolic state. The different roles of FAD2 and FAD3 may be reflected in the subcellular localization patterns. The distinct Golgi-association of EYFP-FAD2 and EYFP-FAD3 is consistent with a role of FAD2 and FAD3 in controlling global membrane homeostasis and subcellular lipid distribution through action of the secretory pathway in vegetative tissues. The increased fluorescence intensity of mCherry-FAD3 upon coexpression with WR11 together with the observed interactions of FADs with acyltransferases at the ER highlight a direct role of FAD2 and FAD3 in oil biogenesis, for which a relocalization of FAD2 to the ER membrane is conceivable.

Zusammenfassung

Ungesättigte Fettsäuren beeinflussen die physiologische Funktion von Membranen und sind eingebaut in Triacylglycerin (TAG) ein Hauptbestandteil des Speicheröls von Samen. Die Fettsäure-desaturasen FAD2 und FAD3 wandeln Ölsäure (18:1^{Δ9}) sequenziell zu Linolsäure (18:2^{Δ9,12}) bzw. Linolensäure (18:3^{Δ9,12,15}) um. Es wird angenommen, dass FAD2 und FAD3 im endoplasmatischen Retikulum (ER) angesiedelt sind, wo sie Phospholipid-assoziierte Fettsäuren modifizieren. Die Acyltransferasen DGAT1, DGAT2 und PDAT befinden sich vermutlich ebenfalls im ER, wo sie TAG produzieren, indem sie Fettsäuren auf Diacylglycerin (DAG) übertragen. DGAT1 und DGAT2 verwenden CoA-gebundene Fettsäuren als Acyldonor, während PDAT Phosphoglycerolipide als Acyldonor verwendet. Bisherige Forschungen deuten darauf hin, dass neben dem metabolischen Kontext und der Interaktion und Kooperation der Enzyme, die an der Fettsäure-desaturierung und dem TAG-Aufbau beteiligt sind, offenbar auch die subzelluläre Lokalisierung eine Rolle bei der TAG-Produktion spielt. In dieser Arbeit wurden Fusionsvarianten von FAD2 und FAD3 mit N-terminalen Fluoreszenz-Markierungen erzeugt, die bei der Expression in Hefe (*Saccharomyces cerevisiae*) erfolgreich Ölsäure bzw. Linolsäure umsetzten. Darüber hinaus komplementierte die ektopische Expression von EYFP-FAD2 oder EYFP-FAD3 die makroskopischen und biochemischen Phänotypen der Arabidopsis *fad2-1* bzw. *fad3-2* Mutanten, was die Funktionalität der fluoreszierenden Fusionsproteine bestätigte. In den erzeugten Pflanzenlinien markierten EYFP-FAD2 oder EYFP-FAD3 ER-assoziierte Donut-förmige Strukturen. Die Koexpression in Arabidopsis Mesophyllprotoplasten mit verschiedenen Organellmarkern brachte diese Strukturen mit Golgi-Partikeln in Verbindung. Quantitative Auswertungen der Kolo-kalisationen bestätigten die Golgi-Assoziation von EYFP-FAD2, und Vergleiche mit anderen Organellmarkern zeigten, dass die beobachtete Kolo-kalisation kein Produkt einer zufälligen Verteilung im Zytosol war. Im Gegensatz zur punktuellen Verteilung von EYFP-FAD3 in komplementierten Pflanzen waren die fluoreszenzmarkierten FAD3-Varianten in Arabidopsis Mesophyllprotoplasten mit dem ER-Netzwerk assoziiert. Die Expression von FAD3 unter der Kontrolle seines endogenen Promotors wurde durch Koexpression mit dem Transkriptionsfaktor für die Lipidbiosynthese WRINKLED1 (WRI1) verstärkt, was auf eine wichtige Rolle von FAD3 in ölbildenden Geweben hinweist. Interaktionsanalysen mit dem *split-ubiquitin*-basierten Hefe-Zwei-Hybrid-System zeigten neue Interaktionen der Fettsäure-desaturasen FAD2 und FAD3 mit den Acyltransferasen PDAT, DGAT1 und DGAT2. Die Expression von fluoreszenzmarkierten Varianten von PDAT und DGAT1 führte zur Produktion von TAG in der Acyltransferase-Vierfachmutante *S. cerevisiae*

H1246, die nicht in der Lage ist TAG herzustellen, was auf die Funktionalität der fluoreszierenden Fusionen hinweist. Lokalisierungsanalysen in Arabidopsis Mesophyllprotoplasten zeigten eine ER-Assoziation von fluoreszenzmarkierten PDAT- und DGAT1-Varianten. Bimolekulare Fluoreszenzkomplementationsanalysen verifizierten die beobachteten Interaktionen von FAD2 mit FAD3 und PDAT. Die rekonstituierte EYFP-Fluoreszenz bildete eine netzwerkartige Struktur, die dem Erscheinungsbild des ER in Protoplasten ähnelte. Dies lässt darauf schließen, dass die ER-Membran der Ort der Interaktion ist. Insgesamt deuten die Daten darauf hin, dass FAD2 und FAD3 je nach Zelltyp und/oder Stoffwechszustand unterschiedliche Rollen spielen. Diese unterschiedlichen Rollen spiegeln sich in unterschiedlichen subzellulären Lokalisierungsmustern wider. Die ausgeprägte Golgi-Assoziation von EYFP-FAD2 und EYFP-FAD3 steht im Einklang mit einer Rolle von FAD2 und FAD3 bei der Kontrolle der globalen Membranhomöostase und der subzellulären Lipidverteilung durch Sekretion im vegetativen Gewebe. Die erhöhte Fluoreszenzintensität von mCherry-FAD3 bei Koexpression mit WRI1 und die beobachteten Interaktionen der FADs mit Acyltransferasen am ER weisen zusammen auf eine direkte Rolle von FAD2 und FAD3 bei der Ölbiogenese hin, für die eine verstärkte Lokalisierung von FAD2 an der ER-Membran denkbar ist.

1. Introduction

Membranes play important roles in the physiology of all eukaryotes. The cytosol and cell organelles are surrounded by membranes, allowing the formation of physiologically distinct specialized compartments. The biological challenge for a membrane is to form a selective barrier, that restricts chemical reactions on one side, while allowing for the selective exchange of substances and the perception of signals across the divide. In plants, biomembranes consist mostly of a bilayer of amphiphilic lipids, including glycerolipids, sphingolipids and sterols. To form a membrane bilayer, the hydrophobic lipid moieties associate, excluding any water. The hydrophilic lipid headgroups orient towards the aqueous surroundings, resulting in a semi-stable fluidic membrane bilayer (Berg et al., 2013). The distinct lipid composition of a membrane bilayer may vary between different types of membranes or organelles and can have substantial influence on the function of the respective membrane. Therefore, to understand the biological function of membranes, it is important to consider the lipid composition of individual membranes. Lipids are a structurally and functionally diverse group of hydrophobic molecules. Besides serving as the building blocks for cellular membranes, lipids also have other important functions in plant cells. Neutral lipids such as triacylglycerol, are used as energy and carbon storage. Wax esters are secreted from cells and form a water-repellent physical barrier within and on top of the extracellular cell wall matrix surrounding each plant cell (Ohlrogge and Browse, 1995). Many hydrophobic components in the plant derive from fatty acids, including glycerolipid classes, triacylglycerol, surface waxes and others. Linolenic acid for example is the precursor for the phytohormone jasmonic acid, which is an important regulator of plant development and stress responses (Wasternack and Feussner, 2018; Delker et al., 2006).

The roles of lipids and fatty acids in plant cells are diverse. Fatty acids found in *Arabidopsis thaliana* (*Arabidopsis*, *A. thaliana*) differ mainly in their chain length and their degree of unsaturation. Historically, the initial studies on plant fatty acid desaturation have been motivated largely by an interest in understanding seed oil modification and were focused on the biochemical or physiological analysis of lipid (oil)-associated fatty acid patterns. Successes and failures of using the key enzymes of fatty acids biosynthesis and modification for the metabolic engineering of oilseeds revealed that the spatial distribution and functional cooperation is an important factor for the efficient interplay of the relevant enzymes (Lou et al., 2014; Dyer and Mullen, 2008). As information on the subcellular localization and interactions of key enzymes of plant fatty acid metabolism are still rather scarce, research in this thesis focuses on elucidating the subcellular localization and interplay of several key enzymes involved in fatty acid desaturation and lipid assembly.

1.1 Structure and function of glycerolipids in plants

Lipids are an important group of organic molecules, which constitute the structural basis of all cells, together with carbohydrates, proteins, and nucleic acids. Lipids are molecules insoluble in water, that are solely defined by their hydrophobic nature, and therefore represent a variety of structurally unrelated molecules (Ohlrogge and Browse, 1995). This thesis focuses on fatty acids and their association with glycerolipids, which play important roles in energy storage and membrane formation. Glycerolipids are based on a glycerol backbone that can incorporate up to three fatty acids via ester bonds. The carbon atoms at the glycerol backbone are numbered according to stereospecific aspects (stereospecific number: *sn*-1, *sn*-2 and *sn*-3). The most relevant glycerolipids in plants are the storage lipid triacylglycerol (TAG), the phospholipids phosphatidylcholine (PC), phosphatidylethanolamine (PE), phosphatidylserine (PS), phosphatidylglycerol (PG), phosphatidylinositol (PI) and phosphatidic acid (PA) and the galactolipids monogalactosyldiacylglycerol (MGDG) and digalactosyldiacylglycerol (DGDG), whose structures are depicted in Figure 1.1. In the storage lipid TAG, three fatty acid moieties are bound to the glycerol backbone (Figure 1.1A). In amphiphilic membrane forming lipids, two of the three positions hold acyl moieties. At the *sn*-3 position, different hydrophilic headgroups can be found (Ohlrogge and Browse, 1995). Figure 1.1B shows the general structure of amphiphilic, membrane forming glycerolipids. Figure 1.1C illustrates various headgroups found in eukaryotic phospholipids. This group of membrane lipids is characterized by the binding of a phosphate group to the glycerol backbone. The simplest phospholipid is phosphatidic acid with only the phosphate group at the *sn*-3 position. Other headgroups can be bound to the phosphate by ester bonds creating PC, PE, PS, PG and PI. PC and PE are the most abundant extraplastidial membrane lipids followed by PG and PS (Li-Beisson et al., 2010). PI and its phosphorylated derivatives are only found in minor amounts and function as signaling lipids (Heilmann, 2016). In chloroplasts, the thylakoid membranes are formed mostly from galactolipids (Li-Beisson et al., 2010). In these lipids, galactosyl residues are bound to the *sn*-3-position of the glycerol backbone instead of phosphoester-bound headgroups found in phospholipids. The structures of the most abundant galactolipids MGDG and DGDG with either one or two bound galactosyl moieties are shown in Figure 1.1D.

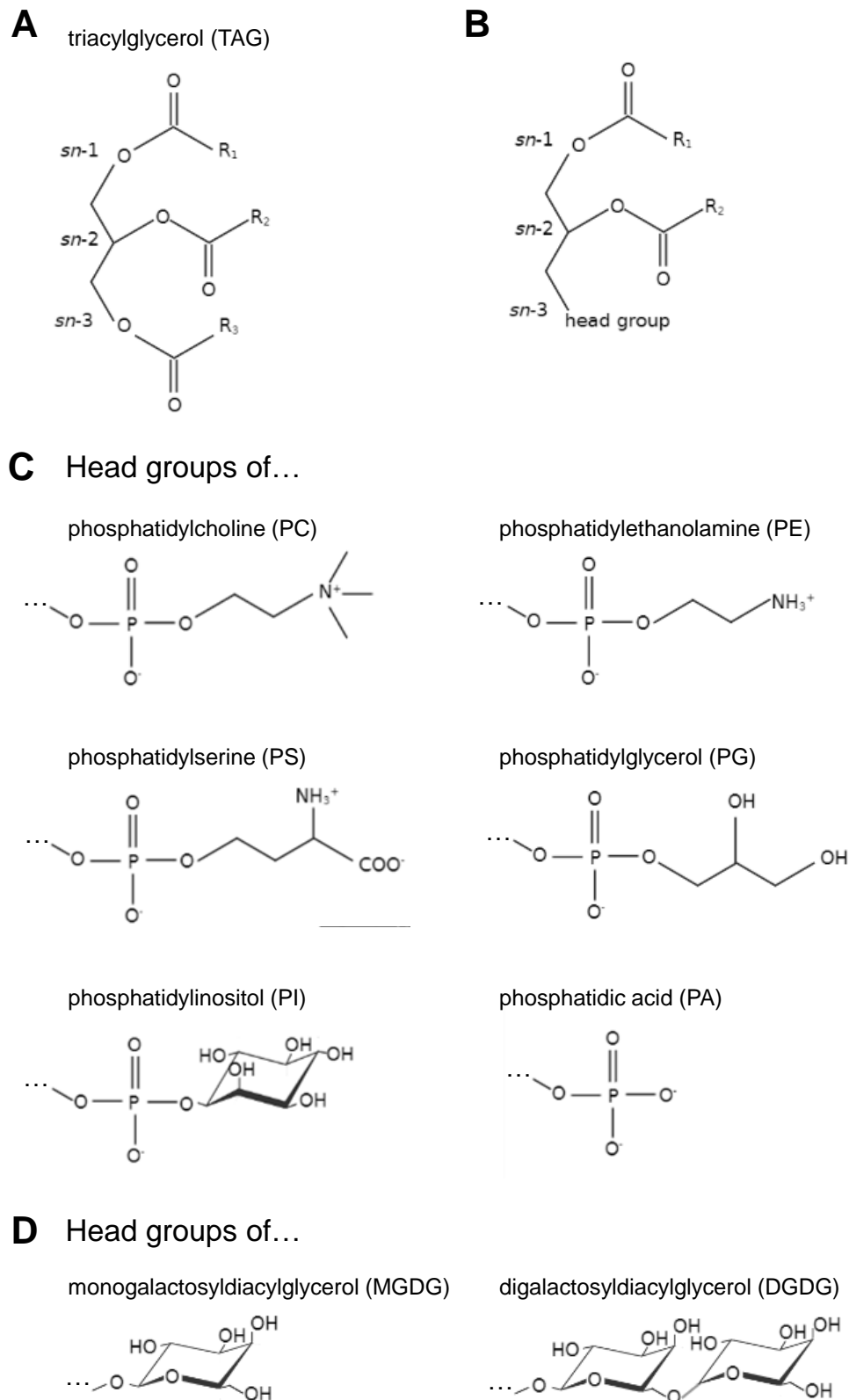


Figure 1.1. Structures of different lipid classes. **A**, Structure of triacylglycerol (TAG). Acyl groups (R_x) are esterified to all three hydroxy groups of the glycerol backbone. **B**, General structure of an amphiphilic membrane glycerolipid. The *sn*-1- and *sn*-2 positions are occupied with acyl groups. At the *sn*-3 position different head groups can be bound. Diacylglycerol possesses a hydroxy group at the *sn*-3 position. **C**, Structures of the headgroups of phospholipids. **D**, Structures of the most common glycolipids in plastids. This image was created with BioRender.com.

The hydrophilic head groups as well as the fatty acid residues influence membrane properties and a variety of membrane bound processes. For instance, the different head groups can affect the shape and curvature of membranes (Cooke and Deserno, 2006). A more specific effect of lipid head groups can be observed when analyzing the role of signaling lipids, that are found in lower amounts in membranes. For instance, the head groups of PI and its phosphorylated derivatives can be recognized by proteins, which are thus recruited to specific membrane regions (Heilmann, 2016). It has been found that PI derivatives accumulate in certain membrane regions, so-called membrane nanodomains. The local lipid composition can thus define membrane areas for specific membrane-localized processes (Heilmann, 2016; Furt et al., 2010). Membrane lipids can not only influence curvature but also the fluidity of a membrane and thus the lateral diffusive mobility of lipids and membrane-embedded or associated proteins (Heilmann, 2016; Mukherjee et al., 1999). In this regard, the degree of unsaturation of the lipid-associated fatty acids is most relevant. The most abundant naturally occurring fatty acids are aliphatic monocarboxylic acids with even numbers of carbon atoms with 16 or 18 carbon atoms in length. Unsaturated fatty acids contain one or more double bonds in contrast to saturated fatty acids, which contain no double bonds. The position of the double bonds can be annotated in two different ways. Using a delta (Δ) followed by a number gives the position of the double bond counting from the carboxylic end. When giving the position of the double bond in relation to the methyl end of the fatty acid, an omega (ω) is used. The monounsaturated fatty acid linoleic acid for example contains two double bonds at positions $\Delta 9$ and $\Delta 12$, respectively, and can be abbreviated as $18:2^{\Delta 9,12}$, where $x:y^{\Delta z}$ is a fatty acid containing x carbons and y double bonds in position z counting from the carboxyl end. $18:2^{\Delta 9,12}$ is an example for a $\omega 6$ fatty acid. The number of double bonds changes the melting point of the fatty acid. Acyl chains with a higher degree of unsaturation have a lower melting point (Berg et al., 2013; Guschina and Harwood, 2006). Therefore, the membrane fatty acid composition influences the membrane fluidity especially under changing temperatures. The remodeling of the membrane composition is thus a mean to cope with temperature changes and other (abiotic) stresses (He and Ding, 2020; Guschina and Harwood, 2006; Miquel et al., 1993; Falcone et al., 2004; Zhang et al., 2012).

Neutral lipids such as TAG do not form membranes and are found in large amounts in the seeds of oilseeds where they serve as energy and carbon storage for the seedling development. The composition of the storage oil highly depends on the plant species but is also adjusted depending on the environmental conditions (Menard et al., 2017; Baud, 2018). TAG also accumulates in non-oil-storing tissues for example in senescent leaves (Li-Beisson et al., 2010; Kaup et al., 2002). In vegetative tissues only a minor amount of

3, The fatty acid synthase multi-protein complex synthesizes fatty acids in cyclic reactions starting with acetyl-CoA and malonyl-ACP. Fatty acids with a chain length of 16 carbon atoms are released and elongated to 18:0. 4, The soluble Δ^9 stearoyl-ACP desaturase (SAD) introduces the first double bond into 18:0-ACP. 5, Two acyl moieties are transferred to glycerol-3-phosphate (G3P) by glycerol-3-phosphate acyltransferase (GPAT) and lyso-phosphatidic acid acyltransferase (LPAAT). The plastidial LPAAT prefers acyl moieties with 16 carbon atoms. 6, Phosphatidic acid (PA) is dephosphorylated to diacylglycerol (DAG) by phosphatidic acid phosphatase (PAP). 7, UDP-galactose is transferred to DAG by MGDG transferase creating MGDG. 8, The DGDG synthase transfers a second galactosyl-moiety to MGDG thereby creating DGDG. 9, Plastidial fatty acid desaturases modify fatty acids bound to MGDG and DGDG (and PG). 10, Fatty acids can be exported to the cytosol where they are incorporated into the acyl-CoA-pool. 11, Acyl-moieties can be transferred to G3P by GPAT and LPAAT at the ER to form PA. The ER localized LPAAT prefers acyl chains with a length of 18 carbon atoms. 12, PA can be dephosphorylated by PAP forming DAG. 13, DAG can be converted to CDP-DAG, which is the precursor for phosphatidylglycerol (PG), phosphatidylserine (PS) and phosphatidylinositol (PI). 14, The most abundant extraplastidial membrane lipids phosphatidylcholine (PC) and phosphatidylethanolamine (PE) are synthesized directly from DAG. 15, The Δ^{12} -desaturase FAD2 introduces a double bond into PC-bound 18:1 Δ^9 thereby creating 18:2 $\Delta^{9,12}$. 16, 18:2 $\Delta^{9,12}$ can be further desaturated to 18:3 $\Delta^{9,12,15}$ by FAD3. 17, Through actions of acyltransferases (e.g. LPCAT) acyl chains can be exchanged between the PC-pool and the acyl-CoA-pool with intermediate generation of lyso-PC (LPC). This cycle is called acyl-editing. 18, DGATs transfer acyl chains from the acyl-CoA-pool onto DAG to create triacylglycerols (TAG). TAGs accumulate between the lipid bilayer of the ER membrane before budding to form lipid droplets. 19, Alternatively to the action of DGATs, PDATs use acyl-chains derived from the PC-pool to form TAG from DAG. This also creates LPC, which can be re-acylated by LPCATs in the acyl-editing cycle. Reviewed by Li-Beisson et al. (2010). This image was created with BioRender.com.

1.2.1 Fatty acid synthesis in the plastid

The *de novo* synthesis of fatty acids in plants takes place in the plastid, in contrast to other eukaryotes, where the fatty acid synthesis machinery is located in the cytosol (Ohlrogge and Browse, 1995). In a first reaction step, malonyl-CoA is formed from acetyl-CoA and CO₂. This reaction is catalyzed by the acetyl-CoA carboxylase (ACC), requires biotin as coenzyme and is adenosine triphosphate (ATP) dependent (Ohlrogge and Browse, 1995; Li-Beisson et al., 2010). In the next step, the malonyl-group is transferred from coenzyme A (CoA) to an acyl carrier protein (ACP) by malonyl-CoA:ACP malonyltransferase. The synthesis of fatty acids is performed by the fatty acid synthase complex (FAS) in a cyclic sequence of four reactions. Starting with an acetyl moiety, the FAS elongates the carbon chain by two carbon atoms from malonyl-ACP in each elongation cycle thereby releasing CO₂. The following three reactions consist of a reduction, a dehydration and another reduction step before a new elongation cycle starts (Ohlrogge and Browse, 1995; Li-Beisson et al., 2010). When the acyl chain reaches 16 or 18 carbon atoms, the fatty acid is released from the FAS complex. 18:0-ACP is efficiently desaturated to 18:1 Δ^9 -ACP by the soluble Δ^9 stearoyl-ACP desaturase (SAD) (Li-Beisson et al., 2010). *De novo* produced palmitic acid (16:0), stearic acid (18:0) or oleic acid (18:1 Δ^9) are available for lipid synthesis in plants. Lipid assembly can either take place in the plastid (prokaryotic pathway) or the fatty acids are exported, and the lipid assembly occurs at the ER (eukaryotic pathway) (Ohlrogge and Browse, 1995). To enter the eukaryotic pathway, acyl moieties are hydrolyzed by acyl-ACP thioesterases, exported from the plastid, and

reactivated by binding to CoA through long-chain acyl-CoA synthetase (LACS) at the outer chloroplast envelope (Li-Beisson et al., 2010; Bates et al., 2013; Koo et al., 2004).

1.2.2 Lipid assembly in the chloroplast: the prokaryotic pathway

The plastidial thylakoid membranes consist mainly of the galactolipids MGDG and DGDG and under standard conditions neither of these lipids are found outside the plastid (Li-Beisson et al., 2010). MGDG and DGDG are synthesized at the envelope membranes of the chloroplasts. In the initial biosynthetic reactions 18:1^{A9} and 16:0 are transferred from ACP to the *sn*-1 and *sn*-2 positions of glycerol-3-phosphate (G3P) by glycerol-3-phosphate acyltransferase (GPAT) and lysophosphatidic acid (LPA) acyltransferase (LPAAT), respectively, resulting in the production of PA (Li-Beisson et al., 2010; Kunst et al., 1988). PA can be activated by the transfer of cytidine diphosphate (CDP) from cytidine triphosphate (CTP) catalyzed by the CDP-DAG synthase. The resulting CDP-DAG is transformed to PG by reacting with G3P, catalyzed by phosphatidylglycerol phosphate (PGP) synthase. PGP is then dephosphorylated by PGP phosphatase to form PG (Li-Beisson et al., 2010; Andrews and Mudd, 1985). Alternatively, the phosphate group of PA can be hydrolyzed by PA phosphatase, creating diacylglycerol (DAG), the precursor for the plastid specific glycolipids MGDG and DGDG (Ohlrogge and Browse, 1995). To form these membrane lipids, galactosyl moieties are subsequently transferred from uridine diphosphate (UDP) activated galactose (UDP-galactose) to DAG by the MGDG transferase and to MGDG by the DGDG synthase (Ohlrogge and Browse, 1995; Li-Beisson et al., 2010; Kelly and Dörmann, 2002). Besides the plastid-derived DAG from the prokaryotic pathway, ER-originated DAG from the eukaryotic pathway can also be used for glycolipid synthesis. The transfer mechanism for DAG from the ER into the plastid is still unknown (Li-Beisson et al., 2010; He et al., 2020). Due to the distinct fatty acid specificity of the acyltransferases (LPAAT) transferring the acyl moieties to the *sn*-2 position of LPA in the plastid and at the ER, the origin of the DAG-precursor for galactolipid formation can be distinguished. The ER-localized LPAAT specifically transfers fatty acids with 18 carbon atoms, while the plastid-localized LPAAT prefers acyl groups with 16 carbon atoms. *A. thaliana* belongs to the so called 16:3-plants, referring to the presence of 16:3^{A7,10,13} at the *sn*-2 position of galactolipids through usage of the prokaryotic pathway for DAG-synthesis (Ohlrogge and Browse, 1995; Li-Beisson et al., 2010).

1.2.3 Lipid assembly and fatty acid modification at the ER: the eukaryotic pathway

The biosynthesis of fatty acid and lipid assembly in plastids (the prokaryotic pathway) is not the only route of lipid biogenesis in plants, and an additional pathway for extraplasmidial lipid biogenesis exists, the "eukaryotic pathway" located at the ER. The first two steps in the assembly of membrane lipids at the ER follow the same principle as in the plastid, except that the responsible acyltransferases use CoA-bound fatty acids. Acyl moieties from CoA are transferred to the *sn*-1 and *sn*-2 positions of G3P by the enzymes GPAT and LPAAT, resulting in the production of PA (Li-Beisson et al., 2010). PA can be converted to CDP-DAG by a CDP-DAG synthase at the ER, similar to reactions in the plastid. As in the plastid, CDP-DAG serves as a precursor for the production of PG by the addition of G3P by PGP synthase followed by PGP phosphatase-mediated dephosphorylation. CDP-DAG is also the precursor for the formation of PI by PI synthase (Li-Beisson et al., 2010).

The production of the most abundant membrane lipids outside the plastids, PC and PE, occurs by head group activation. The dephosphorylation of PA results in the formation of DAG, which can be combined with CDP-choline or CDP-ethanolamine. Aminoalcoholphosphotransferases are responsible for these reactions and exhibit a dual role for the transfer of choline or ethanolamine headgroups to DAG (Li-Beisson et al., 2010).

Through actions of lyso-PC:acyl-CoA acyltransferases (LPCAT), fatty acids can be exchanged between the PC-pool and the acyl-CoA-pool, the latter providing fatty acid substrates for the *de novo* lipid synthesis catalyzed by GPAT and LPAAT (Stymne and Stobart, 1984; Bates et al., 2013; Bates et al., 2012). This exchange of acyl-groups is termed acyl-editing and does not result in net production or degradation of lipids. The deacetylation of PC leads to the production of lyso-PC and released fatty acids. Lyso-PC is then re-acylated with fatty acids from the acyl-CoA pool. The flux from newly synthesized fatty acids into PC via the acyl-editing cycle is faster than the *de novo* synthesis of lipids catalyzed by GPAT or LPAAT (Li-Beisson et al., 2010; Bates et al., 2007).

Importantly, the phospholipid-bound fatty acids at the ER are subject to further modification. Fatty acid desaturases (FADs) can introduce double bonds into the acyl chains and thereby exert a profound influence on the biophysical properties on fatty acids present in membrane lipids. The closely related fatty acid hydroxylases and epoxygenases occurring in some plant species share reaction mechanism and topology with fatty acid desaturases (Shanklin and Cahoon, 1998; Shanklin et al., 2009; Cahoon and Li-Beisson, 2020), but instead of a double bond, those enzymes can introduce hydroxy groups and epoxy groups, respectively. Hydrogenated and epoxygenated fatty acids are uncommon

fatty acids, that are often found channeled away from membranes into storage oil (Cahoon and Li-Beisson, 2020) and are also important components in hydrophobic lipid polyesters found, e.g., in cutin (Cahoon and Li-Beisson, 2020).

1.2.4 Fatty acid desaturation by membrane-bound FADs

In *Arabidopsis*, seven different membrane bound fatty acid desaturases are described. Five of them, FAD4, FAD5, FAD6, FAD7 and FAD8, contain plastidial targeting signals, are all localized in the plastid and act on fatty acids bound to MGDG, DGDG or PG formed by the prokaryotic pathway (Dar et al., 2017; Li-Beisson et al., 2010; Shanklin and Cahoon, 1998). Two desaturases, FAD2 and FAD3, use the membrane lipid PC as substrate and are proposed to act in the eukaryotic pathway at the ER membrane (Li-Beisson et al., 2010; Sperling et al., 1993; Browse et al., 1993; Okuley et al., 1994; McCartney et al., 2004). As mentioned above, membrane-bound FADs are thought to share a membrane topology and active site architecture with hydroxylases and epoxygenases (Shanklin and Cahoon, 1998; Shanklin et al., 2009). The enzymes are anchored in the membrane with at least four membrane-spanning transmembrane domains. The active site consists of three histidine-rich motifs called histidine boxes that coordinate two iron ions necessary for catalytic activity (Shanklin et al., 1994; Shanklin et al., 2009; Shanklin and Cahoon, 1998). The histidine boxes contain a total of eight conserved histidines. In some desaturases the first histidine of the third box is exchanged to a glutamine, resulting in the general description of the motif as H X₍₃₋₄₎ H X₍₇₋₄₁₎ H X₍₂₋₃₎ HH X₍₆₁₋₁₈₉₎ (H/Q) X₍₂₋₃₎ HH (Shanklin and Cahoon, 1998). Experiments using site-directed mutagenesis revealed that all eight histidines are essential for catalytic activity (Shanklin et al., 1994). This motif is conserved in integral membrane desaturases and related enzymes and exhibits equivalent spacing relative to the membrane spanning domains (Shanklin and Cahoon, 1998; Shanklin et al., 1994). The catalytic site as well as both termini are located at the cytosolic face of the ER membrane or for plastidial enzymes are accordingly oriented towards the plastid stroma (Dyer and Mullen, 2001; Dyer et al., 2002). A generic topology model is shown in Figure 1.3.

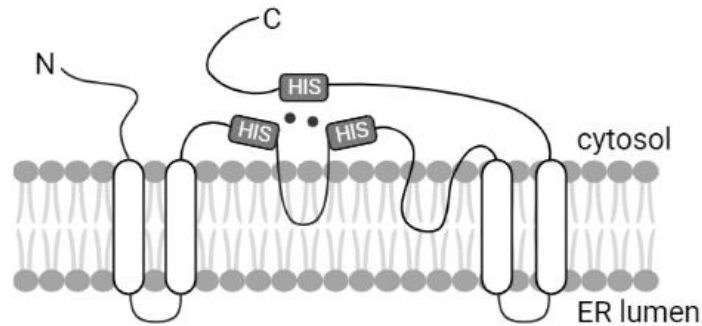


Figure 1.3. Topology model of integral membrane desaturases. Membrane bound desaturases, hydroxylases and epoxygenases share a common topology. At least four transmembrane domains anchor the protein in the membrane with the termini and the catalytic site facing the cytosol or the plastidial stroma. The catalytic site consists of three histidine-rich motifs (HIS) that coordinate two iron ions (black circles). The model was designed according to Dyer et al. (2002). This image was created with BioRender.com.

The desaturation of fatty acids is a redox reaction that requires oxygen and two electrons. The electron transport chain differs between plastidial and ER-localized desaturases, as these compartments contain different electron donors for the respective desaturases (ferredoxin in the plastid, cytochrome b_5 at the ER). In the plastid, the electrons are provided by nicotinamide adenine dinucleotide phosphate (NADPH) and transferred to ferredoxin by ferredoxin-NADP⁺ oxidoreductase. In illuminated photosynthetic tissues, ferredoxin receives electrons directly from photosystem I. By contrast, at the ER the electrons are transferred from nicotinamide adenine dinucleotide (NADH) to cytochrome b_5 by cytochrome b_5 reductase (Shanklin and Cahoon, 1998).

The substrate specificity of desaturases depends on a variety of factors. The lipid head group and the acyl chain length or the existence of previous double bonds all contribute to the enzyme-substrate interactions. For instance, double bonds can be introduced relative to the carboxyl group, the methyl end of the acyl chain or to an already existing double bond. FADs categorized as ΔX -desaturases use the carboxy group as reference for the introduction of the double bond, whereas FADs that use the methyl end of the acyl chain are specified as ωX -desaturases.

1.3 Seed oil biogenesis and oil body formation

TAGs are a major component of most seed oils. They are used as energy storage and carbon source during germination (Baud, 2018). Besides in seeds, TAG can also accumulate in other tissues, for example senescing leaves (Li-Beisson et al., 2010; Kaup et al., 2002). Transient TAG pools also exist in vegetative tissues, probably as reservoir for fatty acids to allow fast membrane remodeling under changing environmental conditions (He and Ding, 2020; Tan et al., 2018). The assembly of TAG takes place at the

ER. Arabidopsis seeds contain 30 % of linoleic acid (18:2^{Δ9,12}) and 20 % of α-linolenic acid (18:3^{Δ9,12,15}) (Li-Beisson et al., 2010; Li et al., 2006). These polyunsaturated fatty acids require the activity of the fatty acid desaturases FAD2 and FAD3 for their synthesis and further enzymes routing the fatty acids away from the ER membrane into the seed oil (Lemieux et al., 1990; Bates et al., 2013).

1.3.1 Synthesis of seed oils

The *de novo* synthesis of TAG occurs via the so-called Kennedy pathway and shares the first several steps of membrane lipid synthesis in the eukaryotic pathway, where two acyl-groups are transferred from acyl-CoA to the *sn*-1 and *sn*-2 positions of G3P by GPAT and LPAAT, respectively (Li-Beisson et al., 2010; Bates et al., 2013). The resulting PA is dephosphorylated to DAG by PA phosphatase, and TAG is formed by transferring a third acyl group to the free *sn*-3 position of DAG (Zou et al., 1999). This third acyl chain can derive from different substrate pools. Diacylglycerol:acyl-CoA acyltransferases (DGATs) use CoA-bound fatty acids as acyl-donor. A different class of acyltransferases uses fatty acids from PC. These enzymes are called phosphatidylcholine:diacylglycerol acyltransferases (PDATs) (Dahlqvist et al., 2000; Bates et al., 2013). The transfer of the fatty acid from the *sn*-2 position of PC to DAG by PDAT leads to the formation of lyso-PC as a byproduct (Ståhl et al., 2004). The lyso-PC destabilizes membrane bilayers and is thus toxic, and it can be re-acylated by the action of the enzymes of the acyl-editing cycle (Stymne and Stobart, 1984; Xu et al., 2012).

The efficient accumulation of TAG at the ER relies on the supply of fatty acids from the plastid. The rate of fatty acid synthesis therefore substantially influences the amount of TAG that can be formed (Chapman and Ohlrogge, 2012). The abundance of key enzymes of lipid and TAG biosynthesis is coordinated at the transcriptional level by the transcription factor WRINKLED1 (WRI1), which has been described as a “master regulator” of fatty acid synthesis (Chapman and Ohlrogge, 2012). The Arabidopsis mutant *wri1* has reduced levels of the WRI1 protein and displays drastically reduced amounts of seed oil (up to a reduction of 80 %) (Focks and Benning, 1998). Reciprocally, overexpression of *WRI1* can increase the TAG content in both seeds and even in leaves (Chapman and Ohlrogge, 2012; Vanhercke et al., 2018; Xu and Shanklin, 2016). In line with its effect on the TAG amount, *WRI1* is mostly expressed in siliques during seed maturation (Baud et al., 2007). The WRI1-mediated increase of TAG results mainly from an increased flux of carbohydrates into the fatty acid synthesis to provide the necessary acyl chains and glycerol backbones (To et al., 2012). Some of the known target genes of WRI1 encode proteins acting at the interface between carbohydrate metabolism and fatty acid *de novo*

synthesis, for example for a subunit of the pyruvate dehydrogenase complex, that generates acetyl-CoA, or for a subunit of the ACC, which catalyzes the carboxylation of acetyl-CoA to malonyl-CoA, initiating fatty acid biosynthesis (Baud et al., 2007). By contrast, enzymes involved in the desaturation or elongation of fatty acids and in lipid assembly seem to be not directly regulated by WRI1 in *Arabidopsis* (To et al., 2012; Baud et al., 2007).

1.3.2 Lipid droplets engulf accumulating TAG that would destabilize the bilayer

TAGs are synthesized at the ER membrane. As TAGs are not amphiphilic lipids, they accumulate in between the two leaflets of the ER membrane bilayer, thereby destabilizing it (Napier et al., 1996; Pyc et al., 2017). The integrity of the ER membrane in areas of TAG accumulation is maintained by the formation and release of oil bodies, which are also called lipid droplets (LDs). LD formation at the cytosolic face of TAG-accumulating ER areas involves the association of oil body-proteins, which stabilize the bulging membrane during TAG accumulation (Shao et al., 2019; Pyc et al., 2017). In addition, a number of other proteins transiently associates with LDs at different stages of LD formation (Shao et al., 2019; Ischebeck et al., 2020). Even though the exact mechanisms initiating the LD formation at the ER and catalyzing the release of the oil body are still unknown, some proteins are known to be involved in LD biogenesis and proliferation. As LDs derive from the cytosolic leaflet of the ER membrane, the TAG cargo is surrounded by a phospholipid monolayer. This monolayer is stabilized by embedded coat proteins. The major coat proteins for lipid droplets in seeds are oleosins (Napier et al., 1996). Oleosins have a hairpin-like structure with a proline-rich knot as a turning point (Huang and Huang, 2017). The hydrophobic hairpin is inserted through the phospholipid monolayer into the oil body. Both termini of the oleosin proteins face the oil body surface (Huang and Huang, 2017). Oleosins stabilize the lipid droplets, prevent LD-LD fusions and protect the engulfed TAG against uncontrolled degradation by lipases (Napier et al., 1996; Shao et al., 2019). In vegetative tissues, lipid-droplet associated proteins (LDAPs) are the most abundant coat proteins on LDs (Ischebeck et al., 2020; Horn et al., 2013; Gidda et al., 2016). While coat proteins are mainly necessary for the stabilization of oil bodies and the regulation of their degradation, other proteins have been found to be involved in the separation of LDs from the ER. Seipins for example localize to the ER-LD contact sites and their expression level has an influence on the size and number of oil bodies (Cai et al., 2015; Taurino et al., 2018). Seipins cooperate with LDAP-interacting protein (LDIP) and vesicle-associated

protein 27-1 (VAP27-1) in stabilizing ER-LD junctions and are thought to play a role in controlling the flux of TAG into nascent LDs (Greer et al., 2020; Pyc et al., 2021).

1.3.3 The role of PC in seed oil biogenesis

The phospholipid PC has a dominant role in plant cells as a major structural component of extraplastidial membranes. In addition, PC-associated fatty acids are the substrates for FAD2- and FAD3-mediated desaturation at the ER membrane. Furthermore, PC is also a key intermediate in the generation of TAG. PC-derived fatty acids can be transferred to TAG in two different ways: First, PC can be used directly as acyl-donor for PDAT-mediated TAG assembly. Second, acyl groups from PC can enter the acyl-CoA pool through the acyl-editing cycle and are then used as acyl-donors for DGAT-mediated TAG assembly (Bates et al., 2012; Bates et al., 2013). A third role is the generation of a PC-derived DAG pool. The phosphocholine headgroup can be exchanged between DAG and PC by a phosphatidylcholine:diacylglycerol cholinetransferase (PDCT) (Lu et al., 2009). Due to its substrate specificity, PDCT directs monounsaturated fatty acids (18:1^{Δ9}) back to the PC pool for desaturation, whereas the polyunsaturated fatty acids 18:2^{Δ9,12} and 18:3^{Δ9,12,15} associate with DAG in the TAG biosynthesis pathway (Lu et al., 2009). The desaturation of PC-bound fatty acids by FAD2 and FAD3 and the coordinated metabolic interplay of the PC-pool, DAG-pool and acyl-CoA-pool play an important role in determining plant membrane lipid organization and the seed oil composition (Bates et al., 2012; Bates et al., 2013).

1.4 Characterization of FAD2 and FAD3 from *A. thaliana*

As outlined above, PC is an important intermediate in seed oil biogenesis, and the desaturation of PC-bound fatty acids has a large influence on TAG composition. In *Arabidopsis*, the two fatty acid desaturases FAD2 and FAD3 are responsible for the desaturation of PC-bound fatty acids at the ER membrane (Sperling et al., 1993; Lemieux et al., 1990). By sequentially modifying 18:1^{Δ9} exported from the plastid, FAD2 and FAD3 produce 18:2^{Δ9,12} and 18:3^{Δ9,12,15}, respectively (Miquel and Browse, 1992; Okuley et al., 1994; Browse et al., 1993). FAD2 is a Δ12-desaturase that prefers PC-bound 18:1^{Δ9} but can also use fatty acids with an acyl chain of 16 carbon atoms as substrate (Kajiwara et al., 1996). The desaturation of 18:2^{Δ9,12} to 18:3^{Δ9,12,15} is catalyzed at the ER by the ω3-desaturase FAD3 (Browse et al., 1993; Yadav et al., 1993). FAD3, similar to FAD2, prefers PC-bound acyl chains with 18 carbon atoms.

While the focus of experiments in this thesis is on the extraplastidial enzymes FAD2 and FAD3, it shall be mentioned that conversion of 18:1^{Δ9} to 18:2^{Δ9,12} and further to 18:3^{Δ9,12,15}

can also occur in plastids by various plastidial fatty acid desaturases acting on fatty acids esterified to the plastidial membrane lipids MGDG, DGDG or PG (Dar et al., 2017; Li-Beisson et al., 2010; Shanklin and Cahoon, 1998). For instance, the conversion of 18:1^{Δ9} to 18:2^{Δ9,12} is catalyzed in the plastid by FAD6, which is an ω6-desaturase (Browse et al., 1989; Falcone et al., 1994) and also uses 16:1^{Δ7} as an acyl substrate for the production of 16:2^{Δ7,10} (Browse et al., 1989). Conversion of 18:2^{Δ9,12} to 18:3^{Δ9,12,15} in plastids is mediated by the isoenzymes FAD7 and FAD8, which can also desaturate 16:2^{Δ7,10} to 16:2^{Δ7,10,13} (Iba et al., 1993; McConn et al., 1994). In contrast to FAD2 and FAD3, the plastidial fatty acid desaturases mentioned all contain plastidial transit peptides.

Intensive metabolic studies and lipid analyses indicate that FAD2 and FAD3 desaturate fatty acids associated with PC, a lipid prominent in the ER membrane (Kajiwara et al., 1996; Sperling et al., 1993; Fouillen et al., 2018; Brown and Dupont, 1989). Both FAD2 and FAD3 are proposed to reside in the ER, and their sequences contain C-terminal ER retention motifs. The ER retention signal at the C-terminus of FAD3 consists of a well-characterized dilysine motif (-KXXXX: in the case of Arabidopsis FAD3: -KSKIN) (McCartney et al., 2004). FAD2 possesses a motif at its C-terminus enriched in aromatic amino acid, that was first described as an ER retrieval motif in this particular enzyme (McCartney et al., 2004). The FAD2-like ER retention motif can generally be described as Φ-X-X-K/R/D/E-Φ-COOH, where Φ stands for large hydrophobic amino acids. The addition of a single amino acid at the C-terminus after the ER retention motif abolished ER association of GFP-marker constructs and resulted in a localization of the marker at the plasma membrane (McCartney et al., 2004). McCartney and coworkers showed that the motifs at the C-termini of FAD2 and FAD3 were necessary and sufficient to target proteins to the ER (McCartney et al., 2004). They proposed that the motif of FAD2 functioned as a retrieval motif for escaped proteins to be transported back from the Golgi to the ER but noted that in the absence of high-resolution imaging data the dynamic localization of FAD2 to the ER and the Golgi needed further investigation (McCartney et al., 2004). A variety of localization analyses were performed using orthologous FAD2 or FAD3 enzymes from different plants. FAD2 from *A. thaliana* and tung tree (*Vernicia fordii*, Vf) as well as FAD3 from rapeseed (*Brassica napus*) localized to the ER when overexpressed in tobacco BY-2 cell culture and detected by immunostaining (Dyer and Mullen, 2001; Dyer et al., 2002). Evidence from live cell imaging supports the association of FAD2 to the ER in root epidermal cells of Arabidopsis (Nguyen et al., 2019). The molecular and biochemical interactions between FAD2 and FAD3 were analyzed by Lou and coworkers, demonstrating that FAD2 and FAD3 were able to both self-interact and interact with each other in yeast two-hybrid experiments (Lou et al., 2014). FAD2 and FAD3 are therefore

thought to form homo- or heterodimers. Furthermore, it was shown that FAD2 and FAD3 heterodimers can facilitate substrate channeling. This means, that to a certain extent 18:1^{Δ9} is directly converted to 18:3^{Δ9,12,15} by the FAD2/FAD3 complex without intermittent release of the 18:2^{Δ9,12} intermediate (Lou et al., 2014).

1.5 TAG assembly by DGATs and PDAT

The desaturation of fatty acids is an important aspect of plant seed oil biogenesis and well-studied. By contrast, information on the molecular details of the transfer of acyl groups into TAG is much less detailed. The last step in the formation of TAG is catalyzed by different classes of acyltransferases that can be distinguished according to their substrate preferences. The first group of enzymes is called diacylglycerol:acyl-CoA acyltransferase (DGAT) and these enzymes use acyl-CoA as an acyl donor. DGATs can be classified in three gene families (Xu et al., 2018). Enzymes belonging to the family of DGAT1 and DGAT2 are membrane bound (Zou et al., 1999; Zhou et al., 2013; Liu et al., 2012), whereas DGAT3 is a soluble acyltransferase and represents the least well investigated enzyme class (Hernández et al., 2012; Xu et al., 2018). Even though DGAT1 and DGAT2 catalyze the same reaction, the enzymes have little amino acid similarity, which is also reflected in prominent differences in their proposed membrane topology (Figure 1.4; Turchetto-Zolet et al., 2016; Shockey et al., 2006; Liu et al., 2012). Enzymes belonging to the family of DGAT1 have eight to ten transmembrane domains, while DGAT2 enzymes are significantly smaller and possess only two membrane spanning domains (Shockey et al., 2006; Liu et al., 2012). A topology model of DGAT1 and DGAT2 from *Vernicia fordii* is shown in Figure 1.4 (Shockey et al., 2006).

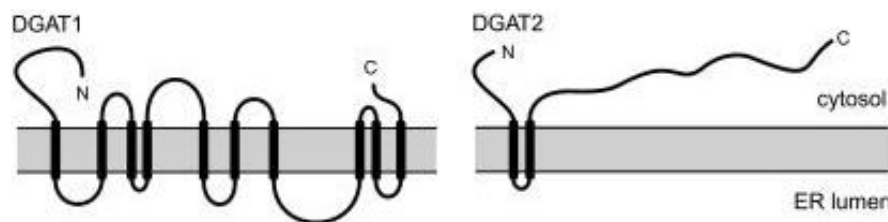


Figure 1.4. Proposed membrane topology of DGAT1 and DGAT2 from tung tree. Tung tree and Arabidopsis DGAT1 enzymes contain 10 putative transmembrane domains, DGAT2 from tung tree and Arabidopsis contain two putative transmembrane domains. The N- and C-terminus of VfDGAT1 and VfDGAT2 face the cytosol. Picture from Shockey et al. (2006).

Shockey and coworkers experimentally confirmed that the N- and C-termini of VfDGAT1 and VfDGAT2 face the cytosol (Shockey et al., 2006). The Arabidopsis DGAT1 and DGAT2 contain ten and two transmembrane domains, respectively (based on sequence analyses) (Liu et al., 2012; Shockey et al., 2006). Immunostaining experiments revealed

that *V*DGAT1 and *V*DGAT2 both localized to the ER in BY-2 cells, but to different ER areas that hardly overlapped (Shockey et al., 2006). ER retention motifs similar to that of FAD2 were identified at the C-termini of DGAT1 and DGAT2. However, in contrast to the motif found in FAD2, the ER retention signals in DGAT1 and DGAT2 are not located at the extreme C-termini. For the orthologous enzymes from tung tree it was experimentally shown that their ER retention motifs were sufficient for ER localization of *V*DGAT1 and *V*DGAT2, but not sufficient to mediate the localization to the distinct ER domains (Shockey et al., 2006).

Physiologically, Arabidopsis DGAT1 is a major determinant for oil accumulation in seeds. An Arabidopsis *tag1-1* mutant defective in *DGAT1* (also called *dgat1-1* or in older literature AS11) has a reduced oil content in seeds with only 60 % of the TAG amount compared to wild type seeds (Zou et al., 1999). The fatty acid composition of TAG in the *tag1-1* mutant is also changed, as shown by the reduced accumulation of the TAG marker fatty acid 20:1^{Δ11} and a concomitant increase in 18:3^{Δ9,12,15} (Katavic et al., 1995). The opposite effect was observed when *DGAT1* was overexpressed, resulting in increased TAG amounts in seeds and even in TAG accumulation in vegetative tissues not normally forming detectable amounts of TAG (Zhou et al., 2013). By contrast, a *dgat2-like* mutant defective in *DGAT2* does not show a seed oil phenotype (Zhang et al., 2009). Furthermore, a *dgat1-1 dgat2-like* double mutant defective in *DGAT1* and *DGAT2* did not show a more severe phenotype than the *dgat1-1* mutant alone (Zhang et al., 2009). First experiments with expression of *DGAT2* in yeast showed that DGAT2 was not able to complement the TAG deficiency in the yeast strain H1246 defective in intrinsic acyl transferase activity (Zhang et al., 2009). Later publications revealed that *DGAT2* optimized for the expression in yeast is able to produce TAG in yeast (Aymé et al., 2014). However, the contribution of DGAT2 to TAG production in Arabidopsis is still unclear and the physiological role of DGAT2 remains largely unknown. In other plant species, DGAT2 homologs are responsible for the incorporation of unusual fatty acids into TAG (tung tree, Xu et al., 2018; Li et al., 2010; Kroon et al., 2006; Burgal et al., 2008; Shockey et al., 2006). Likewise, it has been demonstrated that the Arabidopsis DGAT2 preferably incorporates polyunsaturated fatty acids into TAG, whereas DGAT1 shows no such preference (Zhou et al., 2013). The different localization patterns together with different substrate preferences indicate, that DGAT1 and DGAT2 may indeed not be functionally redundant and play different roles in the plant TAG biogenesis. While the most prominent role of DGAT1 lays in the seed oil biogenesis, emerging evidence suggests further physiological roles for DGAT1 and TAG in vegetative tissues. For example, it has been shown, that DGAT1-mediated TAG accumulation is essential for freezing tolerance in Arabidopsis, possibly by converting the

membrane destabilizing DAG produced during freezing to TAG (Tan et al., 2018).

Plants contain another group of acyltransferases that are not found in mammals (Chapman and Ohlrogge, 2012; Dahlqvist et al., 2000). Enzymes termed PDAT use acyl moieties from PC to form TAG instead of acyl-CoA (Dahlqvist et al., 2000; Ståhl et al., 2004). As a byproduct, lyso-PC is generated. Arabidopsis contains two close relatives of the yeast-*PDAT* homolog, but only PDAT1 (in this thesis from now on termed PDAT) accounts for the PDAT-activity in Arabidopsis (Xu et al., 2018; Ståhl et al., 2004; Zhang et al., 2009). Biochemical characterization revealed that PDAT prefers acyl moieties at the *sn*-2 positions of PC and PE (Ståhl et al., 2004). Furthermore, the enzyme activity was influenced by the transferred acyl chain with the highest activities for polyunsaturated fatty acids and fatty acids containing functional groups like epoxy or hydroxy groups (Ståhl et al., 2004). The high activity against unusual fatty acids may facilitate an effective shuttling of these fatty acids into TAG, where they often accumulate (van Erp et al., 2011; Kim et al., 2011; Xu et al., 2018; Bates et al., 2013), possibly as part of a mechanism to keep unusual fatty acids with particular physical properties away from membranes (Thelen and Ohlrogge, 2002; Drexler et al., 2003).

Structural analyses of PDAT sequences have only been performed *in silico* and suggest that PDAT has at least one putative transmembrane domain (Xu et al., 2018). By sequence comparison, McCartney and coworkers found an amino acid sequence at the C-terminus of PDAT resembling the described ER retention motif of FAD2, suggesting a localization at the ER (McCartney et al., 2004). The transient expression of fluorescence-tagged PDATs from castor bean (*Ricinus communis*, R_cPDAT) in tobacco leaves revealed a localization pattern resembling that of an ER marker supporting the hypothesis of PDAT localizing to the ER membrane (Kim et al., 2011). The membrane orientation of the termini remains currently unresolved.

Similar to observations on *dgat2-like* mutants, a knockout mutant for *PDAT* (*pdat1-1*) does not have an influence on the seed oil content in Arabidopsis (Mhaske et al., 2005). Interestingly, an RNAi (ribonucleic acid interference) knockdown of *PDAT* in the *dgat1-1* mutant background resulted in a further decrease of TAG in the seed by 63 % compared to the *dgat1-1* mutant alone and displayed defects in the seed and pollen development (Zhang et al., 2009). This indicates that in the *dgat1-1* mutant, PDAT might complement at least partially for the loss of DGAT1 during seed oil biogenesis. Nonetheless, PDAT may play a more important role in vegetative tissues than in seed oil biogenesis. The TAG decrease in developing leaves was more severe in the *PDAT* mutants than in the *dgat1-1* mutant (Fan et al., 2013b). The results from overexpression studies for both enzymes were also consistent with these findings: Overexpression of *PDAT* resulted in a sevenfold

increase of TAG in leaves, whereas upon overexpression of *DGAT1* only a minor increase was shown (Xu et al., 2018; Fan et al., 2013b). It has been shown that in vegetative tissues PDAT is involved in the control of membrane lipid homeostasis. Fatty acids for degradation by β -oxidation in the peroxisome are channeled through TAG in vegetative tissues (Xu et al., 2018; Fan et al., 2013b; Fan et al., 2013a; Fan et al., 2014; Fan et al., 2017). PDAT's physiological roles may thus be different in vegetative and in oil-forming tissues, namely channeling of membrane-bilayer disturbing modified fatty acid into TAG in oleogenic tissues (Ståhl et al., 2004; Kim et al., 2011; Xu et al., 2018) and regulating membrane homeostasis by directing fatty acids to transient storage in TAG and degradation in vegetative tissues (Xu et al., 2018).

1.6 Technical modification of oil biogenesis and its challenges

Plant lipids and fatty acids play an important role in human nutrition as well as in industrial applications. Increasingly, attention is given to the consumption of valuable and essential polyunsaturated fatty acids (ω 3- and ω 6-fatty acids) as part of the human diet. Besides the nutritional value, a variety of specific fatty acids can be used as precursors for industrial feedstocks and have the potential to replace limited fossil petroleum-based chemicals (Dyer et al., 2008; Dyer and Mullen, 2008). Energy dense storage lipids from plants are already in use for the production of biofuels as “green” alternative to petroleum-based fuels (Dyer et al., 2008). For an efficient use in the industry, high amounts of particular preferred fatty acids in a uniform lipid matrix are desired to facilitate downstream processing (Dyer and Mullen, 2008; Thelen and Ohlrogge, 2002). Oil crops like rapeseed and soybean or, as a model organism *Arabidopsis*, have been targets for metabolic engineering with the aims of increasing the amounts of oil or of altering seed oil composition (Dyer and Mullen, 2008; Cahoon et al., 1999; Broun and Somerville, 1997; van Erp et al., 2011; Kim et al., 2011; Chen et al., 2015). The ectopic expression of the transcription factor *WR11*, which controls fatty acid biosynthesis at the transcriptional level, leads to the accumulation of TAG in vegetative tissues (Grimberg et al., 2015; Vanhercke et al., 2014; Vanhercke et al., 2018; Xu and Shanklin, 2016). The overexpression of acyltransferases like *DGAT1*, that catalyze the last step in TAG biogenesis, also lead to elevated TAG levels in seeds and in leaves (Zhang et al., 2009; Xu et al., 2018; Vanhercke et al., 2018). The engineering of plants with the aim of the production of unusual fatty acids has been performed by using empiric approaches, so far with often unpredictable results. Unusual fatty acids, that can be of interest for industry, are often identified in exotic plants. While such plants might exhibit high amounts of specific valuable fatty acids in their seed oil, they usually have no desirable agronomic traits, are toxic, require particular culture conditions, or might not be

tractable for immediate cultivation for other reasons (Dyer and Mullen, 2008). Nonetheless, such plants are sources for gene discovery approaches to identify enzymes suitable to produce a certain fatty acid in transgenic crops. Many enzymes responsible for the production of desirable fatty acids have been identified and were introduced into well-established oil crop plants. Surprisingly, this often led to low yields of the desired fatty acids in the seed oil of the transgenic plants compared to accumulation in the native plant species (Dyer and Mullen, 2008; Drexler et al., 2003; Thomæus et al., 2001). For instance, the transgenic expression of specialized FAD related genes (for example encoding hydroxylases) alone has not been sufficient to efficiently alter the TAG composition in seeds (Dyer et al., 2008; Dyer and Mullen, 2008; Haslam et al., 2016; Vanhercke et al., 2019; Drexler et al., 2003; Cahoon et al., 1999; Thomæus et al., 2001). The possible reasons for such divergence in performance of a gene in the native organism or in a transgenic crop are diverse. For instance, the encoded enzymes might exhibit catalytic plasticity when placed in a non-native metabolic context, possibly resulting in the production of unwanted side products (Heilmann et al., 2004b). Similarly, a heterologous enzyme must compete with the endogenous enzyme machinery for substrates, possibly limiting the yield (Dyer et al., 2008). It has been shown that non-native introduced fatty acids formed by a heterologous enzyme accumulate not as desired in seed oil but in other lipid species, for example in PC, likely due to limited ability of endogenous acyltransferases to efficiently transfer the unusual fatty acids into TAG (Cahoon et al., 2006; Thomæus et al., 2001). The coexpression of specialized DGAT or PDAT enzymes from the source organism may improve the shuttling of non-endogenous fatty acids into the seed oil (Drexler et al., 2003; Dyer et al., 2008; Dahlqvist et al., 2000; Shockey et al., 2006; Burgal et al., 2008; Chen et al., 2015). Thus, to generate high yields of single unusual fatty acids in seed oil, a whole range of modifications of the metabolic pathway leading to TAG are necessary (Haslam et al., 2016; Vanhercke et al., 2019). The expression of divergent FADs initially creating the desired fatty acid and acyltransferases capable of transferring the created fatty acids into TAG combined with the knockout of endogenous enzymes competing for the substrate may improve the yield (van Erp et al., 2011; Haslam et al., 2016). Another obstacle becomes evident when considering the substrates. Different enzymes involved in the biosynthesis of fatty acids and lipids use different substrate pools. For example, the desaturation of fatty acids usually occurs on fatty acids bound to membrane lipids, whereas elongases act on acyl-CoA (Haslam et al., 2016). Moreover, even enzymes catalyzing the same reaction might use different substrate pools. Results from Regmi and coworkers indicate that different DGATs use distinct PC-derived DAG pools as substrate (Regmi et al., 2020). Overall, it is evident that the endogenous fatty acid

and TAG metabolism is rather complex.

Part of this complexity might be related to the metabolic state of a plant, and how lipids and fatty acids contribute to the current physiological requirements. While oil is a commodity for the agricultural engineer, plants use lipids for various physiological purposes, and the interplay between alternative metabolic routes is currently not well understood. Unsaturated fatty acids in membrane lipids have a profound effect on membrane properties, and plants can change membrane lipid unsaturation during acclimation to changing environmental conditions and in response to a variety of biotic and abiotic stresses. For instance, the degree of desaturation in membrane lipids influences membrane fluidity and is therefore adjusted in response to temperature changes, especially during chilling and cold stress (He and Ding, 2020; Miquel et al., 1993; Falcone et al., 2004; Matsuda et al., 2005). The *Arabidopsis fad2-1* mutant is deficient in FAD2 activity and shows reduced levels of 18:2^{Δ9,12} in extraplastidial lipids and in seed oil. The *fad2-1* mutant is furthermore sensitive to salt and low temperatures (Miquel and Browse, 1992; Wallis and Browse, 2002; Zhang et al., 2012). Reversely, overexpression of FAD2 from *Arabidopsis* increases salt tolerance in yeast (Zhang et al., 2012) and improves cold tolerance of rice (*Oryza sativa*) (He and Ding, 2020). Linolenic acid, 18:3^{Δ9,12,15}, is the precursor of jasmonates, a group of important phytohormones involved in wound signaling and in growth regulation (Delker et al., 2006; Wasternack and Feussner, 2018). A *fad3-2 fad7-2 fad8* triple mutant is unable to produce jasmonic acid due to the lack of the lipid precursor 18:3^{Δ9,12,15} (Wasternack and Feussner, 2018; Wallis and Browse, 2002; McConn and Browse, 1996). This results in plants being male sterile (McConn and Browse, 1996). Overexpression of *FAD3* genes in different plants increased the tolerance to cold, drought and salt (He and Ding, 2020; Dar et al., 2017). Evidently, stress conditions influence the capability of plants to produce TAG, and a complex network of alternative uses for membrane lipids is in place.

A little explored aspect of research on plant lipid modifying enzymes has been the precise subcellular localization, which has been shown in some instances to be essential for the efficient interplay of heterologous enzymes in metabolic pathway engineering (e.g., Heilmann et al., 2012; Iven et al., 2016). Therefore, the metabolic context, endogenous substrate channeling and spatial distributions of the enzymes involved have to be considered in the engineering of oil crops. To improve the rational design of oil crops more research is needed (Dyer and Mullen, 2008; Haslam et al., 2016; Dyer et al., 2008).

2. Aims and Objectives

Despite a fundamental importance of fatty acid desaturases for plant physiology and biotechnology, precise information on the subcellular distribution of the relevant enzymes has been scarce even for otherwise well-known enzymes, such as Arabidopsis FAD2 or FAD3. The experiments reported so far on the subcellular localization of enzymes involved in the fatty acid desaturation and TAG production were often performed in artificial systems and *ex vivo* (for example immunolocalization) and non-endogenous context or were not analyzed in detail. High-resolution imaging data in the endogenous plant system is still missing.

Therefore, the focus of this thesis lays on the investigation of the subcellular distribution and interplay of the biochemically well-known enzymes responsible for fatty acid desaturation (FAD2 and FAD3) and for TAG assembly (DGAT1, DGAT2 and PDAT) from the model organism *A. thaliana*. The goals were in detail:

- to generate functional fluorescence-tagged enzyme variants and analyze their functionality by expression in yeast.
- to use Arabidopsis mutants deficient in fatty acid desaturation (*fad2-1* and *fad3-2*) and examine whether fluorescence-tagged FAD2 and FAD3 could restore the mutant phenotypes regarding macroscopic traits and lipid composition.
- to analyze the subcellular distribution of functional fluorescence-tagged FAD2 and FAD3 fusions in different tissues in respective complemented Arabidopsis mutants.
- to examine the localization of FAD2, FAD3, DGAT1 and PDAT in a transient plant expression system relative to a variety of different organelle markers.
- to analyze the interaction of key enzymes mediating fatty acid modification and TAG assembly by yeast two-hybrid analyses and in plant cells by using bimolecular fluorescence complementation.

3. Results

The metabolic context, subcellular localization and compartmentalization play an essential role in the engineering of oil crops, but only little has been done to characterize the endogenous system of fatty acid desaturation and oil biogenesis (reviewed by Dyer and Mullen, 2008). While the enzymes involved in the desaturation of fatty acids and the assembly of TAG are biochemically well-characterized, the subcellular distribution and the molecular interplay of FADs and acyltransferases has not been addressed in great detail so far. Therefore, it was the goal of this work to analyze the subcellular localization of functional fluorescence-tagged FADs and acyltransferases from the model organism *A. thaliana* and to explore the interplay of these enzymes.

3.1 Fluorescence-tagged enzyme variants of FAD2 and FAD3 are functional in yeast

For subcellular localization analyses with live cell imaging, functional variants of FAD2 and FAD3 fused to a fluorescence protein are required. To avoid the masking of the C-terminal ER-retention motif (McCartney et al., 2004), the fluorescence proteins EYFP or mCherry were fused to the N-terminus of FAD2 and FAD3. The fusion proteins were first tested for their functionality by expression in yeast. Yeast only produces non or monounsaturated fatty acids (Klug and Daum, 2014; Stukey et al., 1989, 1990) and is therefore suited to observe the subsequent desaturation of monounsaturated fatty acids by the expressed fluorescent fusions of FAD2 and FAD3. The yeast strain INVSc1 was transformed with *pESC-TRP*-vectors (described in section 5.13.1) containing the cDNA for tagged or untagged FAD2 and FAD3 as described in section 5.15. Cells were grown in liquid SD-minimal medium for 3 days at 18-20 °C (described in section 5.20.1). Cells harboring a vector with an empty expression cassette were used as negative control. Cells equivalent to 20 OD-units (the volume corresponding to 20 ml with an OD₆₀₀ of 1) were harvested, the lipids extracted and fatty acids trans methylated. The resulting fatty acid methyl esters (FAMES) were analyzed by gas chromatography with flame ionization detection (GC-FID) (described in sections 5.21.7 and 5.21.8). Representative chromatograms and the quantification of the individual FAMES are shown in Figure 3.1A for the expression of FAD2-variants and in Figure 3.1B for FAD3-variants, respectively. As seen in Figure 3.1A, the chromatograms for FAD2, EYFP-FAD2 and mCherry-FAD2 contained additional fatty acid peaks compared to the empty vector control. The arrow indicates the signal for 18:2^{Δ9,12}, the product of FAD2-mediated conversion of 18:1^{Δ9}, a signal not detected in yeast harboring the empty control vector.

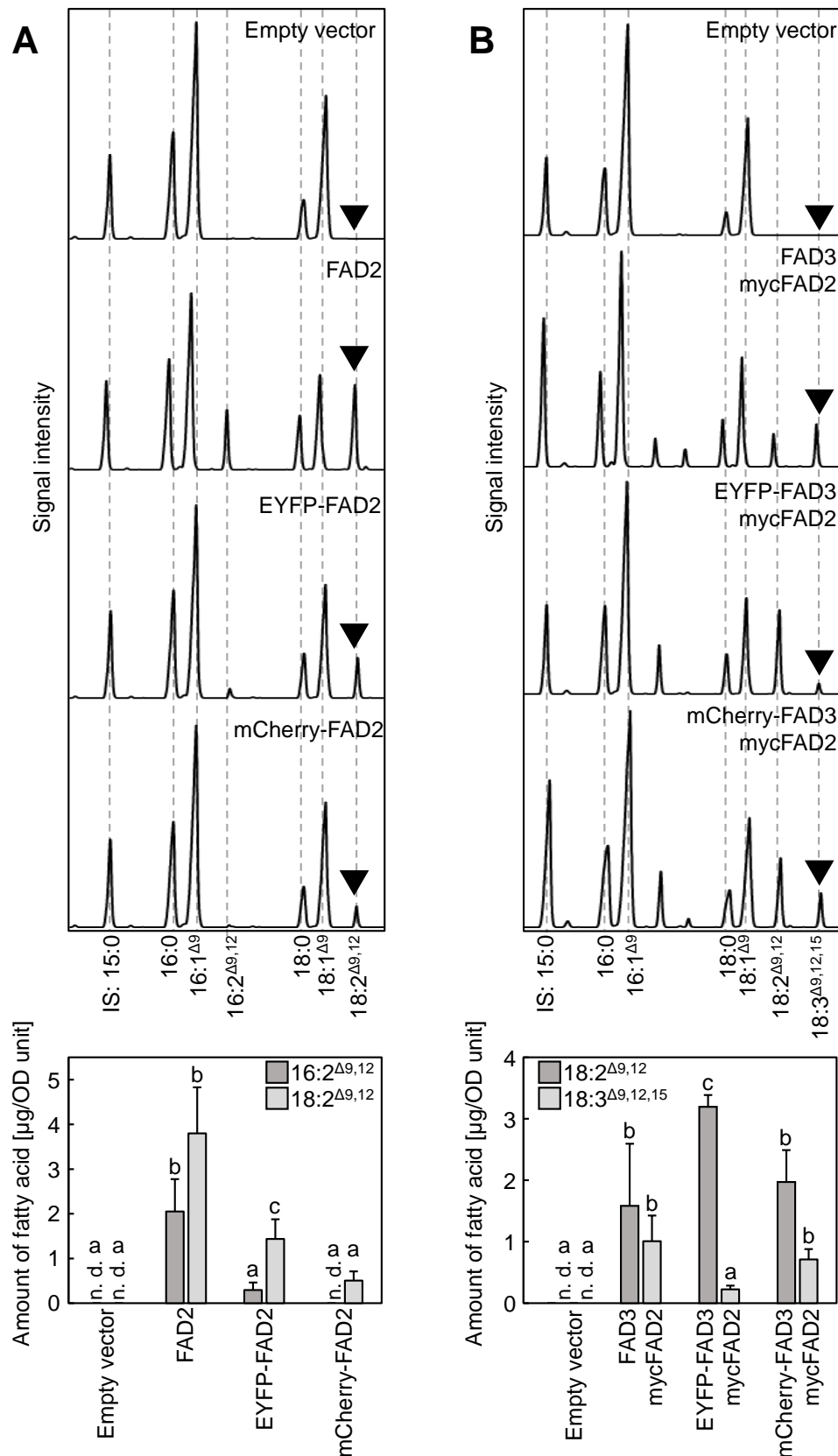


Figure 3.1. Functionality of fluorescence-tagged fatty acid desaturases FAD2 and FAD3 from Arabidopsis heterologously expressed in yeast. The functionality of fluorescence-tagged variants of Arabidopsis FAD2 and FAD3 was assessed upon heterologous expression in yeast. Fusion proteins were expressed in the yeast strain INVSc1 in liquid SD-minimal yeast medium without tryptophane containing

2 % (w/v) galactose at room temperature (FAD2 and variants) or at 18 °C (FAD3 and variants) for 3 days. The fatty acids from 20 OD-units were extracted, trans methylated and analyzed by GC-FID. Significant differences were determined using one-way ANOVA with a Tukey's post-hoc test ($p < 0.05$). Abbreviations: IS, internal standard (50 μ g tripentadecanoin); n. d., not detectable. **A**, Representative chromatograms of yeast expressing FAD2-variants. Arrows indicate the signal for 18:2 $\Delta^{9,12}$, the main product of FAD2. The amounts of 16:2 $\Delta^{9,12}$ and 18:2 $\Delta^{9,12}$ from four independent experiments with two biological replicates each were quantified and are presented in the bar chart. Data represent mean \pm sample standard deviation. **B**, FAD3, EYFP-FAD3 or mCherry-FAD3 was coexpressed with mycFAD2. Representative chromatograms are shown. Arrows indicate the product of FAD3: 18:3 $\Delta^{9,12,15}$. The amounts of 18:2 $\Delta^{9,12}$ and 18:3 $\Delta^{9,12,15}$ from two (EYFP-FAD3 and mCherry-FAD3) or five (empty vector control, untagged FAD3) independent experiments with two to three biological replicates each were quantified and are presented in the bar chart. Data represent mean \pm sample standard deviation.

The quantification shows that yeast transformed with the untagged FAD2 contained the most 18:2 $\Delta^{9,12}$ and 16:2 $\Delta^{9,12}$. 16:2 $\Delta^{9,12}$, a byproduct of the FAD2 mediated desaturation, was also detectable in yeast expressing EYFP-FAD2 but not in cells expressing mCherry-FAD2. Nonetheless, the formation of 18:2 $\Delta^{9,12}$ indicates that EYFP-FAD2 as well as mCherry-FAD2 were active in yeast expression experiments. Since 18:2 $\Delta^{9,12}$ is not produced by yeast itself but is needed as a substrate to assess the functionality of FAD3 in yeast experiments, FAD3-variants were coexpressed with N-terminally myc-tagged FAD2 (mycFAD2). In Figure 3.1B representative chromatograms are presented. The chromatograms of yeast expressing FAD3, EYFP-FAD3 or mCherry-FAD3 together with mycFAD2 contained additional signals for 18:2 $\Delta^{9,12}$ and 18:3 $\Delta^{9,12,15}$, the latter signal indicated by the arrow. The quantification shows that yeast cells expressing EYFP-FAD3 contained the least amount of 18:3 $\Delta^{9,12,15}$ and the most amount of 18:2 $\Delta^{9,12}$, while the product and substrate amounts did not differ significantly ($p < 0.05$) between yeast expressing FAD3 or mCherry-FAD3. Thus, both fluorescence-tagged FAD3-variants proved to be functional in yeast experiments.

3.2 Fluorescence-tagged enzyme variants of FAD2 and FAD3 complement Arabidopsis mutants

As N-terminal fluorescence fusion proteins of FAD2 and FAD3 proved to be functional in yeast, the functionality of these fusions was next tested by mutant complementation assays in the Arabidopsis mutants *fad2-1* and *fad3-2* respectively transformed with EYFP-FAD2 or EYFP-FAD3. For the complementation of *fad2-1*, expression of EYFP-FAD2 was driven by the endogenous *FAD2* promoter (*pFAD2*). The promoter sequence used in this study consisted of 2,281 bp of the genomic sequence upstream of the start codon for the *FAD2* gene. Plants were transformed by floral dipping (Clough and Bent, 1998) using *A. tumefaciens* as described in section 5.17. T1 plants were treated with glufosinate and resistant individuals were propagated. *fad2-1* mutants complemented with EYFP-FAD2 under the *FAD2* promoter are termed EYFP-FAD2 plants. From among the T2 generation,

three lines (L5, L9, L15) were chosen for further experiments. The *fad3-2* mutant was similarly complemented with EYFP-FAD3 under the control of the *cauliflower mosaic virus* 35S promoter (*pCaMV35S*) and propagated as described above. Three EYFP-FAD3 lines (L4, L7, L9) were chosen for further experiments.

3.2.1 Phenotypic defects of *fad2-1* and *fad3-2* are restored by the respective expression of EYFP-FAD2 or EYFP-FAD3

As a first indication for successful complementation, phenotypic traits were analyzed, such as growth and overall appearance. Col-0 wild type controls, *fad2-1* mutants and EYFP-FAD2 plants of generation T2 were grown on soil under short-day conditions for 9 weeks followed by long-day conditions until the end of their life cycle. Growth was documented after 8 and 12 weeks and representative images are shown in Figure 3.2. The complemented lines, wild type controls and *fad2-1* mutants did not differ in the leaf area of the rosette or the height of the shoots. Therefore, based on macroscopic phenotypes, no evaluation of the success of the complementation could be made.

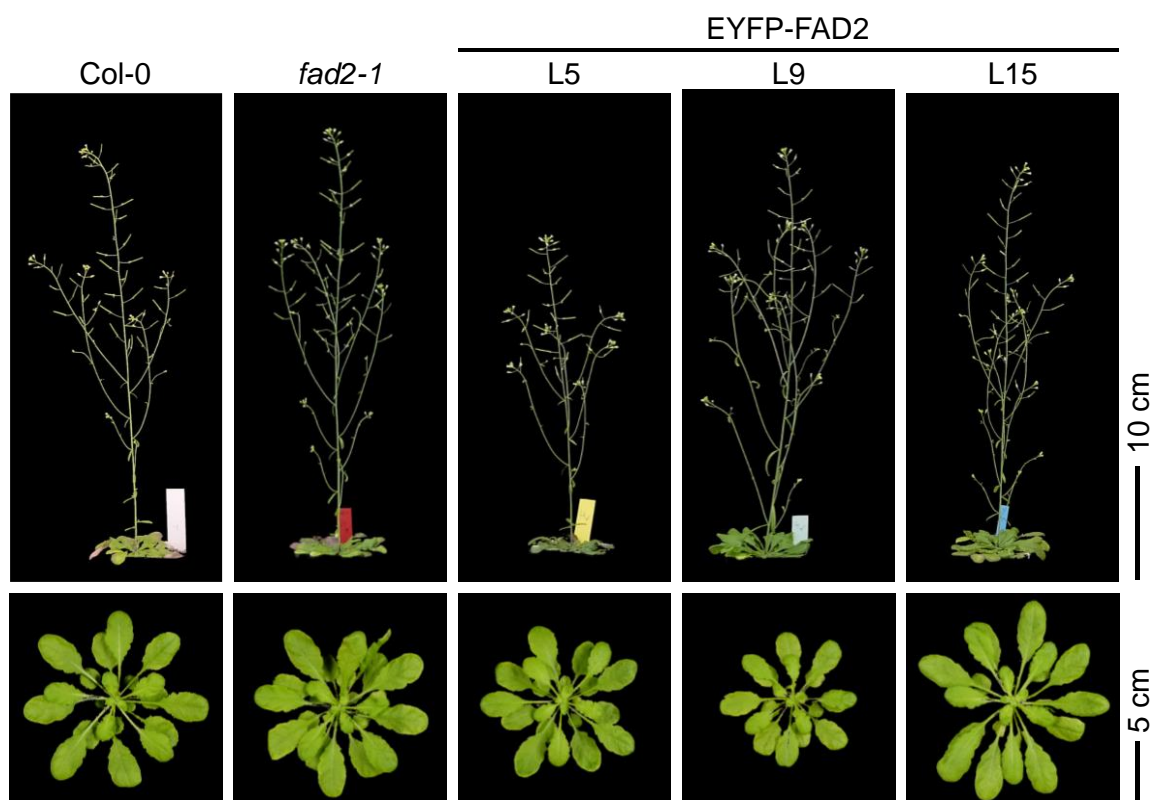


Figure 3.2. Phenotypic comparison of Col-0 wild type, *fad2-1* and *fad2-1* lines expressing EYFP-FAD2. EYFP-FAD2 was expressed in the Arabidopsis *fad2-1* mutant background under the control of an endogenous promoter fragment. 12-week-old (upper panels) and 8-week-old (lower panels) plants are shown. All plants were grown under short-day conditions (8 h light, 16 h dark) for 9 weeks, followed by long-day conditions (16 h light, 8 h dark). Images are representative for 11 plants analyzed for each genotype.

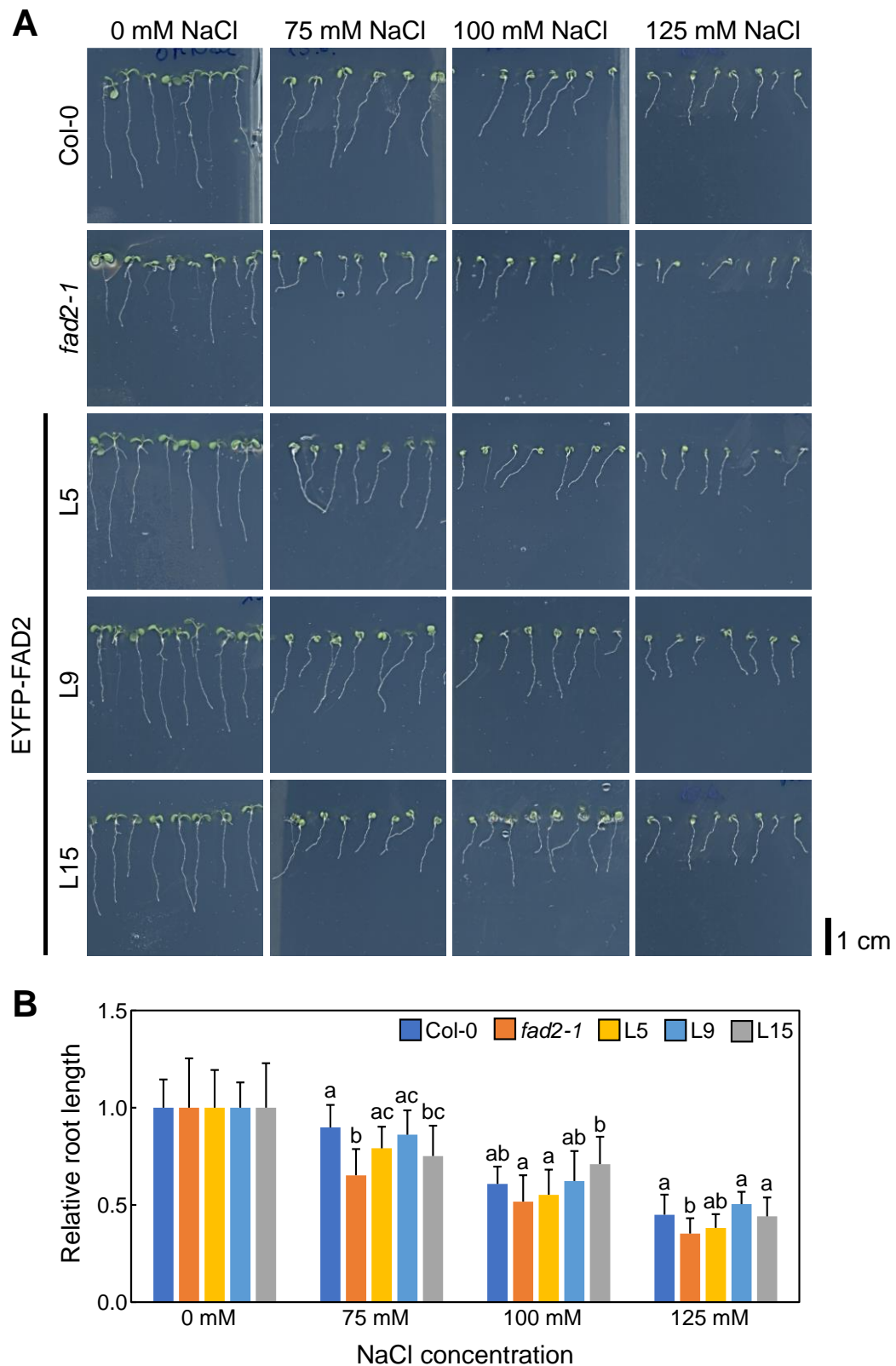


Figure 3.3. Complementation of *fad2-1* salt sensitivity by expression of EYFP-FAD2. The functionality of the EYFP-FAD2 fusion was assessed by testing for complementation of the salt intolerance displayed by the Arabidopsis *fad2-1* mutant. **A**, Plants were grown on vertical plates of $\frac{1}{2}$ MS medium containing the indicated amount of NaCl for 7 days under long-day conditions (16 h light, 8 h dark) after two days of stratification. **B**, Root lengths were measured, and the relative root length compared to mock-treated plants is shown in the bar chart. Data represent mean \pm sample standard deviation. Significant differences were determined using one-way ANOVA with a Tukey's post-hoc test ($p < 0.05$) for each salt concentration. Letters indicate

significantly different categories of samples. The experiments were performed with 12 to 19 seedlings per line and salt concentration.

As the *fad2-1* mutant is sensitive to salt, salt stress experiments were performed to assess the complementation by fluorescence-tagged FAD2. T2 seedlings were grown on ½ MS medium containing 0 mM, 75 mM, 100 mM or 125 mM NaCl for seven days under long-day conditions. The root growth was observed and quantified (see section 5.8). Representative seedlings together with the measured root length related to 0 mM NaCl are shown in Figure 3.3. As seen in Figure 3.3A, all plants responded to increasing amounts of salt with reduced root length. Even though the *fad2-1* mutant had generally the shortest roots, the reaction to salt was more severe in the mutant than in the wild type or the EYFP-FAD2 lines (Figure 3.3B). By contrast, the reduction of the root length in EYFP-FAD2 lines did not differ significantly ($p > 0.05$) compared to the wild type. EYFP-tagged FAD2 under the control of the *FAD2* promoter was able to complement the salt sensitivity of the *fad2-1* mutant.

Phenotypic complementation was easier tested for the *fad3-1* mutant because this mutant displays a macroscopic phenotype. To assess the complementation of *fad3-2* by EYFP-tagged FAD3, wild type Col-0 controls, the *fad3-2* mutant and EYFP-FAD3 plants of generation T2 were grown on soil under short-day conditions for 9 weeks followed by long-day conditions until the end of their life cycle. The growth was documented after 9 and 14 weeks. Representative images are shown in Figure 3.4. As seen in Figure 3.4A, the *fad3-2* mutant displayed a smaller rosette and reduced shoot length compared to the wild type. EYFP-FAD3 lines were similar in appearance to the wild type regarding rosette size and shoot lengths. To confirm the notion of the reduced growth of *fad3-2*, the leaf areas of 9-week-old plants were measured using Fiji. The quantification of the leaf area is shown in Figure 3.4B. The leaf areas of *fad3-2* were significantly lower ($p < 0.05$) than that of the wild type, whereas the leaf areas of EYFP-FAD3 plants covered a broader range and did not differ significantly ($p > 0.05$), neither from the *fad3-2* mutant nor from the wild type controls. The overall larger appearance and the on average larger leaf area of EYFP-FAD3 plants compared to the mutant indicate that EYFP-tagged FAD3 at least partially complemented the growth phenotype of the *fad3-2* mutant.

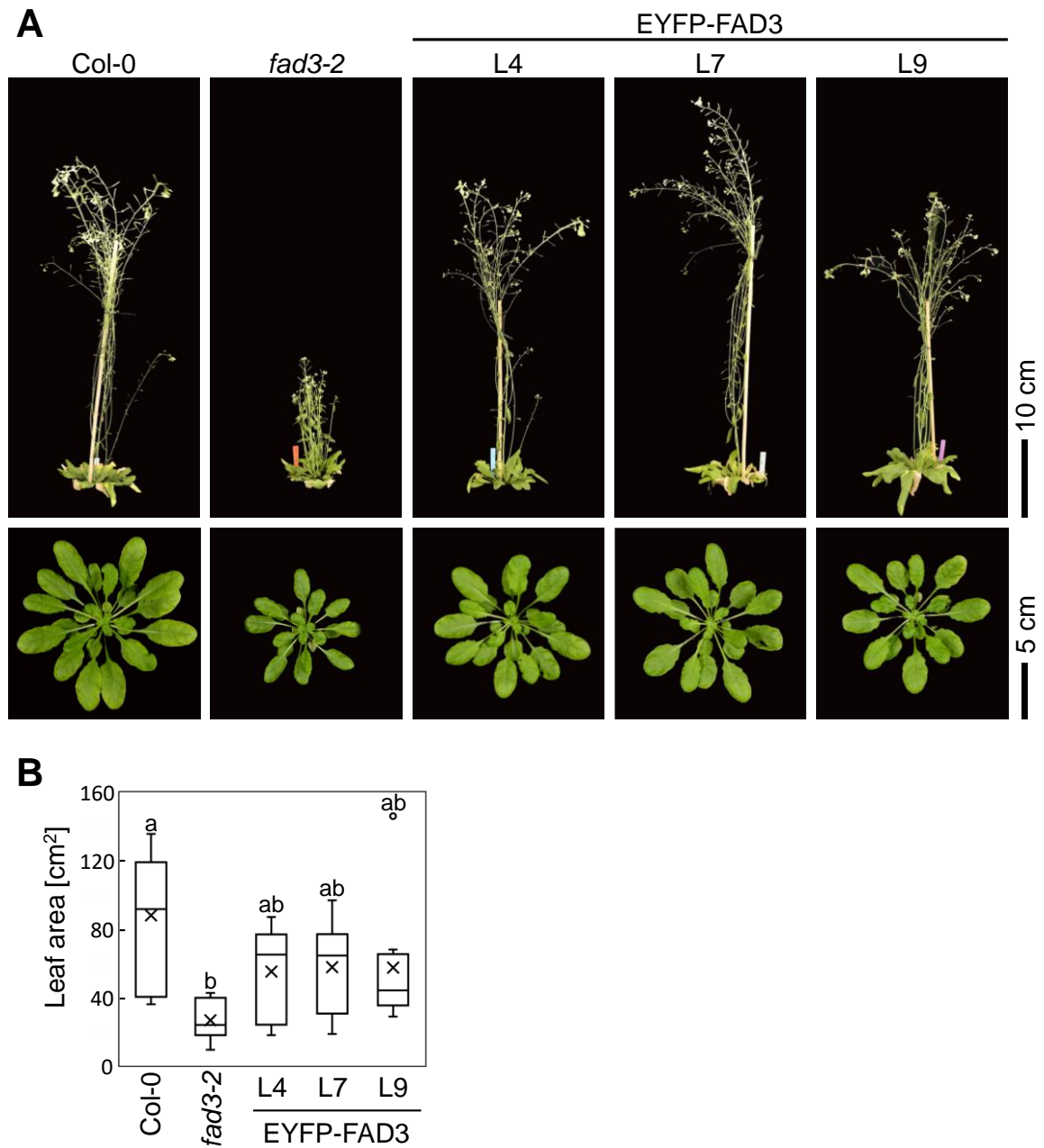


Figure 3.4. Expression of EYFP-FAD3 complements the phenotypic growth defect of the Arabidopsis *fad3-2* mutant. The functionality of an EYFP-FAD3 fusion was assessed by testing for macroscopic complementation of the Arabidopsis *fad3-2* mutant phenotype. EYFP-FAD3 was expressed in the *fad3-2* mutant under the control of the *pCaMV35S* promoter. **A**, 14-week-old (upper panels) and 9-week-old (lower panels) plants are shown. The plants were grown under short-day conditions (8 h light, 16 h dark) for 9 weeks, followed by long-day conditions (16 h light, 8 h dark). **B**, The box plot shows the quantification of the leaf area of 10 (Col-0) or 8 (*fad3-2*, L4, L7, L9) rosettes, respectively, of 9-week-old plants, measured with Fiji (Schindelin et al., 2012). Significant differences were determined using one-way ANOVA with a Tukey's post-hoc test ($p < 0.05$). Letters indicate significantly different categories of samples.

3.2.2 Fatty acid compositions of *fad2-1* and *fad3-2* are restored by the respective expression of EYFP-FAD2 or EYFP-FAD3

In addition to the macroscopic appearance, the EYFP-FAD2 and EYFP-FAD3 plants were also characterized regarding the complementation of their fatty acid composition in different tissues.

Fatty acids extracted from single seeds of EYFP-FAD2 plants were trans methylated and analyzed by GC-FID as described in section 5.21.5 and section 5.21.8, respectively. Ten seeds were analyzed for each transgenic line, the wild type Col-0 and for the *fad2-1* mutant and the results are depicted in Figure 3.5A. The relative amount of 18:2^{Δ9,12} in the *fad2-1* mutant was reduced to approx. 5 % of the total seed fatty acids compared to approx. 30 % of the total seed fatty acids in wild type. The EYFP-FAD2 plants contained approx. 15-25 % of 18:2^{Δ9,12} in seeds which is significantly higher ($p < 0.05$) than in the *fad2-1* mutant (box plot, upper left). The bar chart in Figure 3.5A (upper right) shows the fatty acid composition of seeds from complemented plants and the controls. Besides 18:2^{Δ9,12}, 18:3^{Δ9,12,15} was also reduced in the *fad2-1* mutant, whereas the metabolic precursor 18:1^{Δ9} accumulated. The complemented EYFP-FAD2 plants overall had a similar fatty acid composition in seeds as the wild type. The fatty acid composition is also shown for the individual seeds. The single seed analysis illustrates that in the selected EYFP-FAD2 lines some seeds exhibited a fatty acid composition resembling that of the mutant background and were thus not complemented, possibly because of weak expression of the transgene. Data from these seeds were omitted in the analyses of the fatty acid profile and the calculation of the relative amount of 18:2^{Δ9,12} (box plot, upper left).

In addition to the analysis of seed fatty acids, the fatty acid composition of plant lipids from 14-day-old seedlings was also examined. The membrane lipids PC, MGDG and DGDG were isolated, and the fatty acid composition was analyzed according to section 5.21. The relative amount of PC-bound 18:2^{Δ9,12} was reduced to below 5 % of the PC-associated fatty acids in the *fad2-1* mutant, compared to more than 35 % of the PC-associated fatty acids in wild type (Figure 3.5B, PC). The bar chart representing the fatty acid composition shows that concomitantly with these changes 18:1^{Δ9} accumulated in PC. The EYFP-FAD2 lines contained PC with around 30 % of associated 18:2^{Δ9,12}, which is significantly more ($p < 0.05$) 18:2^{Δ9,12} than in the PC in the *fad2-1* mutant. Except for line EYFP-FAD2 L9, the amounts of 18:2^{Δ9,12} in the complemented EYFP-FAD2 lines were not significantly different ($p > 0.05$) from values for the wild type.

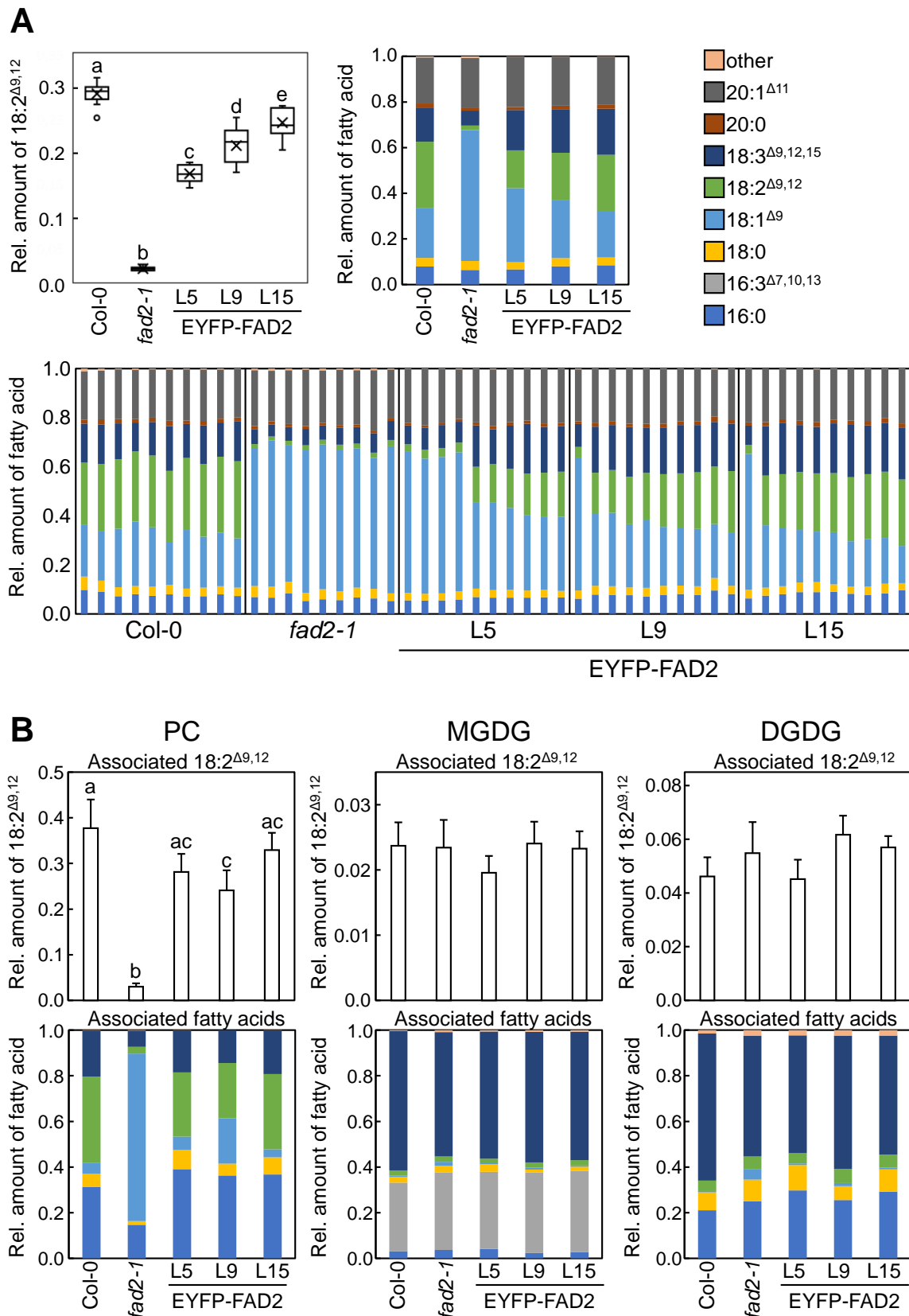


Figure 3.5. Expression of EYFP-FAD2 reconstitutes a wild type-like fatty acid composition in the *Arabidopsis fad2-1* mutant. The fatty acid composition of seeds and seedlings from *fad2-1* mutants complemented with EYFP-FAD2 under the control of its intrinsic promoter (*pFAD2*) was analyzed. **A**, Fatty acid analyses from single seeds (T2). Left, the relative amount of 18:2^{Δ9,12} in single (complemented) seeds is

depicted in the box plot. Significant differences were determined using one-way ANOVA with a Tukey's post-hoc test ($p < 0.05$). Letters indicate significantly different categories of samples. Right, the mean relative fatty acid composition in seeds from the different plant lines is shown in the bar chart. Bottom, single seed fatty acid profiles. $n = 10$. **B**, Fatty acid analyses of different lipid classes isolated from 14-day-old seedlings. Seedlings were grown on $\frac{1}{2}$ MS medium under long-day-conditions (16 h light, 8 h dark). Top panels, the mean relative amounts of 18:2 $^{\Delta 9,12}$ associated with PC, MGDG and DGDG, as indicated. Bottom panels, the mean relative fatty acid compositions of PC, MGDG and DGDG, as indicated. Significant differences were determined using one-way ANOVA with a Tukey's post-hoc test ($p < 0.05$). Letters indicate significantly different categories of samples. $n = 3$.

The data so far are consistent with functionality of EYFP-FAD2 in the context of fatty acids associated with seed oil or the extraplasmidial lipid PC. The plastid-specific lipids MGDG and DGDG contained in general low amounts of 18:2 $^{\Delta 9,12}$ with less than 3 % of associated fatty acids in MGDG and less than 6 % of associated fatty acids in DGDG, respectively (Figure 3.5B). A reduction of 18:2 $^{\Delta 9,12}$ in these lipids in the *fad2-1* mutant was not observed and not expected. Likewise, the fatty acid profile of MGDG and DGDG did not differ much between Col-0, *fad2-1* and the EYFP-FAD2 lines. Only a slight increase of 18:1 $^{\Delta 9}$ in DGDG in the mutant background was observed. Overall, EYFP-tagged FAD2 could complement the lipid composition phenotype of the *fad2-1* mutant in seeds as well as in membrane lipids from seedlings.

Fatty acid analyses of seeds and membrane lipids as described for EYFP-FAD2 plants were performed also for EYFP-FAD3 plant lines to address functionality of the EYFP-FAD3 fusion in comparison to the *fad3-2* mutant and wild type controls. The results are depicted in Figure 3.6, with the analysis of seed fatty acids shown in panel A and the examination of membrane lipids in panel B. The amount of 18:3 $^{\Delta 9,12,15}$ in seed lipids of the *fad3-2* mutant was significantly reduced ($p < 0.05$) to approx. 1 % of the total seed fatty acids, compared to approx. 15 % of the total seed fatty acids in the wild type (Figure 3.6A). The complemented EYFP-FAD3 lines contained significantly increased ($p < 0.05$) amounts of 18:3 $^{\Delta 9,12,15}$ of approx. 20 % of total lipids in the seeds compared to wild type. The reduction of 18:3 $^{\Delta 9,12,15}$ in *fad3-2* mutants was accompanied by the accumulation of 18:2 $^{\Delta 9,12}$, whereas no such accumulation was observed in the wild type controls or EYFP-FAD3 plant lines (Figure 3.6A, upper right). The fatty acid profile of individual seeds from EYFP-FAD3 plants showed that all tested seeds were complemented regarding the fatty acid distribution in the seed oil and no seeds resembling the mutant background were found.

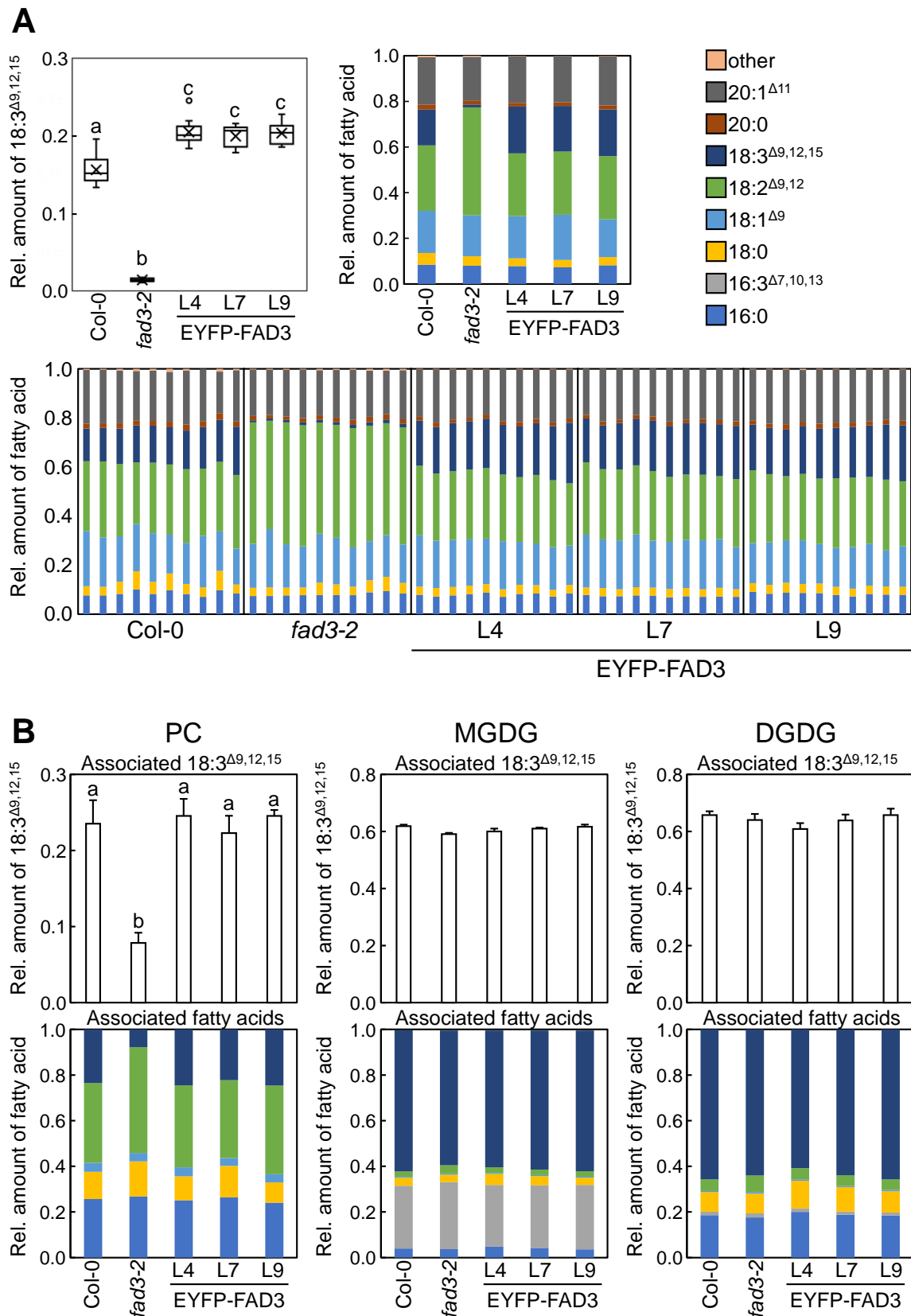


Figure 3.6. Expression of EYFP-FAD3 reconstitutes a wild type-like fatty acid composition in the *Arabidopsis fad3-2* mutant. The fatty acid composition of seeds and seedlings from *fad3-2* mutants complemented with EYFP-FAD3 under the control of *pCaMV35S* was analyzed. **A**, Fatty acid analyses from single seeds (T2). Left, the relative amount of 18:3 $\Delta^{9,12,15}$ in single seeds is depicted in the box plot. Significant

differences were determined using one-way ANOVA with a Tukey's post-hoc test ($p < 0.05$). Letters indicate significantly different categories of samples. Right, the mean relative fatty acid compositions in seeds from the different plant lines are shown in the bar chart. Bottom, single seed fatty acid profiles. $n = 10$. **B**, Fatty acid analyses of different lipids from 14-day-old seedlings. Seedlings were grown on $\frac{1}{2}$ MS medium under long-day-conditions (16 h light, 8 h dark). Top panels, the relative amounts of 18:3 ^{Δ 9,12,15} associated with PC, MGDG and DGDG, as indicated. Bottom panels, the mean relative fatty acid compositions of PC, MGDG and DGDG, as indicated. Significant differences were determined using one-way ANOVA with a Tukey's post-hoc test ($p < 0.05$). Letters indicate significantly different categories of samples. $n = 3$.

The analysis of membrane lipids from 14-day-old seedlings revealed that in *fad3-2* mutants the relative amount of 18:3 ^{Δ 9,12,15} associated with PC was decreased to less than 10 % of the associated fatty acids compared to approx. 25 % of the associated fatty acids in the wild type (Figure 3.6B). EYFP-FAD3 seedlings exhibited wild type levels of PC-bound 18:3 ^{Δ 9,12,15}. The reduction of 18:3 ^{Δ 9,12,15} in the *fad3-2* mutant again resulted in an increase of 18:2 ^{Δ 9,12} associated with PC. By contrast, the relative amount of 18:3 ^{Δ 9,12,15} associated with the plastid-specific membrane lipids MGDG and DGDG did not differ between wild type, *fad3-2* mutant and EYFP-FAD3 lines. In accordance with that, the overall fatty acid profile of MGDG and DGDG was not altered in the *fad3-2* mutant or in EYFP-FAD3 plant lines. Overall, the data indicate that expression of EYFP-tagged FAD3 could complement the lipid composition phenotype of the *fad3-2* mutant.

Taken together, the tests for physiological functionality of the fluorescence-tagged variants of FAD2 or FAD3 indicate that the respective mutant backgrounds were complemented regarding the fatty acid composition of seed oil and membrane lipids. Wild type levels of PC-associated 18:2 ^{Δ 9,12} and 18:3 ^{Δ 9,12,15} were fully restored, respectively, and the *pCaMV35S*-driven overexpression of EYFP-FAD3 in the mutant *fad3-2* even resulted in slightly elevated 18:3 ^{Δ 9,12,15}-levels in the seed oil. Based on these findings, it was concluded that the N-terminal fluorescence fusions of FAD2 and FAD3 were functional and could thus be used for localization studies.

3.3 Functional EYFP-FAD2 and EYFP-FAD3 fusions decorate donut-shaped structures in complemented plant lines

The phenotypic characterization of EYFP-FAD2 and EYFP-FAD3 plants demonstrated that the fluorescent fusion proteins functionally complemented the respective mutants. Therefore, subcellular localization analyses using these fluorescent fusion proteins were feasible. The localization patterns of EYFP-FAD2 and EYFP-FAD3 were first analyzed in roots and leaves of 7-day-old Arabidopsis seedlings expressing the respective fusions. EYFP-FAD2 and EYFP-FAD3 plants were grown on $\frac{1}{2}$ MS medium for seven days under long-day conditions. The subcellular distribution of EYFP-FAD2 and EYFP-FAD3 in different tissues was examined by laser scanning confocal microscopy (LSM) using a Zeiss LSM880 system as described in section 5.23.1. Figure 3.7 shows the localization pattern

of EYFP-FAD2 expressed from its intrinsic promoter in roots (A) or leaf epidermal cells (B). EYFP-FAD2 fluorescence is depicted in green together with bright field images (gray). The distribution of EYFP-FAD2 differed between roots and leaves. In root tissues, a distribution of rather diffuse fluorescence was visible mostly at the cell periphery. The localization of EYFP-FAD2 was similar in root tips, cells of the elongation zone and fully elongated cells. Fluorescence was also detectable in large circular structures, probably surrounding nuclei (Figure 3.7A, upper panel), suggesting localization to the ER. Without an organelle marker, it is not easy possible to clearly distinguish cytosolic fluorescence from fluorescence associated with the ER.

By contrast, a distinct fluorescence pattern was visible in leaf epidermal cells. Here, EYFP-FAD2 localized to hollow circular structures or short lines of approx. 1 μm of size. These structures were distributed throughout the cytosol. While the fluorescence distribution pattern of EYFP-FAD2 in roots, thus, resembled ER association, a different pattern was detected in leaves, which did not resemble ER association.

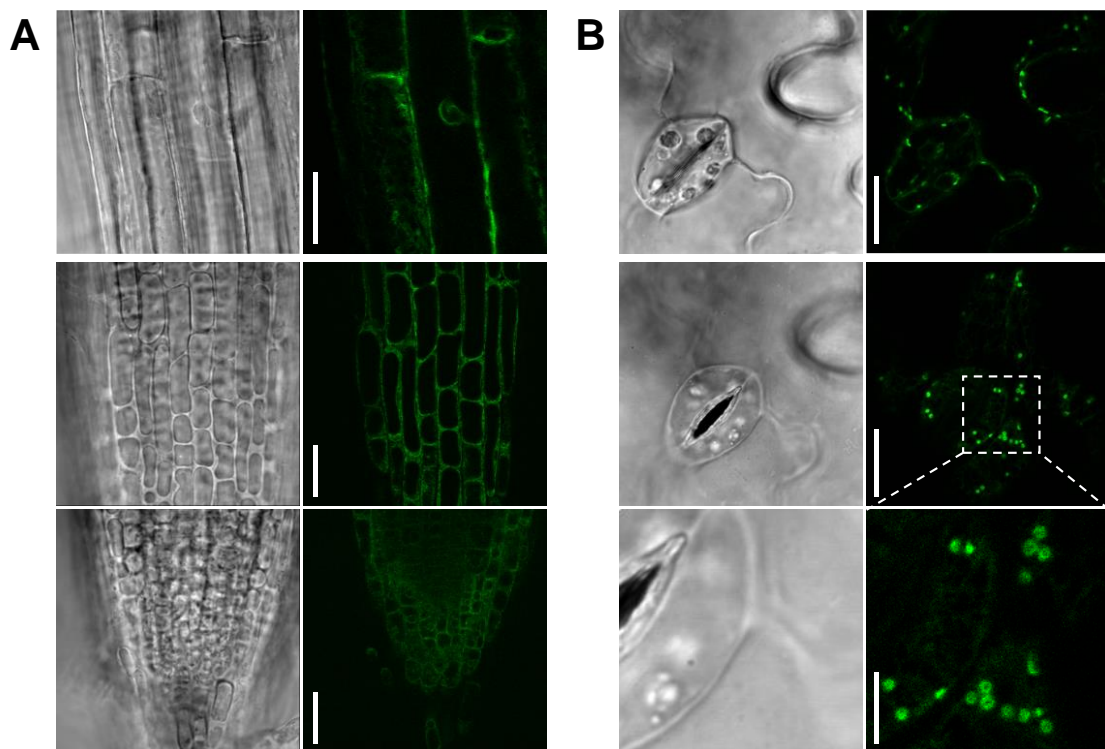


Figure 3.7. Subcellular distribution of EYFP-FAD2 in roots and in leaves of transgenic *Arabidopsis* plants. 7-day-old seedlings of *Arabidopsis* *fad2-1* mutants expressing EYFP-FAD2 under its intrinsic promoter were grown on $\frac{1}{2}$ MS medium under long-day-conditions (16 h light, 8 h dark) and analyzed by laser scanning microscopy (LSM). EYFP-FAD2 fluorescence is depicted in green. **A**, Different areas of the root. Top, elongated root cells; middle, root elongation zone; bottom, root meristematic zone. Scale bars: 25 μm . **B**, Distribution of EYFP-FAD2 in leaf epidermal cells. Top, overview of pavement cells; middle and bottom, overview and magnification of pavement cells and stomata. Dashed box, area of magnification. Scale bars: 15 μm , 5 μm (bottom panel). Images are representative for one experiment using two to three plants representing three independent transgenic lines.

The subcellular localization of EYFP-FAD3 did not differ substantially between root and leaf cells as seen in Figure 3.8A and B, respectively. All tissue types, root tips, elongated root epidermal cells and leaf epidermal cells showed punctuate or circular structures marked by EYFP-FAD3 fluorescence (green). The circular structures were hollow, comparable to the structures highlighted by EYFP-FAD2 fluorescence in leaf epidermal cells (compare Figure 3.7), and at first approximation did not resemble ER association. The observation of both FAD2 and FAD3 fusions in particulate fluorescence distributions, rather than in a diffuse and network-like pattern, was unexpected considering previously published work describing ER association of both proteins (Dyer and Mullen, 2001; Dyer et al., 2002; Nguyen et al., 2019).

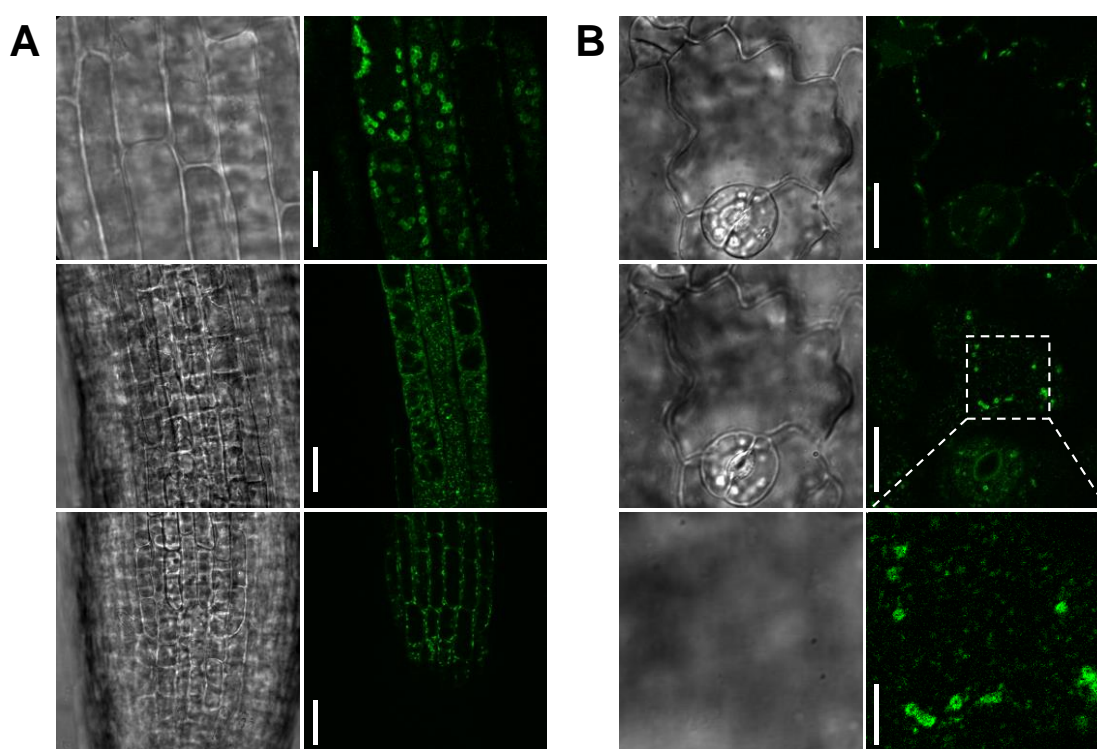


Figure 3.8. Subcellular distribution of EYFP-FAD3 in roots and in leaves of transgenic Arabidopsis plants. 7-day-old seedlings of *Arabidopsis fad3-2* mutants expressing EYFP-FAD3 under the control of *pCaMV35S* were grown on $\frac{1}{2}$ MS medium under long-day-conditions (16 h light, 8 h dark) and analyzed by LSM. EYFP-FAD3 fluorescence is depicted in green. **A**, Different areas of the root. Top, elongated root cells; middle, root elongation zone; bottom, root meristematic zone. Scale bars: 15 μ m (top panel), 25 μ m. **B**, Distribution of EYFP-FAD3 in leaf epidermal cells. Top, overview of leaf pavement cells; middle and bottom, overview and magnification of pavement cells and stomata. Dashed box, area of magnification. Scale bars: 15 μ m, 5 μ m (bottom panel). Images are representative for one experiment using two to five plants representing five independent transgenic lines.

The *Arabidopsis* mutants *fad2-1* and *fad3-2* were successfully complemented by the expression of EYFP-tagged enzyme variants and mutant phenotypes in seeds and seedlings were all restored by expression of EYFP-FAD2 and EYFP-FAD3, respectively (compare Figure 3.2 to Figure 3.6). It is important to note that the successful

complementation indicates functionality of the fluorescent fusions analyzed, and that the subcellular distribution in donut-shaped particulate structures was observed in the same phenotypically complemented respective mutant backgrounds. As the successful mutant complementation indicated functionality of the fluorescent fusions, and therefore biological relevance of the fluorescence distributions observed, it was next attempted to identify the nature of the particulate structures decorated by EYFP-FAD2 in leaves and by EYFP-FAD3 in both leaves and roots.

3.4 Fluorescent fusions of FAD2 associate with Golgi-particles in close proximity to the ER in Arabidopsis mesophyll protoplasts

To determine the nature of the particulate, donut-shaped structures, further analyses were performed using various organelle markers upon expression of fluorescent fusion proteins in Arabidopsis mesophyll protoplasts. The protoplast system combines the advantages of live cell imaging in leaf cells of the homologous organism (Arabidopsis) with fast and easy usage of different organelle markers for coexpression experiments. Protoplasts were isolated from Arabidopsis wild type (Col-0) or ER marker line GFP-HDEL and (co-)transformed with expression vectors for fluorescence-tagged enzyme variants as well as different organelle markers as described in section 5.16. The subcellular fluorescence distributions were analyzed by LSM or by spinning disc microscopy (SD). Images were acquired as Z-stacks covering the cell from one edge to the center and used for image analyses as described in section 5.23. Representative single confocal planes or maximum intensity Z-projections were chosen for representation.

The subcellular distribution of an EYFP-FAD2 fusion was analyzed in mesophyll protoplasts from wild type Arabidopsis plants first without the interference of an additional organelle marker. Representative images are shown in Figure 3.9. A maximum-intensity projection from a Z-stack is shown in Figure 3.9A, Figure 3.9B displays a single confocal plane. EYFP-FAD2 fluorescence is depicted in green, the autofluorescence of chlorophyll A (ChlA) in blue. Bright field images are added in gray. EYFP-FAD2 localized to circular structures or short lines (Figure 3.9A and B). In more detailed images, it is visible that the circular structures were hollow. In Figure 3.9C, the fluorescence intensity distribution is analyzed in detail. The heatmap image of the localization of EYFP-FAD2 illustrates the fluorescence intensity distribution. In addition, the fluorescence intensity was analyzed along the indicated line in a line plot. As seen in the fluorescence intensity map and line plot, the fluorescence intensity was decreased in the center of the circles compared to the periphery.

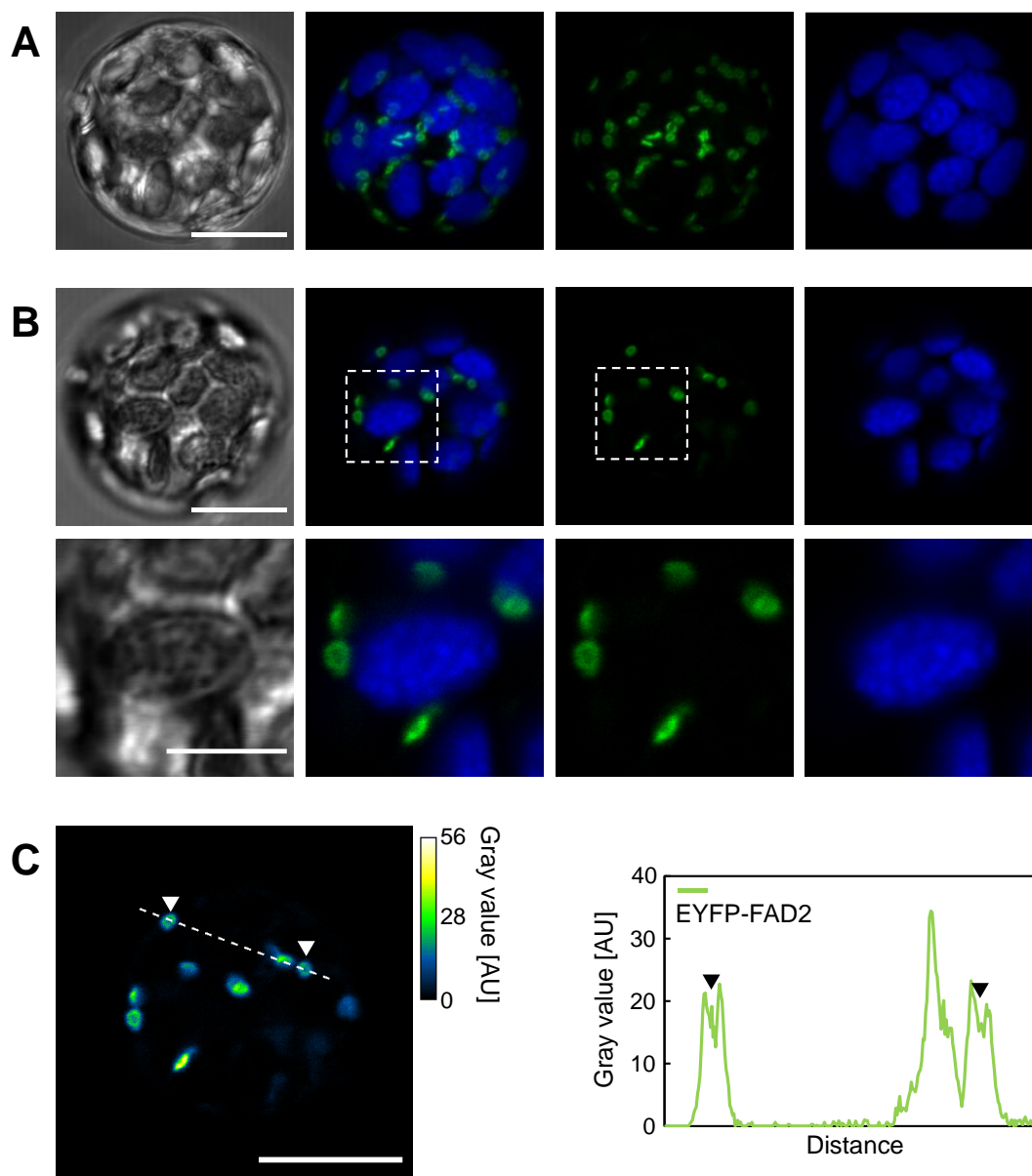


Figure 3.9. Subcellular distribution of EYFP-FAD2 in Arabidopsis mesophyll protoplasts. Protoplasts from *A. thaliana* Col-0 were transformed with *pEntryA-pFAD2::EYFP-FAD2* and analyzed by LSM. Z-stacks covering the cell from one edge to the center were generated with approx. 0.6 μm distance between the slices. EYFP-FAD2 fluorescence is depicted in green, the autofluorescence of chlorophyll A is shown in blue. Scale bars: 10 μm . **A**, Maximum intensity Z-projection of a Z-stack. **B**, Selected single slice of the Z-stack from A. Scale bars: 10 μm (upper panels), 5 μm (lower panels). **C**, Intensity profile for EYFP-FAD2 along the line highlighted in the left panel (slice of the image stack from panel A). Images and analyses are representative for two independent experiments using a total of 15 cells.

The fluorescence distribution pattern in Arabidopsis protoplasts expressing EYFP-FAD2 was comparable to the localization pattern of EYFP-FAD2 in the leaf epidermal cells in stable transformed plant lines (compare Figure 3.9 and Figure 3.7B). To rule out an effect of the EYFP fluorescence protein on the subcellular distribution of the EYFP-FAD2 fusion, the distribution of an mCherry-FAD2 fusion was also analyzed in protoplasts. Representative images are shown in the appendix in Figure 7.1. Figure 7.1A depicts a

maximum intensity Z-projection, Figure 7.1B shows a single confocal plane. mCherry-fluorescence is illustrated in magenta. Importantly, mCherry-FAD2 also decorated donut-shaped particulate structures in a pattern comparable to that of EYFP-FAD2. Thus, the nature of the fluorescence tag did not influence the localization of the fluorescent FAD2 fusions to small circular structures.

To assess the integrity of fluorescent fusions of FAD2, immunodetection of EYFP-FAD2 and mCherry-FAD2 expressed in protoplasts was performed. Proteins from transformed and untransformed protoplasts were separated by SDS-PAGE according to their molecular weight, blotted on membranes and immunodetected using antibodies against GFP or against mCherry, respectively (described in sections 5.18 and 5.19). The results are shown in the appendix in Figure 7.2. Signals were detected at 55 kDa, which is smaller than the expected molecular weight of 69 kDa and 71 kDa for EYFP-FAD2 and mCherry-FAD2, respectively. Free EYFP and mCherry alone have a molecular weight of 27 kDa and 29 kDa, respectively. No proteins were detected at the molecular size of free fluorescence proteins. Proteins from untransformed protoplasts did not result in any signal detection in the western blots. It is therefore assumed that EYFP-FAD2 and mCherry-FAD2 migrated smaller than their expected size and that the observed fluorescence signal originated from full-length fusion proteins.

To next assess the identity of the circular structures decorated by fluorescent fusions of FAD2, colocalization experiments with different organelle markers were performed. Arabidopsis mesophyll protoplasts coexpressing EYFP-FAD2 and various organelle markers were analyzed by LSM. To quantify the degree of colocalization with the individual markers, Pearson's correlation coefficients (PCC) were calculated based on the generated Z-stacks using the Fiji plugin JACoP (Bolte and Cordelières, 2006) as described in section 5.23.3. PCCs analyze the linear relation of two fluorescence images in scatter plots and can range from -1 to 1 with -1 reflecting perfect, linear, inverse relation and 1 indicating perfect, linear correlation of the fluorescence intensities of two channels (Bolte and Cordelières, 2006; Dunn et al., 2011).

To assess the technical limitations of this method, the ER marker *CD3-959-ER-mCherry* (Nelson et al., 2007, see section 5.16) was first transformed into Arabidopsis mesophyll protoplasts derived from the Arabidopsis ER marker line GFP-HDEL (fluorescence is termed ER-GFP), and the PCC was determined as a positive control for further colocalization experiments. The ER marker ER-mCherry consists of the fluorescence protein mCherry with the addition of the C-terminal ER-retention motif HDEL and the signal peptide of *AtWAK2* at the N-terminus (Nelson et al., 2007). Representative images and quantifications are shown in the appendix in Figure 7.3. ER-GFP fluorescence is depicted

in green, ER-mCherry fluorescence is depicted in magenta. Both fluorescence signals colocalized by eye, visible in single confocal slices and Z-projection (appendix Figure 7.3A). The quantification of the colocalization by calculating PCCs confirmed the colocalization of both ER markers. The PCC for both ER markers reached approx. 0.8 on average in comparison to 0.4 when correlating each ER marker to the autofluorescence of chlorophyll A (appendix Figure 7.3B). The difference of the PCCs determined for ER/ER vs ER/plastid comparisons was statistically significant ($p < 0.05$). Alternative analysis of the two ER markers according to their fluorescence intensity distribution along the indicated line in a line plot (appendix Figure 7.3C) also indicates closely resembling distribution patterns for the two ER markers. Based on these control experiments, the respective relative distribution patterns of EYFP-FAD2 vs. different organelle markers were analyzed.

FAD2 is thought to contain a C-terminal ER retention signal and to localize to the ER in root cells of different plants (onion epidermal cells: McCartney et al., 2004, BY-2 cells: Dyer and Mullen, 2001; Arabidopsis root cells: Nguyen et al., 2019). Therefore, the association of EYFP-FAD2 with the ER was first tested, even though the donut-shaped distribution pattern observed in leaves and mesophyll protoplasts did not obviously resemble ER-association. EYFP-FAD2 was expressed under its endogenous promoter in Arabidopsis mesophyll protoplasts together with the ER marker ER-mCherry. Z-stack images were generated as described (section 5.23.1) and PCCs calculated. Representative images and the quantification of the colocalization are shown in Figure 3.10A-C. EYFP-FAD2 fluorescence is depicted in green, the ER marker is shown in magenta. While EYFP-FAD2 was again seen in circular structures, the ER marker formed a diffuse network throughout the cytosol (Figure 3.10A), as would be expected for ER. The PCC of EYFP-FAD2 against the ER ranged between 0.4 and 0.8 with a mean of 0.6. The average PCC was slightly lower than the PCC observed for two ER markers (compare to Figure 7.3B) but was significantly higher ($p < 0.05$) than the correlation of EYFP-FAD2 or ER-mCherry against the autofluorescence of chlorophyll A. Evidently, the subcellular localization patterns of EYFP-FAD2 and the ER marker did not fully coincide. Importantly, the synchronous imaging of the donut-shaped EYFP-FAD2 pattern and the more diffuse ER marker indicates that the EYFP-FAD2 distribution is not merely a reflection of an unusual appearance of the ER, for instance as fusiform bodies induced by stress or development (e.g., Yamada et al., 2011). Instead, the particulate distribution of EYFP-FAD2 appeared together with a diffuse distribution of the ER marker. To assess the spatial relationship between the two markers in more detail, in Figure 3.10C a line plot of EYFP-FAD2 and ER-mCherry is shown. Despite the overall lower fluorescence intensity of EYFP-

FAD2, high intensity values of EYFP-FAD2 fluorescence correlated with high fluorescence intensity of ER-mCherry. Thus, even though EYFP-FAD2 was not evenly distributed throughout the ER, the punctuate structures marked by EYFP-FAD2 nonetheless probably associated with the ER network.

Based on the appearance of the localization pattern of EYFP-FAD2, a localization to Golgi stacks was hypothesized and the distribution of EYFP-FAD2 was tested relative to a coexpressed Golgi marker. As Golgi marker, mCherry with the N-terminal addition of the first 49 amino acids from α -1,2-mannosidase I from *Glycine max.* (*GmMan1*) was used (Saint-Jore-Dupas et al., 2006; Nelson et al., 2007, Golgi-mCherry). *GmMan1* has previously been observed to localize to the *cis*-cite of Golgi stacks (Saint-Jore-Dupas et al., 2006). Arabidopsis protoplasts coexpressing EYFP-FAD2 and Golgi-mCherry were analyzed with LSM or SD. A representative Z-projection taken with the spinning disc microscope as described in section 5.23.2 is presented in Figure 3.10D. EYFP-FAD2 as well as the Golgi marker localized to the same circular structures or short lines. PCCs were calculated from Z-stacks generated by LSM. The resulting values ranged from 0.5 to 0.8 with a mean of 0.66 for the correlation of EYFP-FAD2 and the Golgi marker (Figure 3.10E). The correlation coefficients against the autofluorescence of chlorophyll A were significantly lower ($p < 0.05$). The PCC for the colocalization of EYFP-FAD2 and Golgi-mCherry was slightly higher than for the colocalization of EYFP-FAD2 with the ER marker and less scattered (compare to Figure 3.10B), but still did not reach the value of 0.8 seen for the colocalization of two ER markers (compare to appendix Figure 7.3B). The side-by-side assessment of fluorescence distribution patterns for EYFP-FAD2 and the Golgi marker indicates a clear and obvious similarity (e.g., Figure 3.10B). The rather low PCCs for the coexpressed EYFP-FAD2/Golgi markers (Figure 3.10E), when compared to the ER/ER relations (appendix Figure 7.3), might be a consequence of the high mobility of the protoplasts and the particulate structures during live imaging. A line plot analyzed from an SD image illustrates a high concurrence of EYFP-FAD2 and Golgi-mCherry fluorescence (Figure 3.10E). The circular structures marked by EYFP-FAD2 are regarded as Golgi stacks seen in face-on views with an appearance as short lines when imaged from the side, suggesting a flattened disc shape (Nebenführ et al., 1999).

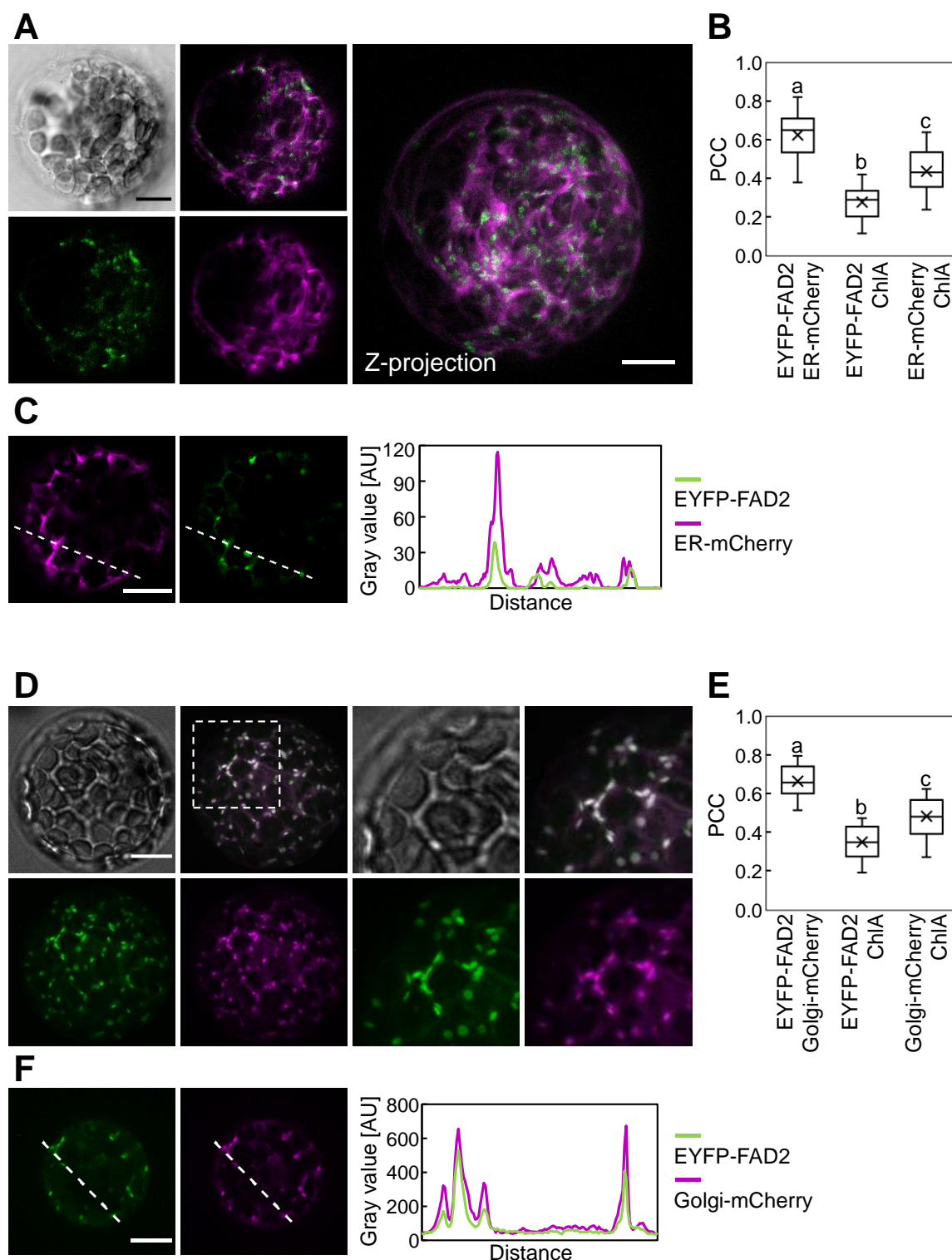


Figure 3.10. Subcellular distribution of EYFP-FAD2 relative to the ER and the Golgi in Arabidopsis mesophyll protoplasts. Protoplasts from *A. thaliana* Col-0 were cotransformed with *pEntryA-pFAD2::EYFP-FAD2* and either the ER marker construct *CD3-959-ER-mCherry* (**A-C**) or the Golgi marker construct *CD3-967-Golgi-mCherry* (**D-F**) and analyzed by LSM or SD. Z-stacks covering the cell from one edge to the center were generated with approx. 0.6 μm distance. EYFP-FAD2 fluorescence is depicted in green, the organelle markers in magenta. Scale bars: 10 μm ; ChlA, chlorophyll A. **A**, Coexpression of EYFP-FAD2 with an ER marker (ER-mCherry) analyzed by LSM. **B+E**, Pearson's correlation coefficients (PCCs) were calculated based on 22 (EYFP-FAD2+ER marker, B) or 14 (EYFP-FAD2+Golgi marker, E) Z-stacks taken by LSM from two independent experiments, respectively. Significant differences were determined using one-way ANOVA with a Tukey's post-hoc test ($p < 0.05$). Letters indicate categories of significantly different samples.

C, Intensity profile for EYFP-FAD2 and the ER marker along the line highlighted in the left panels. **D**, Coexpression of EYFP-FAD2 with a Golgi marker (Golgi-mCherry). The images shown were taken by SD for faster image acquisition. **F**, Intensity profile for EYFP-FAD2 (green) and the Golgi marker (magenta) along the line highlighted in the left panels. The image shown was taken by SD. Images are representative for two independent experiments using 22 (A-C) or 14 (D-F) cells.

To further elucidate the nature of the localization of EYFP-FAD2 to Golgi stacks and the ER, the relations of EYFP-FAD2-marked Golgi with the ER were analyzed. The goal of these experiments was to clarify whether EYFP-FAD2-marked Golgi particles occurred independently of the ER. The Fiji-plugin “Colocalization” marks colocalizing pixels fulfilling the set thresholds and ratio as white pixels, allowing an easy visual evaluation of colocalization (Bourdoncle, 2003). A representative image of the coexpression of EYFP-FAD2 and ER-mCherry is shown in Figure 3.11A. EYFP-FAD2 fluorescence is depicted in green, red illustrates ER-mCherry fluorescence. White colocalizing pixels are seen encircling each EYFP-FAD2-marked Golgi stack indicating that Golgi stacks are surrounded by ER. In 24 analyzed Z-stack images no EYFP-FAD2-marked Golgi was seen independently of ER-mCherry.

During the imaging of EYFP-FAD2 in *Arabidopsis* mesophyll protoplasts and leaf epidermal cells, EYFP-FAD2 fluorescence was often visible as hollow donut-like shapes, whereas this hollow shape was not observed for the marker Golgi-mCherry. This difference was confirmed by line plots derived from SD images (Figure 3.11B). The fluorescence intensity of Golgi-mCherry (red) reached a maximum in the middle of the Golgi stack in face-on views. EYFP-FAD2 fluorescence intensity (green) slightly decreased in the center of the Golgi stack compared to the periphery (indicated by the arrows). The dimensions of the EYFP-FAD2 marked structures and Golgi-mCherry marked structures coincided well, both in face-on views and in side views, respectively (Figure 3.11B).

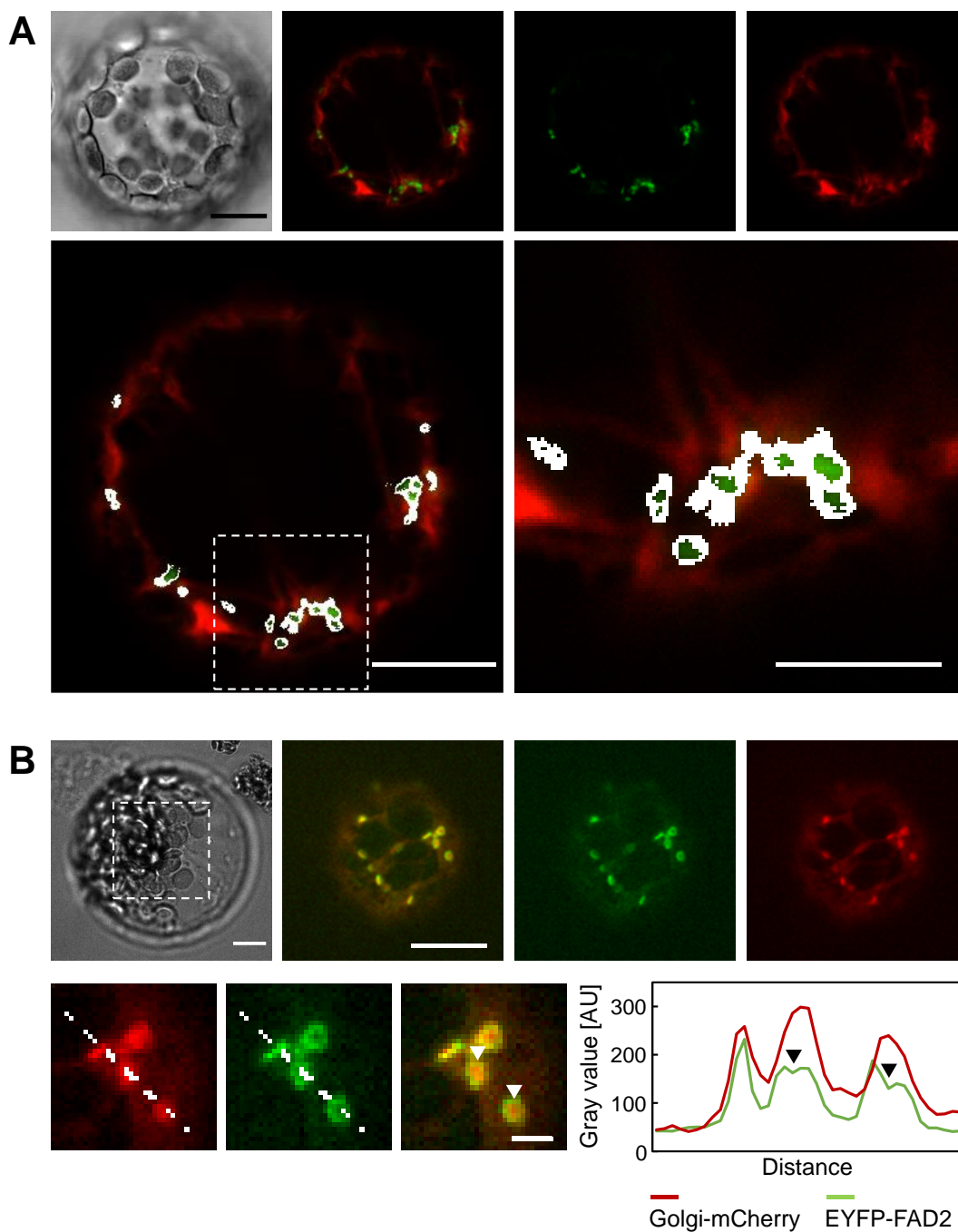


Figure 3.11. Detailed analysis of the subcellular distribution of EYFP-FAD2 relative to the ER and to Golgi stacks. Mesophyll protoplasts from *A. thaliana* Col-0 were cotransformed with *pEntryA-pFAD2::EYFP-FAD2* and either the ER marker construct *CD3-959-ER-mCherry* (A) or the Golgi marker construct *CD3-967-Golgi-mCherry* (B). EYFP-FAD2 fluorescence is depicted in green, the respective organelle markers in red. Selected single confocal planes from Z-stacks are shown. Scale bars: 10 μ m. **A**, Relative localization of EYFP-FAD2 with the ER marker in protoplasts analyzed by LSM. Colocalizing pixels (white) were highlighted using the Fiji plugin “Colocalization” with the following settings: ratio: 50, threshold for the green and red channel: 10. **B**, Relative localization of EYFP-FAD2 with the Golgi marker in protoplasts analyzed by SD. The graph shows the fluorescence intensity distribution along the illustrated line. Scale bar in the line plot images: 2 μ m. Arrowheads in the line plot in panel B (bottom right) indicate the lack of green fluorescence in the center of the “donuts” decorated by EYFP-FAD2, a pattern not reflected by the corresponding red fluorescence pattern of the Golgi marker. Images are representative for 24 cells (A) or 15 cells (B) analyzed in three (A) or one (B) independent experiments.

To assess whether the observed colocalization of EYFP-FAD2 with the Golgi marker was coincidental, further experiments were performed, in which EYFP-FAD2 was coexpressed with peroxisome- and oil-body-markers, two other mainly circular cell organelles. The relative distribution of EYFP-FAD2 and peroxisomes was assessed using peroxisome-targeted CFP (CFP-SKL), as shown in Figure 3.12A-C. A single confocal slice and a detailed image are presented in Figure 3.12A with EYFP-FAD2 fluorescence depicted in green and the peroxisome marker depicted in magenta. CFP-SKL marked circular structures of a similar size as EYFP-FAD2, but both fluorescence signals did not palpably colocalize. The PCCs for the correlation of EYFP-FAD2 and CFP-SKL ranged from 0.25 to 0.67 with a mean of 0.46 and were not significantly different ($p > 0.05$) from the values obtained for EYFP-FAD2 vs. chlorophyll A (Figure 3.12B). This supports that EYFP-FAD2 did not colocalize with CFP-SKL. The line plot presented in Figure 3.12C also illustrates the incongruent fluorescence distribution of EYFP-FAD2 and CFP-SKL.

As an oil body marker, Oleosin3 (OLE3) fused to mCherry was used. Similar to coexpression of EYFP-FAD2 and CFP-SKL, OLE3-mCherry (magenta) and EYFP-FAD2 (green) both localized in circular structures of approximately similar size but without obvious colocalization. The structures marked by OLE3-mCherry varied more in size than EYFP-FAD2 signals. A representative maximum intensity Z-projection and a detailed image of a single confocal slice are presented in Figure 3.12D. The PCCs depicted in Figure 3.12E for EYFP-FAD2 vs. OLE3-mCherry ranged from 0.05 to 0.67 with a mean of 0.34 and were not significantly different ($p > 0.05$) from both correlations to ChlA. A line plot of EYFP-FAD2 and OLE3-mCherry fluorescence distribution was analyzed in Figure 3.12F and illustrates the previous findings of EYFP-FAD2 fluorescence and OLE3-mCherry fluorescence not correlating with each other.

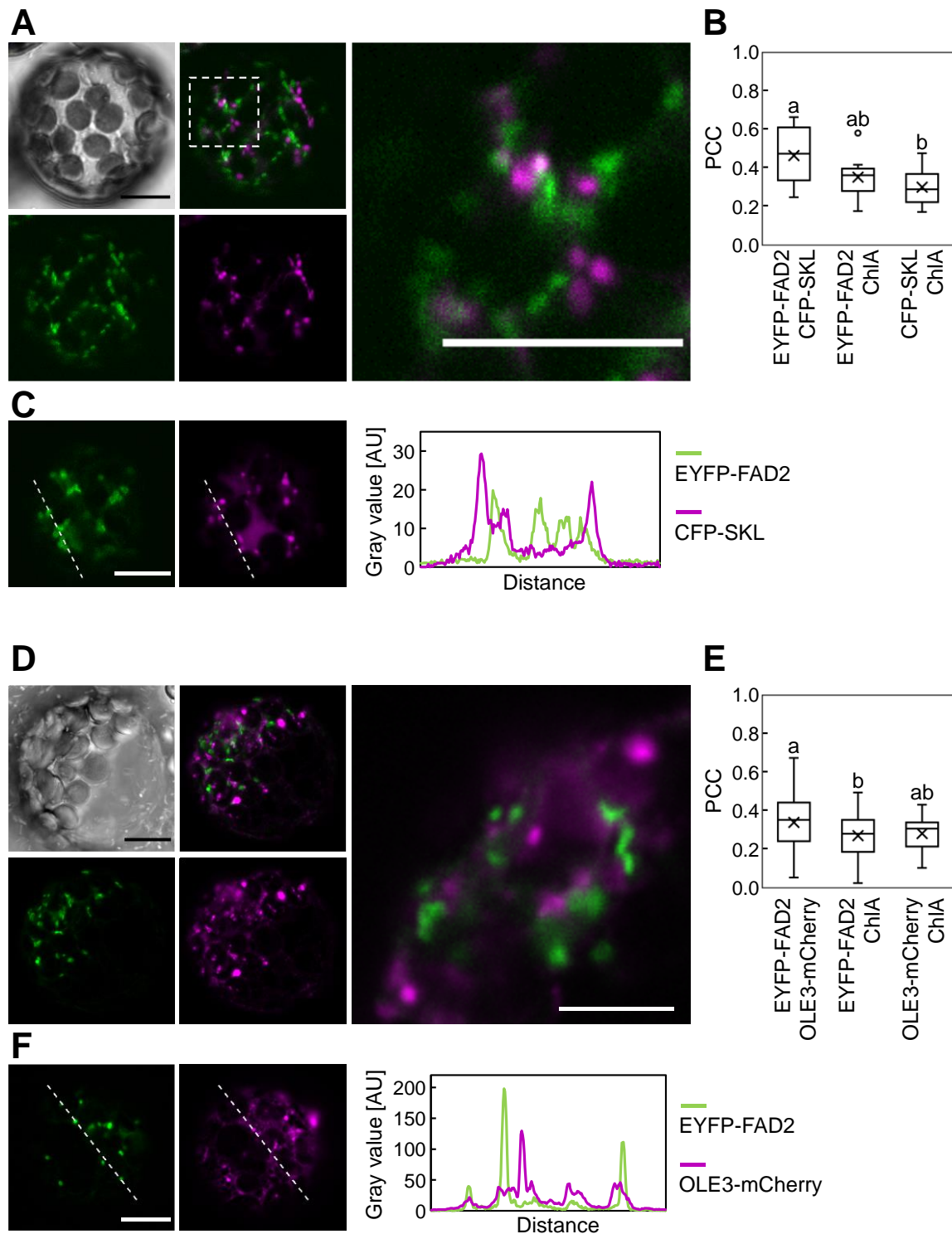


Figure 3.12. Subcellular distribution of EYFP-FAD2 relative to peroxisomes and oil bodies in *Arabidopsis mesophyll* protoplasts. Protoplasts from *A. thaliana* Col-0 were cotransformed with *pEntryA-pFAD2::EYFP-FAD2* and either the peroxisome marker construct *pEntryD-pCaMV35S::CFP-SKL* (**A-C**) or the oil body marker construct *pCAMBIA3300.0GS-pCaMV35S::OLE3-mCherry* (**D-F**). Z-stacks covering the cell from one edge to the center with approx. 0.6 μm distance between the slices were generated by LSM. EYFP-FAD2 fluorescence is depicted in green, the respective organelle markers in magenta. Scale bars: 10 μm . Significant differences were determined using one-way ANOVA with a Tukey's post-hoc test ($p < 0.05$). Letters indicate categories of significantly different samples. **A**, Coexpression of EYFP-FAD2 with a peroxisome marker (CFP-SKL). A single confocal slice is shown. **B**, Pearson's correlation coefficients (PCCs) between EYFP-FAD2 and the peroxisomal marker or chlorophyll A (ChlA) were calculated based on 10 Z-stacks acquired by LSM. **C**, Intensity profile for EYFP-FAD2 (green) and the peroxisome-marker (magenta) along the

line highlighted in the left panels. **D**, Coexpression of EYFP-FAD2 with OLE3-mCherry (oil body marker). A maximum intensity Z-projection is shown. The detail image (right) represents a merged image from a single confocal plane. **E**, PCCs between EYFP-FAD2 and the OLE3-mCherry or ChIA were calculated based on 33 Z-stacks from three independent experiments acquired by LSM. Two of three experiments were performed by Georg Steinert (master's student). **F**, Intensity profile for EYFP-FAD2 (green) and the oil body marker (magenta) along the line highlighted in the left panels. Images are representative for one (A-C) or three (D-F) independent experiments using a total of 10 (A-C) or 33 (D-F) cells.

In addition to the calculation of PCCs to assess the relative fluorescence distribution patterns of various markers, Manders' colocalization coefficients (MCC) were also calculated for selected experiments. Other than the PCCs, the MCCs indicate the fraction of fluorescence signal that overlaps another fluorescence signal and vice versa. Therefore, for one coexpression experiment, two coefficients can be calculated (see section 5.23.3). MCCs are independent of signal proportionality and rather evaluate the spatial coincidence of two fluorescence signals (Dunn et al., 2011). The results of these additional analyses are shown in the appendix in Figure 7.4. As for PCCs (appendix Figure 7.3), the MCCs for two ER markers were calculated to obtain a positive control (appendix Figure 7.4A). The MCCs for ER-mCherry overlapping ER-GFP and vice versa were both in a similar high range with mean values of 0.76 and 0.8, respectively, illustrating a high spatial coincidence of these markers, as expected. As a negative control, the MCCs for EYFP-FAD2 coexpressed with CFP-SKL were calculated. Both corresponding MCC values were low, with 0.31 and 0.23, respectively (appendix Figure 7.4B). These values support the previous observation of an incongruent localization of EYFP-FAD2 and peroxisomes. The MCCs for EYFP-FAD2 vs. ER-mCherry were high, with an average of 0.83, indicating spatial coincidence of EYFP-FAD2 with the ER marker, despite an overall dissimilar pattern. By contrast, only a small fraction (MCC of 0.37) of ER-mCherry signal overlapped with the EYFP-FAD2 signal, leading to the conclusion that the EYFP-FAD2-marked Golgi stacks distribute in a different pattern than the ER marker, but are all overlapping with the ER-network, which itself is further spread throughout the cell.

For the calculation of MCCs for colocalization of EYFP-FAD2 with the Golgi marker, individual thresholds were manually chosen for each image, so that for the Golgi marker only the fluorescence intensity in circular Golgi stacks was considered. Thus, weak ER-labeling sometimes observed for the Golgi marker was excluded. The calculated MCCs revealed that a fraction of approx. 0.69 of EYFP-FAD2 signal coincided with the Golgi marker, while only a fraction of 0.33 of the Golgi marker cooccurred with EYFP-FAD2 fluorescence (appendix Figure 7.4.D). This notion is consistent with the observation that EYFP-FAD2 did not colocalize evenly with all Golgi signals and that the Golgi marker decorated further signal that were not at the same time decorated by EYFP-FAD2 (hollow circles from EYFP-FAD2 fluorescence vs. filled circles from the Golgi marker).

Taken together, EYFP-FAD2 displayed an equivalent subcellular distribution pattern in mesophyll protoplast experiments as it was observed in leaf epidermal cells. The analysis of different coexpressed organellar markers indicates that EYFP-FAD2 mostly colocalized with the *cis*-Golgi marker, as supported by high PCC and MCC values for spatial correlation. Furthermore, coexpression of EYFP-FAD2 with an ER marker also revealed high PCC and MCC values, highlighting that EYFP-FAD2-marked Golgi stacks were in close proximity to the ER-network. By contrast, EYFP-FAD2 did not colocalize with markers for peroxisomes or for oil bodies, as indicated by low values for the corresponding PCC and MCC analyses, demonstrating that the EYFP-FAD2 distribution in relation to Golgi stacks was not coincidental.

3.5 FAD3 associated with the ER of Arabidopsis mesophyll protoplasts

As Arabidopsis protoplasts were successfully used to investigate the subcellular distribution of fluorescence-tagged FAD2 fusions relative to various organellar markers, equivalent experiments were initiated to also assess the subcellular distribution of fluorescence-tagged FAD3. The subcellular localization of mCherry-FAD3 was analyzed in mesophyll protoplasts of Arabidopsis wild type plants first without interference of an organelle marker. Figure 3.13A shows the distribution of mCherry-FAD3 in a single confocal plane acquired by LSM. mCherry-FAD3 fluorescence is depicted in magenta, ChlA-autofluorescence in blue. In contrast to the distribution of EYFP-FAD3 seen in leaf epidermal cells in the complemented *fad3-2* mutant plants (compare Figure 3.8B), in the protoplasts mCherry-FAD3 was more evenly distributed throughout a network in the cytoplasm.

FAD3 has previously been shown to possess a C-terminal ER-retention motif (McCartney et al., 2004), and therefore the distribution of mCherry-FAD3 was next assessed relative to a coexpressed ER marker. Mesophyll protoplasts from the Arabidopsis ER marker line GFP-HDEL (ER-GFP) transiently expressing mCherry-FAD3 were analyzed by LSM. Figure 3.13B shows a representative single confocal plane and a maximum intensity Z-projection. The ER-GFP fluorescence is shown in green, mCherry-FAD3 is depicted in magenta. Both fluorescence fusion proteins showed a similar network-like distribution throughout the cell. PCCs were calculated based on Z-stack images acquired by LSM. The PCC values for mCherry-FAD3 vs. ER-GFP ranged from 0.6 to almost 1, with a mean of approx. 0.8 (Figure 3.13C). At an average, these values were similar to those obtained for the correlation of two bona fide ER markers (compare appendix Figure 7.3B) and significantly higher ($p < 0.05$) than the PCCs obtained for either mCherry-FAD3 or ER-GFP vs. the autofluorescence of ChlA. The line plot shown in Figure 3.13D further

illustrates colocalization of mCherry-FAD3 with the ER-maker. Please note that the mCherry-FAD3 distribution resembled that of the ER marker, even though the overall fluorescence intensity of mCherry-FAD3 was comparably low. Equivalent experiments were performed using EYFP-tagged FAD3 coexpressed with ER-mCherry in wild type protoplasts, and these experiments additionally confirmed localization of EYFP-FAD3 at the ER (appendix Figure 7.5).

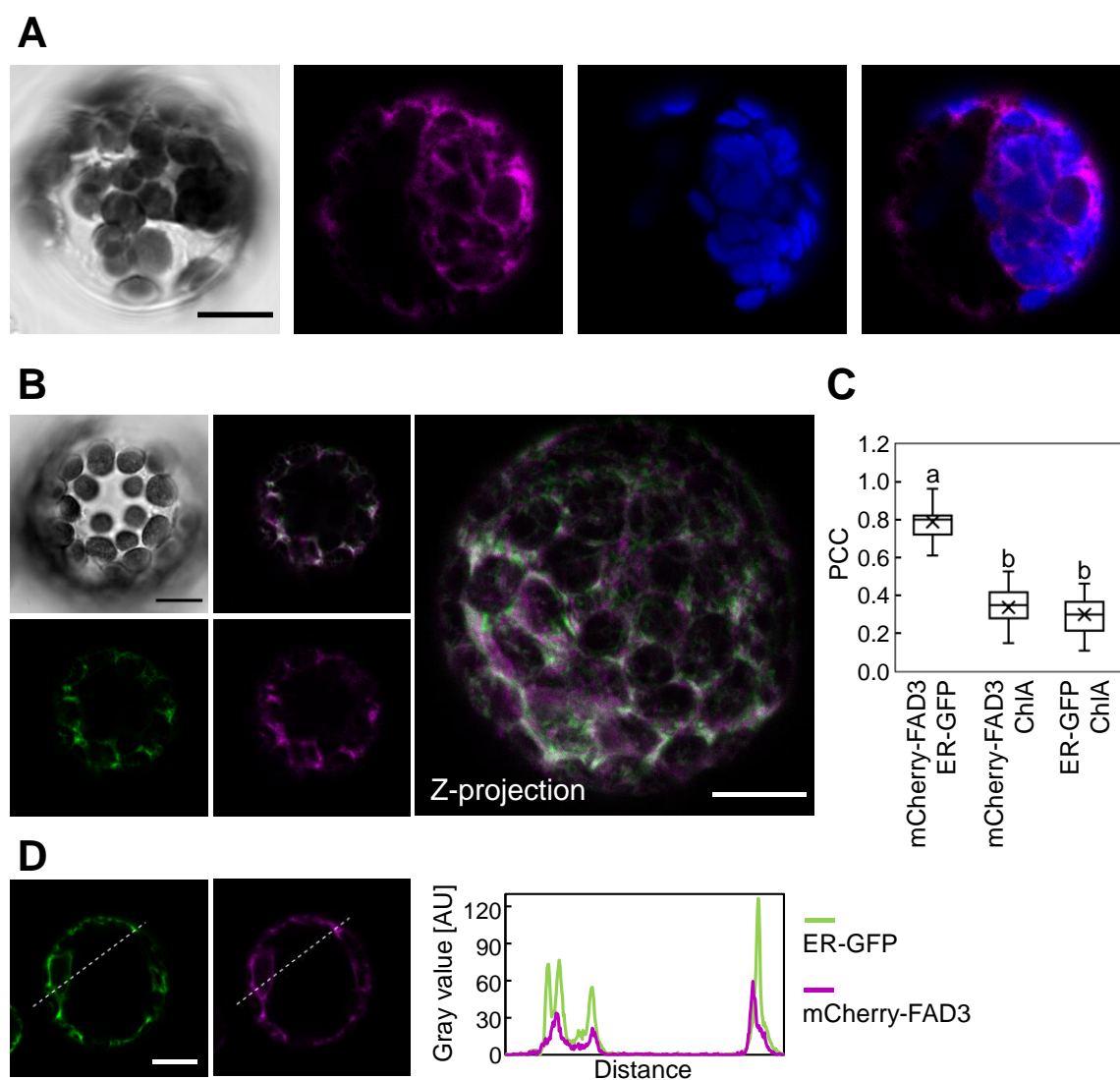


Figure 3.13. Subcellular distribution of mCherry-FAD3 in Arabidopsis mesophyll protoplasts. Protoplasts from *A. thaliana* Col-0 or GFP-HDEL were transformed with *pEntryA-pCaMV35S::mCherry-FAD3* and analyzed by LSM. Z-stacks covering the cell from one edge to the center with approx. 0.6 μm distance between the slices were generated. Magenta, mCherry-FAD3 fluorescence; green, ER-GFP; blue, chlorophyll A (ChlA) autofluorescence. Scale bar: 10 μm . **A**, *A. thaliana* Col-0 protoplasts expressing mCherry-FAD3. Depicted is a single confocal plane. **B**, Protoplast from *A. thaliana* GFP-HDEL expressing mCherry-FAD3 for colocalization analyses. **C**, PCCs between mCherry-FAD3 and the ER marker GFP-HDEL or ChlA were calculated based on 11 Z-stacks acquired by LSM. Significant differences were determined using one-way ANOVA with a Tukey's post-hoc test ($p < 0.05$). Letters indicate categories of significantly different samples. **D**, Intensity profile for mCherry-FAD3 (magenta) and ER-GFP (green) along the line highlighted in the left panels. Images are representative for single experiments using 10 (A) or 11 (B-D) cells.

3.6 Partial colocalization of FAD2 and FAD3 in Arabidopsis mesophyll protoplasts

FAD2 and FAD3 are known to interact with each other and to cooperate metabolically through substrate channeling (Lou et al., 2014). Therefore, experiments with EYFP-FAD2 and mCherry-FAD3 were performed in Arabidopsis mesophyll protoplasts to assess their relative subcellular distribution upon coexpression. Figure 3.14A shows representative images from these analyses, with EYFP-FAD2 fluorescence depicted in green and mCherry-FAD3 fluorescence in magenta. As seen in previous localization experiments, EYFP-FAD2 localized to punctuate structures identified as Golgi stacks along a network marked by mCherry-FAD3 fluorescence resembling the ER network. Accordingly, the PCCs resembled the values for the colocalization of EYFP-FAD2 with the ER marker ranging from 0.5 to 0.86 with a mean of 0.63 (compare Figure 3.14B and Figure 3.10B in section 3.4). The line plot depicted in Figure 3.14C illustrates the colocalization of EYFP-FAD2 marked Golgi stacks with mCherry-FAD3 at the ER. High intensity peaks corresponding to EYFP-FAD2 cooccurred with high intensity peaks of mCherry-FAD3 fluorescence. To confirm the spatial association of EYFP-FAD2 with the network marked by mCherry-FAD3, images were further evaluated using the Fiji plugin “Colocalization” (see section 5.23.3 and 3.4). A selected single confocal plane and a maximum intensity Z-projection are depicted in Figure 3.14D. As for the coexpression of EYFP-FAD2 with the ER marker, no Golgi stacks marked by EYFP-FAD2 fluorescence were detected without association to the mCherry-FAD3 network. To assess whether the intermediate PCCs resulted from a partial colocalization, MCCs were calculated and are presented in Figure 3.14E. On average a fraction of 0.8 of the pixels showing EYFP-FAD2 fluorescence coincided with mCherry-FAD3 fluorescence. Inversely, on average a fraction of less than 0.5 of mCherry-FAD3 fluorescence cooccurred with EYFP-FAD2 fluorescence, which is consistent with the general localization of mCherry-FAD3 to the whole ER network. Even though FAD2 and FAD3 localized to different organelles, partial colocalization at Golgi-ER-interaction sites was visible in Arabidopsis mesophyll protoplasts.

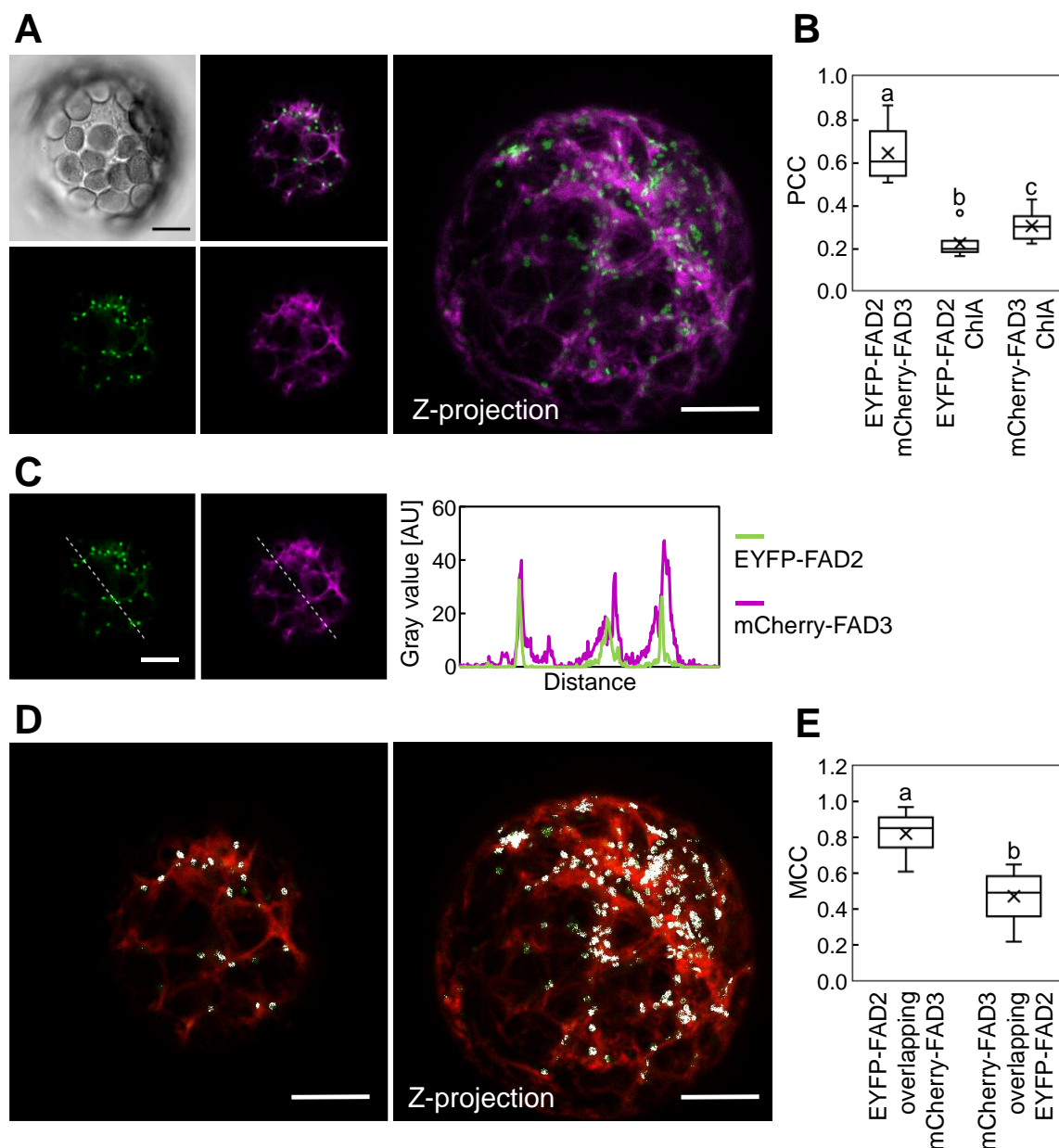


Figure 3.14. Relative subcellular distribution of EYFP-FAD2 and mCherry-FAD3 in *Arabidopsis* mesophyll protoplasts. Protoplasts from *A. thaliana* Col-0 were cotransformed with *pEntryA-pFAD2::EYFP-FAD2* and *pEntryA-pCaMV35S::mCherry-FAD3* and analyzed by LSM. Z-stacks covering the cell from one edge to the center were acquired with approx. 0.6 μm distance between the slices. EYFP-FAD2 fluorescence is depicted in green, mCherry-FAD3 fluorescence in magenta (**A-C**) or red (**D**). Scale bar: 10 μm ; ChlA, chlorophyll A. **A**, Single confocal plane and maximum intensity Z-projection of the relative localization of EYFP-FAD2 and mCherry-FAD3. **B**, Pearson's correlation coefficients (PCCs) were calculated based on 14 Z-stacks taken by LSM. Significant differences were determined using one-way ANOVA with a Tukey's post-hoc test ($p < 0.05$). Letters indicate categories of significantly different samples. **C**, Intensity profile for EYFP-FAD2 (green) and mCherry-FAD3 (magenta) along the line highlighted in the left panels. **D**, Relative localization of EYFP-FAD2 (green) and mCherry-FAD3 (red) in a single confocal plane (left) and maximum intensity Z-projection (right). Colocalizing pixels (white) were highlighted using the Fiji plugin "Colocalization" with the following settings: ratio: 50; threshold for the green channel (EYFP-FAD2): 5; threshold for the red channel (mCherry-FAD3): 10. **E**, Manders' colocalization coefficients (MCCs) were calculated from the same set of images used for PCCs. Individual thresholds were chosen for each image and channel to omit background signals. Significant differences were determined using one-way ANOVA with a Tukey's post-hoc test ($p < 0.05$). Letters indicate categories of significantly different samples. Images are representative for one experiment using 14 cells.

3.7 Coexpression of the transcription factor WRINKLED1 enables detection of mCherry-FAD3 expressed from its intrinsic promoter in Arabidopsis mesophyll protoplasts

The previously described experiments assessing the subcellular distribution of EYFP-FAD3 or mCherry-FAD3 were all performed using the *pCaMV35S* promoter to drive gene expression, thereby overexpressing the fluorescence-tagged FAD3 variants. The *pCaMV35S*-driven regime had been chosen because no fluorescence was observed in protoplasts upon expression of mCherry-FAD3 driven by an intrinsic *FAD3* promoter fragment consisting of 1,632 bp upstream of the *FAD3* start-codon. Since the linolenic acid produced by FAD3 is found mostly in the seed oil of Arabidopsis, and in green tissues the plastidial desaturases FAD7 and FAD8 contribute the majority of cellular linolenic acid (Browse et al., 1993), it is possible that FAD3 plays a major role mainly during seed filling. As mesophyll cells do not produce large amounts of TAG under normal conditions, the localization of FAD3 could differ in oleogenic tissues from the observed pattern. In oleogenic plant tissues, oil biogenesis is orchestrated by the master-regulatory transcription factor WRINKLED1 (WRI1, Chapman and Ohlrogge, 2012). To mimic a state of oil biosynthesis in Arabidopsis mesophyll protoplasts and therefore probably enabling the expression of FAD3 from its intrinsic promoter, *pFAD3::mCherry-FAD3* was coexpressed with the transcription factor WRI1 tagged with EYFP (WRI1-EYFP).

pFAD3::mCherry-FAD3 was cloned together with *pCaMV35S::CFP-SKL* as transformation control or a cassette for the expression of WRI1-EYFP (*pCaMV35S::WRI1-EYFP*) on the same vector backbone (*pCambia3300.0GS*). The constructs were transformed in Arabidopsis mesophyll protoplasts and analyzed by LSM (see sections 5.13.4, 5.16 and 5.23). Figure 3.15 shows representative images from these analyses, with mCherry-FAD3 fluorescence depicted in magenta, CFP-SKL fluorescence in cyan and WRI1-EYFP fluorescence in green.

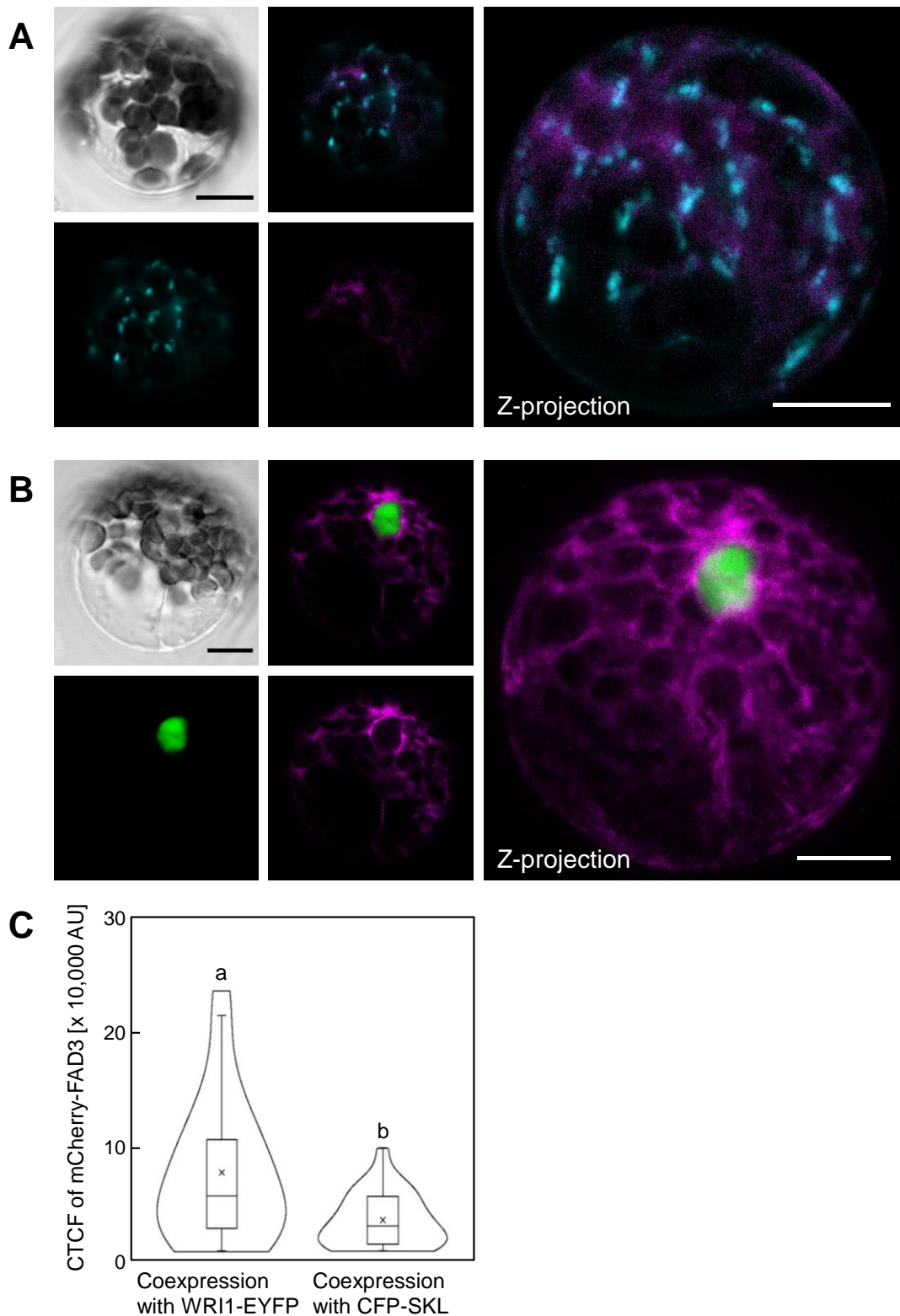


Figure 3.15. Subcellular distribution of mCherry-FAD3 driven by an intrinsic promoter fragment upon coexpression with WRI1-EYFP. Mesophyll protoplasts from *A. thaliana* Col-0 were transformed with *pCAMBIA3300.0GS-pFAD3::mCherry-FAD3-pCaMV35S::CFP-SKL* (A) or *pCAMBIA3300.0GS-pFAD3::mCherry-FAD3-pCaMV35S::WRI1-EYFP* (B) and analyzed by LSM. Z-stacks covering the cell from one edge to the center with approx. 1 μ m distance between the slices were acquired. mCherry-FAD3 fluorescence is depicted in magenta, WRI1-EYFP fluorescence in green. The peroxisomal marker CFP-SKL functions as a control for successful transformation and is depicted in cyan. For each construct, a single confocal plane and a maximum intensity Z-projection are shown. Images are representative for four

experiments using a total of 42 cells. Scale bars: 10 μm . **C**, Corrected total cell fluorescence (CTCF) of mCherry-FAD3 was measured from sum intensity Z-projections of cells expressing mCherry-FAD3 together with either WR11-EYFP or CFP-SKL. A total of 27 (coexpression with WR11-EYFP) and 22 (coexpression with CFP-SKL) cells from two independent experiments were used. Care was taken to use the same settings for image acquisition. Significant differences were determined using Kruskal-Wallis test ($p < 0.05$). Letters indicate categories of significantly different samples.

Whereas mCherry-FAD3 fluorescence was hardly detectable in control cells coexpressing a CFP-SKL control instead of WR11-EYFP (Figure 3.15A), protoplasts expressing WR11-EYFP showed mCherry-FAD3 fluorescence in network-like structures (Figure 3.15B). The network decorated by mCherry-FAD3 surrounded the nucleus, which was brightly marked by WR11-EYFP (Figure 3.15B). The subcellular distribution of mCherry-FAD3 under the control of its endogenous promoter was similar to that observed for mCherry-FAD3 driven by *pCaMV35S* (compare Figure 3.13A). To numerically confirm the impression of higher mCherry-FAD3 fluorescence intensity in cells coexpressing WR11-EYFP compared to control cells coexpressing CFP-SKL, the corrected total cell fluorescence (CTCF) was determined (see section 5.23.3) and is presented in Figure 3.15C. The CTCF of mCherry-FAD3 was significantly higher ($p < 0.05$) in protoplasts expressing the transcription factor than in the control cells expressing CFP-SKL.

To assess the integrity of mCherry-FAD3 and WR11-EYFP, the proteins were isolated from transformed *Arabidopsis* protoplasts, separated by SDS-PAGE according to their molecular weight, blotted to membranes and immunodetected using antibodies against mCherry or against GFP, respectively (see sections 5.18 and 5.19). The results are presented in the appendix in Figure 7.6. The mCherry-FAD3 fusion protein and WR11 tagged with EYFP had an expected molecular weight of 71 kDa and 76 kDa, respectively. However, by using the anti-mCherry antibody, protein signals were detected at a molecular weight of approx. 55 kDa (appendix Figure 7.6A). No signals were detected at the height of 29 kDa, the molecular weight of mCherry. As noticed for fluorescence-tagged FAD2 (see section 3.4 and Figure 7.2), mCherry-tagged FAD3 might migrate smaller than the expected molecular weight. Using the anti-GFP antibody, a protein signal above the height corresponding to 100 kDa was detected, which is larger than the expected size of WR11-EYFP (approx. 76 kDa). Again, no signal corresponding to EYFP (molecular weight: 27 kDa) was observed. Therefore, it is assumed that the observed fluorescence signals in protoplasts corresponded to full-length proteins of mCherry-FAD3 and WR11-EYFP, respectively.

The localization patterns of fluorescent FAD3-fusions in protoplasts differed from the subcellular distribution in transformed plant lines. Coexpression experiments revealed that in *Arabidopsis* mesophyll protoplasts FAD3 localized to the ER and partially colocalized with FAD2. The expression of FAD3 under its endogenous promoter was enhanced by

coexpression with the transcription factor for lipid biosynthesis WRI1, but this effect did not influence the subcellular distribution of fluorescence-tagged FAD3 fusions.

3.8 FAD2 and FAD3 interact with acyltransferases in yeast two-hybrid studies

Seed oil biogenesis is orchestrated by the master transcription factor WRI1, which enables the coordinated expression of factors required for seed oil biogenesis in the correct tissues and at the correct stages during Arabidopsis development (Chapman and Ohlrogge, 2012; Baud et al., 2007). As it was shown above (Figure 3.15), the fluorescence intensity of mCherry-FAD3 under the endogenous promoter was increased by coexpression of WRI1-EYFP in (non-oleogenic) Arabidopsis mesophyll protoplasts. These findings suggest that the interplay of fatty acid desaturases with other factors involved in oil biogenesis might contribute to the function of FAD2 and/or FAD3. Therefore, experiments were performed to identify other elements of the biological machinery for oil biogenesis that may influence the precise localization of FAD2 or FAD3 in membrane subdomains at the ER-Golgi continuum. The focus of these analyses was on possible interactions of FAD2 or FAD3 with key ER-associated acyltransferases with known roles in Arabidopsis oil biogenesis. FAD2 and FAD3 act on fatty acids that are mostly bound to the membrane lipid PC, and the unsaturated fatty acids produced by FAD2 and FAD3 are major components in the seed oil of Arabidopsis (Li-Beisson et al., 2010; Li et al., 2006). Arabidopsis seed oil consists of TAG, which is produced by transferring fatty acids from phospholipids or CoA onto DAG. These reactions are catalyzed by acyltransferases, such as PDAT, DGAT1 and DGAT2. While interaction and cooperative action in the form of substrate channeling were previously shown for FAD2 and FAD3 (Lou et al., 2014), an equivalent interplay of fatty acid desaturases with acyltransferases responsible for TAG formation remains largely to be elucidated.

To address possible links between desaturases and acyltransferases, yeast two-hybrid analyses were performed to test for interactions between FAD2 or FAD3 and the acyltransferases PDAT, DGAT1 or DGAT2. Since all proteins of interest possess transmembrane domains and are therefore integral membrane proteins, classical yeast two-hybrid systems testing for interactions between soluble proteins in the nucleus is not suitable, and instead a split-ubiquitin based yeast two-hybrid system was employed (Johnsson and Varshavsky, 1994). Moreover, previous studies showed that DGAT2 is not efficiently produced in yeast when the Arabidopsis cDNA sequence is transformed (Aymé et al., 2014). Therefore, a *DGAT2*-sequence optimized for the codon usage of yeast (*DGAT2_{opt}*) was used in these experiments. The yeast strain NMY51 was cotransformed

with bait and prey vectors as described in section 5.15, and interaction tests were performed as described in section 5.22.1. Bait proteins were either C-terminally or N-terminally fused to the C-terminal half of ubiquitin (Cub) and the transcription factor (Figure 3.16A and B, respectively). The wild type ubiquitin halves can reconstitute autonomically and are therefore suited for a positive control. For this purpose, Alg5 was fused to the N-terminal ubiquitin half (Nub). To avoid the autoassembly, a mutated Nub with a point-mutation at amino acid position 13 from isoleucine to glycine (NubG) was used for the negative control and all interaction tests with the proteins of interest. Yeast cells were spotted on SD medium without leucine and tryptophane (SD-LW) as a control for cell density and selective growth indicating the presence of the relevant plasmids. Growth on SD-selection medium without leucine, tryptophane and histidine (-LWH) was only possible if the proteins under investigation interacted with each other.

As it was already published, interactions between FAD2 and FAD3 were seen with both proteins used as bait in both fusion-variants as indicated by growth on SD-LWH selection medium (Figure 3.16). Prey proteins N-terminally fused to NubG produced the clearest results (data for C-terminal fusions are not shown). While interaction between FAD2 and FAD3 was known (Lou et al., 2014) and was confirmed here, additional interactions of FAD3 with PDAT and DGAT2_{opt} were observed with C-terminal fusion of Cub to FAD3 (Figure 3.16A) but not with N-terminal fusions (Figure 3.16B). In addition, both FAD2 bait fusions were able to interact with DGAT2_{opt}.

PDAT used as bait protein as C-terminal fusion variant did not produce interpretable results, because no growth of the positive control was visible on SD-LWH medium (Figure 3.16A). By contrast, N-terminal fusion variants of PDAT did result in yeast growth of the positive control on SD-LWH medium (Figure 3.16B). Furthermore, novel interactions of PDAT were observed with FAD2, with FAD3 and with PDAT itself.

Interaction analyses with DGAT1 as a bait protein were only interpretable when C-terminal fusion variants were used because expression of N-terminal fusion proteins did not lead to a distinct growth of the positive control on SD-LWH selection medium. Yeast growth on SD-LWH was visible with FAD2, with FAD3 or with PDAT used as prey proteins indicating the ability of DGAT1 to interact with these proteins.

The expression of C-terminal fusions of DGAT2_{opt} resulted in weak but detectable growth of the negative control (Figure 3.16A). Therefore, the growth observed for the interaction tests with FAD2, FAD3 and PDAT cannot be interpreted with any degree of certainty. By contrast, no growth of the negative control was observed when the N-terminal fusion variant of DGAT2_{opt} was expressed and the previously observed interactions with FAD2

and FAD3 were confirmed. In addition, interaction of DGAT2_{opt} with PDAT was observed (Figure 3.16B).

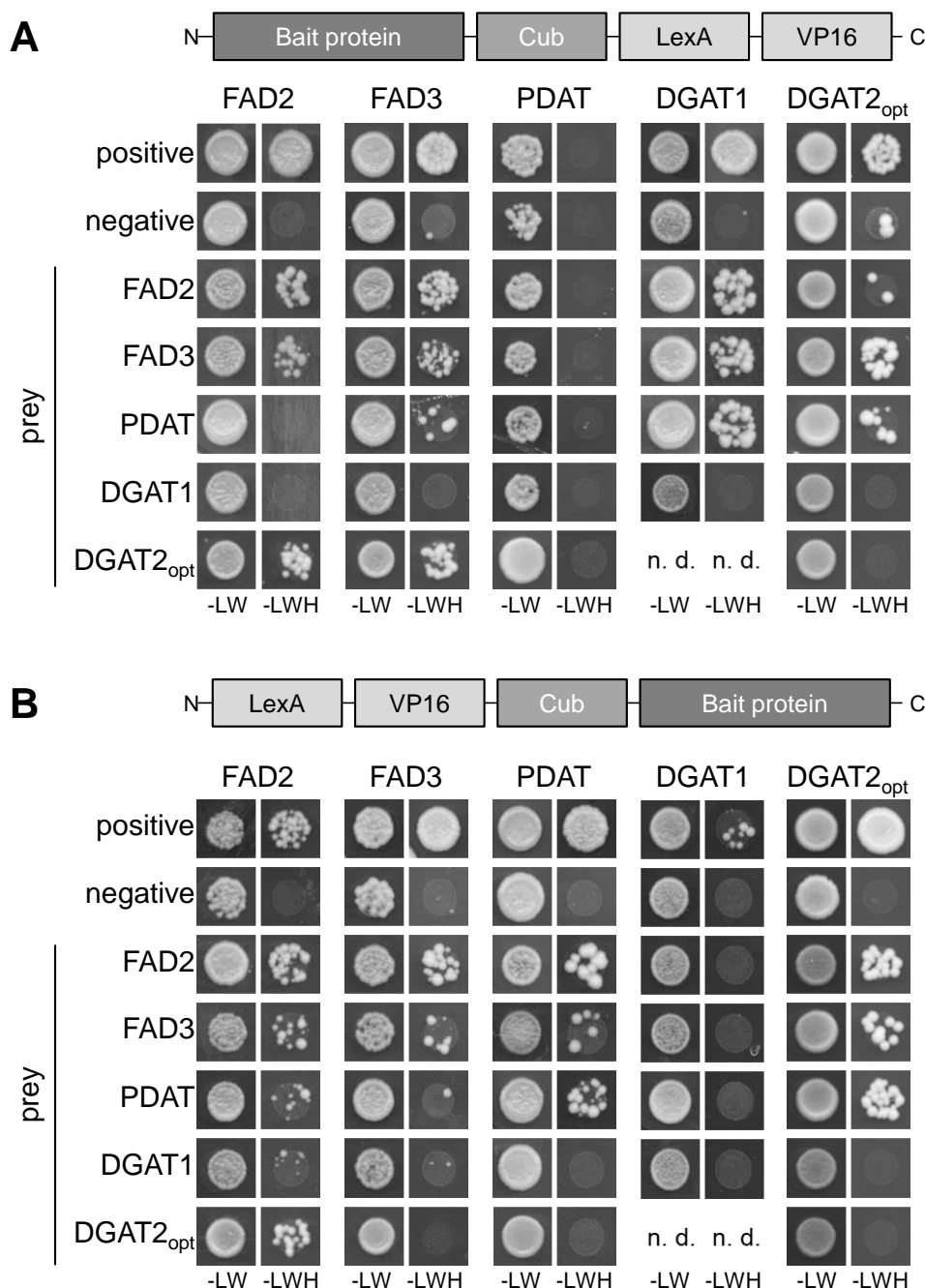


Figure 3.16. Interaction of enzymes involved in fatty acid desaturation and TAG assembly according to split-ubiquitin based yeast two-hybrid analyses. Protein-protein interactions were analyzed between fatty acid desaturases and selected acyltransferases, using the split-ubiquitin based yeast two-hybrid system. Cotransformation of the bait constructs with *pAI-Alg5* and *pDL2-Alg5* served as positive and negative controls, respectively. Prey proteins were N-terminally fused to NubG (*pPR3-N*-vectors). n. d., not determined. **A**, Test with FAD2, FAD3, PDAT, DGAT1 and DGAT2_{opt} (cDNA for DGAT2 codon optimized for expression in yeast) as bait proteins fused C-terminally to Cub and transcription factors. **B**, Test with FAD2, FAD3, PDAT, DGAT1 and DGAT2_{opt} as bait proteins fused N-terminally to Cub and transcription factors. Results are representative for at least three independent experiments with four colonies of each combination (except for DGAT2_{opt} as bait with C-terminal fusions to Cub or as prey protein: two independent experiments with four colonies each were performed). Some replications were performed by Luise Jäckel (bachelor's student).

Besides the known interaction between FAD2 and FAD3 it was shown that both desaturases also interacted with acyltransferases responsible for the assembly of TAG. The interactions of FAD2 or FAD3 with DGAT2_{opt} were observed with each enzyme as bait protein. Furthermore, FAD3 and DGAT2_{opt} exhibited additional interactions with PDAT. DGAT1 showed interactions with both fatty acid desaturases and PDAT. The orientation of the fusion of the bait protein to Cub played an essential role for the interaction analyses of PDAT, DGAT1 and DGAT2_{opt} and interpretable results were respectively obtained for these enzyme combinations with only one specific orientation.

3.9 Fluorescence-tagged enzyme variants of PDAT and DGAT1 are functional in yeast

The interactions of FAD2 or FAD3 with different acyltransferases made these latter enzymes interesting for further analyses of the subcellular distribution of protein complexes involving FAD2 and FAD3 at the ER. Therefore, experiments were initiated to assess the subcellular localization of PDAT and DGAT1 in *Arabidopsis* mesophyll protoplasts. Before commencing these localization analyses, fusion proteins of PDAT and DGAT1 with N- and/or C-terminal fluorescence tags were generated and tested for functionality in yeast. The functionality of the PDAT or DGAT1 fusion proteins was analyzed by complementation tests of a yeast mutant defective in acyltransferase activity. The yeast strain *S. cerevisiae* H1246 used in these experiments is an acyltransferase quadruple mutant deficient in TAG and sterol ester production (Sandager et al., 2002). While this yeast mutant, thus, cannot form any TAG or sterol esters by itself, the expression of suitable functional acyltransferases re-enables TAG production, which can easily be detected. Fluorescence-tagged fusions of *Arabidopsis* PDAT or DGAT1 were expressed in this yeast strain as described in section 5.20.2. Lipids were extracted and analyzed for the presence of TAG by thin-layer chromatography (TLC) (described in section 5.21.1 and 5.21.4). Representative TLC plates and signal intensity quantifications from three biological replicates on two TLC plates are depicted in Figure 3.17. Yeast cells transformed with a control vector carrying an empty expression cassette were used as a negative control. Furthermore, untagged PDAT and DGAT1 were expressed for comparison. Figure 3.17A and B present the results for fluorescence-tagged PDAT variants. Both N- and C-terminal fusions of fluorescence proteins to PDAT were analyzed. Yeast transformed with the empty control vector did not produce TAG. By contrast, the expression of untagged PDAT as well as the tested fusion-proteins resulted in substantial TAG production, indicating that all expressed PDAT variants were able to complement the lack of endogenous acyltransferase activity in the yeast strain H1246. The quantification of the produced TAG

levels indicated no statistical difference ($p > 0.05$) in TAG-forming performance between the expressed fluorescence-fusion proteins (Figure 3.17B), however, without testing for the expression levels of the individual proteins.

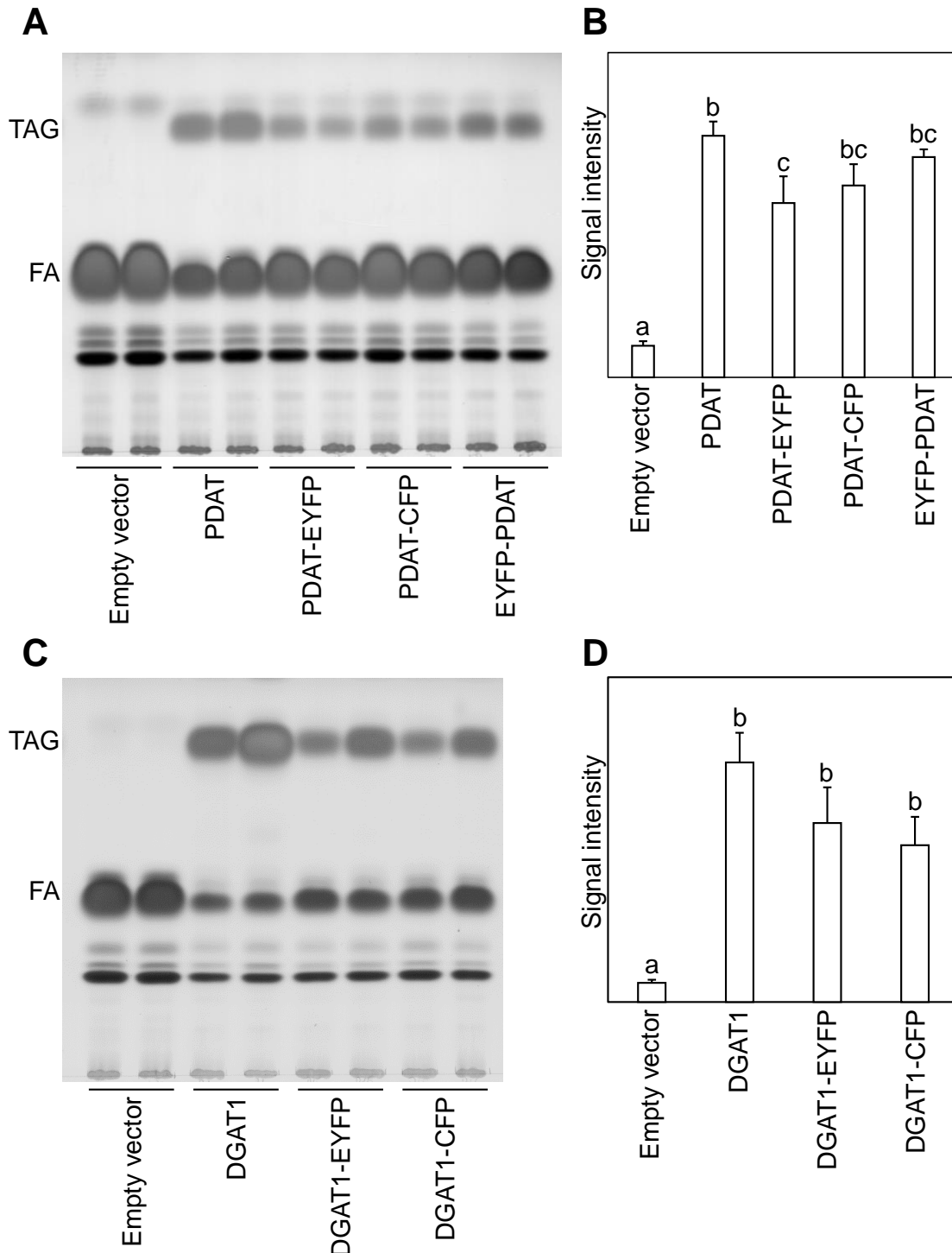


Figure 3.17. Functionality of the fluorescence-tagged acyltransferases PDAT and DGAT1 in the yeast strain H1246. The functionality of fluorescence-tagged variants of PDAT and DGAT1 was assessed in yeast deficient in TAG synthesis. **A**, The yeast strain H1246 was transformed with *pESC-URA*-vectors containing the cDNA coding for PDAT, PDAT-EYFP, PDAT-CFP or EYFP-PDAT, respectively. Cells were grown in liquid SD-minimal yeast medium without uracil containing 2 % (w/v) galactose at 30 °C for 4 days. The lipids from

40 OD-units were isolated and analyzed by TLC. Depicted is one representative result from a total of five independent experiments with two to three biological replicates each. **C**, The yeast strain H1246 was transformed with *pESC-URA*-vectors containing the cDNA coding for DGAT1, DGAT1-EYFP or DGAT1-CFP, respectively. Cells were grown in liquid SD-minimal yeast medium without uracil containing 2 % (w/v) galactose at 30 °C for 3-4 days. The lipids from 20 OD-units were isolated and analyzed by TLC. Depicted is one representative result from three independent experiments with two to three biological replicates each.

B+D, Quantification of the signal intensity corresponding to TAG for one representative, independent experiment with three biological replicates. The signal intensity of A and C together with signal from samples on a second TLC plate from the same experiment was quantified using Fiji. Significant differences were determined using one-way ANOVA with a Tukey's post-hoc test ($p < 0.05$). Letters indicate categories of significantly different samples. TAG, triacylglycerol; FA, fatty acid.

The results from yeast H1246 expressing DGAT1 variants are shown in Figure 3.17C and D. While no TAG was formed by yeast transformed with the empty control vector, TAG was present in all yeast cultures expressing the untagged or the fluorescence-tagged DGAT1 variants. Again, the amounts of produced TAG did not differ significantly ($p > 0.05$) between cells expressing the tagged or untagged enzymes (Figure 3.17D).

Based on the yeast H1246 complementation tests, fluorescent fusion variants of PDAT or DGAT1 proved to be fully functional compared with the performance of the non-tagged enzyme variants. Furthermore, no difference was observed in the functionality of N- or C-terminal tagged PDAT variants, and the fusion proteins were thus used for further localization studies in *Arabidopsis mesophyll* protoplasts.

3.10 PDAT and DGAT1 localize to the ER in *Arabidopsis mesophyll* protoplasts

The subcellular distribution of PDAT and DGAT1 were investigated in *Arabidopsis mesophyll* protoplasts using the functional fluorescent fusion proteins characterized in section 3.9. The proteins were expressed under the *pCaMV35S* promoter, as described in the sections 5.16 and 5.23.

Figure 3.18A shows the subcellular distribution of EYFP-PDAT in a network-like structure throughout the cytosol without the expression of an additional organelle marker. EYFP-PDAT fluorescence is depicted in yellow, the autofluorescence of ChlA in blue. A single confocal plane is presented. Images were taken by LSM. Expression of mCherry-PDAT in mesophyll protoplasts of *Arabidopsis* plants stably expressing the ER marker GFP-HDEL (ER-GFP) revealed colocalization of mCherry-PDAT (magenta) with the ER-GFP (green, Figure 3.18B). For quantification of the degree of colocalization, PCCs were calculated from 13 Z-stack images and from 8 single confocal slices. The PCCs for mCherry-PDAT vs. ER-GFP ranged from 0.63 to 0.95 with a mean of 0.82. These values are similar to the values obtained when coexpressing two ER markers (compare appendix Figure 7.3B), indicating that the mCherry-PDAT fusion localized to the ER. Colocalization of mCherry-PDAT with the ER marker is also illustrated by the line plot in Figure 3.18D where the

fluorescence intensities of mCherry-PDAT and ER-GFP showed very similar distribution patterns.

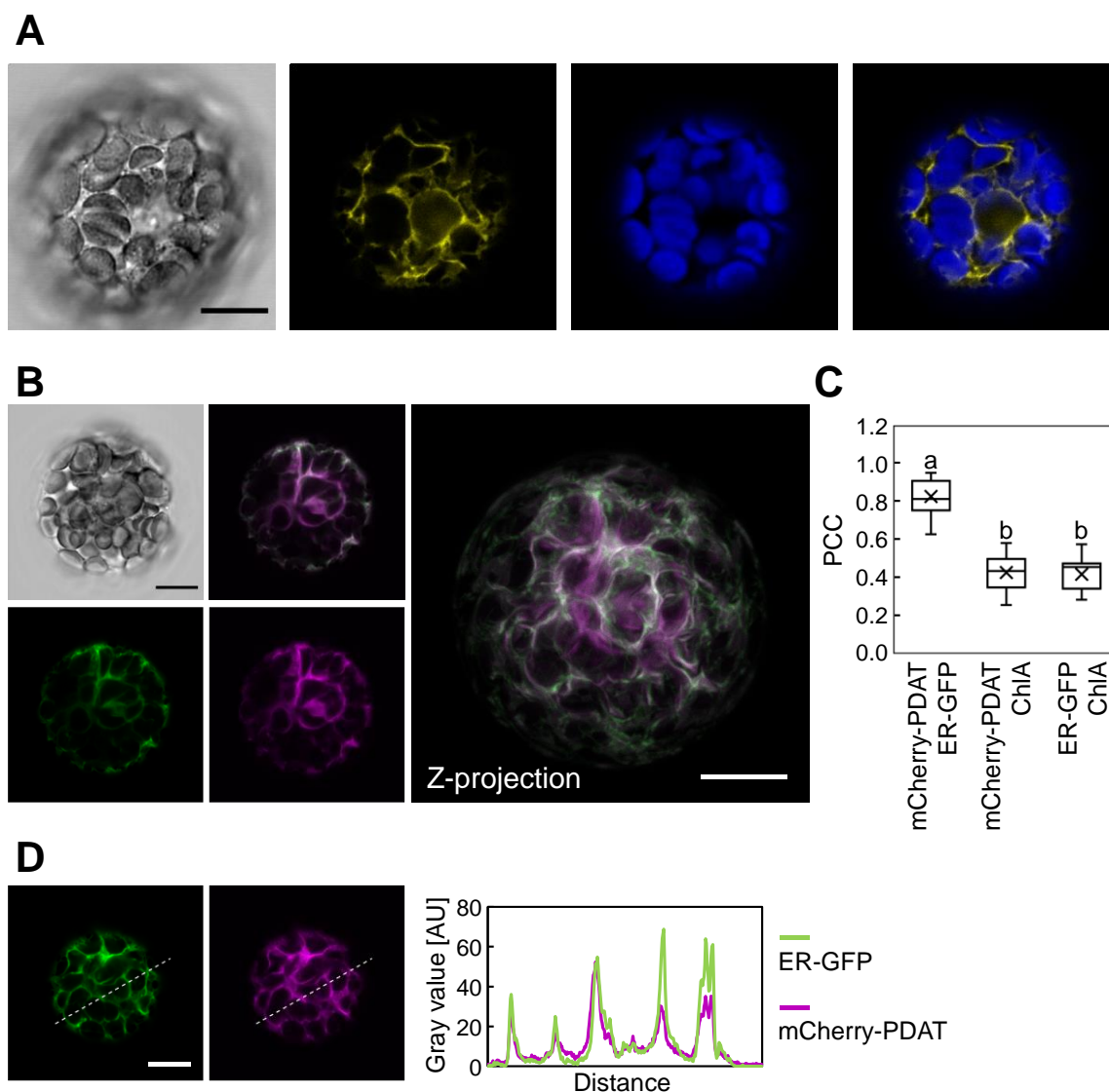


Figure 3.18. Subcellular distribution of fluorescence-tagged PDAT in *Arabidopsis mesophyll* protoplasts. Protoplasts from *A. thaliana* Col-0 or GFP-HDEL were transformed with *pEntryD-pCaMV35S::EYFP-PDAT* (**A**) or *pEntryD-pCaMV35S::mCherry-PDAT* (**B-D**), respectively, and analyzed by LSM. Z-stacks covering the cell from one edge to the center with approx. 0.6 μm distance between the slices were acquired. Scale bars: 10 μm . **A**, Protoplasts from *A. thaliana* Col-0 expressing EYFP-PDAT. EYFP-PDAT fluorescence is shown in yellow, the autofluorescence of chlorophyll A (ChlA) in blue. A single confocal plane is shown. Images are representative for six cells. **B**, Protoplast from *A. thaliana* GFP-HDEL expressing mCherry-PDAT. mCherry-PDAT fluorescence is shown in magenta, the ER marker (GFP-HDEL) in green. Selected single confocal slice (left) and maximum intensity Z-projection of a Z-stack (right). **C**, Pearson's correlation coefficients (PCCs) were calculated based on 13 Z-stacks and 8 single confocal images from two independent experiments taken by LSM. Significant differences were determined using one-way ANOVA with a Tukey's post-hoc test ($p < 0.05$). Letters indicate categories of significantly different samples. **D**, Intensity profile for mCherry-PDAT (magenta) and ER-GFP (green) along the line highlighted in the left panels. Images are representative for two independent experiments using a total of 21 (B-D) cells.

The integrity of the fusion-proteins EYFP-PDAT and mCherry-PDAT was tested by isolating the proteins from protoplasts, separation by SDS-PAGE, followed by blotting and

immunodetection using anti-GFP or anti-mCherry antibodies (see sections 5.18 and 5.19). The result is presented in the appendix in Figure 7.7. The expected molecular weights for EYFP-PDAT or mCherry-PDAT are 99 kDa and 101 kDa, respectively. Protein signals were detected just above 100 kDa with both antibodies. Proteins extracted from untransformed protoplasts did not give a signal when detected with the anti-mCherry antibody as a negative control. No signal was seen in neither western blot at the molecular weight of free EYFP or mCherry proteins (27 kDa and 29 kDa, respectively). It is therefore concluded that the fluorescence observed by LSM indicated the distribution of full-length fluorescent fusion variants of PDAT.

As for fluorescence-tagged PDAT variants, subcellular localization analyses were also performed for DGAT1 fused to EYFP. DGAT1-EYFP was coexpressed with the ER marker ER-mCherry in *Arabidopsis mesophyll* protoplasts. Figure 3.19A shows a representative Z-projection. DGAT1-EYFP is depicted in green, ER-mCherry in magenta and the autofluorescence of ChlA in blue. Both DGAT1-EYFP and ER-mCherry decorated a diffuse network-like pattern with the localization patterns clearly resembling each other in appearance. PCCs were calculated and are depicted in Figure 3.19B. The PCC values for DGAT1-EYFP vs. ER-mCherry ranged from 0.5 to 0.84 with a mean value of 0.7. The correlation was slightly lower than for the correlation of two ER markers (compare appendix Figure 7.3B) but were significantly higher ($p < 0.05$) than values calculated for either fluorophore vs. ChlA. A line plot of the fluorescence intensities of DGAT1-EYFP and ER-mCherry is shown in Figure 3.19C. The fluorescence distribution illustrates close colocalization of DGAT1 with the ER marker.

The proteins expressed in *Arabidopsis mesophyll* protoplasts were isolated and separated by SDS-PAGE, followed by blotting and immunodetection using anti-GFP antibody (see sections 5.18 and 5.19). The result is shown in the appendix in Figure 7.8. The expected molecular weight of DGAT1-EYFP is 86 kDa, and a protein signal was detected at the expected molecular weight. An additional signal was detected at the molecular weight of approx. 30 kDa, probably corresponding to the presence of free EYFP (molecular weight: 27 kDa). Thus, in these experiments it cannot be ruled out that the fluorescence distribution pattern shown in Figure 3.19 partly resulted from the cytosolic fluorescence of free EYFP.

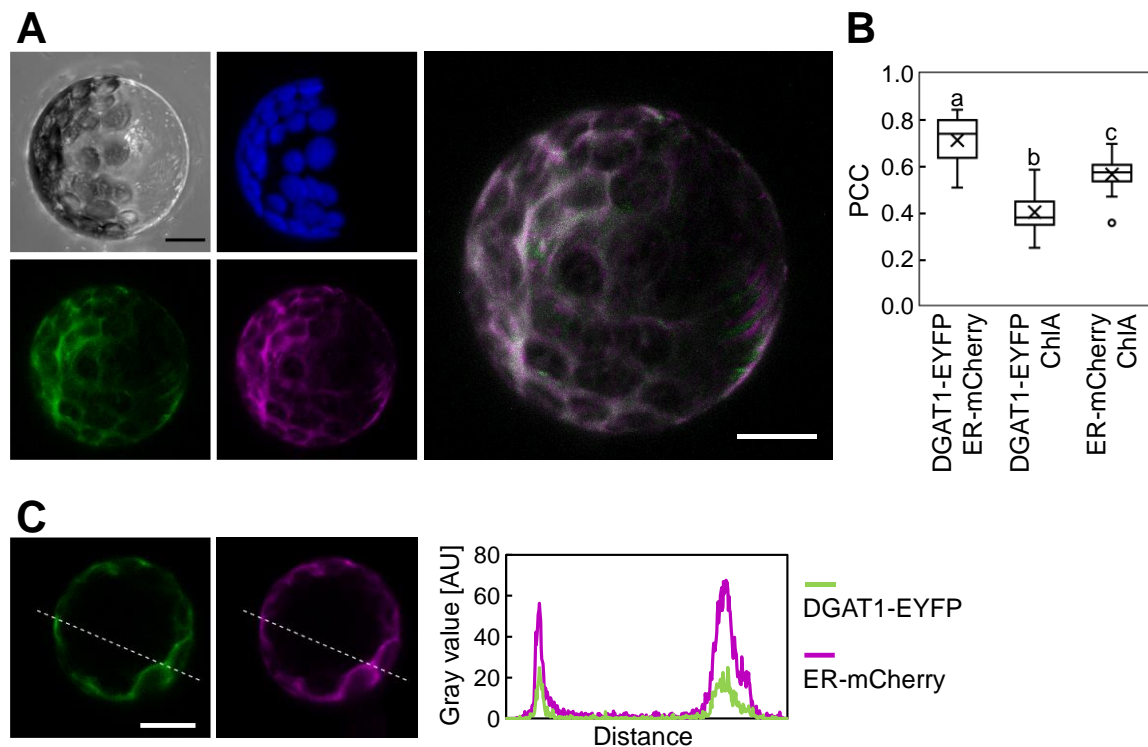


Figure 3.19. Subcellular distribution of DGAT1 in Arabidopsis mesophyll protoplasts. Mesophyll protoplasts from *A. thaliana* Col-0 were cotransformed with *pEntryD-pCaMV352::DGAT1-EYFP* and the ER marker construct *CD3-959-ER-mCherry* and analyzed by LSM. Z-stacks covering the cell from one edge to the center with approx. 0.6 μ distance between the slices were acquired. Scale bars: 10 μ m. **A**, Protoplast from *A. thaliana* Col-0 expressing DGAT1-EYFP and the ER marker ER-mCherry. DGAT1-EYFP fluorescence is shown in green, the ER marker in magenta. The autofluorescence of chlorophyll A (ChlA) is depicted in blue. A maximum intensity Z-projection is shown. **B**, Pearson's correlation coefficients (PCCs) were calculated based on 16 Z-stacks from two independent experiments taken by LSM. Significant differences were determined using one-way ANOVA with a Tukey's post-hoc test ($p < 0.05$). Letters indicate categories of significantly different samples. **C**, Intensity profile for DGAT1-EYFP (green) and ER-mCherry (magenta) along the line highlighted in the left panels. Images are representative for two experiments using a total of 16 cells (A-C).

Taken together, PDAT and possibly DGAT1 from Arabidopsis localized to the ER when expressed in Arabidopsis mesophyll protoplasts. This localization pattern is in accordance with previous findings for the related enzymes *RcPDAT* from *Ricinus communis* and *VfDGAT1* from *Vernicia fordii* (Kim et al., 2011; Shockey et al., 2006).

3.11 FAD2 interacts with FAD3 and PDAT in BiFC experiments at ER-like structures

Experiments so far had shown interaction between the fatty acid desaturases FAD2 and FAD3 with the acyltransferase PDAT based on yeast two-hybrid analyses (compare Figure 3.16). FAD3 and PDAT localized to the ER of Arabidopsis mesophyll protoplasts whereas FAD2 mainly localized to Golgi stacks. To verify the observed interactions and to determine the subcellular site of interaction, bimolecular fluorescence complementation (BiFC) analyses were performed. The constructs were introduced via *pBiFct2in1-NC-*

vectors into *Arabidopsis* mesophyll protoplasts. The vector encodes free RFP as a transformation control that fluoresces independent from any reconstituted fluorescence based on interaction of the partner proteins tested. The N-terminal half of EYFP was fused to the N-terminus of the first tested protein, the C-terminal half was fused to the C-terminus of the second protein of interest. Two images from different confocal planes of each cell showing RFP-fluorescence were acquired by LSM. As negative controls, Alg5, which was already used as a control in the yeast two-hybrid experiments (compare Figure 3.16), was tested against itself for interaction as well as against each tested protein of interest. Representative images are shown in Figure 3.20. RFP-fluorescence indicating successful transformation is depicted in red, reconstituted EYFP-fluorescence in yellow, and the autofluorescence of ChlA in blue. In the three negative controls consisting of Alg5 vs. Alg5, Alg5 vs. FAD3 and Alg5 vs. PDAT no reconstituted EYFP-fluorescence was detected (Figure 3.20A, C and D, respectively). By contrast, the Alg5 vs. FAD2 control displayed EYFP-fluorescence in round structures. These structures were partially detectable in the RFP channel as well (Figure 3.20B, indicated by the arrows) and based on the distinct observed spatial distribution likely represent an overexpression artifact.

EYFP-fluorescence was positively reconstituted in cells expressing FAD2 together with FAD3 and in cells expressing FAD2 and PDAT, respectively (Figure 3.20E and F). For both combinations, the reconstituted fluorescence patterns showed a network-like pattern throughout the cell and around the nucleus, resembling the appearance of the ER in the mesophyll protoplasts.

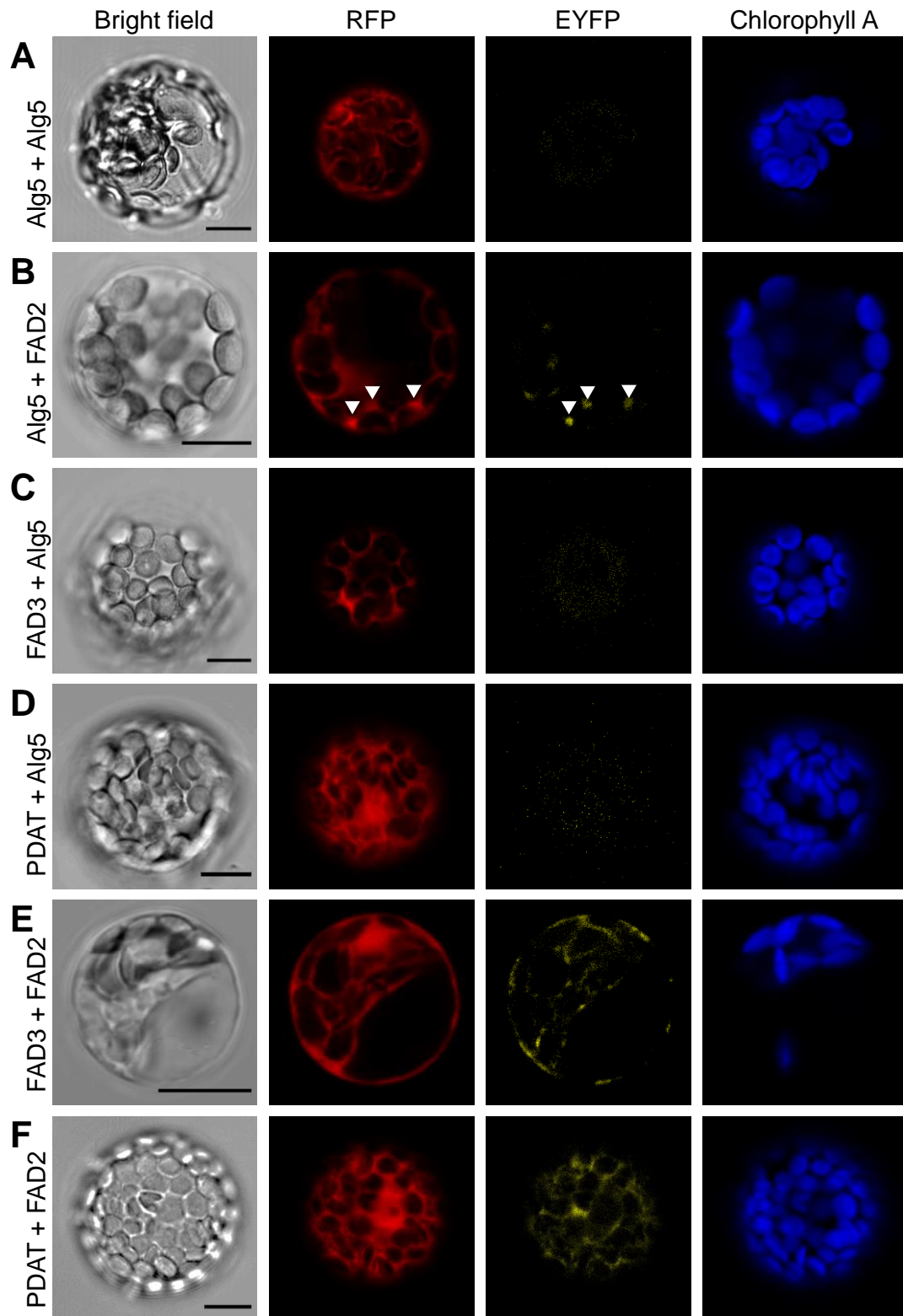


Figure 3.20. BiFC-analyses for *in vivo* interactions between FAD2, FAD3 and PDAT. The previously observed interactions of FAD2 with FAD3 and with PDAT were verified using bimolecular fluorescence complementation analyses in Arabidopsis protoplasts. Transformed protoplasts were analyzed by LSM. For each cell that showed RFP-fluorescence two confocal planes were recorded. RFP-fluorescence (red) was used as a control for successful transformation. Yellow shows reconstituted EYFP-fluorescence, the autofluorescence of chlorophyll A is depicted in blue. Scale bars: 10 μ m. **A-D**, As negative controls, the vectors *pBiFCt2in1-NC-Alg5-Alg5* (**A**, n = 18), *pBiFCt2in1-NC-Alg5-FAD2* (**B**, n = 17), *pBiFCt2in1-NC-FAD3-Alg5* (**C**, n = 9) and *pBiFCt2in1-NC-PDAT-Alg5* (**D**, n = 15). were used. **E**, Protoplasts transformed with *pBiFCt2in1-*

NC-FAD3-FAD2 show interaction of FAD3 and FAD2, $n = 31$. **F**, Protoplasts transformed with *pBiFCt2in1-NC-PDAT-FAD2* show interaction of PDAT and FAD2, $n = 28$. Images are representative for two independent experiments using 18 (Alg5+ Alg5), 17 (Alg5 + FAD2), 9 (FAD3 + Alg5), 15 (PDAT + Alg5), 31 (FAD3 + FAD2) and 28 (PDAT + FAD3) cells in total.

To numerically assess the results from the BiFC experiments, protoplasts showing RFP-fluorescence for each construct were counted and classified in three different groups: i) no EYFP-fluorescence was detectable at all, ii) EYFP-fluorescence showed artifacts (comparable to Figure 3.20B), or iii) EYFP-fluorescence with an appearance similar to the ER (comparable to Figure 3.20E and F). Large round structures visible in both the RFP and EYFP-channel were considered to be artifacts due to the overexpression of the EYFP-fusion proteins. Each cell was only included in one class. The relative number of cells for each tested protein combination is illustrated in Figure 3.21.

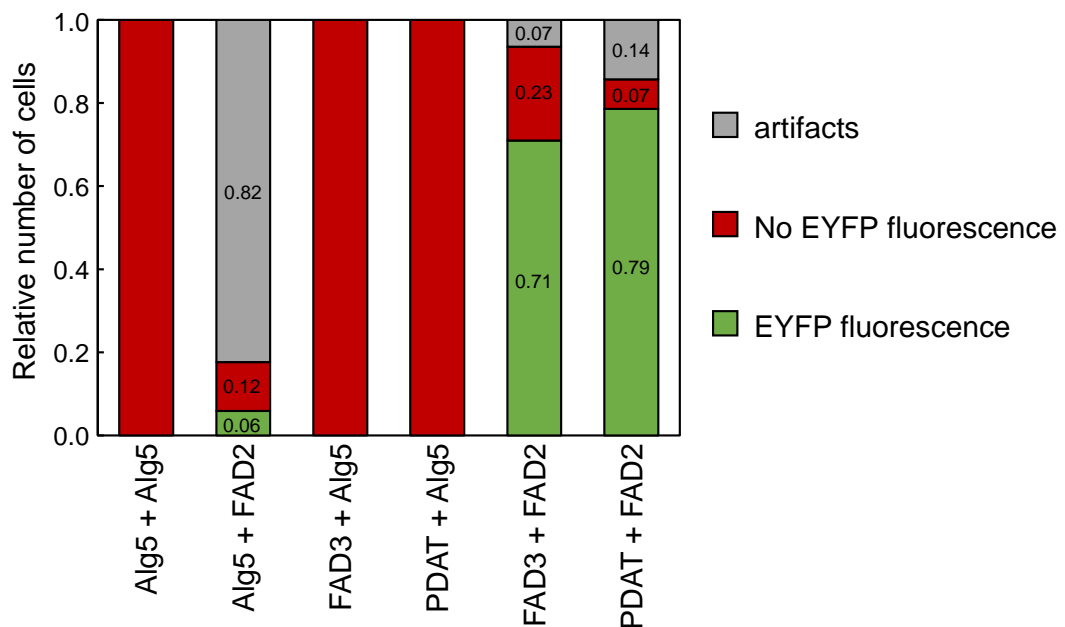


Figure 3.21. Quantitative evaluation of BiFC analyses. Arabidopsis mesophyll protoplasts were transformed with *pBiFCt2in1-NC* vectors and analyzed by LSM as shown in Figure 3.20. The cells were counted and categorized into three groups: i) no EYFP-fluorescence was detectable (red), ii) the EYFP-fluorescence showed artifacts similar to Fig. 3.20B (grey), iii) EYFP-fluorescence was observed in an ER-like network pattern. Experiments were performed twice with 18 (Alg5+ Alg5), 17 (Alg5 + FAD2), 9 (FAD3 + Alg5), 15 (PDAT + Alg5), 31 (FAD3 + FAD2) and 28 (PDAT + FAD3) cells in total.

The negative controls of Alg5 against itself, against FAD3 or against PDAT did not show EYFP reconstitution in any cell observed. When Alg5 was expressed together with FAD2, almost 90 % of cells showed EYFP-fluorescence, but in over 80 % of cells the EYFP-fluorescence was found in artifact-like structures. The interaction tests between FAD2 and FAD3 or PDAT resulted in 71 % and 79 % of cells showing a valid EYFP-fluorescence distribution with no artifacts visible, respectively.

To assess the expression and integrity of the proteins used in BiFC-assays, proteins were isolated from transformed *Arabidopsis* mesophyll protoplasts, separated by SDS-PAGE, and blotted to membranes (see sections 5.18 and 5.19). Immunodetections using anti-nYFP and anti-cYFP antibodies did not show any specific protein signals, neither from protoplasts transformed with the negative controls nor from protoplasts showing reconstituted EYFP-fluorescence (data not shown). Therefore, no statement on the protein expression and protein integrity could be made.

The fluorescence reconstitution in ER-like structures verified the interaction of FAD2 with FAD3 and with PDAT, respectively. Despite the localization of FAD2 to Golgi stacks in localization studies, the site of interaction with FAD3 and PDAT in BiFC experiments seemed to be at the ER. Reciprocally, the observed patterns indicate no influence of the interaction of FAD2 with FAD3 or with PDAT on the donut-shaped Golgi particles decorated by fluorescence-tagged FAD2 alone.

4. Discussion

Metabolic pathways for plant fatty acid desaturation and lipid assembly in plants have long been of interest in the context of industrial applications. Research in this field has focused mainly on the modification of seed oil – with mixed results. In the past decade, it became evident that the spatial distribution and the molecular interaction of the enzymes involved in the generation of modified fatty acids and the formation of seed oil are important factors to be considered for metabolic pathway engineering (Dyer and Mullen, 2008). However, information on the precise subcellular distribution of the relevant enzymes has been limited.

The ER is the site of TAG biogenesis and the majority of proteins involved in fatty acid modification and lipid assembly in the eukaryotic pathway are thought to reside in the ER membrane. For instance, the acyltransferases DGAT1 and DGAT2 from tung tree have been shown to localize to the ER, where they occupy distinct ER subdomains, indicating the existence of TAG producing protein clusters in ER microdomains (Lou et al., 2014). Functional ER retention signals have been found and analyzed for the fatty acid desaturases FAD2 and FAD3 (McCartney et al., 2004), suggesting their localization in the ER membrane, which nonetheless has not been clearly demonstrated. Overall, the published information on the subcellular distribution of enzymes of fatty acid modification and oil biogenesis has been surprisingly scarce or appear not fully conclusive, despite their essential contribution to seed oil biology and a long-standing industrial interest.

Previous studies on the subcellular localization of fatty acid desaturases and related enzymes used transient protein expression in heterologous systems, mostly without demonstrating functionality of the fluorescent fusions used or based on immunodetection of fixed cells (Dyer and Mullen, 2001; Dyer et al., 2002; McCartney et al., 2004). Therefore, the work presented in this thesis focused on a detailed analysis of the subcellular distribution and the interaction of enzymes involved in fatty acid desaturation and TAG assembly in the endogenous metabolism of *Arabidopsis*. Functional fluorescence-tagged enzymes were examined in transiently and stably transformed plant cells with quantitative *in vivo* imaging analysis. Besides the expected localization to the ER membrane, a novel localization of FAD2 to Golgi stacks was observed. The distinct Golgi-association of EYFP-FAD2 in the cells analyzed is consistent with a role of FAD2 in contributing to the control of membrane unsaturation in cellular membranes, which are physiologically linked by the secretory pathway.

4.1 Fluorescence-tagged enzyme variants of FAD2 and FAD3 are functional and complement the respective Arabidopsis mutants

To assess subcellular localization of FAD2 or FAD3 in live cell imaging, functional fluorescence-tagged enzymes were created. Fluorescence tags were cloned to the N-termini of FAD2 or FAD3, respectively, to avoid a possible interference of the fluorescence tag with the C-terminal ER-retention motifs of the enzymes (McCartney et al., 2004). The fusion proteins generated were functional in yeast, as the production of 18:2^{Δ9,12} or 18:3^{Δ9,12,15} could be detected, respectively, upon expression of the fusion proteins. While the amounts of the detected products were generally lower compared to the expression of untagged proteins when the fluorescence-tagged proteins were expressed (see section 3.1, Figure 3.1), this does not necessarily mean that the fluorescence tag impaired enzyme activity. Alternatively, the protein abundance might vary between cells expressing the differently sized proteins, and thus influence the amount of fatty acid produced. As different approaches to detect the fusion proteins in western blots remained unsuccessful, no information on the protein amounts could be obtained to resolve this point.

From a qualitative perspective, the fatty acid patterns of the transgenic yeasts supported functionality of the fusion proteins. Besides the FAD2-product, 18:2^{Δ9,12}, 16:2^{Δ9,12} was also detected in all yeast cells expressing different FAD2-variants, consistent with previous work by Kajiwara and coworkers also reporting the desaturation of 16:1^{Δ9} to 16:2^{Δ9,12} by FAD2 expressed in yeast (Kajiwara et al., 1996). The positions of the double bonds in 16C-fatty acids differ between yeast and plants. Yeast natively contains only one desaturase, the Δ9-desaturase ScOLE1, which introduces a single double bond at position Δ9 of fatty acids with a chain length of 16 and 18 carbon atoms (Klug and Daum, 2014; Stukey et al., 1989, 1990). By contrast, in chloroplasts FAD5 introduces a double bond into 16:0 at position Δ7, resulting in the formation of 16:1^{Δ7}, which can be further desaturated by FAD6 and FAD7/FAD8 to 16:2^{Δ7,10} and 16:3^{Δ7,10,13}, respectively (Heilmann et al., 2004a; Browse et al., 1989; Iba et al., 1993; McConn et al., 1994). 16:1^{Δ7} is not exported from the plastid and can thus not enter the extraplastidial eukaryotic pathway of lipid assembly (Li-Beisson et al., 2010). Since 16:1^{Δ9} present in yeast does not occur naturally in Arabidopsis, the ability of FAD2 (and FAD3) to desaturate fatty acids with 16 carbon atoms might not be physiologically relevant. However, the yeast experiment illustrates the plasticity of fatty acid substrates accepted by desaturases depending on the metabolic context.

Constructs for the fluorescence-tagged variants of FAD2 and FAD3 were transformed into the respective Arabidopsis mutants. The expression of EYFP-FAD2 and EYFP-FAD3 resulted in complementation of the respective mutants with regard to both fatty acid composition and macroscopic defects (see section 3.2.1 and 3.2.2). When the

endogenous promoter sequence was used to drive the expression of *EYFP-FAD2*, it is expected that the gene activity of *EYFP-FAD2* in the complemented lines reflects that of *FAD2* in the wild type. The amounts of 18:2^{Δ9,12} in seed TAG or the membrane lipid PC in the complemented *fad2-1* *EYFP-FAD2* lines were substantially higher than in the *fad2-1* mutant control, indicating functional complementation. However, 18:2^{Δ9,12} levels reached in the complemented lines were only at 50-85 % of wild type levels (see Figure 3.5). In combination with the results from the yeast experiments, which only revealed general functionality of *EYFP-FAD2*, it cannot be ruled out that the *EYFP*-tag negatively influenced the apparent functionality of the *FAD2* fusion protein. The fluorescent fusion might have not been fully functional, possibly due to an effect of the *EYFP*-tag on translation efficiency, protein stability or catalytic activity. In any case, with the substantial complementation observed, such a negative effect - if at all present - must have been small. There are hints that the activity and abundance of *FAD2* from *Glycine max* are regulated on the protein level by phosphorylation and proteasomal degradation (Tang et al., 2005), and in analogy the abundance of *EYFP-FAD2* might have been lower in the complemented *Arabidopsis* plants compared to the abundance of *FAD2* in the wild type. Alternatively, a lower protein abundance of the *EYFP-FAD2* protein might have resulted from posttranslational effects of the ectopic expression, even though the intrinsic *FAD2* promoter was used to drive expression of the transgene.

The *fad3-2* mutant was complemented with *EYFP-FAD3* under the control of the *pCaMV35S* promoter. This promoter is active in almost all tissues and leads to a strong expression (Holtorf et al., 1995). Consequently, the amount of 18:3^{Δ9,12,15} in the seed oil was slightly elevated in the complemented mutant compared to the wild type (see Figure 3.6). The fatty acid composition of the membrane lipid PC in the complemented lines resembled that of wild type seedlings and did not show increased levels of 18:3^{Δ9,12,15}. The fatty acid compositions of the plastidial membrane lipids MGDG and DGDG were not altered in the *fad3-2* mutant nor the complemented plant lines. This is consistent with the role of *FAD3* in the desaturation of extraplastidial membrane lipids (Browse et al., 1993). In our hands, the *fad3-2* mutant exhibited smaller rosettes and a reduced shoot height compared to wild type plants, a phenotype not reported in the literature so far. Expression of *EYFP-FAD3* in the mutant background resulted in normal growth of the rosette leaves and the shoot, indicating that the observed phenotype resulted from the defect in the *FAD3* gene locus and that *EYFP-FAD3* could complement for this defect. As it was discussed for *EYFP-FAD2*, an influence of the *EYFP*-tag on the enzyme activity or posttranslational modification of *FAD3* cannot be ruled out. Furthermore, O'Quin and coworkers found that the N-termini of *BnFAD3* and *VfFAD3* have an effect on the protein half-life via

proteasomal degradation, which is a regulatory mechanism to increase FAD3 activity under changing temperatures (O'Quin et al., 2010). The overexpression under the *pCaMV35S* promoter might complement for negative effects of the tag on FAD3 activity or stability. In the future, protein and transcript abundance might need to be considered to further evaluate the influence of the EYFP-tag.

4.2 A possible role of FAD2 at the Golgi

Previous research on the subcellular localization of fatty acid desaturases pointed to a localization of FADs at the ER. However, these studies often made use of transient protein expression in non-endogenous plant cell systems (e. g. onion epidermal cells, BY-2 cells) and were performed without demonstrating functionality of the fluorescent fusions (Dyer and Mullen, 2001; Dyer et al., 2002; McCartney et al., 2004). In this study, the localization of EYFP-FAD2 was analyzed in different tissues in stably or in transiently transformed plant cells in combination with different organelle markers and using quantitative live cell imaging. The analyses revealed a novel localization of FAD2 to Golgi stacks with slightly different localization patterns observed depending on the cell type (see section 3.3 Figure 3.7 and section 3.4).

In root epidermal cells of complemented *fad2-1* mutants, the localization of EYFP-FAD2 resembled an ER-like pattern, which is consistent with previous findings (see section 3.3, Figure 3.7; Dyer and Mullen, 2001; Dyer et al., 2002; McCartney et al., 2004; Nguyen et al., 2019; Lee et al., 2016). Surprisingly, in leaf epidermal cells, instead of an expected ER localization, EYFP-FAD2 localized predominantly to circular structures. To identify the subcellular site of the EYFP-FAD2 localization, colocalization experiments in transiently transformed *Arabidopsis* mesophyll protoplasts were performed. This system allows the simple and rapid localization analysis of the protein of interest in combination with different organelle markers in the endogenous plant background. The fluorescence distribution pattern of EYFP-FAD2 in *Arabidopsis* protoplasts resembled that observed in stably transformed *Arabidopsis* leaf epidermal cells (compare Figure 3.7 and Figure 3.9). Coexpression with different organelle markers revealed that the structures marked by EYFP-FAD2 in leaf cells closely resemble Golgi stacks (see Figure 3.10), whereas other organellar markers did not colocalize, including for peroxisomes or oil bodies (see Figure 3.10 and Figure 3.12). Quantitative image analyses supported the colocalization of EYFP-FAD2 with the Golgi marker with high PCC and MCC values. Interestingly, EYFP-FAD2 localized to Golgi stacks but did not mark the whole Golgi (see Figure 3.10 and Figure 3.11). Two different perspectives of Golgi stacks were observed. In face-on views, the marker showed round filled circles with approx. 1 μm diameter (Nebenführ et al., 1999).

By contrast, EYFP-FAD2 localized only to the rim of these circles. Nebenführ and coworkers sometimes observed ring-like structures in the fluorescence distribution pattern of *GmMan1-GFP*, the protein on which the Golgi marker used in this work is based upon (Nebenführ et al., 1999). At that time, the authors interpreted this fluorescence distribution as osmotically collapsed Golgi stacks. In this study, ring structures were only observed with EYFP-FAD2 and never in the fluorescence distribution of the marker. Therefore, collapsed Golgi stacks do not seem to be the cause for the observed ring-like structures in the EYFP-FAD2 fluorescence distribution. When imaging the side views of the Golgi stacks, the marker protein and EYFP-FAD2 appeared as lines with a length of approx. 1 μm , the diameter of the Golgi stacks in face-on views. When considering Golgi-localization, ER-proximal *cis*-Golgi and ER-averted *trans*-Golgi can be distinguished for some proteins. For instance, Saint-Jore-Dupas and coworkers could clearly distinguish the localization to *cis*-Golgi-localized proteins from *trans*-Golgi-localization in confocal microscopy images, and the fluorescence of a *cis*-Golgi-localized protein and a *trans*-Golgi-localized protein only partially overlapped (Saint-Jore-Dupas et al., 2006). The Golgi marker used in this study is published as a *cis*-Golgi marker (Nelson et al., 2007; Nebenführ et al., 1999). In side-views of Golgi stacks, the fluorescence intensities of EYFP-FAD2 and the *cis*-Golgi marker correlated well, and the maximal fluorescence intensity of both fluorophores closely overlapped (see Figure 3.11B). Nonetheless, to clearly distinguish *cis*-Golgi from *trans*-Golgi localization, further localization experiments using an additional *trans*-Golgi-marker (for example fluorescence-tagged α -2,6-sialyltransferase from *rattus norvegicus*) in high-resolution microscopy are necessary (Boevink et al., 1998; Wee et al., 1998; Saint-Jore-Dupas et al., 2006). Alternatively – or in addition, the Golgi-localization of EYFP-FAD2 could be specified by transmission electron microscopy. So far, these results indicate that EYFP-FAD2 localizes specifically to the peripheral region of the *cis*-face of Golgi stacks.

The Golgi associated membrane region decorated by EYFP-FAD2 was always found in immediate proximity to the ER (see Figure 3.11). Quantitative image analyses of cells coexpressing EYFP-FAD2 and an ER marker resulted in high PCC and MCC values (see section 3.4, Figure 3.10). In image analyses using the Fiji Plugin “Colocalization”, which highlights colocalizing pixels, it was evident that every EYFP-FAD2-marked Golgi stack was surrounded by the ER (see Figure 3.11). This finding is consistent with a general association of Golgi stacks with the ER. Boevink and coworkers analyzed the movements of Golgi stacks in *Nicotiana clevelandii* leaves and found that the Golgi stacks moved along the ER network on underlying actin cables (Boevink et al., 1998). They hypothesized that the moving Golgi stacks allowed the transfer of products (e. g. membrane lipids, proteins)

from the ER to the *cis* site of Golgi stacks (Boevink et al., 1998). In light of this interpretation, the precise localization of EYFP-FAD2 at the ER-Golgi continuum might similarly indicate a role for FAD2 in the transfer of modified fatty acids between ER and *cis*-Golgi to facilitate distribution via the secretory pathway. The molecular signal and retention mechanism guiding FAD2 to this specific localization remain to be elucidated.

McCartney and coworkers performed an in-depth biochemical study on the insertion of FAD2 into the ER membrane and FAD2's C-terminal retention motif. They found that FAD2 is co-translationally inserted into the ER membrane, with the first transmembrane domain likely mediating the membrane insertion event (McCartney et al., 2004). Whereas integral membrane proteins inserted into the ER membrane are generally subject to outbound trafficking via the secretory pathway, proteins might be retained at the ER or other stations of the pathway by retrieval motifs, also called retention signals. ER retrieval motifs mediate the retrograde transport of escaped proteins at the Golgi back to the ER membrane. Disturbance of these retrieval motifs normally results in the transport of the proteins via the secretory pathway to the plasma membrane, where they accumulate (McCartney et al., 2004). FAD2 contains a C-terminal ER-retention motif, which was found to be sufficient to target marker proteins to the ER membrane. The addition of a single amino acid at the extreme C-terminus disrupted ER localization (McCartney et al., 2004). To avoid interference with the ER retention motif, the fluorescence tag was added to the N-terminus. In the present study, EYFP-FAD2 was not ever observed at the plasma membrane, suggesting that the proteins did not travel uncontrolled through the secretory pathway and that the C-terminal localization sequence was undisturbed. Besides the ER-association, McCartney and coworkers observed an additional localization of FAD2 to Golgi particles in onion epidermal cells (McCartney et al., 2004). They suggested that the localization of FAD2 to Golgi particles reflected a saturation of the retrograde transport machinery between ER and Golgi at high expression levels of FAD2. By contrast, in the present study, the localization of FAD2 to Golgi stacks dominated with hardly any fluorescence signal at the ER membrane, suggesting that the Golgi is the actual target localization of FAD2 in leaf cells, which might be reached before first saturating the ER with marker protein. Whether the published C-terminal ER retention signal of FAD2 is responsible for this localization or additional signal sequences play a role will require further investigation.

The observed localization at the Golgi is likely linked to the physiological role of FAD2 in the cells analyzed. In previous studies, FAD2 has been mostly analyzed in the context of (seed) oil biogenesis. By contrast, cells of the root cortex or the leaf epidermis used for localization analyses in this study under normal conditions do not accumulate high amounts of oil. In the vegetative tissues studied, the localization of FAD2 to the Golgi

possibly reflects FAD2's role in controlling the degree of lipid desaturation in extraplastidial membranes. Since lipid assembly and fatty acid desaturation do not occur on all plant membranes, lipids need to be distributed from their site of origin at the ER to other endomembranes and the plasma membrane. Membrane lipids are transported to a large extent via vesicular trafficking to other sites in the plant cell, a process in which the Golgi is an important player (Park et al., 2021; Dupree and Sherrier, 1998). The localization of FAD2 at the Golgi, a dynamic intermediate organelle between the ER and the endomembrane system, places this enzyme in the central organelle for lipid distribution and may allow FAD2 to quickly change between the roles in membrane lipid desaturation and fatty acid desaturation meant for TAG generation. As membrane lipid desaturation is also involved in plant responses to a variety of stresses (He and Ding, 2020), the localization of FAD2 at the Golgi is also consistent with its reported role in mediating stress responses, including responses to cold or salt treatments (Miquel et al., 1993; Zhang et al., 2012; Wallis and Browse, 2002). Preliminary results on the subcellular distribution of EYFP-FAD2 during treatment of protoplasts with salt stress suggest a dynamic transient dissociation of EYFP-FAD2 from the punctate Golgi-particles. Future experiments will be required to address the physiological relevance and underlying molecular mechanisms of such dynamic relocalization.

4.3 FAD2 and FAD3 interact with each other at the ER membrane

As for FAD2, FAD3 was proposed to localize to the ER membrane and *BnFAD3* was previously shown to associate with the ER upon expression in BY-2 cells (Dyer and Mullen, 2001). A classical C-terminal ER retention motif different from that of FAD2 has been shown to be able to localize a fluorescent marker protein to the ER membrane (McCartney et al., 2004). In contrast to the expected ER localization, in transformed Arabidopsis plants a functional EYFP-FAD3 fusion protein was not seen in ER like structures. Instead, circular structures similar to the distribution pattern of EYFP-FAD2 were observed in the root cortex and in leaf epidermal cells (see section 3.3, Figure 3.8). Since for EYFP-FAD2 these structures were found to be Golgi stacks, it is assumed that EYFP-FAD3 also localizes to the Golgi in stable plant lines. This assumption needs to be verified, for example by crossing the generated plant lines with plants expressing different organelle markers. When compared to the analyses of EYFP-FAD2, EYFP-FAD3 presented some experimental challenges. Notably, localization analyses in stably transformed plant lines was performed with 7-day-old seedlings. In older plants EYFP-FAD3 fluorescence was no longer detectable despite the lipid profile and the physical appearance of the complemented mutants resembling wild type plants.

To elucidate the subcellular distribution of fluorescence-tagged FAD3, localization analyses were performed in *Arabidopsis* mesophyll protoplast. Surprisingly, the ring structures marked by EYFP-FAD3 fluorescence in intact seedlings were not observed in protoplasts. Instead, a net-like structure was visible and colocalization with an ER marker revealed that the net-like structure marked by mCherry-FAD3 fluorescence was the ER network (see section 3.5, Figure 3.13). Quantitative image analyses resulted in high PCCs substantiating the localization of FAD3 to the ER. The experiments were performed with both EYFP- and mCherry-tagged FAD3 variants and did not differ in the outcome. These results indicate that the nature of the tag did not influence the subcellular localization of FAD3.

The differences in the localization of FAD3 in leaves of stably transformed plants and in *Arabidopsis* mesophyll protoplasts was unexpected, and several factors might have contributed to the divergent observations. For instance, the isolation of protoplasts from leaves causes substantial physiological stress to the cells. The leaves were cut in stripes, meaning that the cells experienced wounding stress. With isolating single cells from the tissue, cell-cell contacts were destroyed. Furthermore, the cells were kept in the dark for an extended period during protein expression. It is also possible that enhanced membrane trafficking in consequence of the digested cell wall might influence the subcellular distribution of EYFP-FAD3 in protoplasts. Another reason could be the age of the plants analysed. The localization of FAD3 in whole leaf tissue was analysed in seedlings, while the plants for protoplast isolation were 6 to 8 weeks old and therefore resembled a different developmental stage. It is also possible that endogenous FAD3 in the wild type protoplasts influenced the localization of the ectopically overexpressed fluorescence-tagged FAD3. These notions were not experimentally addressed in this thesis. Overall, in contrast to the observations for EYFP-FAD2, the EYFP-FAD3 fusion did not display an equivalent distribution pattern when expressed in *Arabidopsis* mesophyll protoplasts (compare 3.3 Figure 3.8 and Figure 3.13), suggesting additional factors governing the subcellular distribution of EYFP-FAD3 in these cells.

The mutant complementation and localization analyses were performed with fluorescence-tagged FAD3 variants under the expression control of the *pCaMV35S* promoter. This expression regime was chosen, because usage of the endogenous *FAD3* promoter had not resulted in detectable fluorescence signal in protoplasts. A possible explanation is that FAD3's dominant physiological role lies in the biogenesis of seed oil and that thus FAD3 might not be expressed to large amounts in non-oleogenic vegetative tissues. To test this hypothesis, mCherry-FAD3 was coexpressed with the transcription factor WRI1 tagged to EYFP. While the *FAD3* gene is not a known target of WRI1, WRI1 is described as the

“master regulator” of fatty acid biosynthesis, and it plays a major role in the transcriptional regulation of seed oil biogenesis (Baud et al., 2007; Chapman and Ohlrogge, 2012). In this thesis, the coexpression of WRI1-EYFP substantially enhanced the abundance of mCherry-FAD3 expressed under the control of its native promoter. However, the subcellular localization of mCherry-FAD3 was not altered by the coexpression with WRI1-EYFP (see section 3.7, Figure 3.15). These observations support the assumption that FAD3’s predominant role might lie in the generation of desaturated fatty acid for seed oil biogenesis rather than in the desaturation of fatty acids in vegetative tissues, as it was proposed for FAD2 in this work. This notion is also consistent with the overall fatty acid composition of extraplastidial membrane lipids, which contain mostly 18:2^{Δ9,12} and only a minor proportion of 18:3^{Δ9,12,15}, thus differing in their degree of unsaturation from plastidial galactolipids, which mostly contain the trienoic linolenic or hexadecatrienoic acids (see Figure 3.6, Miquel and Browse, 1992). Since the *FAD3* gene is no known target of WRI1-mediated transcriptional regulation, the mechanism by which FAD3-occurrence is influenced by WRI1-coexpression remains to be elucidated. It is conceivable that a different factor, which is activated by WRI1, stabilizes FAD3 at the ER membrane, resulting in a higher protein abundance of FAD3. The stability of FAD3 might be regulated by posttranslational modifications, as it has been proposed to play a role in FAD2 stability and protein abundance (Tang et al., 2005; O’Quin et al., 2010; Dyer and Mullen, 2001). To clarify on which level the occurrence of FAD3 is regulated by the activity of WRI1, further research will be needed.

FAD2 and FAD3 are homologous enzymes, which have been shown to interact and to functionally cooperate with each other (Lou et al., 2014). The interaction of FAD2 and FAD3 could also be observed in yeast two-hybrid studies presented in this work (see section 3.8, Figure 3.16). With functional and differently tagged enzyme variants at hand, colocalization experiments with FAD2 and FAD3 were the next logical step. EYFP-FAD2 and mCherry-FAD3 were coexpressed in *Arabidopsis* mesophyll protoplasts. EYFP-FAD2 localized in circular Golgi stacks associated with mCherry-FAD3-fluorescence in the ER network (see section 3.6, Figure 3.14). The colocalization of EYFP-FAD2 and mCherry-FAD3 resembled the relative localization of EYFP-FAD2 and the ER marker. Accordingly, quantitative image analyses resulted in similar PCC values for the colocalization of FAD2 and FAD3 as for the colocalization of FAD2 and the ER marker (see section 3.6, Figure 3.14).

The interaction of FAD2 and FAD3 was verified in BiFC-experiments. Protoplasts expressing FAD2 and FAD3 fused to one half each of EYFP showed reconstituted EYFP-fluorescence in a network-like structure resembling the ER network (see section 3.11,

Figure 3.20). This indicates that besides the different localization pattern of FAD2 and FAD3, the enzymes are able to interact with each other and that the interaction site is likely the ER membrane. Since FAD2 alone predominantly localized to Golgi stacks in leaf cells, the interaction and substrate channeling of FAD2 and FAD3 may especially occur under oil producing conditions for which FAD2 might need to dynamically redistribute from the Golgi to other regions in the ER membrane.

4.4 Novel interactions between fatty acid desaturases and acyltransferases

The finding that WRI1-expression enhanced the mCherry-FAD3 abundance when under the expression control of the endogenous promoter indicates a direct involvement of the fatty acid desaturases in the seed oil biogenesis. Therefore, it was tested whether other elements involved in TAG biosynthesis may influence the precise localization of FAD2 and FAD3. The last step in the formation of TAG in Arabidopsis is catalyzed by the acyltransferases DGAT1, DGAT2 and PDAT. In yeast two-hybrid assays, interactions of both fatty acid desaturases, FAD2 and FAD3, with the acyltransferases PDAT, DGAT1 and DGAT2 were analyzed. Besides the published interactions between FAD2 and FAD3 (Lou et al., 2014), novel interactions between both desaturases and all three tested acyltransferases were observed (see section 3.8, Figure 3.16). These results indicate that these enzymes can physically associate, as has previously been proposed for substrate channeling during fatty acid modification and oil assembly (Lou et al., 2014). The yeast two-hybrid experiments were performed with the ubiquitin halves fused in different orientations to the proteins of interest. As it is common with such experiments, not all interactions were seen in all tested directions. Hence, the orientation of the tag may influence the ability of the proteins to interact with each other, or alternatively may influence protein expression. For example, when PDAT was used as bait protein with the ubiquitin half and the transcription factor fused to its C-terminus, no growth of the positive control was observed. Since the unaltered ubiquitin halves used in the positive controls reconstitute on their own, this observation indicates that the fusion protein may not be (fully) expressed. Similar effects were observed for interaction analyses using DGAT1. Only the combination of C-terminally tagged DGAT1 as a bait protein and N-terminally tagged prey proteins resulted in interpretable data. It has been hypothesized, that the active form of DGAT1 is represented by homodimers and homotetramers and that the N-terminus may be responsible for oligomerization (Regmi et al., 2020; Xu et al., 2018). Accordingly, Regmi and coworkers could show an interaction of DGAT1 with itself, that could not be observed in this work (Regmi et al., 2020). It is possible that the N-terminal

fusion of the ubiquitin half to DGAT1 disturbs the self-interaction.

The localization patterns of fluorescence-tagged FAD2 and FAD3 indicated at least partial association with the Golgi, or at least with membrane regions not strictly covering the ER. Therefore, it was next tested whether other enzymes that are involved in plant oil biogenesis and thought to reside in the ER (PDAT and DGAT1) might also display unexpected distribution patterns. To analyze the subcellular distribution of PDAT and DGAT1, fluorescence-fusion constructs were generated, and their functionality examined first in yeast mutant complementation experiments. Fluorescent fusion variants of PDAT were able to complement the TAG deficiency in the acyltransferase deficient yeast strain H1246, regardless of which fluorescence protein was used or to which terminus it was fused. Similarly, the N-terminally tagged DGAT1-variants tested also proved to be functional in yeast complementation experiments (see section 3.9, Figure 3.17).

The subcellular localizations of the functional fusions of DGAT1 or PDAT were analyzed upon transient expression in *Arabidopsis* mesophyll protoplasts. Both enzymes contain ER retrieval motifs similar to that of FAD2 at their C-termini. In DGAT1, the ER retention signal is not found at the extreme C-terminus (McCartney et al., 2004; Shockey et al., 2006). In accordance with previous studies (Shockey et al., 2006; Kim et al., 2011), both acyltransferases localized to the ER membrane. The colocalizations of PDAT and DGAT1 with an ER marker were quantified and revealed high PCCs, respectively (see section 3.10, Figure 3.18 and Figure 3.19). Since the *Arabidopsis* mesophyll protoplasts used in this study do not accumulate TAG under normal conditions and the proteins were overexpressed under the control of the *pCaMV35S* promoter, the localization of both enzymes in oil forming tissues remains to be addressed, ideally under the control of their respective endogenous promoter and in a mutant background.

In BiFC experiments, reconstituted EYFP-fluorescence from the EYFP halves fused to PDAT and FAD2, respectively, was seen in structures resembling the ER network (see section 3.11, Figure 3.20). This finding verified the interactions between FAD2 and PDAT observed in yeast two-hybrid studies and revealed the ER as the site of interaction. The relevance of the observed interactions on the subcellular localization, the enzyme activity or substrate channeling will require further investigation.

The finding that both FAD2 and FAD3 were able to interact with acyltransferases supports an involvement of FAD2 and FAD3 in TAG biogenesis. Furthermore, the data suggest the occurrence of specialized TAG-forming protein clusters at the ER membrane, bringing proteins involved in the generation of TAG into close proximity and facilitating their cooperation. To what extent the observed interactions occur and play a role in plant cells remains to be elucidated. It is conceivable that the interactions may be dynamic and may

vary depending on the cell type and the metabolic context. An interaction of FAD2 and FAD3 with PDAT could improve the shuttling of membrane-disturbing fatty acids into TAG. Even though in *Arabidopsis* the extraplastidial FADs (FAD2 and FAD3) do not produce unusual, membrane disturbing fatty acids, the ability of those three enzymes to interact with each other hints to an effective shuttling of fatty acids away from membranes into TAG. In oil forming tissues, interaction between the desaturases with the major TAG forming enzyme DGAT1 may facilitate TAG formation. Since PC-bound fatty acids are not a substrate for DGAT1-mediated TAG production, the interactions of DGAT1 with FAD2 and FAD3 are an interesting finding. To metabolically connect DGAT1 and FAD activities, further enzyme activities are needed. For instance, LPCATs exchange fatty acids between the PC-pool and the acyl-CoA-pool (Stymne and Stobart, 1984; Bates et al., 2012; Bates et al., 2013), connecting the fatty acid desaturation mediated by FADs with the TAG assembly mediated by DGAT1. It is possible that FADs and DGATs are found together with LPCATs in a functional metabolic cluster increasing the flux of desaturated fatty acids into TAG. Preliminary data from yeast two-hybrid analyses indicated the ability of LPCAT1 (AT1G12640) and LPCAT2 (AT1G63050) to interact with FAD2, FAD3 and PDAT, respectively. LPCAT2 also displayed additional interactions with DGAT1 and DGAT2_{opt}. Further interactions and the subcellular localization underlying this functional clusters need to be elucidated and possible additional players identified.

4.5 In a nutshell and future perspectives

The results presented in this thesis reveal a novel localization of the key oleoyl desaturase FAD2 to Golgi stacks. Even though FAD2 is a known interaction partner of the linoleoyl desaturase FAD3, in protoplasts the localization of FAD2 differed from that of FAD3, which resided at the ER network. FAD3-abundance has been shown to be influenced by WRI1, which indicates a relevant role of FAD3 in the oil biogenesis. Together with novel interactions between FAD2 or FAD3 and acyltransferases, the newly discovered Golgi association of FAD2 may illustrate differential roles of fatty acid desaturases in vegetative tissues or under TAG producing conditions. The localization of FAD2 to Golgi stacks positions the enzyme in a central organelle for the distribution of membrane components via the secretory pathway, with contact to the site of lipid assembly, the ER membrane. Localization analyses using BiFC constructs illustrated the ability of FAD2 to dynamically localize to the ER membrane when interacting with FAD3 or PDAT.

The plant lines generated in this thesis expressing EYFP-tagged FAD2 and FAD3 in the respective mutant background will be useful tools for further investigation of the localization of FAD2 and FAD3 under different conditions and in different developmental stages.

Crossing of these plants with lines expressing different organelle markers will allow the verification of the observed localizations to Golgi stacks and the ER membrane in intact tissues. The localization of FAD2 to Golgi stacks provides the basis for further investigations. By using immunogold electron microscopy, the observed localization of FAD2 to the rim of the *cis* site of Golgi stacks could be further resolved. Different chemical treatments influencing the vesicle transport and the protein transport between the ER and the Golgi combined with live cell imaging could provide new insights in the dynamic of the ER-Golgi localization of FAD2. The molecular mechanisms of ER-retention of FAD2 or FAD3 might involve posttranslational modifications of FAD2 and FAD3, a topic that is currently not well explored. Further research will be needed to determine the nature and position of possible modifications and their influence on localization, enzyme activity and protein stability. Moreover, the existence of Golgi-derived sugar modifications could further verify FAD2's localization to the Golgi.

Besides these conceptual aspects, further progress in microscopic technology might aid future work. While in this thesis FAD2 was analyzed in easily accessible cells from vegetative tissues, FAD2's localization also needs to be addressed in the context of oil formation. Such experiments might require the coexpression of FADs with acyltransferases in tissues involved in seed filling, such as developing siliques. However, due to the limited depth of optical penetration, these tissues are currently not feasible for detailed microscopic scrutiny. The well-characterized WR11 transcription factor, that was already used in this work for localization analysis of FAD3, could help to mimic oil-forming conditions in other vegetative tissues. Additional lipid analyses from plant material expressing FADs, acyltransferases and WR11 could help to elucidate functional connections between these enzymes.

In this context, the interaction analyses performed here by yeast two-hybrid tests or BiFC experiments might be verified in more detail by protein crosslinking combined with mass spectrometry, possibly leading to the identification of additional components, that could be relevant in the establishment of TAG forming clusters at the ER membrane.

Taken together, the results presented in this thesis highlight different roles of FAD2 and other enzymes in vegetative and oil forming tissues and hint to the existence of TAG forming clusters in the ER membrane. While a new and unexpected localization has been observed for an important enzyme, and many other important observations were made, the outcome of this work leads to new questions to be addressed in future research.

5. Materials and Methods

5.1 Devices and Equipment

All specific devices are listed in the appendix in Table 7.1.

5.2 Chemicals

Specific chemicals are listed in the appendix in Table 7.2. All chemicals not specifically mentioned were purchased from Sigma-Aldrich/Merck (Munich/Darmstadt, Germany), Carl Roth GmbH (Karlsruhe, Germany) or AppliChem (Darmstadt, Germany). All solvents used in this work were purchased from Carl Roth GmbH (Karlsruhe, Germany) or Honeywell International Inc. (Offenbach, Germany).

5.3 Standards, enzymes, molecular size markers

Lipid and fatty acid standards are listed in the appendix in Table 7.3. All restriction enzymes used in this work were purchased from New England Biolabs Inc. (Frankfurt am Main, Germany). If available, high-fidelity enzyme variants were chosen. Other enzymes and molecular size markers are listed in the appendix in Table 7.4.

5.4 Consumables and kits

Kits and consumables are listed in the appendix in Table 7.5.

5.5 Microorganisms

Escherichia coli (*E. coli*) NEB5 α (New England Biolabs Inc., Frankfurt am Main, Germany)
Genotype: *fhuA2* Δ (*argF-lacZ*)*U169 phoA glnV44 Φ 80 Δ (lacZ)M15 gyrA96 recA1 relA1 endA1 thi-1 hsdR17*

Agrobacterium tumefaciens (*Agrobacterium/A. tumefaciens*) AGL-0 (Lazo et al., 1991)
Genotype: *C58 pTiBo542; recA::bla Tregion deletiert Mop(+)* *Cb(R)*

Saccharomyces cerevisiae INVSc1 (Invitrogen™, Thermo Fisher Scientific, Schwerte, Germany)

Genotype: *MAT α his3 Δ 1 leu2 trp1-289 ura3-52/MAT α his3 Δ 1 leu2 trp1-289 ura3-52*

Saccharomyces cerevisiae H1246 (Sandager et al., 2002)

Genotype: *MAT α ade2-1 can 1-100 his3-11,15 leu2-3,112 trp1-1 ura3-1 are1- Δ ::HIS3 are2- Δ ::LEU2 dga1- Δ ::KanMX4 Iro1- Δ ::TRP1 ADE2*

Saccharomyces cerevisiae NMY51 (Dualsystems Biotech AG, Zurich, Switzerland)

Genotype: *MATa*, *his3Δ200*, *trp1-901*, *leu2-3,112*, *ade2*, *LYS2::(lexAop)4-HIS3*, *ura3::(lexAop)8-lacZ (lexAop)8-ADE2 GAL4*)

5.6 Plants

The experiments performed in this study were conducted in *Arabidopsis* lines with the ecotype *Arabidopsis thaliana* Columbia-0 (Col-0, wild type) if not stated otherwise.

Col-0	originally obtained from Lehle Seeds (http://www.arabidopsis.com)
<i>fad2-1</i>	EMS mutant, defective in fatty acid desaturase 2 (Lemieux et al., 1990; Okuley et al., 1994)
<i>fad3-2</i>	EMS mutant, defective in fatty acid desaturase 3 (Browse et al., 1993)
GFP-HDEL	ER marker line. Overexpression of ER-targeted GFP (gift from Prof. Dr. Staffan Persson, Copenhagen)

5.7 Culture media and growth conditions

All media and amino acid stock solutions were autoclaved for 15 min at 121 °C before use. Glucose and galactose stock solutions were sterilized by filtration. The antibiotics used for bacteria selection were purchased from Duchefa (Haarlem, Netherlands) and are listed together with other media supplements in Table 5.1.

Table 5.1. Antibiotics and supplements.

Antibiotic	Stock concentration	final concentration	solvent
Carbenicillin	100 mg/ml	100 µg/ml	H ₂ O
Kanamycin	50 mg/ml	50 µg/ml	H ₂ O
Rifampicin	50 mg/ml	50 µg/ml	Methanol
Spectinomycin	50 mg/ml	50 µg/ml	H ₂ O
isopropyl β-D-1-thiogalactopyranoside (IPTG)	1 M	50-100 mM	H ₂ O
5-bromo-4-chloro-3-indolyl-β-D-galactopyranoside (β-X-gal)	80 mg/ml	8-16 mg/ml	di-methyl formamide (DMF)

5.7.1 Growth conditions for *E. coli*

E. coli cells were grown at 37 °C. Liquid cultures were shaken at 180 rpm.

LB medium: 0.5 % (w/v) yeast extract, 1 % (w/v) tryptone, 0.5 % (w/v) NaCl
1.5 % (w/v) micro-agar for solid medium

5.7.2 Growth conditions for *A. tumefaciens*

A. tumefaciens cells were grown at 28-30 °C. Liquid cultures were shaken at 180 rpm.

YEB medium: 0.5 % (w/v) beef extract, 0.1 % (w/v) yeast extract, 0.1 % (w/v) tryptone, 0.5 % (w/v) saccharose, 0.123 % (w/v) MgSO₄ • 7 H₂O
1.5 % (w/v) micro-agar for solid medium

5.7.3 Growth conditions for yeast

Yeast cells were grown at 30 °C, if not stated otherwise. Liquid cultures were shaken at 180 rpm. For the maintenance of yeast strains, colonies were plated out on YPAD medium every two weeks. For long term storage, glycerol stocks were prepared from YPAD overnight cultures with a final glycerol concentration of 12.5 % (v/v) and stored at -80 °C. Transformed yeast was plated out on SD medium. For selection, the transformed yeast cells were spread on medium lacking the corresponding amino acids. The composition for the yeast media and the amino acid stock solutions used are listed below.

YPAD: 1 % (w/v) yeast extract, 2 % peptone, 0.004 % (w/v) adenine hemi sulfate,
2 % (w/v) glucose
2 % (w/v) micro-agar for solid medium

SD: 0.17 % (w/v) yeast nitrogen base without amino acids and ammonium sulfate, 0.5 % (w/v) (NH₄)₂SO₄
2 % (w/v) micro-agar for solid medium
2 % (w/v) glucose or galactose added after autoclaving
1x amino acid stock solution added after autoclaving

Amino acid stock solutions (10x):

-W: 200 mg/l L-adenine hemi sulfate, 200 mg/l L-arginine HCl, 200 mg/l L-histidine HCl monohydrate, 300 mg/l L-isoleucine, 200 mg/l L-leucine, 300 mg/l L-lysine HCl, 200 mg/l L-methionine, 500 mg/l L-phenylalanine, 2000 mg/l L-threonine, 300 mg/l L-tyrosine, 200 mg/l uracil, 1500 mg/l L-valine und 200 mg/l L-serine

- LW: same as -W but without L-leucine
 -LWH: same as -W but without L-leucine and L-histidine HCl monohydrate
 -Ura: same as -W but with 200 mg/l L-tryptophan and without uracil

5.7.4 Growth conditions for Arabidopsis

Arabidopsis plants were cultivated in Adaptis A1000 plant chambers (Conviron, Cambridgeshire, United Kingdom) or PERCIVAL AR-66/L3 plant chambers (Percival Scientific, Perry, IA, USA).

Nine parts of Substrate 1 (Klasmann-Deilmann GmbH, Geeste, Germany) with one part of vermiculite were used as soil substrate. The soil substrate was steamed at 80 °C for 8-10 h before use. Plants used for protoplast isolation were grown under short-day conditions (8-10 h light at 21 °C, 14-16 h dark at 18 °C) for 6-8 weeks. Plants for stable transformation and seed propagation were grown for 4-6 weeks under short-day conditions, followed by long-day conditions (16 h light at 21 °C, 8 h darkness at 18 °C) to induce shoot growth.

For growth on solid ½ MS medium, seeds were surface sterilized in 1 ml of 6 % (v/v) sodium-hypochlorite solution with 0.01 % (v/v) Triton-X-100 for 10 minutes. The seeds were washed 4-6 times with sterile water, resuspended in 0.1 % (w/v) agarose solution and stratified for 2 days at 4 °C in the dark either in agarose solution or on ½ MS plates.

½ MS medium: 0.22 % (w/v) Murashige & Skoog medium incl. modified vitamins, 1 % (w/v) sucrose, 0.8 % (w/v) micro-agar, pH 5.6 with 1 M KOH

5.8 Salt treatment and root length measurements of Arabidopsis

Plants for salt stress experiments were grown sterile on ½ MS medium (as described in section 5.7.4) containing 0 mM (control), 75 mM, 100 mM, and 125 mM NaCl. The amounts of NaCl were added directly to the medium. Seedlings were grown for 7 days under long-day conditions. To document root growth the plates were scanned, and root lengths were measured using Fiji (Schindelin et al., 2012).

5.9 Vectors

pEntryA-pCaMV35S *Amp^R*, based on *pUC18*, contains two different SfiI-cutting sites for the introduction of a promoter sequence and a multiple cloning site (mcs) followed by the polyA-terminator from the octopin synthase gene (OCS) from *Agrobacterium tumefaciens*. The promoter, mcs and OCS terminator are flanked by *att*-sites

- (*attL1* and *attL4*) for recombination with the dual Gateway™ system. (Dr. Mareike Heilmann, Halle)
- pEntryD-pCaMV35S* *Amp^R*, based on pUC18, contains two different *SfiI*-cutting sites for the introduction of a promoter sequence and a mcs followed by the polyA-terminator from OCS. The promoter, mcs and OCS terminator are flanked by att-sites (*attR4* and *attL2*) for recombination with the dual Gateway™ system. (Dr. Mareike Heilmann, Halle)
- pCAMBIA3300.0GS* *Kan^R* in bacteria, *Basta^R* in plants. Contains a *ccdB* gene flanked by *attR1* and *attR2* recombination sites. Serves as a target vector of the Clonase™-mediated dual Gateway™ reaction. Contains the left border sequence and right border sequence for Agrobacterium mediated stable transformation in plants. (Dr. Ellen Hornung, Göttingen)
- pESC-TRP* *Amp^R*, based on *pUC*, contains two mcs with a FLAG-tag and c-myc-tag, respectively. mcsI is flanked by *GAL10* promoter and *ADH1* terminator. mcsII is flanked by *GAL1* promoter and *CYC1* terminator. Contains the open reading frame (ORF) of *TRP1* for selection in yeast. (Agilent Technologies, VWR International GmbH, Darmstadt, Germany)
- pESC-URA* *Amp^R*, based on *pUC*, contains two mcs with a FLAG-tag and c-myc-tag, respectively. mcsI is flanked by *GAL10* promoter and *ADH1* terminator. mcsII is flanked by *GAL1* promoter and *CYC1* terminator. Contains the ORF of *URA3* for selection in yeast. (Agilent Technologies, VWR International GmbH, Darmstadt, Germany)
- pBT3-C* *Kan^R*, bait vector for yeast two-hybrid analyses. Contains the ORF of *LEU2* for selection in auxotrophic yeast. Contains a mcs for C-terminal fusions to the C-terminal ubiquitin half (Cub, amino acids 35 to 76) and transcription factor LexA-VP16. The gene expression is controlled by *CYC1* promoter and terminator. (Dualsystems Biotech AG, Zürich, Schweiz)

<i>pBT3-N</i>	<i>Kan^R</i> , bait vector for yeast two-hybrid analyses. Contains the ORF of <i>LEU2</i> for selection in auxotrophic yeast. Contains a mcs for N-terminal fusions to Cub and transcription factor LexA-VP16. The gene expression is controlled by <i>CYC1</i> promoter and terminator. (Dualsystems Biotech AG, Zürich, Schweiz)
<i>pPR3-N</i>	<i>Amp^R</i> , prey vector for yeast two-hybrid analyses. Contains the ORF of <i>TRP1</i> for selection in auxotrophic yeast. Contains a mcs for N-terminal fusions to a mutated N-terminal ubiquitin half (NubG, amino acids 1 to 34, point mutation: isoleucine 13 to glycine). The gene expression is controlled by <i>CYC1</i> promoter and terminator. (Dualsystems Biotech AG, Zürich, Schweiz)
<i>pAI-Alg5</i>	<i>Amp^R</i> , prey vector for yeast two-hybrid analyses as positive control. <i>TRP1</i> auxotrophic marker for selection in yeast. Contains Nub fused to the cDNA of <i>dolichyl-phosphate beta-glucosyl-transferase</i> (<i>Alg5</i>). (Dualsystems Biotech AG, Zürich, Schweiz)
<i>pDL2-Alg5</i>	<i>Amp^R</i> , prey vector for yeast two-hybrid analyses as negative control. <i>TRP1</i> auxotrophic marker for selection in yeast. Contains NubG fused to <i>Alg5</i> . (Dualsystems Biotech AG, Zürich, Schweiz)
<i>pDONR221-P1P4</i>	<i>Kan^R</i> , <i>attP1</i> and <i>attP4</i> recombination sites flank a <i>ccdB</i> gene and chloramphenicol resistance gene, which can be exchanged against the cDNA of a gene of interest. Serves as a donor vector for Clonase TM -mediated dual Gateway TM reaction. (Grefen and Blatt, 2012)
<i>pDONR221-P3P2</i>	<i>Kan^R</i> , <i>attP3</i> and <i>attP2</i> recombination sites flank a <i>ccdB</i> gene and chloramphenicol resistance gene, which can be exchanged against the cDNA of a gene of interest. Serves as a donor vector for Clonase TM -mediated dual Gateway TM reaction. (Grefen and Blatt, 2012)
<i>pBiFCt-2in1-NC</i>	<i>Spec^R</i> , <i>attR3</i> and <i>attR2</i> recombination sites flank a <i>lacZ</i> expression cassette and allow for recombination with

pDONR221-P3P2 to form N-terminal fusion proteins with the N-terminal half of EYFP and an HA tag. *attR1* and *attR4* recombination sites flank a *ccdB* gene and chloramphenicol resistance gene and allow for recombination with *pDONR221-P1P4* to form C-terminal fusion proteins with a myc-tag and the C-terminal half of EYFP. Contains the cDNA of RFP as transformation control. All expression cassettes are under the control of the *pCaMV35S* promoter and terminator. Contains the left border sequence and right border sequence for Agrobacterium mediated stable transformation in plants. (Grefen and Blatt, 2012)

5.10 Molecular biology methods

5.10.1 Isolation of RNA from seeds and siliques

For the isolation of RNA, 15-20 mg seeds or 60 mg siliques were homogenized in liquid nitrogen with mortar and pestle, resuspended in 2 ml extraction buffer and incubated overnight at 4 °C. The extracts were centrifuged for 4 s at 15,870 x *g* to get rid of cell debris. The supernatant was centrifuged at 15,870 x *g* and 4 °C for 30 min. The sediment was washed with 500 µl 75 % (v/v) ethanol and centrifuged again for 5 min at 15,870 x *g* and 4 °C. The sediment was dissolved in 500 µl solubilization buffer. The nucleic acids were extracted twice with 500 µl phenol (pH 4.3), once with 500 µl phenol:chloroform:isoamyl alcohol (IAA) (25:24:1, v/v/v) and twice with 500 µl chloroform:IAA (24:1, v/v). In between the extraction steps the samples were centrifuged for 5 min at 15,870 x *g* at room temperature. The upper phase was transferred to a fresh reaction tube after each centrifugation. For precipitation 0.1 volumes sodium acetate (pH 5) and 1.5 volumes ethanol were added to the extract and mixed by inverting. The samples were incubated at -80 °C for 0.5 to 2 hours. The RNA was sedimented by centrifugation at 15,870 x *g* and 4 °C for 10 min. The sedimented RNA was washed with 500 µl 75 % ethanol (v/v) and centrifuged again at 4 °C and 15,870 x *g* for 5 min. The ethanol was discarded, and the RNA dried at room temperature for approx. 10 min. The RNA was dissolved in 20 µl H₂O.

Extraction buffer: 8 M lithium chloride, 2 % (v/v) β-mercaptoethanol

Solubilization buffer: 0.5 % (w/v) sodium dodecyl sulfate (SDS), 100 mM NaCl, 25 mM ethylenediaminetetraacetic acid (EDTA), 10 mM tris base, pH 7.6

5.10.2 Isolation of RNA from leaves and seedlings

For the isolation of RNA from leaves and seedlings, 30-50 mg plant material were homogenized with mortar and pestle in liquid nitrogen. The homogenized material was resuspended in 1 ml TRIzol and centrifuged at 15,870 x *g* and 4 °C for 10 min. The supernatant was mixed with 200 µl chloroform, and incubated at room temperature for 2-3 min. The samples were centrifuged again as described. The upper phase was mixed with 0.5 volumes of isopropanol and 0.5 volumes of high salt precipitation buffer (HSPB). After incubation for 10 min at room temperature the samples were centrifuged at 15,870 x *g* and 4 °C for 15 min. The sedimented RNA was washed with 900 µl 75 % (v/v) ethanol and centrifuged again at 15,870 x *g* and 4 °C for 5 min. The supernatant was discarded, and the sediment was dried at room temperature for approx. 10 min. The RNA was dissolved in 20 µl H₂O.

TRIzol: 38 % (v/v) phenol (saturated with 0.1 M citrate, pH 4.3), 0.8 M guanidinium thiocyanate, 0.4 M ammonium thiocyanate, 0.1 M sodium acetate, pH 5.0, 5 % (v/v) glycerol

HSPB: 0.8 M sodium citrate, 1.2 M NaCl

5.10.3 Concentration measurements of nucleic acid

The concentration of nucleic acid solution was determined by photometric measurements. The “NanoDrop 2000 spectrophotometer” (Thermo Fisher Scientific, Schwerte, Germany; software version 1.4.1) was used to measure the absorption at a wavelength of 260 nm. An absorption of 1 equaled 50 µg/ml DNA and 40 µg/ml RNA, respectively.

5.10.4 cDNA-Synthesis

For the synthesis of complementary DNA (cDNA) from RNA the “RevertAid H Minus First Strand cDNA Synthesis Kit” (Thermo Fisher Scientific, Schwerte, Germany) was used according to the manufacturer’s manual. cDNA was synthesized from 1-5 µg of RNA in a total reaction volume of 20 µl.

5.10.5 Isolation of genomic DNA

To isolate genomic DNA from Arabidopsis as template for PCRs, the “GeneJET™ Plant Genomic DNA Purification Kit” (Thermo Fisher Scientific, Schwerte, Germany) was used. For this purpose, 80-100 mg of fresh plant leaf material were harvested and grinded in liquid nitrogen with a pestle in 1.5 ml reaction tubes. The Lysis Buffer A was added to the

performed as described in section 5.10.7. The desired DNA bands were cut out and dissolved in 400-500 μ l binding buffer. The extraction was performed as described in the manufacturer's manual. The DNA was eluted with 22 μ l elution buffer.

5.10.9 Restriction of DNA fragments

For cloning purposes, 10 μ l vector-DNA were digested in a total volume of 50 μ l containing each of the appropriate restriction enzymes and 1x CutSmart reaction buffer. Purified PCR-products were digested with 1 μ l of each enzyme solution in 1x CutSmart reaction buffer in a total volume of 25 μ l. The reactions were incubated overnight at the enzyme's optimal reaction temperature. The reaction was stopped by incubation at 80 °C for 10-20 min. Digested vector DNA was purified by agarose gel electrophoreses as described in section 5.10.7 and extracted as described in section 5.10.8.

From *E. coli* isolated plasmid DNA was verified by restriction. For this purpose, 1-3 μ l of plasmid DNA were mixed with 0.2-0.5 μ l enzyme solution in 1x CutSmart buffer in a total volume of 20 μ l. The reaction mixture was incubated for 0.5-1 h at the enzyme's optimal reaction temperature. The DNA-fragments were analyzed by agarose gel electrophoresis as described in section 5.10.7.

5.10.10 Ligation of DNA fragments

To ligate PCR products in vector backbones, 1 μ l of restricted vector and 3 μ l of restricted PCR product were mixed with 1 μ l T4-DNA-Ligase (New England Biolabs Inc., Frankfurt am Main, Germany) in 1x reaction buffer in a total volume of 20 μ l. The reaction was incubated for one hour at room temperature (approx. 20 °C) or overnight at 16 °C. The mixture was transformed into chemo competent *E. coli* for amplification as described in 5.11.2.

5.10.11 Clonase™-mediated Gateway™ reaction

To transfer expression cassettes from *pEntry*-vectors into the plant expression vector *pCAMBIA3300.0GS*, the Gateway™ LR Clonase™ II Enzyme Mix (Invitrogen™, Thermo Fisher Scientific, Schwerte, Deutschland) was used according to the manufacturer's manual. The reaction mixture was scaled down to a final volume of 5 μ l and incubated over night at 25 °C. For each recombination, a *pEntryA*-vector and a *pEntryD*-vector were combined with *pCAMBIA3300.0GS*.

To generate vectors for bimolecular fluorescence complementation analyses, purified PCR products were introduced into *pDONR221*-vectors with the Gateway™ BP Clonase™ II

Enzyme Mix (Invitrogen™, Thermo Fisher Scientific, Schwerte, Deutschland). The resulting plasmids were used to clone the corresponding cDNAs into the target vector *pBiFCt-2in1-NC* by using the Gateway™ LR Clonase™ II enzyme mix.

5.11 Amplification of plasmid-DNA in *E. coli*

5.11.1 Preparation of chemo competent *E. coli*

The preparation of chemo competent *E. coli* was performed as described by Inoue and coworkers (Inoue et al., 1990). For this purpose, 500 ml LB-medium were inoculated with 3-5 ml of an overnight culture of the *E. coli* strain NEB5 α . The cells were grown at 30 °C while shaking at 180 rpm until an OD₆₀₀ of 0.4-0.6 was reached. After incubation for 10 min on ice, the cells were harvested in 50 ml aliquots by centrifugation at 3220 x *g* and 4 °C for 10-15 min. The sedimented cells were resuspended in 10 ml transformation buffer (TFB) and incubated on ice for 10 min. The cells were centrifuged again as described and the sedimented cells were resuspended in 4 ml TFB buffer. The aliquoted cells were pooled and DMSO was added to a final concentration of 7.5 % (v/v). After incubation for 10 min on ice, the cells were aliquoted and frozen in liquid nitrogen. The competent cells were stored at -80°C.

TFB: 10 mM 4-(2-hydroxyethyl)-1-piperazineethanesulfonic acid (HEPES),
15 mM CaCl₂, 250 mM KCl pH 6.7 (KOH)
The buffer was autoclaved at 121 °C for 15 min.
55 mM MnCl₂ (sterile filtered) were added after autoclaving.

5.11.2 Transformation of chemo competent *E. coli*

The transformation of chemo competent *E. coli* was performed as described by Inoue and coworkers (Inoue et al., 1990). Either 1 μ l of plasmid DNA, 20 μ l ligation mixture (see section 5.10.10) or 5 μ l Gateway™-reaction mixture (see section 5.10.11) were used to transform 50-100 μ l of competent cells (see section 5.11.1). The mixtures were incubated on ice for 30 min. A heat shock was applied for 30-60 s at 42 °C. The cells were chilled on ice for 1 min, 900 μ l LB-medium were added and the mixture was incubated at 37 °C for 1 h. For the transformation of ligation and Gateway™ reactions, the cells were precipitated at 15,000 x *g* for 3-5 min and plated on solid LB-medium containing the appropriate antibiotic. For the transformation of plasmid DNA, 50-100 μ l of the transformation reaction were plated on LB-plates with appropriate antibiotics. The plates were incubated over night at 37 °C.

Blue-white selection was performed to identify positive generated *pBiFCt-2in1-NC*

plasmids. For this purpose, β -X-gal and IPTG were added to the LB medium in addition to the antibiotic. The media supplements are listed in Table 5.1.

5.11.3 Isolation of plasmid DNA from *E. coli*

For isolation of plasmid DNA from *E. coli*, 2.5 ml of LB-medium with appropriate antibiotic were inoculated with a single transformed colony and allowed to grow over night at 37 °C while shaking at 180 rpm. The cells were harvested by sedimentation at 15,000 x g for 3-5 min. The plasmid DNA was isolated with the “GeneJET™ Plasmid Miniprep Kit” (Thermo Fisher Scientific, Schwerte, Germany) according to the manufacturer’s instructions.

To isolate larger amounts and achieve higher plasmid concentrations, plasmid DNA was isolated from 50-100 ml of *E. coli* overnight cultures using the “CompactPrep Plasmid Midi Kit” (Qiagen, Hilden, Germany) according to the manufacturer’s instructions.

5.12 Sequencing

Generated plasmids were checked by sequencing. For this purpose, 1 μ g plasmid DNA was mixed with 5 μ l of 5 μ M oligonucleotides in a total volume of 10 μ l. The samples were sequenced by GATC Biotech AG (Eurofins Genomics Germany GmbH, Ebersberg, Germany). The oligonucleotides used for sequencing are listed in the appendix in Table 7.8. The results were analyzed with Chromas (version 2.6.6, Technelysium Pty Ltd, South Brisbane, Australia).

5.13 Cloning strategies

5.13.1 Recombinant plasmids for heterologous protein expression in yeast

For heterologous expression of fatty acid desaturases and acyltransferases from *Arabidopsis* in yeast, the vectors *pESC-TRP* and *pESC-URA*, respectively, were used. Either the cDNA coding for the untagged enzyme or for a fusion to a fluorescence protein were introduced into the vector. As template for cDNA amplification existing *pEntry*-plasmids were used (for *pEntry*-vectors see section 5.13.4). To create coexpression constructs, the cDNA encoding FAD3-variants and the cDNA encoding FAD2 were cloned into the *mcsI* and the *mcsII* of the *pESC-TRP* plasmids, respectively. Cloning techniques were performed as described in section 5.10. The oligonucleotides used for cDNA amplification are listed in Table 7.7. The resulting constructs and the corresponding restriction sites are described in Table 5.2.

Table 5.2. Recombinant plasmids for protein expression in INVSc1 cloned or used in this work. S. Scheer: Plasmids were generated by Sebastian Scheer during his bachelor's thesis in this group. GOI: gene of interest.

Vector	cDNA	restriction sites (fusion protein)	restriction site between GOI and tag	source
<i>pESC-TRP</i>	<i>FAD2</i>	EcoRI, NotI	-	this work
	<i>EYFP-FAD2</i>	EcoRI, NotI	XhoI	S. Scheer
	<i>mCherry-FAD2</i>	Sall, NheI	XhoI	S. Scheer
	<i>FAD3</i> <i>mycFAD2</i>	FAD3: EcoRI, NotI FAD2: XhoI, NheI	-	this work
	<i>EYFP-FAD3</i> <i>mycFAD2</i>	EYFP-FAD3: EcoRI, NotI FAD2: XhoI, NheI	XhoI -	this work
	<i>mCherry-FAD3</i> <i>mycFAD2</i>	mCherry-FAD3: EcoRI, NotI FAD2: XhoI, NheI	XhoI -	this work
<i>pESC-URA</i>	<i>DGAT1</i>	BamHI, NheI	-	this work
	<i>DGAT1-EYFP</i>	BamHI, NheI	XhoI	this work
	<i>DGAT1-CFP</i>	BamHI, NheI	XhoI	this work
	<i>PDAT</i>	Sall, KpnI	-	this work
	<i>PDAT-CFP</i>	Sall, KpnI	NheI	this work
	<i>PDAT-EYFP</i>	Sall, KpnI	NheI	this work
	<i>EYFP-PDAT</i>	Sall, KpnI	AscI	this work

5.13.2 Recombinant plasmids for yeast two-hybrid analyses

For yeast two-hybrid analyses, the bait vectors *pBT3-C* and *pBT3-N* and the prey vector *pPR3-N* were used. The cDNAs coding for the gene of interest (GOI) were introduced into the mcs by SfiI restriction sites. The cDNAs were cloned in frame with Cub, LexA and VP16 or NubG in bait or prey vectors, respectively. The cDNA template for DGAT2 optimized for expression in yeast (DGAT2_{opt}) was kindly provided by Prof. Dr. Thierry Chardot (Aymé et al., 2014). The cloning techniques were performed as described in section 5.10. The oligonucleotides used for the vector generation are listed in the appendix in Table 7.7. The resulting vectors are listed in Table 5.3.

Table 5.3. Recombinant plasmids for yeast two-hybrid analyses cloned or used in this work. S. Scheer: Plasmids were generated by Sebastian Scheer during his bachelor's thesis in this group.

Bait vectors			Prey vectors		
Vector	cDNA	Source	Vector	cDNA	Source
pBT3-C	<i>FAD2</i>	S. Scheer	pPR3-N	<i>FAD2</i>	S. Scheer
	<i>FAD3</i>	S. Scheer		<i>FAD3</i>	S. Scheer
	<i>DGAT1</i>	S. Scheer		<i>DGAT1</i>	S. Scheer
	<i>DGAT2_{opt}</i>	this work		<i>DGAT2_{opt}</i>	this work
	<i>PDAT</i>	S. Scheer		<i>PDAT</i>	S. Scheer
pBT3-N	<i>FAD2</i>	S. Scheer			
	<i>FAD3</i>	S. Scheer			
	<i>DGAT1</i>	S. Scheer			
	<i>DGAT2_{opt}</i>	this work			
	<i>PDAT</i>	S. Scheer			

5.13.3 Recombinant plasmids for bimolecular fluorescence complementation (BiFC)

The cDNAs coding for the GOI were amplified with *att*-recombination sites at the 3' and the 5' end. The amplified cDNAs were introduced into *pDONR221*-vectors by Gateway™ BP Clonase™ mediated recombination. The resulting vectors were combined with the *pBiFCt-2in1-NC* vector by Gateway™ LR Clonase™ mediated recombination. The cloning techniques were performed as described in section 5.10. The oligonucleotides used for cDNA amplification are listed in the appendix in Table 7.7. The resulting constructs and the corresponding restriction sites are listed in Table 5.4.

Table 5.4. Recombinant plasmids for BiFC analyses cloned and used in this work.

Vector backbone	<i>pDONR221-P3P2</i>	<i>pDONR221-P1P4</i>	source
pBiFCt-2in1-NC	<i>Alg5</i>	<i>Alg5</i>	this work
	<i>Alg5</i>	<i>FAD2</i>	this work
	<i>FAD3</i>	<i>Alg5</i>	this work
	<i>PDAT</i>	<i>Alg5</i>	this work
	<i>FAD3</i>	<i>FAD2</i>	this work
	<i>PDAT</i>	<i>FAD2</i>	this work

5.13.4 Recombinant plasmids for heterologous protein expression in plant cells

For localization analyses in transiently transformed plant cells, the plant expression vectors *pEntryA-pCaMV35S* or *pEntryD-pCaMV35S* were used. To generate fluorescent fusion proteins, the cDNA coding for a fluorescence protein (EYFP or mCherry) and the cDNA for the GOI were cloned sequentially into the mcs of the respective vectors. Care was taken to remove the stop codon between the fusion partners and to ensure that both cDNAs were in the same reading frame. For the expression of FAD2 and FAD3 under their endogenous promoter, the genomic sequence upstream of each ATG was amplified and exchanged against the *pCaMV35S* via *SfiI* restriction sites. For the promoter of FAD2 (*pFAD2*), 2,281 bp upstream of the start codon, including the first annotated intron, were chosen. For the promoter of FAD3 (*pFAD3*), 1,632 bp upstream of the start codon were amplified. The cloning techniques were performed as described in section 5.10. The oligonucleotides used for cDNA amplification are listed in the appendix in Table 7.7. The resulting constructs and the corresponding restriction sites are described in Table 5.5.

Table 5.5. Recombinant plasmids for transient transformation of Arabidopsis protoplasts cloned or used in this work. S. Scheer: Plasmids were generated by Sebastian Scheer during his bachelor's thesis in this group. GOI: gene of interest.

Vector	Promoter	cDNA	restriction sites GOI	restriction sites tag	source
<i>pEntryA</i>	<i>pCaMV35S</i>	<i>mCherry-FAD2</i>	XhoI, NotI	Ascl, XhoI	this work
	<i>pFAD2</i>	<i>EYFP-FAD2</i>	XhoI, NotI	Ascl, XhoI	this work
	<i>pCaMV35S</i>	<i>EYFP-FAD3</i>	XhoI, NotI	Ascl, XhoI	S. Scheer
	<i>pFAD3</i>	<i>mCherry-FAD3</i>	XhoI, NotI	Ascl, XhoI	this work
	<i>pCaMV35S</i>	<i>mCherry-FAD3</i>	XhoI, NotI	Ascl, XhoI	S. Scheer
<i>pEntryD</i>	<i>pCaMV35S</i>	<i>DGAT1-EYFP</i>	Ascl, XhoI	XhoI, NotI	S. Scheer
	<i>pCaMV35S</i>	<i>EYFP-PDAT</i>	Ascl, NheI	Sall, Ascl	this work
	<i>pCaMV35S</i>	<i>mCherry-PDAT</i>	Ascl, NheI	Sall, Ascl	this work
	<i>pCaMV35S</i>	<i>WR11-EYFP</i>	Sall, XhoI	XhoI, NotI	this work

For Agrobacterium-mediated stable transformation of Arabidopsis and for simultaneous coexpression of two constructs, the cDNAs in the *pEntryA*- and *pEntryD*-vectors were combined into the plant transformation vector *pCAMBIA3300.0GS* using Gateway™ technology (as described in section 5.10.11). The resulting and used constructs are listed in Table 5.6.

Table 5.6. Recombinant plasmids for stable and transient transformation of *Arabidopsis* generated and used in this work.

Vector	pEntryA		pEntryD		source
	promoter	cDNA	promoter	cDNA	
pCAMBIA 3300.0GS	<i>pFAD2</i>	<i>EYFP-FAD2</i>	empty vector		this work
	<i>pCaMV35S</i>	<i>EYFP-FAD3</i>	empty vector		this work
	<i>pFAD3</i>	<i>EYFP-FAD3</i>	<i>pCaMV35S</i>	<i>WRI1-EYFP</i>	this work
	<i>pFAD3</i>	<i>EYFP-FAD3</i>	<i>pCaMV35S</i>	<i>CFP-SKL</i>	this work

5.14 Preparation and transformation of chemo competent *A. tumefaciens*

The preparation of chemo competent *A. tumefaciens* was performed as described by An (1987). For this purpose, 200 ml YEB medium containing rifampicin were inoculated with *A. tumefaciens* from an overnight culture to an OD₆₀₀ of 0.1-0.2. The cells were grown at 30 °C while shaking at 180 rpm to an OD₆₀₀ of 0.5. The cells were harvested by centrifugation at 3,220 x *g* and 4 °C for 10 min. The sedimented cells were resuspended in 40 ml 150 mM NaCl and sedimented again by centrifugation as described. The cells were resuspended in 4 ml 75 mM CaCl₂ (chilled on ice) and aliquoted. The aliquots were frozen in liquid nitrogen and stored at -80 °C.

The transformation of chemo competent *A. tumefaciens* was performed as described by Lazo and coworkers (Lazo et al., 1991). After thawing, 200 µl cells were mixed with 2-3 µg of plasmid DNA. The mixture was incubated on ice for 30 min. The cells experienced a cold shock by freezing them in liquid nitrogen and were thawed again for 10 min at 37 °C. After addition of 800 µl YEB medium the mixture was incubated at 30 °C for 1.5-2 h. The cells were sedimented by centrifugation at 13,000 x *g* for 5 min and plated on solid YEB medium containing rifampicin and kanamycin. The plates were incubated at 30 °C for two days.

5.15 Preparation and transformation of competent *S. cerevisiae*

The preparation of chemo competent yeast cells was performed by the lithium acetate (LiAc) method (Ito et al., 1983). As preculture, 30-50 ml of YPAD medium were inoculated with cells from the desired yeast strain and grown overnight at 30 °C while shaking at 180 rpm. YPAD-medium was inoculated with preculture at an OD₆₀₀ of 0.15-0.2 and allowed to grow to an OD₆₀₀ of 0.6 at 30 °C while shaking at 180 rpm. The yeast cells were precipitated in 50 ml aliquots by centrifugation at 2,500 x *g* for 5 min and washed once with

10-15 ml TE buffer. The cells were resuspended in 1 ml LiAc/TE buffer, sedimented again and resuspended in 700 μ l LiAc/TE-buffer. The yeast cells were now competent and prepared for transformation.

For transformation, 100 μ l of yeast cells in LiAc/TE buffer and 0.5-1 μ g of plasmid-DNA were mixed. For yeast two-hybrid analyses equal amounts of bait- and prey constructs were used. The cells were subsequently mixed with 700 μ l of PEG/LiAc mix and the reaction mixture was incubated at 30 °C for 30 min while shaking at 180 rpm. Afterwards, 80 μ l of DMSO were added and the mixture was incubated at 42 °C for 15 min. The cells were sedimented at 750 x g for 5 min, the supernatant was dismissed, and the cells were washed with 300 μ l of 0.9 % (w/v) NaCl. After sedimentation by centrifugation at 15,000 x g for 30 s, the cells were resuspended in 100 μ l of 0.9 % (w/v) NaCl and plated on SD-selection medium (see section 5.7.3). The plates were incubated at 30 °C for 3-4 days.

Yeast of strain NMY51 was transformed with bait and prey plasmids (see section 5.13.2) for yeast two-hybrid analyses and selected on SD-LW medium. Yeast of strain INVSc1 or H1246 was transformed with respective *pESC*-based constructs for protein expression (see section 5.13.4) and selected on respective SD-selection medium. After three days at 30 °C, individual positive colonies were streaked on fresh SD-selection medium and allowed to grow again for two days at 30 °C to obtain more cell material for the subsequent protein-protein interaction or protein expression tests.

TE buffer: 10 mM Tris, 1 mM EDTA, pH 7.5

LiAc/TE buffer: 0.1 M lithium acetate (LiAc), 10 mM Tris, 1 mM EDTA, pH 7.5

PEG/LiAc mix: 0.1 M LiAc, 40 % (w/v) polyethylene glycol 4000 (PEG 4000), 10 mM Tris pH 7.5, 1 mM EDTA

5.16 Preparation and transformation of Arabidopsis mesophyll protoplasts

The preparation of protoplasts from Arabidopsis was performed as described by Yoo and coworkers (Yoo et al., 2007). Leaves from 6–8-week-old Arabidopsis plants grown under short-day conditions were cut into 1-2 mm fine strips and were subsequently infiltrated with enzyme solution in an exicator for 30-45 min in the dark. Then, the leaf strips were first left unmoved for 2.5 h in the dark followed by incubation for 30 min with gentle shaking in the enzyme solution in the dark. The protoplasts were filtered through nylon sieves (100 μ m) and centrifuged at 200 x g for 2 min at 12 °C. The supernatant was discarded, the cells were carefully resuspended in 3 ml W5 buffer and incubated for 40 min on ice in the dark

for slow sedimentation. Subsequently, the supernatant was discarded, the cells were carefully resuspended in 3 ml W5 buffer and incubated on ice in the dark for another 40 min. Again, the supernatant was discarded, and the protoplasts were resuspended in MMG buffer to obtain a cell amount of approx. 2×10^5 cells/ml.

Plasmid constructs used for protoplast transformation are listed in Table 5.5 and Table 5.6, organelle markers for colocalization experiments are listed in Table 5.7, and BiFC constructs used are listed in Table 5.4.

For the transformation 50 µg of total plasmid DNA in a max. volume of 50 µl were mixed with 500 µl of protoplast solution. For cotransformation of two vectors, equal amounts of plasmid DNA were used. The protoplasts were mixed with 550 µl PEG solution and the mixture incubated at room temperature for 15 min. Afterwards, the transformation mixture was diluted with 2.2 ml of W5 buffer, and the protoplasts were sedimented at $200 \times g$ for 2 min. The supernatant was discarded, the protoplasts were resuspended in 500 µl WI buffer and incubated overnight in the dark at room temperature. Transformed protoplasts were used for microscopic analyses (see section 5.23), and/or analyzed by SDS-PAGE and immunodetection (see sections 5.18 and 5.19).

Enzyme solution:	0.4 M mannitol, 20 mM KCl, 20 mM 2-(N-morpholino) ethanesulfonic acid (MES) pH 5.7, 1.5 % (w/v) Cellulase "Onozuka R-10" from <i>Trichoderma viride</i> ca. 1 U/mg, 0.4 % (w/v) Maceroenzyme R-10 from <i>Rhizopus sp. lyophile.</i> , 1 M CaCl ₂ , 0.1 g/ml BSA filtered through 0.45 µm syringe filter
W5 buffer:	2 mM MES pH 5.7, 154 mM NaCl, 125 mM CaCl ₂ , 5 mM KCl
MMG buffer:	4 mM MES pH 5.7, 0.4 M mannitol, 15 mM MgCl ₂
PEG solution:	40 % (w/v) PEG-4000, 0.2 M mannitol, 0.1 M CaCl ₂
WI buffer:	4 mM MES pH 5.7, 0.5 mM mannitol, 20 mM KCl

Table 5.7. Organelle markers used for colocalization experiments in Arabidopsis protoplasts.

Marker	Source
<i>CD3-959-ER-mCherry</i>	Nelson et al., 2007
<i>CD3-967-Golgi-mCherry</i>	Nelson et al., 2007
<i>pEntryD-pCaMV35S::CFP-SKL</i>	Dr. Mareike Heilmann, Halle (Saale)
<i>pCAMBIA3300.0GS pCaMV35S::OLE3-mCherry</i>	Dr. Mareike Heilmann, Halle (Saale)

5.17 Generation of stably transformed Arabidopsis plants

Arabidopsis plants were transformed with the help of *A. tumefaciens* (Clough and Bent, 1998). Plants were grown as described in section 5.7.4 until flowering. As preculture, 30-50 ml YEB medium with appropriate antibiotics were inoculated with Agrobacteria containing the desired plasmid (Table 5.6) and incubated over night at 28-30 °C while shaking at 180 rpm. The preculture was used to inoculate 400 ml of YEB medium to an OD₆₀₀ of 0.15. The cells were incubated at 28-30 °C while shaking at 180 rpm until the culture reached an OD₆₀₀ of 0.8. The cells were harvested by centrifugation at 3,220 x g and 4 °C for 20 min. The sedimented cells were washed in 5 % (w/v) saccharose and centrifuged again as described above. The cells were resuspended in 200 ml of 5 % (w/v) saccharose and incubated on ice for 30 min. To reduce the surface tension of the solution, 0.05 % (v/v) Silwet® L-77 were added, and the flowers were dipped in the solution for 4-5 s. The plants were placed back in the growth chambers under long-day conditions. The transformation procedure was repeated within a time interval of one to two weeks. The seeds were harvested (T1) and grown on soil under short-day conditions until four true leaves were formed. The seedlings were sprayed with 0.045 % (v/v) Basta® (glufosinate ammonium, Bayer, Leverkusen, Germany) for selection of transgenic plants. The Basta®-treatment was repeated after two and after four weeks. Resistant plants were transferred to long-day growth conditions approx. 8 weeks after germination to induce shoot and seed production. The T2-seeds were harvested and used for further experiments.

5.18 SDS-PAGE

Proteins expressed in Arabidopsis protoplasts were separated according to their molecular weight by SDS-PAGE (Laemmli, 1970). Aliquots of 400-500 µl transformed protoplasts (see section 5.16) were sedimented by centrifugation at 200 x g for 2 min and resuspended in 10-15 µl 4x sample buffer. Proteins were separated either on self-cast polyacrylamide gels or SERVAGel™ Neutral HSE gels (SERVA Electrophoresis GmbH, Heidelberg, Germany). Self-prepared polyacrylamide gels were prepared in a Multiple Gel Caster (SE 200 series) (Hofer Inc., SERVA Electrophoresis GmbH, Heidelberg, Germany). The composition of self-cast polyacrylamide gels is described in Table 5.8. As molecular size marker 5 µl of "PageRuler™ Prestained Protein Ladder" (Thermo Fisher Scientific, Schwerte, Germany) were used. The gel electrophoresis was performed in SE250 Electrophoresis Chambers (Hofer Inc., SERVA Electrophoresis GmbH, Heidelberg, Germany) with running buffer at constant 35 mA/gel (pre-casted gels) or at constant 25 mA/gel (self-casted gels) for 30-40 min. Protein transfer by western blotting

and subsequent immunodetection of specific proteins was performed as described in section 5.19.

4x sample buffer: 240 mM Tris-HCl pH 6.8, 8 % (w/v) sodium dodecyl sulfate (SDS), 0.08 % (w/v) bromophenol blue, 40 % (v/v) glycerol, 20 % (v/v) 2-mercaptoethanol or 0.05 M dithiothreitol (DTT) (Julkowska et al., 2013)

running buffer: 0.3 % (w/v) Tris, 1.44 % (w/v) glycine, 0.1 % (w/v) SDS

Table 5.8. Composition of self-cast SDS-PAGE-gels.

Component	Separation gel	Stacking gel
Rotiphorese® Gel 30 (37,5:1)	10 % (w/v)	5 % (w/v)
Tris-HCl pH 8.8	370 mM	-
Tris-HCl pH 6.8	-	120 mM
ddH ₂ O	45 % (v/v)	62 % (v/v)
SDS	0.1 % (w/v)	0.1 % (w/v)
ammonium persulfate (APS)	0.06 % (w/v)	0.09 % (w/v)
N,N,N',N'-tetramethyl-ethylenediamine (TEMED)	0.01 % (v/v)	0.01 % (v/v)

5.19 Western blotting and immunodetection of specific proteins

Proteins from SDS-PAGE gels (see section 5.18) were transferred to nitrocellulose membranes (Amersham Protran 0,45 NC, Cytiva, Freiburg im Breisgau, Germany) (Towbin et al., 1979). The transfer was performed in Mini-PROTEAN® Tetra System Blotting Chamber (BioRad Laboratories GmbH, Munich, Germany) in transfer buffer at constant 60 V and 400 mA for 60-75 min. The membranes were blocked in 3 % (w/v) milk powder in tris buffered saline (TBS) for 30 min at room temperature. The primary antibody was diluted in 3 % (w/v) milk powder in TBS according to the manufacturer's instruction and incubated with the membrane at room temperature for 1 h or at 4 °C overnight while shaking. The membrane was washed three times for 10 min in 10 ml TBS each time while shaking. The secondary antibody was diluted according to the manufacturer's instruction in 3 % (w/v) milk powder in TBS and incubated on the membrane at room temperature for 45 to 60 min. The membrane again was washed three times as previously described. The antibodies used in this work are listed in Table 5.9. The proteins were detected by horse radish peroxidase (HRP) generated chemiluminescence and the "SuperSignal™ West

Femto Maximum Sensitivity Substrate” (Thermo Fisher Scientific, Schwerte, Germany) was used. The chemiluminescence signals were detected and documented with the “Fusion Solo S” (Vilber Lourmat Deutschland GmbH, Eberhardzell, Germany) and the software “FusionCapt Advance Solo 7” (version 17.01).

Transfer buffer: 0.582 % (w/v) Tris, 0.293 % (w/v) glycine, 0.375 % (w/v) SDS, 20 % (v/v) methanol

Tris-buffered saline (TBS): 50 mM Tris-HCl pH 7.5, 150 mM NaCl

Table 5.9. Primary and secondary polyclonal antibodies.

Epitope	Host organism	Conjugate	Dilution	Supplier
anti-GFP	rabbit	-	1:5,000	Invitrogen™, Thermo Fisher Scientific, Schwerte, Deutschland (#A-11122)
anti-mCherry	goat	-	1:2,500	Sicgen, Cantanhede, Portugal (#AB0040-200)
anti-nYFP	rabbit	-	1:2,000	Agrisera, Vännäs, Sweden
anti-cYFP	rabbit	-	1:10,000	Agrisera, Vännäs, Sweden
anti-goat	rabbit	HRP	1:7,500	Merck, Darmstadt, Germany (#A5420)
anti-rabbit	goat	HRP	1:7,000	Merck, Darmstadt, Germany (#A6154)

5.20 Heterologous expression of different cDNA clones in yeast

Functional characterization of fatty acid desaturases and acyltransferases was performed by heterologous expression in yeast. The yeast strains INVSc1 and H1246 were used. The strain INVSc1 is auxotrophic for histidine, leucine, tryptophan and uracil and the strain H1246 is auxotrophic for uracil. These auxotrophies were exploited to select for cells successfully transformed with plasmids containing the desired cDNA (see section 5.9 for yeast expression vectors). The cloning of the recombinant plasmids for heterologous expression is described in the section 5.13.1. The *pESC*-vectors used each contain a galactose-inducible promoter, *GAL1* or *GAL10*, upstream of the cloned cDNAs.

5.20.1 Heterologous expression of FAD2 and FAD3 in the yeast strain INVSc1

For transgene expression precultures consisting of 30-50 ml SD-W medium with 2 % (w/v) glucose were inoculated with the appropriate transformed yeast clones and incubated at

30 °C for 24-48 h while shaking at 180 rpm. The expression cultures consisting of 50 ml SD-W medium were inoculated with the preculture to an OD₆₀₀ of 0.3, and expression was induced by adding 2 % (w/v) galactose.

The expression of FAD2-variants was performed at room temperature (20 °C) while shaking at 180 rpm. The expression cultures of FAD3-variants were incubated at 18 °C shaking at 180 rpm. mycFAD2 was coexpressed with the FAD3-variants to provide the necessary 18:2^{Δ9,12} substrate for FAD3.

After 3-4 days, 20 OD-units (the volume corresponding to 20 ml cell culture with an OD₆₀₀ of 1) were harvested by centrifugation at 2,500 x g for 5 min, washed once in 2-5 ml of TE buffer (see section 5.15) and centrifuged again. The yeast sediments were frozen in liquid nitrogen and stored at -20 °C until fatty acid analysis was performed (described in section 5.21.7).

5.20.2 Heterologous expression of PDAT and DGAT1 in the yeast strain H1246

The yeast strain H1246, an acyltransferase quadruple mutant (see section 5.5) which is deficient in TAG production and sterol ester synthesis, was transformed with *pESC-URA* vectors (see Table 5.2) containing the cDNA for tagged and untagged PDAT and DGAT1 variants as described in section 5.15. The expression was performed as described for FAD2 in section 5.20.1. After 3-4 days growth and expression at 30 °C, 20-50 OD-units were harvested by centrifugation and stored at -20 °C until lipid extraction and analyses (see section 5.21.1) were performed.

5.21 Lipid extraction and fatty acid analyses

The methods used to isolate and analyze lipids and fatty acids from yeast and plant material are described below. Lipid extractions and analyses were performed in glass vials and with glass Pasteur pipettes whenever possible.

5.21.1 Isolation of total lipids from yeast

To analyze the formation of TAG after expression of PDAT- and DGAT1-variants in yeast, 30-50 OD-units of yeast cells were used (see section 5.20.2) for lipid extraction (Bligh and Dyer, 1959). The yeast cells were incubated in 2 ml chloroform:methanol (1:2, v/v) at room temperature for 1 hour and additionally mechanically disrupted by vigorous mixing with glass beads (3 mm). The extracts were mixed with 750 µl H₂O and 500 µl chloroform and phase separation was performed by centrifugation at 200 x g for 2 min. The lower, organic phase was transferred to a fresh glass vial. The remaining aqueous phase was re-

extracted one more time with 500 μ l chloroform as described above. The combined organic phases were evaporated under air stream. The dried lipids were dissolved in 20 μ l chloroform and separated with thin layer chromatography (TLC) as described in 5.21.4.

5.21.2 Isolation of total lipids from plant material

Total lipids were extracted from approx. 50-100 mg of 14-day-old Arabidopsis seedlings grown on $\frac{1}{2}$ MS-medium under long-day conditions (Bligh and Dyer, 1959). The seedlings were ground with mortar and pestle in liquid nitrogen and mixed with 4 ml chloroform:methanol (2:1, v/v). To extract the lipids the samples were incubated at room temperature for 30 min. The samples were mixed with 1.5 ml chloroform and 1.5 ml H₂O. Phase separation was achieved by centrifugation at 200 x g for 2 min. The lower organic phase was transferred to a fresh glass vial and the aqueous phase was subsequently extracted again with 1.3 ml chloroform, until the organic phase was colorless (in total four extraction steps). The combined organic phases were washed once with 2 ml H₂O. The chloroform was evaporated under air stream. The lipids were dissolved in 1 ml chloroform and lipid classes were separated with solid phase adsorption chromatography (see section 5.21.3).

5.21.3 Separation of lipid classes with solid phase adsorption chromatography

The separation of the lipid classes, neutral lipids, galactolipids and phospholipids, was carried out with silica solid phase extraction (SPE) columns with capacity for 100 mg starting material (HF Bond Elut 1CC LRC-SI, 100 mg, Agilent Technologies, VWR International GmbH, Darmstadt, Germany) (Launhardt et al., 2021). The SPE columns were equilibrated with 1 ml chloroform. The lipid extracts were loaded on the columns and the solvent allowed to pass the column completely. Neutral lipids were eluted with 2 ml chloroform. Glycolipids were eluted with 2 ml acetone:methanol (9:1, v/v). Phospholipids were eluted with 2 ml methanol:acetic acid (100:1, v/v). The neutral lipid fraction was discarded. The glycolipids were dried under air stream. The phospholipids were extracted from the elution fraction by addition of 2 ml chloroform and 2 ml H₂O. The phases were separated by centrifugation at 200 x g for 2 min. The lower organic phase was transferred to a fresh glass vial. The remaining aqueous phase was extracted one more time with 1.5 ml chloroform. The chloroform of the combined organic phases was evaporated under air stream. All dried lipid fractions were dissolved in 100 μ l chloroform and separated with TLC as described in section 5.21.4.

5.21.4 Thin layer chromatography (TLC)

Total lipid extracts from yeast (section 5.21.1) or phospholipid and glycolipid fractions from seedlings (section 5.21.3) were separated by TLC (Launhardt et al., 2021). The samples were spotted onto silica gel plates (TLC silica gel plates 60, 20 x 20 cm, glass supported, Merck, Darmstadt, Germany) next to 5 µg of each of the corresponding lipid standards (see appendix Table 7.3). The TLC plates were developed with appropriate developing solvent using glass TLC developing chambers. The used developing solvents and the incubation times are listed in Table 5.10.

Table 5.10. Developing solvents and developing time for thin layer chromatography.

Lipid class	Developing solvent	Developing time
Neutral lipids	petrol ether:diethylether:acetic acid, 70:30:2 (v/v/v)	30 min
Glycolipids	acetone:toluene:H ₂ O, 90:30:7 (v/v/v)	30 min
Phospholipids	chloroform:methanol:acetic acid, 65:25:8 (v/v/v)	60 min

Neutral lipids were visualized by immersing the TLC plates in CuSO₄-solution (10 % (w/v) CuSO₄, 0.8 % (v/v) H₃PO₄) followed by drying and heating the TLC plates to 180 °C. Isolation of phospholipid or glycolipid subclasses, such as PC, MGDG and DGDG was achieved by scraping the corresponding lipids from the developed TLCs. For this purpose, the TLC plates were sprayed with 0,02 % primulin (in acetone:water, 4:1, v/v) and the lipids visualized under UV light. Afterwards, the isolated lipids could be used for transmethylation with sodium methoxide as described in section 5.21.5.

5.21.5 Extraction and transmethylation of fatty acids from single seeds

To analyze the fatty acid composition from single Arabidopsis seeds, fatty acid methyl esters (FAMES) were prepared by trans-esterification with trimethyl sulfonium hydroxide (TMSH) (Butte et al., 1982). For this purpose, single seeds were homogenized in 10 µl 0.2 M TMSH in a GC-vial insert. Trans-esterification took place by incubating the samples at room temperature until the TMSH was evaporated. The generated FAMES were dissolved in 10 µl acetonitrile and analyzed by gas chromatography coupled to flame ionization detection (GC-FID) as described in section 5.21.8.

5.21.6 Base-catalyzed transmethylation of fatty acids with sodium methoxide

Fatty acid methyl esters of lipids purified via TLC were prepared by trans-esterification with sodium methoxide (Launhardt et al., 2021). As internal standard 10 µg tripentadecanoin were added to each sample. The samples were mixed with 333 µl methanol:toluene (2:1, v/v) and 167 µl 0.5 M sodium methoxide (0.5 M CH₃ONa in methanol) and incubated for 20 min at room temperature while shaking. The FAMES were extracted with 0.5 ml of 5 M NaCl and 1.5 ml n-hexane. Phases were separated by centrifugation at 200 x g for 2 min. The upper organic phase was transferred to a new glass vial and evaporated under air stream. The samples were dissolved in 100 µl acetonitrile and transferred to GC-vials with 250 µl inserts. The acetonitrile was evaporated, and the FAMES resolved in a final volume of 10 µl acetonitrile. The samples were analyzed by GC-FID as described in section 5.21.8.

5.21.7 Acid-catalyzed transmethylation of fatty acids

To analyze the fatty acid composition of yeast, sedimented cells were resuspended in 2 ml FAME solution for transmethylation (Miquel and Browse, 1992). To quantify the fatty acids, 50 µg tripentadecanoin were added as an internal standard. The reaction was incubated in a water bath at 80 °C for 60 min. To extract the formed FAMES, 200 µl of 5 M NaCl and 2 ml n-hexane were added and mixed. The phases were separated by centrifugation at 200 x g for 2 min. the upper n-hexane phase was transferred to a fresh glass vial and the remaining fraction was extracted again with 2 ml n-hexane. The organic phases were combined, and the n-hexane evaporated under air stream. The FAMES were resolved in 100 µl acetonitrile, 10 µl were analyzed by GC-FID (see section 5.21.8).

FAME solution: 2.75 % (v/v) H₂SO₄, 2 % (v/v) dimethoxy propane, in methanol

5.21.8 Gas chromatography of FAMES

The analysis of FAMES was performed as described (Launhardt et al., 2021) with GC-2010Plus (Shimadzu Deutschland GmbH, Duisburg, Germany) coupled to a flame ionization detector. A DB-23 column (30 m x 0.25 mm; 0.25 µm coating thickness, Agilent Technologies, VWR International GmbH, Darmstadt, Germany) with helium as carrier gas was used. The samples were injected at 220 °C (AOC-20i Auto Injector, Shimadzu Deutschland GmbH, Duisburg, Germany). The chromatography was performed using a temperature gradient: After one minute at 150 °C, the oven temperature was increased to 200 °C at a rate of 25 °C/min, followed by an increase to 250 °C at a rate of 4 °C/min and kept at 250 °C for 6 min. The FAMES were identified by comparison to menhaden fish oil

as authentic reference substance. The "GC Solution" software (version 2.31.00, Shimadzu Deutschland GmbH, Duisburg, Germany) was used for measurement and data analysis

5.22 Protein-protein interaction studies

The split-ubiquitin-based yeast two-hybrid system was used to screen for protein-protein interactions. The observed interactions were verified with bimolecular fluorescence complementation in *Arabidopsis mesophyll* protoplasts.

5.22.1 Split-ubiquitin-based yeast two-hybrid system

For protein-protein interaction analyses in yeast, the split-ubiquitin-based yeast two-hybrid system was used (Dualsystems Biotech AG, Zurich, Switzerland) (Johnsson and Varshavsky, 1994). This system utilizes the protease-mediated cleavage of proteins and peptides labeled with ubiquitin. The N- and C-terminal halves of ubiquitin are each fused to the proteins of interest. Upon interaction of the fusion proteins, the ubiquitin halves are in proximity to each other and can reconstitute. The reconstituted ubiquitin is recognized by endogenous ubiquitin-specific proteases, which cleave of the transcription factor LexA-VP16. The free transcription factor then activates the reporter genes *HIS3*, *ADE2* and *lacZ*, which allows the yeast to grow on selection medium lacking histidine. For the positive control the wild type N-terminal ubiquitin half (Nub, amino acids 1 to 34) fused to Alg5 ensures the reconstitution of ubiquitin. To avoid the auto-assembly of the ubiquitin halves in the interaction tests and the negative control, a mutated Nub with a mutation at position 13 from isoleucine to glycine (NubG) was used. The vectors are described in section 5.9 and the used yeast two-hybrid constructs are described in section 5.13.2. The C-terminal ubiquitin half (Cub, amino acids 35 to 76) was fused to the bait proteins, the NubG was fused to the prey proteins.

5.22.2 Yeast two-hybrid tests

Positive transformed yeast colonies (see section 5.14) were used for protein-protein interaction tests on selection medium lacking leucine, tryptophane and histidine (SD-LWH). For this purpose, cells were resuspended and diluted in 500 µl TE buffer (see section 5.15) to an OD₆₀₀ of 0.5. Then, 4 µl were spotted on SD-LW and SD-LWH selection medium (see section 5.7.3). The cell growth was monitored over a period of 5 days at 30 °C and documented using a scanner.

5.22.3 Interaction analysis by bimolecular fluorescence complementation

Bimolecular fluorescence complementation (BiFC) assays were performed to validate the protein-protein interactions found with yeast two-hybrid analyses. In this work, BiFC studies were performed in *Arabidopsis mesophyll* protoplasts. The underlying principle of the BiFC experiment is similar to that of the split ubiquitin-based yeast two-hybrid system. The coding sequences of the protein interactors of interest are fused to either the N-terminal or C-terminal half of EYFP. Only when the two proteins to be tested are close to each other through interaction can the two EYFP fragments assemble into a functional EYFP protein and emit fluorescence. For details of the constructs, see section 5.9 and 5.13.3. Constructs were transiently transformed into protoplasts (see section 5.16), and cells were incubated for heterologous protein expression over night until microscopic evaluation (see section 5.23). An RFP protein coexpressed under the control of a *pCaMV35S* promoter was used to identify transformed cells. Reconstitution of EYFP fluorescence indicated protein-protein interaction and provided information about the subcellular localization of the interaction.

5.23 Microscopy and image analysis

5.23.1 Fluorescence microscopy using the LSM880

Laser scanning confocal microscopy was performed using Laser Scanning Microscope LSM880 (Carl Zeiss, Jena, Germany). For imaging of *Arabidopsis mesophyll* protoplasts (subcellular localization analyses and BiFC experiments), a Plan-Apochromat 40x/0.95 Korr M27 objective (Carl Zeiss, Jena, Germany) was used. Seedlings were imaged using a 63x oil immersion objective (Plan-Apochromat 63x/1.4 Oil DIC M27; Carl Zeiss, Jena, Germany). The wavelengths used for excitation, the emission range and the filter sets are listed in Table 5.11. The pinhole was kept at approx. 1 Airy unit. Z-stacks covering the cell from one edge to the center were generated with 0.5-1 μm between each frame, resulting in approx. 20-30 frames per cell. Images were acquired with an 8-bit bit depth using ZEN Black image analysis software (version 14.0.18.201, Carl Zeiss, Jena, Germany).

Table 5.11. Microscopy settings at the LSM880. MBS: main beam splitter.

Fluorescence protein	Excitation [nm]	Emission range [nm]	Filter
CFP	405	460-520	MBS 488/561/633 + MBS -405
Chlorophyll A	633	650-720	MBS 488/561/633 (+ MBS -405)

Fluorescence protein	Excitation [nm]	Emission range [nm]	Filter
EYFP	514	520-570	MBS 458/514
GFP	488	490-550	MBS 488/561/633 or MBS 488
mCherry RFP	561	580-630	MBS 458/561 or MBS 488/561/633

5.23.2 Fluorescence microscopy using a spinning disc microscope

Spinning disc microscopy was performed using Zeiss Cell observer SD with a Yokogawa CSU-X1 spinning disc unit and a 63x oil immersion objective (Carl Zeiss, Jena, Germany). EYFP and GFP were excited at 488 nm, mCherry was excited at 561 nm. A DAPI/FITC/TRITC ET Triple band emitter (AHF Analysetechnik, Tübingen, Germany, F67-000) was used. Images were acquired using ZEN Blue image analysis software (Carl Zeiss, Jena, Germany) and Photometrics Evolve 512 Delta EM-CCD camera.

5.23.3 Image analysis using Fiji

Image processing was performed using the software ImageJ Fiji (version 1.51, Schindelin et al., 2012). Images were contrast enhanced with a maximum of 0.1 % saturated pixels. Z-projections from Z-stacks were generated using the projection type “maximum intensity”. Leaf areas from complemented plant lines were calculated using simple interactive object extraction (SIOX) as a Fiji plugin (Arganda-Carreras et al., 2009).

The Pearson’s correlation coefficients (PCC) and Manders’ colocalization coefficients (MCC) were determined using the Fiji-plugin JACoP (Bolte and Cordelières, 2006). Unprocessed Z-stack images (generated as described in section 5.23.1) of up to 512x512 pixels were used for analysis. For the calculation of MCCs, individual thresholds for every channel were chosen to omit background signals. The underlying mathematical equations for PCC and MCC calculations are as follows (Bolte and Cordelières, 2006):

A_i and B_i : gray value of voxel i in channel A and B, respectively

a , b : average intensity in channel A and B, respectively

PCC:

$$r_p = \frac{\sum_i (A_i - a) \times (B_i - b)}{\sqrt{[\sum_i (A_i - a)^2 \times \sum_i (B_i - b)^2]}}$$

MCCs:

$$M_1 = \frac{\sum_i A_{i,coloc}}{\sum_i A_i} ; M_2 = \frac{\sum_i B_{i,coloc}}{\sum_i B_i}$$

With $A_{i,coloc}$ being A_i if $B_i > 0$ and 0 if $B_i = 0$, and $B_{i,coloc}$ being B_i if $A_i > 0$ and 0 if $A_i = 0$

Line plots were generated using Fiji and illustrated with the plugin “dotted line” (Baler, 2003).

To highlight colocalized areas, the Fiji plugin “Colocalization” (Bourdoncle, 2003) was used. This plugin renders pixels that meet a certain intensity threshold and ratio as white (maximal gray value: 255). Z-stack images generated by LSM were used as input. From the resulting images single confocal planes were chosen or maximum intensity Z-projections were generated.

To compare fluorescence intensities between different samples, Z-stack images were acquired as described in section 5.23.1, and sum intensity Z-projections were generated. During image acquisition, it was taken care that the image acquisition settings were the same for all cells and samples used. The fluorescence intensities in a selected cell and the background were measured. The corrected total cell fluorescence (CTCF) was calculated as:

$$CTCF = \text{area of the selected cell} \times (\text{mean cell fluorescence} - \text{mean background fluorescence})$$

The product of the cell area and mean cell fluorescence was used as equivalent for the integrated density (the sum of the intensity values of the pixels).

5.24 Statistical analyses

Bar charts and box plots were generated using Microsoft Office 365 (Microsoft Corporation, Redmond, WA, USA). Error bars in bar charts represent the sample standard deviation. The box plots depict the inner quartiles with the whiskers indicating the maximum and minimum. Values 1.5 times larger or smaller than the interquartile range (IQR) are regarded as outliers. Outliers are represented by circles. The cross marks the mean, the line in between the quartiles marks the median. Violin plots (Figure 3.15C) were generated according to Spitzer et al. (2014).

Statistical significance was determined using one-way ANOVA with a subsequent Tukey's post-hoc test (significance level $p < 0.05$). Instead of one-way ANOVA, the Kruskal-Wallis test was used to determine the statistical significance of data that did not follow normal distribution (Figure 3.15C, significance level $p < 0.05$). The statistical analyses were performed using the online tool “Statistics Kingdom” (2017).

6. References

- An, G.** (1987). [17] Binary ti vectors for plant transformation and promoter analysis. In *Recombinant DNA Part D* (Elsevier), pp. 292–305.
- Andrews, J., and Mudd, J.B.** (1985). Phosphatidylglycerol synthesis in pea chloroplasts: pathway and localization. *Plant physiology* **79** (1): 259–265.
- Arganda-Carreras, I., Saalfeld, S., and Schindelin, J.** (2009). SIOX (Simple Interactive Object Extraction). <https://imagej.nih.gov/ij/plugins/siox/index.html>. Accessed 27 February 2022.
- Aymé, L., Baud, S., Dubreucq, B., Joffre, F., and Chardot, T.** (2014). Function and localization of the *Arabidopsis thaliana* diacylglycerol acyltransferase DGAT2 expressed in yeast. *PLoS one* **9** (3): e92237.
- Baler, K.** (2003). Dotted Line. <https://imagej.nih.gov/ij/plugins/dotted-line.html>. Accessed 11 February 2022.
- Bates, P.D., Fatihi, A., Snapp, A.R., Carlsson, A.S., Browse, J., and Lu, C.** (2012). Acyl editing and headgroup exchange are the major mechanisms that direct polyunsaturated fatty acid flux into triacylglycerols. *Plant physiology* **160** (3): 1530–1539.
- Bates, P.D., Ohlrogge, J.B., and Pollard, M.** (2007). Incorporation of newly synthesized fatty acids into cytosolic glycerolipids in pea leaves occurs via acyl editing. *Journal of Biological Chemistry* **282** (43): 31206–31216.
- Bates, P.D., Stymne, S., and Ohlrogge, J.** (2013). Biochemical pathways in seed oil synthesis. *Current opinion in plant biology* **16** (3): 358–364.
- Baud, S.** (2018). Seeds as oil factories. *Plant reproduction* **31** (3): 213–235.
- Baud, S., Mendoza, M.S., To, A., Harscoët, E., Lepiniec, L., and Dubreucq, B.** (2007). WRINKLED1 specifies the regulatory action of LEAFY COTYLEDON2 towards fatty acid metabolism during seed maturation in *Arabidopsis*. *The Plant journal for cell and molecular biology* **50** (5): 825–838.
- Berg, J.M., Tymoczko, J.L., Stryer, L., and Gatto, G.J., eds** (2013). *Biochemie* (Berlin, Heidelberg: Springer Spektrum).
- Bligh, E.G., and Dyer, W.J.** (1959). A rapid method of total lipid extraction and purification. *Canadian journal of biochemistry and physiology* **37** (8): 911–917.
- Boevink, P., Oparka, K., Santa Cruz, S., Martin, B., Betteridge, A., and Hawes, C.** (1998). Stacks on tracks: the plant Golgi apparatus traffics on an actin/ER network. *The Plant journal for cell and molecular biology* **15** (3): 441–447.
- Bolte, S., and Cordelières, F.P.** (2006). A guided tour into subcellular colocalization analysis in light microscopy. *Journal of Microscopy* **224** (Pt 3): 213–232.

- Bourdoncle, P.** (2003). Colocalization.
<https://imagej.nih.gov/ij/plugins/colocalization.html>. Accessed 11 February 2022.
- Broun, P., and Somerville, C.** (1997). Accumulation of ricinoleic, lesquerolic, and densipolic acids in seeds of transgenic *Arabidopsis* plants that express a fatty acyl hydroxylase cDNA from castor bean. *Plant physiology* **113** (3): 933–942.
- Brown, D.J., and Dupont, F.M.** (1989). Lipid Composition of Plasma Membranes and Endomembranes Prepared from Roots of Barley (*Hordeum vulgare* L.) Effects of Salt. *Plant physiology* **90** (3): 955–961.
- Browse, J., Kunst, L., Anderson, S., Hugly, S., and Somerville, C.** (1989). A mutant of *Arabidopsis* deficient in the chloroplast 16:1/18:1 desaturase. *Plant physiology* **90** (2): 522–529.
- Browse, J., McConn, M., James, D., and Miquel, M.** (1993). Mutants of *Arabidopsis* deficient in the synthesis of alpha-linolenate. Biochemical and genetic characterization of the endoplasmic reticulum linoleoyl desaturase. *Journal of Biological Chemistry* **268** (22): 16345–16351.
- Burgal, J., Shockey, J., Lu, C., Dyer, J., Larson, T., Graham, I., and Browse, J.** (2008). Metabolic engineering of hydroxy fatty acid production in plants: RcDGAT2 drives dramatic increases in ricinoleate levels in seed oil. *Plant biotechnology journal* **6** (8): 819–831.
- Butte, W., Eilers, J., and Kirsch, M.** (1982). Trialkylsulfonium- and Trialkylselenoniumhydroxides for the Pyrolytic Alkylation of Acidic Compounds. *Analytical Letters* **15** (10): 841–850.
- Cahoon, E.B., Carlson, T.J., Ripp, K.G., Schweiger, B.J., Cook, G.A., Hall, S.E., and Kinney, A.J.** (1999). Biosynthetic origin of conjugated double bonds: production of fatty acid components of high-value drying oils in transgenic soybean embryos. *Proceedings of the National Academy of Sciences of the United States of America* **96** (22): 12935–12940.
- Cahoon, E.B., Dietrich, C.R., Meyer, K., Damude, H.G., Dyer, J.M., and Kinney, A.J.** (2006). Conjugated fatty acids accumulate to high levels in phospholipids of metabolically engineered soybean and *Arabidopsis* seeds. *Phytochemistry* **67** (12): 1166–1176.
- Cahoon, E.B., and Li-Beisson, Y.** (2020). Plant unusual fatty acids: learning from the less common. *Current opinion in plant biology* **55**: 66–73.
- Cai, Y., Goodman, J.M., Pyc, M., Mullen, R.T., Dyer, J.M., and Chapman, K.D.** (2015). *Arabidopsis* SEIPIN Proteins Modulate Triacylglycerol Accumulation and Influence Lipid Droplet Proliferation. *The Plant cell* **27** (9): 2616–2636.

- Chapman, K.D., and Ohlrogge, J.B.** (2012). Compartmentation of triacylglycerol accumulation in plants. *The Journal of biological chemistry* **287** (4): 2288–2294.
- Chen, Y., Cui, Q., Xu, Y., Yang, S., Gao, M., and Wang, Y.** (2015). Effects of tung oilseed FAD2 and DGAT2 genes on unsaturated fatty acid accumulation in *Rhodotorula glutinis* and *Arabidopsis thaliana*. *Molecular genetics and genomics MGG* **290** (4): 1605–1613.
- Clough, S.J., and Bent, A.F.** (1998). Floral dip: a simplified method for *Agrobacterium*-mediated transformation of *Arabidopsis thaliana*. *The Plant journal for cell and molecular biology* **16** (6): 735–743.
- Cooke, I.R., and Deserno, M.** (2006). Coupling between lipid shape and membrane curvature. *Biophysical journal* **91** (2): 487–495.
- Dahlqvist, A., Stahl, U., Lenman, M., Banas, A., Lee, M., Sandager, L., Ronne, H., and Stymne, S.** (2000). Phospholipid:diacylglycerol acyltransferase: an enzyme that catalyzes the acyl-CoA-independent formation of triacylglycerol in yeast and plants. *Proceedings of the National Academy of Sciences of the United States of America* **97** (12): 6487–6492.
- Dar, A.A., Choudhury, A.R., Kancharla, P.K., and Arumugam, N.** (2017). The FAD2 Gene in Plants: Occurrence, Regulation, and Role. *Frontiers in plant science* **8**: 1789.
- Delker, C., Stenzel, I., Hause, B., Miersch, O., Feussner, I., and Wasternack, C.** (2006). Jasmonate biosynthesis in *Arabidopsis thaliana*--enzymes, products, regulation. *Plant biology (Stuttgart, Germany)* **8** (3): 297–306.
- Drexler, H., Spiekermann, P., Meyer, A., Domergue, F., Zank, T., Sperling, P., Abbadi, A., and Heinz, E.** (2003). Metabolic engineering of fatty acids for breeding of new oilseed crops: strategies, problems and first results. *Journal of plant physiology* **160** (7): 779–802.
- Dunn, K.W., Kamocka, M.M., and McDonald, J.H.** (2011). A practical guide to evaluating colocalization in biological microscopy. *American journal of physiology. Cell physiology* **300** (4): C723-42.
- Dupree, P., and Sherrier, D.** (1998). The plant Golgi apparatus. *Biochimica et Biophysica Acta (BBA) - Molecular Cell Research* **1404** (1-2): 259–270.
- Dyer, J.M., Chapital, D.C., Kuan, J.-C.W., Mullen, R.T., Turner, C., McKeon, T.A., and Pepperman, A.B.** (2002). Molecular analysis of a bifunctional fatty acid conjugase/desaturase from tung. Implications for the evolution of plant fatty acid diversity. *Plant physiology* **130** (4): 2027–2038.
- Dyer, J.M., and Mullen, R.T.** (2001). Immunocytological localization of two plant fatty acid desaturases in the endoplasmic reticulum. *FEBS Letters* **494** (1-2): 44–47.

- Dyer, J.M., and Mullen, R.T.** (2008). Engineering plant oils as high-value industrial feedstocks for biorefining: the need for underpinning cell biology research. *Physiologia plantarum* **132** (1): 11–22.
- Dyer, J.M., Stymne, S., Green, A.G., and Carlsson, A.S.** (2008). High-value oils from plants. *The Plant journal for cell and molecular biology* **54** (4): 640–655.
- Falcone, D.L., Gibson, S., Lemieux, B., and Somerville, C.** (1994). Identification of a gene that complements an *Arabidopsis* mutant deficient in chloroplast omega 6 desaturase activity. *Plant physiology* **106** (4): 1453–1459.
- Falcone, D.L., Ogas, J.P., and Somerville, C.R.** (2004). Regulation of membrane fatty acid composition by temperature in mutants of *Arabidopsis* with alterations in membrane lipid composition. *BMC plant biology* **4**: 17.
- Fan, J., Yan, C., Roston, R., Shanklin, J., and Xu, C.** (2014). *Arabidopsis* lipins, PDAT1 acyltransferase, and SDP1 triacylglycerol lipase synergistically direct fatty acids toward β -oxidation, thereby maintaining membrane lipid homeostasis. *The Plant cell* **26** (10): 4119–4134.
- Fan, J., Yan, C., and Xu, C.** (2013a). Phospholipid:diacylglycerol acyltransferase-mediated triacylglycerol biosynthesis is crucial for protection against fatty acid-induced cell death in growing tissues of *Arabidopsis*. *The Plant journal for cell and molecular biology* **76** (6): 930–942.
- Fan, J., Yan, C., Zhang, X., and Xu, C.** (2013b). Dual role for phospholipid:diacylglycerol acyltransferase: enhancing fatty acid synthesis and diverting fatty acids from membrane lipids to triacylglycerol in *Arabidopsis* leaves. *The Plant cell* **25** (9): 3506–3518.
- Fan, J., Yu, L., and Xu, C.** (2017). A Central Role for Triacylglycerol in Membrane Lipid Breakdown, Fatty Acid β -Oxidation, and Plant Survival under Extended Darkness. *Plant physiology* **174** (3): 1517–1530.
- Focks, N., and Benning, C.** (1998). wrinkled1: A novel, low-seed-oil mutant of *Arabidopsis* with a deficiency in the seed-specific regulation of carbohydrate metabolism. *Plant physiology* **118** (1): 91–101.
- Fouillen, L., Maneta-Peyret, L., and Moreau, P.** (2018). ER Membrane Lipid Composition and Metabolism: Lipidomic Analysis. *Methods in molecular biology (Clifton, N.J.)* **1691**: 125–137.
- Furt, F., König, S., Bessoule, J.-J., Sargueil, F., Zallot, R., Stanislas, T., Noirot, E., Lherminier, J., Simon-Plas, F., Heilmann, I., and Mongrand, S.** (2010). Polyphosphoinositides are enriched in plant membrane rafts and form microdomains in the plasma membrane. *Plant physiology* **152** (4): 2173–2187.

- Gidda, S.K., Park, S., Pyc, M., Yurchenko, O., Cai, Y., Wu, P., Andrews, D.W., Chapman, K.D., Dyer, J.M., and Mullen, R.T.** (2016). Lipid Droplet-Associated Proteins (LDAPs) Are Required for the Dynamic Regulation of Neutral Lipid Compartmentation in Plant Cells. *Plant physiology* **170** (4): 2052–2071.
- Greer, M.S., Cai, Y., Gidda, S.K., Esnay, N., Kretzschmar, F.K., Seay, D., McClinchie, E., Ischebeck, T., Mullen, R.T., Dyer, J.M., and Chapman, K.D.** (2020). SEIPIN Isoforms Interact with the Membrane-Tethering Protein VAP27-1 for Lipid Droplet Formation. *The Plant cell* **32** (9): 2932–2950.
- Grefen, C., and Blatt, M.R.** (2012). A 2in1 cloning system enables ratiometric bimolecular fluorescence complementation (rBiFC). *BioTechniques* **53** (5): 311–314.
- Grimberg, Å., Carlsson, A.S., Marttila, S., Bhalerao, R., and Hofvander, P.** (2015). Transcriptional transitions in *Nicotiana benthamiana* leaves upon induction of oil synthesis by WRINKLED1 homologs from diverse species and tissues. *BMC plant biology* **15**: 192.
- Guschina, I.A., and Harwood, J.L.** (2006). Mechanisms of temperature adaptation in poikilotherms. *FEBS Letters* **580** (23): 5477–5483.
- Haslam, R.P., Sayanova, O., Kim, H.J., Cahoon, E.B., and Napier, J.A.** (2016). Synthetic redesign of plant lipid metabolism. *The Plant journal for cell and molecular biology* **87** (1): 76–86.
- He, M., and Ding, N.-Z.** (2020). Plant Unsaturated Fatty Acids: Multiple Roles in Stress Response. *Frontiers in plant science* **11**: 562785.
- He, M., Qin, C.-X., Wang, X., and Ding, N.-Z.** (2020). Plant Unsaturated Fatty Acids: Biosynthesis and Regulation. *Frontiers in plant science* **11**: 390.
- Heilmann, I.** (2016). Phosphoinositide signaling in plant development. *Development* (Cambridge, England) **143** (12): 2044–2055.
- Heilmann, I., Mekhedov, S., King, B., Browse, J., and Shanklin, J.** (2004a). Identification of the *Arabidopsis* palmitoyl-monogalactosyldiacylglycerol delta7-desaturase gene FAD5, and effects of plastidial retargeting of *Arabidopsis* desaturases on the fad5 mutant phenotype. *Plant physiology* **136** (4): 4237–4245.
- Heilmann, I., Pidkowich, M.S., Girke, T., and Shanklin, J.** (2004b). Switching desaturase enzyme specificity by alternate subcellular targeting. *Proceedings of the National Academy of Sciences of the United States of America* **101** (28): 10266–10271.
- Heilmann, M., Iven, T., Ahmann, K., Hornung, E., Stymne, S., and Feussner, I.** (2012). Production of wax esters in plant seed oils by oleosomal cotargeting of biosynthetic enzymes. *Journal of lipid research* **53** (10): 2153–2161.

- Hernández, M.L., Whitehead, L., He, Z., Gazda, V., Gilday, A., Kozhevnikova, E., Vaistij, F.E., Larson, T.R., and Graham, I.A.** (2012). A cytosolic acyltransferase contributes to triacylglycerol synthesis in sucrose-rescued *Arabidopsis* seed oil catabolism mutants. *Plant physiology* **160** (1): 215–225.
- Holtorf, S., Apel, K., and Bohlmann, H.** (1995). Comparison of different constitutive and inducible promoters for the overexpression of transgenes in *Arabidopsis thaliana*. *Plant molecular biology* **29** (4): 637–646.
- Horn, P.J., James, C.N., Gidda, S.K., Kilaru, A., Dyer, J.M., Mullen, R.T., Ohlrogge, J.B., and Chapman, K.D.** (2013). Identification of a new class of lipid droplet-associated proteins in plants. *Plant physiology* **162** (4): 1926–1936.
- Huang, C.-Y., and Huang, A.H.C.** (2017). Unique Motifs and Length of Hairpin in Oleosin Target the Cytosolic Side of Endoplasmic Reticulum and Budding Lipid Droplet. *Plant physiology* **174** (4): 2248–2260.
- Iba, K., Gibson, S., Nishiuchi, T., Fuse, T., Nishimura, M., Arondel, V., Hugly, S., and Somerville, C.** (1993). A gene encoding a chloroplast omega-3 fatty acid desaturase complements alterations in fatty acid desaturation and chloroplast copy number of the *fad7* mutant of *Arabidopsis thaliana*. *Journal of Biological Chemistry* **268** (32): 24099–24105.
- Inoue, H., Nojima, H., and Okayama, H.** (1990). High efficiency transformation of *Escherichia coli* with plasmids. *Gene* **96** (1): 23–28.
- Ischebeck, T., Krawczyk, H.E., Mullen, R.T., Dyer, J.M., and Chapman, K.D.** (2020). Lipid droplets in plants and algae: Distribution, formation, turnover and function. *Seminars in cell & developmental biology* **108**: 82–93.
- Ito, H., Fukuda, Y., Murata, K., and Kimura, A.** (1983). Transformation of intact yeast cells treated with alkali cations. *Journal of bacteriology* **153** (1): 163–168.
- Iven, T., Hornung, E., Heilmann, M., and Feussner, I.** (2016). Synthesis of oleyl oleate wax esters in *Arabidopsis thaliana* and *Camelina sativa* seed oil. *Plant biotechnology journal* **14** (1): 252–259.
- Johnsson, N., and Varshavsky, A.** (1994). Split ubiquitin as a sensor of protein interactions in vivo. *Proceedings of the National Academy of Sciences of the United States of America* **91** (22): 10340–10344.
- Julkowska, M.M., Rankenberg, J.M., and Testerink, C.** (2013). Liposome-binding assays to assess specificity and affinity of phospholipid-protein interactions. *Methods in molecular biology* (Clifton, N.J.) **1009**: 261–271.
- Kajiwara, S., Shirai, A., Fujii, T., Toguri, T., Nakamura, K., and Ohtaguchi, K.** (1996). Polyunsaturated fatty acid biosynthesis in *Saccharomyces cerevisiae*: expression of

- ethanol tolerance and the FAD2 gene from *Arabidopsis thaliana*. *Applied and environmental microbiology* **62** (12): 4309–4313.
- Katavic, V., Reed, D.W., Taylor, D.C., Giblin, E.M., Barton, D.L., Zou, J., Mackenzie, S.L., Covello, P.S., and Kunst, L.** (1995). Alteration of seed fatty acid composition by an ethyl methanesulfonate-induced mutation in *Arabidopsis thaliana* affecting diacylglycerol acyltransferase activity. *Plant physiology* **108** (1): 399–409.
- Kaup, M.T., Froese, C.D., and Thompson, J.E.** (2002). A role for diacylglycerol acyltransferase during leaf senescence. *Plant physiology* **129** (4): 1616–1626.
- Kelly, A.A., and Dörmann, P.** (2002). DGD2, an *Arabidopsis* gene encoding a UDP-galactose-dependent digalactosyldiacylglycerol synthase is expressed during growth under phosphate-limiting conditions. *Journal of Biological Chemistry* **277** (2): 1166–1173.
- Kim, H.U., Lee, K.-R., Go, Y.S., Jung, J.H., Suh, M.-C., and Kim, J.B.** (2011). Endoplasmic reticulum-located PDAT1-2 from castor bean enhances hydroxy fatty acid accumulation in transgenic plants. *Plant & cell physiology* **52** (6): 983–993.
- Klug, L., and Daum, G.** (2014). Yeast lipid metabolism at a glance. *FEMS yeast research* **14** (3): 369–388.
- Koo, A.J.K., Ohlrogge, J.B., and Pollard, M.** (2004). On the export of fatty acids from the chloroplast. *Journal of Biological Chemistry* **279** (16): 16101–16110.
- Kroon, J.T.M., Wei, W., Simon, W.J., and Slabas, A.R.** (2006). Identification and functional expression of a type 2 acyl-CoA:diacylglycerol acyltransferase (DGAT2) in developing castor bean seeds which has high homology to the major triglyceride biosynthetic enzyme of fungi and animals. *Phytochemistry* **67** (23): 2541–2549.
- Kunst, L., Browse, J., and Somerville, C.** (1988). Altered regulation of lipid biosynthesis in a mutant of *Arabidopsis* deficient in chloroplast glycerol-3-phosphate acyltransferase activity. *Proceedings of the National Academy of Sciences of the United States of America* **85** (12): 4143–4147.
- Laemmli, U.K.** (1970). Cleavage of structural proteins during the assembly of the head of bacteriophage T4. *Nature* **227** (5259): 680–685.
- Launhardt, L., Matzner, M., Heilmann, M., and Heilmann, I.** (2021). Analysis of Phosphoinositides from Complex Plant Samples by Solid-Phase Adsorption Chromatography and Subsequent Quantification via Thin-Layer and Gas Chromatography. *Methods in molecular biology (Clifton, N.J.)* **2295**: 379–389.
- Lazo, G.R., Stein, P.A., and Ludwig, R.A.** (1991). A DNA transformation-competent *Arabidopsis* genomic library in *Agrobacterium*. *Bio/technology (Nature Publishing Company)* **9** (10): 963–967.

- Lee, K.-R., Lee, Y., Kim, E.-H., Lee, S.-B., Roh, K.H., Kim, J.-B., Kang, H.-C., and Kim, H.U.** (2016). Functional identification of oleate 12-desaturase and ω -3 fatty acid desaturase genes from *Perilla frutescens* var. *frutescens*. *Plant cell reports* **35** (12): 2523–2537.
- Lemieux, B., Miquel, M., Somerville, C., and Browse, J.** (1990). Mutants of *Arabidopsis* with alterations in seed lipid fatty acid composition. TAG. Theoretical and applied genetics. *Theoretische und angewandte Genetik* **80** (2): 234–240.
- Li, R., Yu, K., Hatanaka, T., and Hildebrand, D.F.** (2010). *Vernonia* DGATs increase accumulation of epoxy fatty acids in oil. *Plant biotechnology journal* **8** (2): 184–195.
- Li, Y., Beisson, F., Pollard, M., and Ohlrogge, J.** (2006). Oil content of *Arabidopsis* seeds: the influence of seed anatomy, light and plant-to-plant variation. *Phytochemistry* **67** (9): 904–915.
- Li-Beisson, Y., Shorrosh, B., Beisson, F., Andersson, M.X., Arondel, V., Bates, P.D., Baud, S., Bird, D., Debono, A., Durrett, T.P., Franke, R.B., Graham, I.A., Katayama, K., Kelly, A.A., Larson, T., Markham, J.E., Miquel, M., Molina, I., Nishida, I., Rowland, O., Samuels, L., Schmid, K.M., Wada, H., Welti, R., Xu, C., Zallot, R., and Ohlrogge, J.** (2010). Acyl-lipid metabolism. *The arabidopsis book* **8**: e0133.
- Liu, Q., Siloto, R.M.P., Lehner, R., Stone, S.J., and Weselake, R.J.** (2012). Acyl-CoA:diacylglycerol acyltransferase: molecular biology, biochemistry and biotechnology. *Progress in lipid research* **51** (4): 350–377.
- Lou, Y., Schwender, J., and Shanklin, J.** (2014). FAD2 and FAD3 desaturases form heterodimers that facilitate metabolic channeling in vivo. *The Journal of biological chemistry* **289** (26): 17996–18007.
- Lu, C., Xin, Z., Ren, Z., Miquel, M., and Browse, J.** (2009). An enzyme regulating triacylglycerol composition is encoded by the ROD1 gene of *Arabidopsis*. *Proceedings of the National Academy of Sciences of the United States of America* **106** (44): 18837–18842.
- Matsuda, O., Sakamoto, H., Hashimoto, T., and Iba, K.** (2005). A temperature-sensitive mechanism that regulates post-translational stability of a plastidial omega-3 fatty acid desaturase (FAD8) in *Arabidopsis* leaf tissues. *Journal of Biological Chemistry* **280** (5): 3597–3604.
- McCartney, A.W., Dyer, J.M., Dhanoa, P.K., Kim, P.K., Andrews, D.W., McNew, J.A., and Mullen, R.T.** (2004). Membrane-bound fatty acid desaturases are inserted co-translationally into the ER and contain different ER retrieval motifs at their carboxy termini. *The Plant journal for cell and molecular biology* **37** (2): 156–173.

- McConn, M., and Browse, J.** (1996). The Critical Requirement for Linolenic Acid Is Pollen Development, Not Photosynthesis, in an Arabidopsis Mutant. *The Plant cell* **8** (3): 403–416.
- McConn, M., Hugly, S., Browse, J., and Somerville, C.** (1994). A Mutation at the *fad8* Locus of Arabidopsis Identifies a Second Chloroplast omega-3 Desaturase. *Plant physiology* **106** (4): 1609–1614.
- Menard, G.N., Moreno, J.M., Bryant, F.M., Munoz-Azcarate, O., Kelly, A.A., Hassani-Pak, K., Kurup, S., and Eastmond, P.J.** (2017). Genome Wide Analysis of Fatty Acid Desaturation and Its Response to Temperature. *Plant physiology* **173** (3): 1594–1605.
- Mhaske, V., Beldjilali, K., Ohlrogge, J., and Pollard, M.** (2005). Isolation and characterization of an Arabidopsis thaliana knockout line for phospholipid: diacylglycerol transacylase gene (*At5g13640*). *Plant physiology and biochemistry PPB* **43** (4): 413–417.
- Miquel, M., and Browse, J.** (1992). Arabidopsis mutants deficient in polyunsaturated fatty acid synthesis. Biochemical and genetic characterization of a plant oleoyl-phosphatidylcholine desaturase. *Journal of Biological Chemistry* **267** (3): 1502–1509.
- Miquel, M., James, D., Dooner, H., and Browse, J.** (1993). Arabidopsis requires polyunsaturated lipids for low-temperature survival. *Proceedings of the National Academy of Sciences of the United States of America* **90** (13): 6208–6212.
- Mukherjee, S., Soe, T.T., and Maxfield, F.R.** (1999). Endocytic sorting of lipid analogues differing solely in the chemistry of their hydrophobic tails. *The Journal of cell biology* **144** (6): 1271–1284.
- Napier, J.A., Stobart, A.K., and Shewry, P.R.** (1996). The structure and biogenesis of plant oil bodies: the role of the ER membrane and the oleosin class of proteins. *Plant molecular biology* **31** (5): 945–956.
- Nebenführ, A., Gallagher, L.A., Dunahay, T.G., Frohlick, J.A., Mazurkiewicz, A.M., Meehl, J.B., and Staehelin, L.A.** (1999). Stop-and-go movements of plant Golgi stacks are mediated by the acto-myosin system. *Plant physiology* **121** (4): 1127–1142.
- Nelson, B.K., Cai, X., and Nebenführ, A.** (2007). A multicolored set of in vivo organelle markers for co-localization studies in Arabidopsis and other plants. *The Plant journal for cell and molecular biology* **51** (6): 1126–1136.
- Nguyen, V.C., Nakamura, Y., and Kanehara, K.** (2019). Membrane lipid polyunsaturation mediated by FATTY ACID DESATURASE 2 (*FAD2*) is involved in endoplasmic reticulum stress tolerance in Arabidopsis thaliana. *The Plant journal for cell and molecular biology* **99** (3): 478–493.
- Ohlrogge, J., and Browse, J.** (1995). Lipid biosynthesis. *The Plant cell* **7** (7): 957–970.

- Okuley, J., Lightner, J., Feldmann, K., Yadav, N., Lark, E., and Browse, J.** (1994). Arabidopsis FAD2 gene encodes the enzyme that is essential for polyunsaturated lipid synthesis. *The Plant cell* **6** (1): 147–158.
- O'Quin, J.B., Bourassa, L., Zhang, D., Shockey, J.M., Gidda, S.K., Fosnot, S., Chapman, K.D., Mullen, R.T., and Dyer, J.M.** (2010). Temperature-sensitive post-translational regulation of plant omega-3 fatty-acid desaturases is mediated by the endoplasmic reticulum-associated degradation pathway. *The Journal of biological chemistry* **285** (28): 21781–21796.
- Park, K., Ju, S., Kim, N., and Park, S.-Y.** (2021). The Golgi complex: a hub of the secretory pathway. *BMB Rep* **54** (5): 246–252.
- Pyc, M., Cai, Y., Greer, M.S., Yurchenko, O., Chapman, K.D., Dyer, J.M., and Mullen, R.T.** (2017). Turning Over a New Leaf in Lipid Droplet Biology. *Trends in plant science* **22** (7): 596–609.
- Pyc, M., Gidda, S.K., Seay, D., Esnay, N., Kretschmar, F.K., Cai, Y., Doner, N.M., Greer, M.S., Hull, J.J., Coulon, D., Bréhélin, C., Yurchenko, O., Vries, J. de, Valerius, O., Braus, G.H., Ischebeck, T., Chapman, K.D., Dyer, J.M., and Mullen, R.T.** (2021). LDIP cooperates with SEIPIN and LDAP to facilitate lipid droplet biogenesis in Arabidopsis. *The Plant cell* **33** (9): 3076–3103.
- Regmi, A., Shockey, J., Kotapati, H.K., and Bates, P.D.** (2020). Oil-Producing Metabolons Containing DGAT1 Use Separate Substrate Pools from those Containing DGAT2 or PDAT. *Plant physiology* **184** (2): 720–737.
- Saint-Jore-Dupas, C., Nebenführ, A., Boulaflous, A., Follet-Gueye, M.-L., Plasson, C., Hawes, C., Driouich, A., Faye, L., and Gomord, V.** (2006). Plant N-glycan processing enzymes employ different targeting mechanisms for their spatial arrangement along the secretory pathway. *The Plant cell* **18** (11): 3182–3200.
- Sandager, L., Gustavsson, M.H., Ståhl, U., Dahlqvist, A., Wiberg, E., Banas, A., Lenman, M., Ronne, H., and Stymne, S.** (2002). Storage lipid synthesis is non-essential in yeast. *Journal of Biological Chemistry* **277** (8): 6478–6482.
- Schindelin, J., Arganda-Carreras, I., Frise, E., Kaynig, V., Longair, M., Pietzsch, T., Preibisch, S., Rueden, C., Saalfeld, S., Schmid, B., Tinevez, J.-Y., White, D.J., Hartenstein, V., Eliceiri, K., Tomancak, P., and Cardona, A.** (2012). Fiji: an open-source platform for biological-image analysis. *Nature methods* **9** (7): 676–682.
- Shanklin, J., and Cahoon, E.B.** (1998). DESATURATION AND RELATED MODIFICATIONS OF FATTY ACIDS¹. *Annual review of plant physiology and plant molecular biology* **49**: 611–641.

- Shanklin, J., Guy, J.E., Mishra, G., and Lindqvist, Y.** (2009). Desaturases: emerging models for understanding functional diversification of diiron-containing enzymes. *Journal of Biological Chemistry* **284** (28): 18559–18563.
- Shanklin, J., Whittle, E., and Fox, B.G.** (1994). Eight histidine residues are catalytically essential in a membrane-associated iron enzyme, stearoyl-CoA desaturase, and are conserved in alkane hydroxylase and xylene monooxygenase. *Biochemistry* **33** (43): 12787–12794.
- Shao, Q., Liu, X., Su, T., Ma, C., and Wang, P.** (2019). New Insights Into the Role of Seed Oil Body Proteins in Metabolism and Plant Development. *Frontiers in plant science* **10**: 1568.
- Shockey, J.M., Gidda, S.K., Chapital, D.C., Kuan, J.-C., Dhanoa, P.K., Bland, J.M., Rothstein, S.J., Mullen, R.T., and Dyer, J.M.** (2006). Tung tree DGAT1 and DGAT2 have nonredundant functions in triacylglycerol biosynthesis and are localized to different subdomains of the endoplasmic reticulum. *The Plant cell* **18** (9): 2294–2313.
- Sperling, P., Linscheid, M., Stöcker, S., Mühlbach, H.P., and Heinz, E.** (1993). In vivo desaturation of cis-delta 9-monounsaturated to cis-delta 9,12-diunsaturated alkenylether glycerolipids. *Journal of Biological Chemistry* **268** (36): 26935–26940.
- Spitzer, M., Wildenhain, J., Rappsilber, J., and Tyers, M.** (2014). BoxPlotR: a web tool for generation of box plots. *Nature methods* **11** (2): 121–122.
- Ståhl, U., Carlsson, A.S., Lenman, M., Dahlqvist, A., Huang, B., Banas, W., Banas, A., and Stymne, S.** (2004). Cloning and functional characterization of a phospholipid:diacylglycerol acyltransferase from *Arabidopsis*. *Plant physiology* **135** (3): 1324–1335.
- Statistic Kingdom** (2017). <http://www.statskingdom.com>. Accessed 11 February 2022.
- Stukey, J.E., McDonough, V.M., and Martin, C.E.** (1989). Isolation and characterization of OLE1, a gene affecting fatty acid desaturation from *Saccharomyces cerevisiae*. *Journal of Biological Chemistry* **264** (28): 16537–16544.
- Stukey, J.E., McDonough, V.M., and Martin, C.E.** (1990). The OLE1 gene of *Saccharomyces cerevisiae* encodes the delta 9 fatty acid desaturase and can be functionally replaced by the rat stearoyl-CoA desaturase gene. *Journal of Biological Chemistry* **265** (33): 20144–20149.
- Stymne, S., and Stobart, A.K.** (1984). Evidence for the reversibility of the acyl-CoA:lysophosphatidylcholine acyltransferase in microsomal preparations from developing safflower (*Carthamus tinctorius* L.) cotyledons and rat liver. *The Biochemical journal* **223** (2): 305–314.

- Tan, W.-J., Yang, Y.-C., Zhou, Y., Huang, L.-P., Le Xu, Chen, Q.-F., Yu, L.-J., and Xiao, S.** (2018). DIACYLGLYCEROL ACYLTRANSFERASE and DIACYLGLYCEROL KINASE Modulate Triacylglycerol and Phosphatidic Acid Production in the Plant Response to Freezing Stress. *Plant physiology* **177** (3): 1303–1318.
- Tang, G.-Q., Novitzky, W.P., Carol Griffin, H., Huber, S.C., and Dewey, R.E.** (2005). Oleate desaturase enzymes of soybean: evidence of regulation through differential stability and phosphorylation. *The Plant journal for cell and molecular biology* **44** (3): 433–446.
- Taurino, M., Costantini, S., Domenico, S. de, Stefanelli, F., Ruano, G., Delgadillo, M.O., Sánchez-Serrano, J.J., Sanmartín, M., Santino, A., and Rojo, E.** (2018). SEIPIN Proteins Mediate Lipid Droplet Biogenesis to Promote Pollen Transmission and Reduce Seed Dormancy. *Plant physiology* **176** (2): 1531–1546.
- Thelen, J.J., and Ohlrogge, J.B.** (2002). Metabolic engineering of fatty acid biosynthesis in plants. *Metabolic engineering* **4** (1): 12–21.
- Thomæus, S., Carlsson, A.S., and Stymne, S.** (2001). Distribution of fatty acids in polar and neutral lipids during seed development in *Arabidopsis thaliana* genetically engineered to produce acetylenic, epoxy and hydroxy fatty acids. *Plant Science* **161** (5): 997–1003.
- To, A., Joubès, J., Barthole, G., Lécureuil, A., Scagnelli, A., Jasinski, S., Lepiniec, L., and Baud, S.** (2012). WRINKLED transcription factors orchestrate tissue-specific regulation of fatty acid biosynthesis in *Arabidopsis*. *The Plant cell* **24** (12): 5007–5023.
- Towbin, H., Staehelin, T., and Gordon, J.** (1979). Electrophoretic transfer of proteins from polyacrylamide gels to nitrocellulose sheets: procedure and some applications. *Proceedings of the National Academy of Sciences of the United States of America* **76** (9): 4350–4354.
- Turchetto-Zolet, A.C., Christoff, A.P., Kulcheski, F.R., Loss-Morais, G., Margis, R., and Margis-Pinheiro, M.** (2016). Diversity and evolution of plant diacylglycerol acyltransferase (DGATs) unveiled by phylogenetic, gene structure and expression analyses. *Genetics and molecular biology* **39** (4): 524–538.
- van Erp, H., Bates, P.D., Burgal, J., Shockey, J., and Browse, J.** (2011). Castor phospholipid:diacylglycerol acyltransferase facilitates efficient metabolism of hydroxy fatty acids in transgenic *Arabidopsis*. *Plant physiology* **155** (2): 683–693.
- Vanhercke, T., Belide, S., Taylor, M.C., El Tahchy, A., Okada, S., Rolland, V., Liu, Q., Mitchell, M., Shrestha, P., Venables, I., Ma, L., Blundell, C., Mathew, A., Ziolkowski, L., Niesner, N., Hussain, D., Dong, B., Liu, G., Godwin, I.D., Lee, J., Rug, M., Zhou, X.-R., Singh, S.P., and Petrie, J.R.** (2018). Up-regulation of lipid

- biosynthesis increases the oil content in leaves of *Sorghum bicolor*. *Plant biotechnology journal* **17** (1): 220–232.
- Vanhercke, T., Dyer, J.M., Mullen, R.T., Kilaru, A., Rahman, M.M., Petrie, J.R., Green, A.G., Yurchenko, O., and Singh, S.P.** (2019). Metabolic engineering for enhanced oil in biomass. *Progress in lipid research* **74**: 103–129.
- Vanhercke, T., El Tahchy, A., Liu, Q., Zhou, X.-R., Shrestha, P., Divi, U.K., Ral, J.-P., Mansour, M.P., Nichols, P.D., James, C.N., Horn, P.J., Chapman, K.D., Beaudoin, F., Ruiz-López, N., Larkin, P.J., Feyter, R.C. de, Singh, S.P., and Petrie, J.R.** (2014). Metabolic engineering of biomass for high energy density: oilseed-like triacylglycerol yields from plant leaves. *Plant biotechnology journal* **12** (2): 231–239.
- Wallis, J.G., and Browse, J.** (2002). Mutants of *Arabidopsis* reveal many roles for membrane lipids. *Progress in lipid research* **41** (3): 254–278.
- Wasternack, C., and Feussner, I.** (2018). The Oxylipin Pathways: Biochemistry and Function. *Annual review of plant biology* **69**: 363–386.
- Wee, E.G., Sherrier, D.J., Prime, T.A., and Dupree, P.** (1998). Targeting of active sialyltransferase to the plant Golgi apparatus. *The Plant cell* **10** (10): 1759–1768.
- Xu, C., and Shanklin, J.** (2016). Triacylglycerol Metabolism, Function, and Accumulation in Plant Vegetative Tissues. *Annual review of plant biology* **67**: 179–206.
- Xu, J., Carlsson, A.S., Francis, T., Zhang, M., Hoffman, T., Giblin, M.E., and Taylor, D.C.** (2012). Triacylglycerol synthesis by PDAT1 in the absence of DGAT1 activity is dependent on re-acylation of LPC by LPCAT2. *BMC plant biology* **12**: 4.
- Xu, Y., Caldo, K.M.P., Pal-Nath, D., Ozga, J., Lemieux, M.J., Weselake, R.J., and Chen, G.** (2018). Properties and Biotechnological Applications of Acyl-CoA:diacylglycerol Acyltransferase and Phospholipid:diacylglycerol Acyltransferase from Terrestrial Plants and Microalgae. *Lipids* **53** (7): 663–688.
- Yadav, N.S., Wierzbicki, A., Aegerter, M., Caster, C.S., Pérez-Grau, L., Kinney, A.J., Hitz, W.D., Booth, J.R., Schweiger, B., and Stecca, K.L.** (1993). Cloning of higher plant omega-3 fatty acid desaturases. *Plant physiology* **103** (2): 467–476.
- Yamada, K., Hara-Nishimura, I., and Nishimura, M.** (2011). Unique defense strategy by the endoplasmic reticulum body in plants. *Plant & cell physiology* **52** (12): 2039–2049.
- Yoo, S.-D., Cho, Y.-H., and Sheen, J.** (2007). *Arabidopsis* mesophyll protoplasts: a versatile cell system for transient gene expression analysis. *Nature protocols* **2** (7): 1565–1572.
- Zhang, J., Liu, H., Sun, J., Li, B., Zhu, Q., Chen, S., and Zhang, H.** (2012). *Arabidopsis* fatty acid desaturase FAD2 is required for salt tolerance during seed germination and early seedling growth. *PLoS one* **7** (1): e30355.

- Zhang, M., Fan, J., Taylor, D.C., and Ohlogge, J.B.** (2009). DGAT1 and PDAT1 acyltransferases have overlapping functions in Arabidopsis triacylglycerol biosynthesis and are essential for normal pollen and seed development. *The Plant cell* **21** (12): 3885–3901.
- Zhou, X.-R., Shrestha, P., Yin, F., Petrie, J.R., and Singh, S.P.** (2013). AtDGAT2 is a functional acyl-CoA:diacylglycerol acyltransferase and displays different acyl-CoA substrate preferences than AtDGAT1. *FEBS Letters* **587** (15): 2371–2376.
- Zou, J., Wei, Y., Jako, C., Kumar, A., Selvaraj, G., and Taylor, D.C.** (1999). The Arabidopsis thaliana TAG1 mutant has a mutation in a diacylglycerol acyltransferase gene. *The Plant journal for cell and molecular biology* **19** (6): 645–653.

7. Appendix

7.1 Additional information to the obtained results

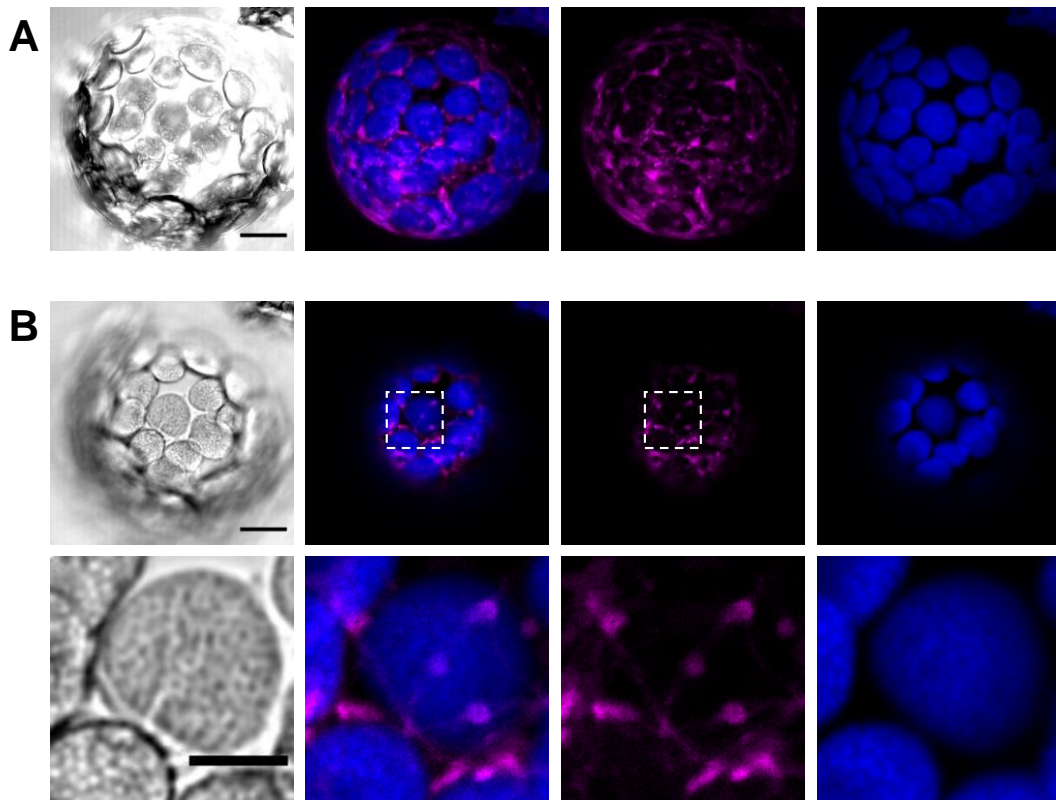


Figure 7.1. Subcellular distribution of mCherry-FAD2 in *Arabidopsis* mesophyll protoplasts. Protoplasts from *A. thaliana* Col-0 were transformed with *pEntryA-pFAD2::mCherry-FAD2* and analyzed by LSM. Z-stacks covering the cell from one edge to the center with approx. 0.6 μm distance between the slices were acquired. mCherry-FAD2 fluorescence is depicted in magenta, the autofluorescence of chlorophyll A in blue. **A**, Maximum intensity Z-projection. Scale bar: 10 μm . **B**, Selected single slice of the Z-stack from A. Scale bars: 10 μm (upper panels), 5 μm (lower panels). Images are representative for three experiments using a total of 19 cells.

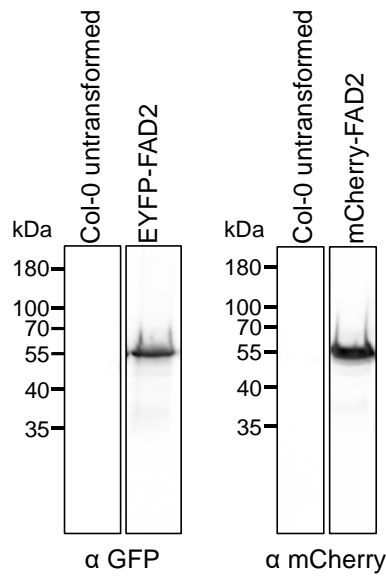


Figure 7.2. Immunodetection of tagged FAD2 expressed in Arabidopsis mesophyll protoplasts. Arabidopsis mesophyll protoplasts used for examination of subcellular localization of tagged FAD2 were tested for transient protein expression. Proteins from transiently transformed protoplasts were separated by SDS-PAGE and transferred to nitrocellulose membranes by western blotting. The tagged proteins were detected with specific anti-GFP or anti-mCherry antibodies and HRP chemiluminescence. Untransformed protoplasts were used as a control for antibody specificity. Expected molecular weights: EYFP-FAD2: 69 kDa, mCherry-FAD2: 71 kDa. Images are representative for nine (EYFP-FAD2) or five (mCherry-FAD2) experiments.

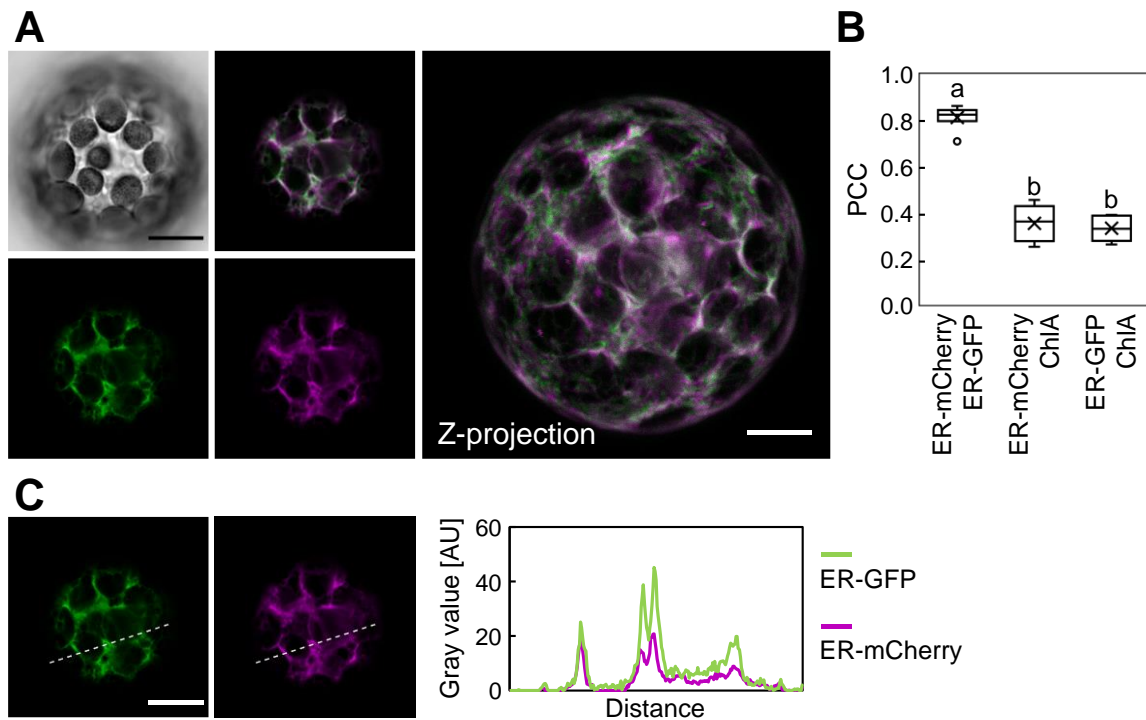


Figure 7.3. Subcellular distribution of two different ER markers. As positive control for quantitative evaluation of colocalization, the relative localization of two ER markers was analyzed. Protoplasts from the Arabidopsis ER-marker line GFP-HDEL were transformed with the ER marker construct *CD3-959-ER-mCherry* and analyzed by LSM. Z-stacks covering the cell from one edge to the center with approx. 0.6 μm distance between the slices were acquired. The ER marker ER-mCherry is shown in magenta, the ER marker ER-GFP in green. Scale bars: 10 μm ; ChlA, chlorophyll A. **A**, Single confocal plane and maximum intensity Z-projection of the relative localization of the two ER markers. **B**, Pearson's correlation coefficients (PCCs) were calculated based on 8 Z-stacks from two independent experiments taken by LSM. Significant differences were determined using one-way ANOVA with a Tukey's post-hoc test ($p < 0.05$). Letters indicate categories of significantly different samples. **D**, Intensity profile for ER-mCherry (magenta) and ER-GFP (green) along the line highlighted in the left panels. Images are representative for two experiments using a total of 8 cells.

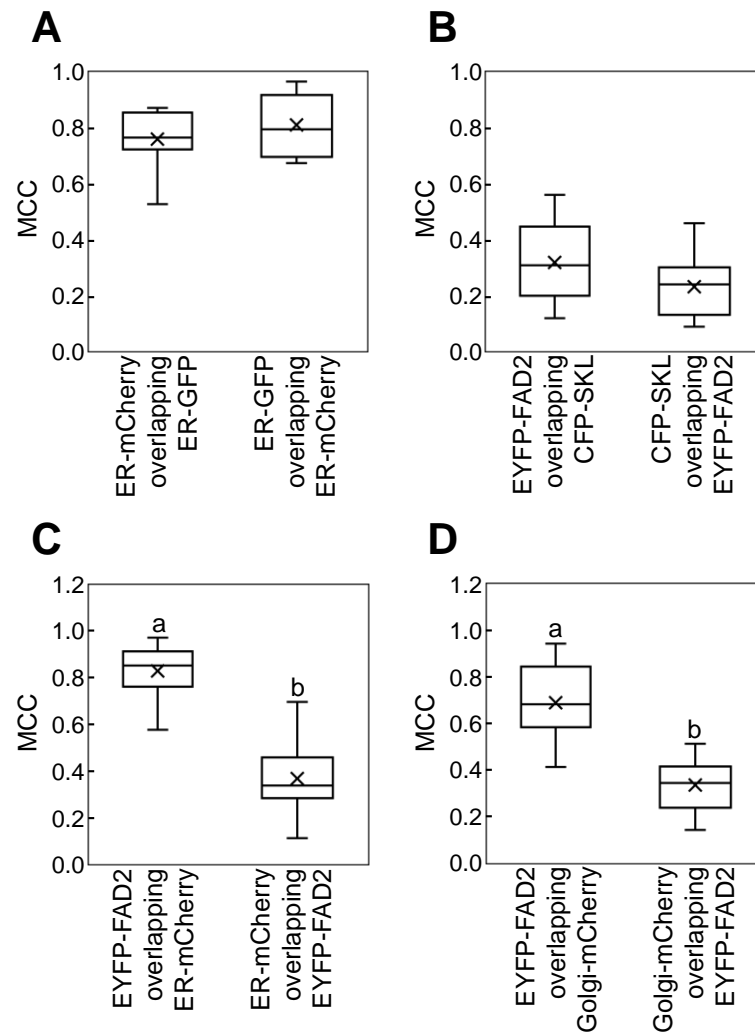


Figure 7.4. MCCs for selected colocalization experiments in *Arabidopsis mesophyll* protoplasts. As a second quantification method of colocalization, Manders' colocalization coefficients (MCCs) were calculated. MCCs calculate the fraction of a probe that coincide with a second probe. MCCs were calculated based on Z-stacks taken by LSM. Individual thresholds were chosen for each image and channel to omit background signals. Significant differences were determined using one-way ANOVA with a Tukey's post-hoc test ($p < 0.05$). Letters indicate categories of significantly different samples. **A**, Protoplasts from *A. thaliana* GFP-HDEL were transformed with the ER marker construct *CD3-959-ER-mCherry*. MCCs were calculated based on 8 Z-stacks from one experiment. **B**, Protoplasts from *A. thaliana* Col-0 were cotransformed with *pEntryA-pFAD2::EYFP-FAD2* and the peroxisome-marker construct *pEntryD-pCaMV35S::CFP-SKL*. MCCs were calculated based on 9 Z-stacks from one experiment. **C**, Protoplasts from *A. thaliana* Col-0 were cotransformed with *pEntryA-pFAD2::EYFP-FAD2* and the ER marker construct *CD3-959-ER-mCherry*. MCCs were calculated based on 21 Z-stacks from two independent experiments. **D**, Protoplasts from *A. thaliana* Col-0 were cotransformed with *pEntryA-pFAD2::EYFP-FAD2* and the Golgi marker construct *CD3-967-Golgi-mCherry*. MCCs were calculated based on 14 Z-stack from two independent experiments.

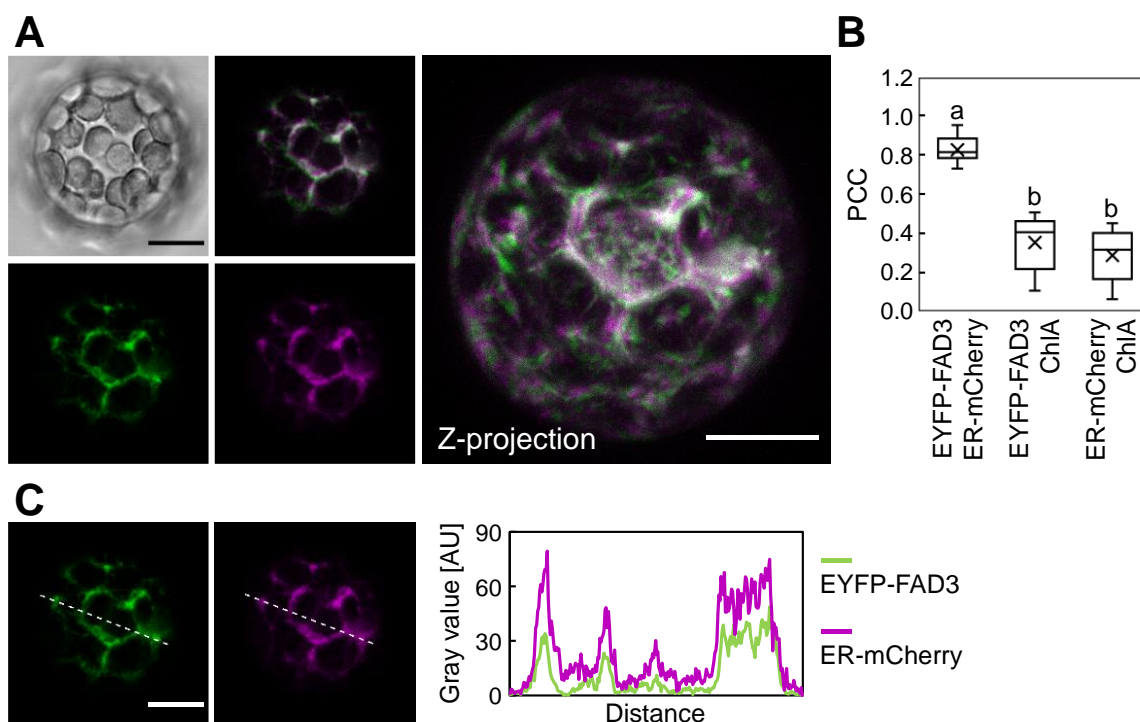


Figure 7.5. Subcellular distribution of EYFP-FAD3 relative to the ER in Arabidopsis mesophyll protoplasts. Protoplasts from *A. thaliana* Col-0 were cotransformed with *pEntryA-pCaMV35S::EYFP-FAD3* and the ER marker construct *CD3-959-ER-mCherry* and analyzed by LSM. Z-stacks covering the cell from one edge to the center with approx. 0.6 μm distance between the slices were acquired. EYFP-FAD3 fluorescence is shown in green, the ER marker (ER-mCherry) in magenta. Scale bar: 10 μm ; ChlA, chlorophyll A. **A**, Protoplast from *A. thaliana* Col-0 coexpressing EYFP-FAD3 and the ER marker. Selected single confocal slice (left) and maximum intensity Z-projection of a Z-stack (right). **B**, Pearson's correlation coefficients (PCCs) were calculated based on 10 Z-stacks from one experiment taken by LSM. Significant differences were determined using one-way ANOVA with a Tukey's post-hoc test ($p < 0.05$). Letters indicate categories of significantly different samples. **C**, Intensity profile for EYFP-FAD3 (green) and ER-mCherry (magenta) along the line highlighted in the left panels. Images are representative for one experiment using 10 cells.

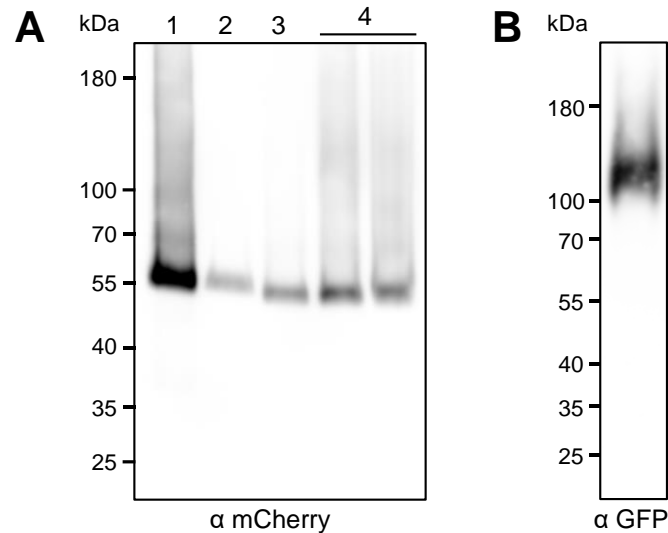


Figure 7.6. Immunodetection of fluorescence-tagged FAD3 expressed in Arabidopsis mesophyll protoplasts. Arabidopsis mesophyll protoplasts used for examination of subcellular localization of tagged FAD3 were tested for transient protein expression. Proteins from transiently transformed protoplasts were separated by SDS-PAGE and transferred to nitrocellulose membranes by western blotting. The tagged proteins were detected using anti-mCherry (A) and anti-GFP (B) antibodies and HRP chemiluminescence. 1, Arabidopsis protoplasts transformed with *pEntryA-pCaMV35S::mCherry-FAD3*; 2, Arabidopsis protoplasts transformed with *pEntryA-pFAD3::mCherry-FAD3*; 3, Arabidopsis protoplasts transformed with *pCAMBIA3300.0GS-pFAD3::mCherry-FAD3-pCaMV35S::CFP-SKL*; 4, Arabidopsis protoplasts transformed with *pCAMBIA3300.0GS-pFAD3::mCherry-FAD3-pCaMV35S::WRI1-EYFP*. Expected molecular weights: mCherry-FAD3: 71 kDa, WRI1-EYFP: 76 kDa. Images are representative for two independent experiments.

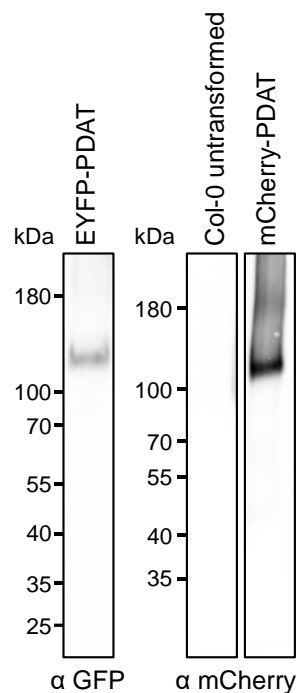


Figure 7.7. Immunodetection of fluorescence-tagged PDAT expressed in Arabidopsis mesophyll protoplasts. Arabidopsis mesophyll protoplasts used for examination of subcellular localization of tagged PDAT were tested for transient protein expression. Proteins from transiently transformed protoplasts were separated by SDS-PAGE and transferred to nitrocellulose membranes by western blotting. The tagged proteins were detected with specific anti-GFP and anti-mCherry antibodies and HRP chemiluminescence. Untransformed protoplasts were used as a control for antibody specificity. Expected molecular weights: EYFP-PDAT: 99 kDa, mCherry-PDAT: 101 kDa. Images are representative for two independent experiments.

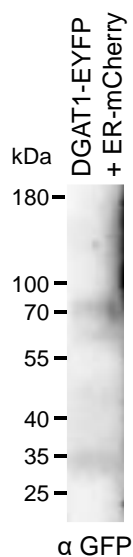


Figure 7.8. Immunodetection of DGAT1-EYFP expressed in Arabidopsis mesophyll protoplasts. Arabidopsis mesophyll protoplasts used for examination of subcellular localization of tagged DGAT1 were tested for transient protein expression. Protoplasts were cotransformed with *pEntryD-pCaMV35S::DGAT1-EYFP* and the ER marker construct *CD3-959-ER-mCherry*. Proteins from transiently transformed protoplasts were separated by SDS-PAGE and transferred to nitrocellulose membranes by western blotting. The tagged proteins were detected with specific anti-GFP antibody and HRP chemiluminescence. Expected molecular weights: DGAT1-EYFP: 86 kDa, EYFP: 27 kDa. n = 1.

7.2 Additional information to materials and methods

7.2.1 Specification of devices

Table 7.1. Devices used in this work.

Device	Manufacturer/Supplier
Plant Chamber Adaptis A1000	Conviron, Cambridgeshire, United Kingdom
Plant Chamber PERCIVAL AR-66/L3	Percival Scientific, Perry, IA, USA
Ultrospec 2100 pro UV/Vis Spectrometer	Biochrom, Cambridge, United Kingdom
Ultrospec 3000 UV/Vis Spectrometer	Pharmacia Biotech AG, Dübendorf, Germany
TADVANCED or TProfessional Thermocycler	Biometra, Göttingen, Germany
Agarose gel chambers, MINI and MIDI with gel slides	cti, Idstein, Germany
Gel Detection System Quantum ST4	Vilber Lourmat Deutschland GmbH, Eberhardzell, Germany
NanoDrop 2000 Spectrophotometer	Thermo Fisher Scientific, Schwerte, Germany
Multiple Gel Caster (SE 200 series)	Hoefer Inc. (SERVA Electrophoresis GmbH, Heidelberg, Germany)
SE250 Electrophorese Chamber	Hoefer Inc. (SERVA Electrophoresis GmbH, Heidelberg, Germany)
Mini-PROTEAN® Tetra System Blotting Chamber	BioRad Laboratories GmbH, Munich, Germany
Fusion Solo S	Vilber Lourmat Deutschland GmbH, Eberhardzell, Germany
Chromatogram Immersion Device III	CAMAG Chemie-Erzeugnisse & Adsorptionstechnik AG, Muttenz, Switzerland
GC-2010 Plus (with FID)	Shimadzu Deutschland GmbH, Duisburg, Germany
30 m DB-23 column	Agilent Technologies (VWR International GmbH, Darmstadt, Germany)
AOC-20i Auto Injector	Shimadzu Deutschland GmbH, Duisburg, Germany
Hydrogen generator, H2PEM-100	Parker Hannifin GmbH, Bielefeld, Germany
Zeiss Laser Scanning Microscope LSM880	Carl Zeiss, Jena, Germany

Device	Manufacturer/Supplier
Zeiss Cell observer SD with a Yokogawa CSU-X1 spinning disc unit with Photometrics Evolve 512 Delta EM-CCD camera	Carl Zeiss, Jena, Germany
DAPI/FITC/TRITC ET Tripleband emitter F67-000	AHF Analysetechnik, Tübingen, Germany

7.2.2 Specification of chemicals

Table 7.2. Chemicals used in this work.

Chemical	Manufacturer/Supplier
5-bromo-4-chloro-3-indolyl- β -D-galactopyranoside (β -x-gal)	Sigma-Aldrich, Munich, Germany
Albumin Fraction V (BSA)	Carl Roth, Karlsruhe, Germany
Basta® (glufosinate ammonium)	Bayer, Leverkusen, Germany
Biozym LE Agarose	Biozym Scientific GmbH, Hessisch Oldendorf, Germany
Isopropyl β -D-1-thiogalactopyranoside (IPTG), dioxane free	Thermo Fisher Scientific, Schwerte, Germany
Lithium chloride, 8 M	Sigma-Aldrich, Munich, Germany
Micro-Agar	Duchefa, Haarlem, Netherlands
Murashige & Skoog-Medium, incl. modified vitamins	Duchefa, Haarlem, Netherlands
Phenol solution, saturated with 0.1 M citrate buffer, pH 4.3	Sigma-Aldrich, Munich, Germany
phenol:chloroform:isoamyl alcohol, 25:24:1, saturated with 10 mM Tris, pH 8.0, 1 mM EDTA	Sigma-Aldrich, Munich, Germany
Primuline	Sigma-Aldrich, Munich, Germany
Rotiphorese® Gel 30 (37.5:1)	Carl Roth, Karlsruhe, Germany
Silwet® L-77	Lehle Seeds, Round Ror, TX, USA
Skim milk powder for blotting	SERVA Electrophoresis GmbH, Heidelberg, Germany
sodium methoxide, 0.5 M CH ₃ ONa in methanol (0.5 N)	Carl Roth, Karlsruhe, Germany
yeast nitrogen base without amino acids and ammonium sulfate	Difco™ (Otto Nordwald, Hamburg, Germany)

7.2.3 Lipid and fatty acid standards

Table 7.3. Lipid- and fatty acid standards.

Lipid-/Fatty acid	Manufacturer/Supplier
linolenic acid (18:1 ^{Δ9})	Sigma-Aldrich, Munich, Germany
triacylglycerol (TAG)	self-made, extracted vegetable oil
diacylglycerol (DAG)	Avanti Polar Lipids Inc. (Merck, Darmstadt, Germany)
monogalactosyldiacylglycerol (MGDG)	Avanti Polar Lipids Inc. (Merck, Darmstadt, Germany)
digalactosyldiacylglycerol (DGDG)	Avanti Polar Lipids Inc. (Merck, Darmstadt, Germany)
phosphatidylcholine (dioleoyl-)	Avanti Polar Lipids Inc. (Merck, Darmstadt, Germany)
tripentadecanoin	Sigma-Aldrich, Munich, Germany
menhaden fish oil	Sigma-Aldrich, Munich, Germany

7.2.4 Molecular size markers and enzymes

Table 7.4. Molecular size markers and enzymes.

Molecular Size Marker	Manufacturer/Supplier
GeneRuler™ 1 kb DNA Ladder	Thermo Fisher Scientific, Schwerte, Germany
PageRuler™ Prestained Protein Ladder, 10 to 180 kDa	Thermo Fisher Scientific, Schwerte, Germany
Enzyme	Manufacturer/Supplier
Cellulase "Onozuka R-10" from <i>Trichoderma viride</i> ca. 1 U/mg	SERVA Electrophoresis GmbH, Heidelberg, Germany
Maceroenzyme R-10 from <i>Rhizopus sp. lyophile</i> .	SERVA Electrophoresis GmbH, Heidelberg, Germany
Phusion® High Fidelity DNA-Polymerase	New England Biolabs Inc., Frankfurt am Main, Germany
T4-DNA-Ligase, 5 Weiss Units/μl	New England Biolabs Inc., Frankfurt am Main, Germany
Gateway™ BP Clonase™ II Enzyme Mix	Invitrogen™, Thermo Fisher Scientific, Schwerte, Deutschland
Gateway™ LR Clonase™ II Enzyme Mix	Invitrogen™, Thermo Fisher Scientific, Schwerte, Deutschland

7.2.5 Consumables and kits

Table 7.5. Consumables and kits.

Product	Manufacturer/Supplier
Amersham Protran 0,45 NC (nitrocellulose membrane)	Cytiva, Solingen, Germany
EASYstrainer™ (100 µm, sterile)	Greiner Bio-One GmbH, Frickenhausen, Germany
Filter paper	Cytiva, Solingen, Germany
Filtropur S 0.45 (filter for syringes)	Sarstedt, Nümbrecht, Germany
HF Bond Elut 1CC LRC-SI, 100 mg	Agilent Technologies (VWR International GmbH, Darmstadt, Germany)
TLC Silica Gel 60, 20 x 20 cm, glass support	Merck, Darmstadt, Germany
250 µl Insert, Polypropylene	Agilent Technologies (VWR International GmbH, Darmstadt, Germany)
Srew Caps N9, center hole, PTFE 1.0 mm	Macherey-Nagel GmbH & Co. KG, Düren, Germany
1.5 ml Vials N9	Macherey-Nagel GmbH & Co. KG, Düren, Germany
Cellview cell culture dish, 35/10 mm, glass bottom	Greiner Bio-One GmbH, Frickenhausen, Germany
SERVAGel™ Neutral HSE, 12 sample well	SERVA Electrophoresis GmbH, Heidelberg, Germany
Kit	Manufacturer/Supplier
CompactPrep Plasmid Midi Kit	Qiagen, Hilden, Germany
DUALmembrane Kit 3	Dualsystems Biotech AG, Zurich, Switzerland
GeneJET™ Plasmid Miniprep Kit	Thermo Fisher Scientific, Schwerte, Germany
GeneJET™ Gel Extraction Kit	Thermo Fisher Scientific, Schwerte, Germany
GeneJET™ Plant Genomic DNA Purification Kit	Thermo Fisher Scientific, Schwerte, Germany
RevertAid H Minus First Strand cDNA Synthesis Kit	Thermo Fisher Scientific, Schwerte, Germany
SuperSignal™ West Femto Maximum Sensitivity Substrate	Thermo Fisher Scientific, Schwerte, Germany

7.2.6 AGI numbers of genes used in this work

Table 7.6. AGI numbers of genes used in this work.

Gene	AGI number	No. of base pairs	protein size [kDa]
<i>FAD2</i>	AT3G12120	1,152	44
<i>FAD3</i>	AT2G29980	1,161	44
<i>PDAT</i>	AT5G13640	2,016	74
<i>DGAT1</i>	AT2G19450	1,563	59
<i>DGAT2</i>	AT3G51520	945	36
<i>WRI1</i>	AT3G54320	1,317	49

7.2.7 Oligonucleotides

Table 7.7. Oligonucleotides used for cloning.

DNA	Sequence of oligonucleotide (5' - 3')	Vector
<i>FAD2</i>	FAD2-for-XhoI ATGCCTCGAGATGGGTGCAGGTGGAAGAAT	<i>pEntryA</i> , <i>pEntryD</i> <i>pESC-TRP</i>
	FAD2-rev-NotI ATGCGCGGCCGCTCATAACTTATTGTTGTACCA	<i>pEntryA</i> , <i>pEntryD</i> <i>pESC-TRP</i>
	FAD2-for-EcoRI ATGCGAATTCATGGGTGCAGGTGGAAGAAT	<i>pESC-TRP</i>
	FAD2-rev-NheI ATGCGCTAGCTCATAACTTATTGTTGTACCA	<i>pESC-TRP</i>
	FAD2-for-SfiI ATGCGGCCATTACGGCCATGGGTGCAGGTGGAAGAAT	<i>pBT3-N</i> , <i>pBT3-C</i> <i>pPR3-N</i>
	FAD2-Nrev-SfiI ATGCGGCCGAGGCCGCTCATAACTTATTGTTGTACCA	<i>pBT3-N</i> , <i>pBT3-C</i> <i>pPR3-N</i>
	FAD2-Crev-SfiI ATGCGGCCGAGGCCGCTCATAACTTATTGTTGTACCA	<i>pBT3-N</i> , <i>pBT3-C</i> <i>pPR3-N</i>
	FAD2-for-attB1 GGGGACAAGTTTGTACAAAAAAGCAGGCTTAATGGGTGCAGGTGGAAGAATG	<i>pDONR221-P1P4</i>
FAD2-rev-attB4- GGGGACAACCTTTGTATAGAAAAGTTGGGTGTAACCTATTGTTGTACCAGT	<i>pDONR221-P1P4</i>	
<i>pFAD2</i>	<i>pFAD2</i> -for AATAAATGGTTGGTGAC	<i>pEntryA</i> , <i>pEntryD</i>
	<i>pFAD2</i> -rev GTTTCTGCAGAAAACC	<i>pEntryA</i> , <i>pEntryD</i>
	<i>pFAD2</i> -for-SfiI ATGCGGCCATTACGGCCAATAAATGGTTGGTGAC	<i>pEntryA</i> , <i>pEntryD</i>
	<i>pFAD2</i> -rev-SfiI ATGCGGCCGAGGCCGCTTTCTGCAGAAAACC	<i>pEntryA</i> , <i>pEntryD</i>

DNA	Sequence of oligonucleotide (5' - 3')	Vector
FAD3	FAD3-for-XhoI ATGCCTCGAGATGGTTGTTGCTATGGACCA	<i>pEntryA</i> , <i>pEntryD</i>
	FAD3-rev-NotI ATGCGCGGCCGCTTAATTGATTTTAGATTTGT	<i>pEntryA</i> , <i>pEntryD</i>
	FAD3-for-EcoRI ATGCGAATTCATGGTTGTTGCTATGGACC	<i>pESC-TRP</i>
	FAD3-for-SfiI ATGCGGCCATTACGGCCATGGTTGTTGCTATGGACCA	<i>pBT3-N</i> , <i>pBT3-C</i> <i>pPR3-N</i>
	FAD3-Nrev-SfiI ATGCGGCCGAGGCGGCCCTTAATTGATTTTAGATTTGT	<i>pBT3-N</i> , <i>pBT3-C</i> <i>pPR3-N</i>
	FAD3-Crev-SfiI ATGCGGCCGAGGCGGCCCTATTGATTTTAGATTTGT	<i>pBT3-N</i> , <i>pBT3-C</i> <i>pPR3-N</i>
	FAD3-for-attB3 GGGGACAACCTTTGTATAATAAAGTTGGAATGGTTGTTGCTATGGACC A	<i>pDONR221-P3P2</i>
	FAD3-rev-attB2+ GGGGACCACTTTGTACAAGAAAGCTGGGTTTAATTGATTTTAGATTT GTC	<i>pDONR221-P3P2</i>
pFAD3	pFAD3-for AGCGGACCTATGACTAC	<i>pEntryA</i> , <i>pEntryD</i>
	pFAD3-rev CGCCGGAGAGAGGGGG	<i>pEntryA</i> , <i>pEntryD</i>
	pFAD3-for-SfiI ATGCGGCCATTACGGCCAGCGGACCTATGACTAC	<i>pEntryA</i> , <i>pEntryD</i>
	pFAD3-rev-SfiI ATGCGGCCGAGGCGGCCCGCCGGAGAGAGGGGG	<i>pEntryA</i> , <i>pEntryD</i>
DGAT1	DGAT1-for-AscI ATGCGGCGCGCCATGGCGATTTTGGATTCTGC	<i>pEntryA</i> , <i>pEntryD</i>
	DGAT1-rev-XhoI ATGCCTCGAGTGACATCGATCCTTTTCGGT	<i>pEntryA</i> , <i>pEntryD</i>
	DGAT1-for-BamHI ATGCGGATCCATGGCGATTTTGGATTCTGC	<i>pESC-URA</i>
	DGAT1-rev-NheI ATGCGCTAGCTCATGACATCGATCCTTTTCG	<i>pESC-URA</i>
	DGAT1-for-SfiI ATGCGGCCATTACGGCCATGGCGATTTTGGATTCTGC	<i>pBT3-N</i> , <i>pBT3-C</i> <i>pPR3-N</i>
	DGAT1-Nrev-SfiI ATGCGGCCGAGGCGGCCCTCATGACATCGATCCTTTTCGGT	<i>pBT3-N</i> , <i>pBT3-C</i> <i>pPR3-N</i>
	DGAT1-Crev-SfiI ATGCGGCCGAGGCGGCCCTTACATCGATCCTTTTCGGT	<i>pBT3-N</i> , <i>pBT3-C</i> <i>pPR3-N</i>
	DGAT2_{opt}	DGAT2 _{opt} -for-SfiI ATGCGGCCATTACGGCCATGGGTGGTTCTAGAGAG
DGAT2 _{opt} -Nrev-SfiI ATGCGGCCGAGGCGGCCCTATAGTATCTTCAGTTCAAG		<i>pBT3-N</i> , <i>pBT3-C</i> <i>pPR3-N</i>

DNA	Sequence of oligonucleotide (5' - 3')	Vector
	DGAT2opt-Crev-Sfil ATGCGGCCGAGGCCGCCCTTAGTATCTTCAGTTCAAG	<i>pBT3-N, pBT3-C pPR3-N</i>
PDAT	PDAT-for-Ascl ATGCGGCGCGCCATGCCCTTATTCATCGGAA	<i>pEntryA, pEntryD</i>
	PDAT-rev-NheI ATGCGCTAGCCAGCTTCAGGTCAATACGCT	<i>pEntryA, pEntryD</i>
	PDAT-for-Sall ATGCGTCGACATGCCCTTATTCATCGGAA	<i>pESC-URA</i>
	PDAT-rev-KpnI ATGCGGTACCTCACAGCTTCAGGTCAATAC	<i>pESC-URA</i>
	CFP-for-NheI ATGCGCTAGCATGAGCAAGGGCGCCGAGCT	<i>pESC-URA</i>
	PDAT-for-Sfil ATGCGGCCATTACGGCCATGCCCTTATTCATCGGAA	<i>pBT3-N, pBT3-C pPR3-N</i>
	PDAT-Nrev-Sfil ATGCGGCCGAGGCCGCCCTCACAGCTTCAGGTCAATACGCT	<i>pBT3-N, pBT3-C pPR3-N</i>
	PDAT-Crev-Sfil ATGCGGCCGAGGCCGCCCTCAGCTTCAGGTCAATACGCT	<i>pBT3-N, pBT3-C pPR3-N</i>
	PDAT-for-attB3 GGGGACAACCTTTGTATAATAAAAGTTGGAATGCCCTTATTCATCGGA A	<i>pDONR221-P3P2</i>
	PDAT-rev-attB2+ GGGGACCACTTTGTACAAGAAAGCTGGGTTACAGCTTCAGGTCAAT AC	<i>pDONR221-P3P2</i>
WRI1	WRI1-for-Sall ATGCGTCGACATGAAGAAGCGCTTAACCAC	<i>pEntryA, pEntryD</i>
	WRI1-rev-XhoI ATGCCTCGAGTTCAGAACCAACGAACAAG	<i>pEntryA, pEntryD</i>
Alg5	Alg5-for-attB3 GGGGACAACCTTTGTATAATAAAAGTTGGAATGAGAGCGTTGAGATTCC T	<i>pDONR221-P3P2</i>
	Alg5-rev-attB2+ GGGGACCACTTTGTACAAGAAAGCTGGGTTAACATTTCTTATTATCT CTAT	<i>pDONR221-P3P2</i>
	Alg5-for-attB1 GGGGACAAGTTTGTACAAAAAAGCAGGCTTAATGAGAGCGTTAGAG ATTCT	<i>pDONR221-P1P4</i>
	Alg5-rev-attB4- GGGGACAACCTTTGTATAGAAAAGTTGGGTGACATTTCTTATTATCTCT AT	<i>pDONR221-P1P4</i>
EYFP mCherry	EYFP/mC-for-Ascl ATGCGGCGCGCCATGGTGAGCAAGGGCGAGGA	<i>pEntryA, pEntryD</i>
	EYFP/mC-rev-XhoI ATGCCTCGAGCTTGTACAGCTCGTCCA	<i>pEntryA, pEntryD</i>
	EYFP/mC-for-XhoI ATGCCTCGAGATGGTGAGCAAGGGCGAGGA	<i>pEntryA, pEntryD</i>

DNA	Sequence of oligonucleotide (5' - 3')	Vector
	EYFP/mC-rev-NotI ATGCGCGGCCGCTTACTTGTACAGCTCGTCCA	<i>pEntryA</i> , <i>pEntryD</i>
	EYFP/mC-for-Sall ATGCGTCGACATGGTGAGCAAGGGCGAGGA	<i>pEntryA</i> , <i>pEntryD</i> <i>pESC-URA</i>
	EYFP/mC+1-rev-Ascl ATGCGGCGCGCCTCTTGTACAGCTCGTCCATGC	<i>pEntryA</i> , <i>pEntryD</i>
	EYFP/mC-for-EcoRI ATGCGAATTCATGGTGAGCAAGGGCGAGGA	<i>pESC-TRP</i>
	EYFP/mC-for-Sall ATGCGTCGACATGGTGAGCAAGGGCGAGGA	<i>pESC-TRP</i>
	EYFP/mC-rev-NheI ATGCGCTAGCTTACTTGTACAGCTCGTCCA	<i>pESC-URA</i>
CFP	CFP-for-XhoI ATGCCTCGAGATGAGCAAGGGCGCCGAGCT	<i>pESC-URA</i>
	CFP-rev-NheI ATGCGCTAGCTCACTTCCACTTGTACAGCT	<i>pESC-URA</i>
	CFP-rev-KpnI ATGCGGTACCTCACTTCCACTTGTACAGCT	<i>pESC-URA</i>

Table 7.8. Oligonucleotides used for sequencing.

Analyzed sequence	Description/Name	Sequence of oligonucleotide (5' - 3')
<i>pEntryA</i>	35S-for	TATATAAGGAAGTTCATTT
<i>pEntryD</i>	OCS-rev	TTTACAACGTGCACAACAGAA
	M13-for	CCCAGTCACGACGTTGTAAAACG
<i>pESC-TRP</i>	<i>pESC-TRP</i> -mcsI-rev	ACCAAACCTCTGGCGAAG
<i>pESC-URA</i>	GAL10-for	GTAATATGATTATTAAC
	GAL1-for	ATTTTCGGTTTGTATTACTTC
	TCyc1-rev	AAATAAATAGGGACCTAG
<i>pBT3-N</i>	<i>pBT3N</i> -for	AAGGAGTCCACCTTACAT
	<i>pBT3N</i> -rev	AATGTAAGCGTGACATAA
<i>pPR3-N</i>	<i>pPR3N</i> -for	ATGCAGATTTTCGTCAAGACTTT
	<i>pPR3N</i> -rev	ATAACTAATTACATGACT
<i>pDONR221-P1P4</i> <i>pDONR221-P3P2</i>	M13fwd-DONR	GTAAAACGACGGCCAGTCTT
<i>EYFP/CFP</i>	VYFP-for	CTGAAGTTCATCTGCACCACCGGCAAG
	VYFP-rev	CTTGCCGGTGGTGAGATGAAGTTCAG
<i>EYFP</i>	HYFP-for	TACCAGTCCGCCCTGAGCAAAGA
	HYFP-rev	TCTTTGCTCAGGGCGGACTGGTA

Analyzed sequence	Description/Name	Sequence of oligonucleotide (5' - 3')
<i>mCherry</i>	HmCherry-for	CTACGACGCTGAGGTCAAGAC
	HmCherry-rev	GTCTTGACCTCAGCGTCGTAG
<i>FAD2</i>	FAD2mfor	ATGTTAACCGTCCAGTTTGT
<i>FAD3</i>	FAD2mrev	ACAAACTGGACGGTTAACAT
	FAD3for265	AAGGAACACTTTTCTG
	FAD3mfor	TCTCTATTTGTGCTACAGAA
	FAD3mrev	TTCTGTAGCACAAATAGAGA
<i>DGAT1</i>	DGAT1mfor	ATTCTGCTTTTTTATCAGGT
	DGAT1mrev	ACCTGATAAAAAAGCAGAAT
<i>DGAT2opt</i>	Dgat2optfor756	GGTTCACCGCTTCCATGTAG
<i>PDAT</i>	PDATfor536	TGGCTGCTGACTACTTTGCT
	PDATrev536	AGTAGATCTATAGCTTCACCA
	PDATfor918	TTCTCTGCTGAAGCAAAGGA
	PDATrev918	TCCTTTGCTTCAGCAGAGAA
	PDATfor1389	TGGTGAAGCTATAGATCTACT
	PDATrev1389	AGCAAAGTAGTCAGCAGCCA
<i>WRI1</i>	WRI1mrev	TCCCAAACACTCTTCCGATC
<i>pFAD2</i>	pFAD2for560	ACGATTCTTTCTTTTCATAT
	pFAD2for1393	CTCGTCTACAAAACGATATG
<i>pFAD3</i>	pFAD3for739	AAATCGGTGATGGCAATTGG

Acknowledgment – Danksagung

Wie jemand einmal so schön bemerkte, steht kein Mensch allein auf weiter Flur – bzw. im Labor. Daher möchte ich mich bei einigen Menschen bedanken, ohne die die Entstehung dieser Arbeit nicht möglich gewesen wäre.

Zuallererst ein großes Dankeschön an Prof. Dr. Ingo Heilmann und Dr. Mareike Heilmann. Ihr gabt mir die Möglichkeit, an einem so vielseitigen und spannenden Thema zu arbeiten. Dankbar bin ich auch für unseren großartigen Ausflug zur Tagung nach Galveston.

Vielen Dank, Ingo, für die Aufnahme in deine Arbeitsgruppe. Die fachlichen Diskussionen, deine Impulse und Denkanstöße und deine Unterstützung bei der Anfertigung dieser Arbeit waren mir eine große Hilfe. Ein Dankeschön auch für deine gute Laune und dass der nächste Witz nicht fern war.

Vielen Dank, Mareike, für deine umfangreiche Betreuung im Labor und für das Fachwissen, das du mit mir teilst. Nicht nur bei der Anfertigung von Vorträgen und Postern, sondern auch bei dieser Arbeit konnte ich auf deine Hilfe zählen. Und vielen Dank für die eine oder andere Stunde des Verquatschens zum Feierabend. Die spannendsten Themen tauchen immer erst auf, wenn man gerade dabei ist zu gehen.

Für die finanzielle Unterstützung bedanke ich mich bei der Graduiertenschule „AgriPoly: Determinants of Plant Performance“ (Projekt-Nr.: J 01 070 339), finanziert durch das Land Sachsen-Anhalt und den Europäischen Sozialfonds.

Bei den Gutachtern möchte ich mich für die Zeit bedanken, die sie sich für die Begutachtung meiner Dissertation genommen haben.

Danke, Marta, dass du mir die SD-Mikroskopie näherbrachtest und für alle Fragen zum Bereich der Mikroskopie ein offenes Ohr hattest. Bei Prof. Dr. Kirsten Bacia und ihrer Arbeitsgruppe möchte ich mich für die Möglichkeit zur Nutzung des SD-Mikroskops bedanken.

Ein Dank gilt auch meinen Studenten, mit denen ich mein Projekt eine Zeit lang teilen durfte. Insbesondere möchte ich Sebastian Scheer, Georg Steinert und Luise Jäckel hervorheben, deren Ergebnisse teilweise Eingang in diese Arbeit fanden.

Vielen Dank an Franzi, meine Leidensgenossin. Du hast die Messlatte hochgesteckt und vorgemacht, wie es richtig geht. Vielen Dank für die wunderbaren Gespräche, das geteilte Leid und die geteilte Freude.

Danke an Christoph und Monique für die vielen konstruktiven Diskussionen und den starken Kaffee.

Ein großer Dank geht an alle aktuellen und ehemaligen Mitglieder der AG Heilmann: Christoph, Franzi, Monique, Lennart, Praveen, Feng, Johanna U., Johanna N., Benita, Marion, Kristin, Irene, Nadine, Alex, Willi, Angela, Julia, Martina, Daniel. Ihr standet mir immer mit Rat und Tat zur Seite. Vielen Dank für die wundervolle Zeit. Eine schönere Arbeitsatmosphäre kann ich mir nicht vorstellen! Und so viel Kuchen!

Besonders dankbar bin ich für die Unterstützung durch meine Familie und meine Freunde. Ihr standet mir immer zur Seite mit Motivation, Aufmunterung und was immer gerade benötigt wurde.

An Stephan: Du passt mir emotional ganz gut in den Kram. Nach wie vor. Danke!

Curriculum vitae

Larissa Launhardt

Date of Birth: November 22nd, 1993
Place of Birth: Buchholz i. d. Nordheide
Nationality: German

Education

Since 12/2017 Ph.D., Scholarship recipient in the graduate school “AgriPoly”
Martin-Luther-University Halle-Wittenberg
Department of Plant Biochemistry (Prof. Dr. Ingo Heilmann)

10/2015 – 11/2017 Master of Science in Biochemistry
Martin-Luther-University Halle-Wittenberg

10/2012 – 9/2015 Bachelor of Science in Biochemistry
Martin-Luther-University Halle-Wittenberg

2012 Abitur
Albert-Einstein-Gymnasium, Buchholz i. d. Nordheide

Publications and Conferences

Larissa Launhardt, Monique Matzner, Mareike Heilmann, Ingo Heilmann (2021) Analysis of Phosphoinositides from Complex Plant Samples by Solid-Phase Adsorption Chromatography and Subsequent Quantification via Thin-Layer and Gas Chromatography. In: Bartels D., Dörmann P. (eds) Plant Lipids. Methods in Molecular Biology, vol 2295. Humana, New York, NY.

Larissa Launhardt, Mareike Heilmann, Ingo Heilmann (June 2019) Spatiotemporal organization of enzymes mediating plant oil biogenesis. “Plant Science Student Conference” (PSSC), Leibniz Institute of Plant Biochemistry, Halle (Saale), Germany (poster).

Larissa Launhardt, Mareike Heilmann, Ingo Heilmann (January 2019) Spatiotemporal organization of enzymes mediating plant oil biogenesis. Gordon Research Conference “Plant Lipids: Structure, Metabolism and Function”, Galveston, Texas, USA (poster).

Larissa Launhardt, Mareike Heilmann, Ingo Heilmann (January 2019) Spatiotemporal organization of enzymes mediating plant oil biogenesis. Gordon Research Seminar “Plant Lipids: Structure, Metabolism and Function”, Galveston, Texas, USA (poster and talk).

Erklärung

Hiermit erkläre ich, dass ich die vorliegende Dissertation selbständig und ohne fremde Hilfe verfasst habe, keine anderen als die angegebenen Quellen und Hilfsmittel benutzt habe und die den benutzten Werken wörtlich oder inhaltlich entnommenen Stellen als solche kenntlich gemacht habe.

Des Weiteren erkläre ich, bisher keine vergeblichen Promotionsversuche unternommen zu haben und die Dissertation in der gegenwärtigen bzw. in einer anderen Fassung nicht bereits an einer anderen Fakultät vorgelegt zu haben.

Halle (Saale), _____

Larissa Launhardt